Deciphering Photoluminescence and Charge Carrier Recombination Dynamics of the Lead Halide Perovskite Nanocrystals at the Single-Particle and Ensemble Level

A Thesis Submitted for the Degree of

Doctor of Philosophy at the University of Hyderabad

by

Sumanta Paul

School of Chemistry

University of Hyderabad

Hyderabad- 500046

India

Declaration

I hereby declare that the matter embodied in the thesis entitled **"Deciphering Photoluminescence and Charge Carrier Recombination Dynamics of the Lead Halide Perovskite Nanocrystals at the Single-Particle and Ensemble Level"** is the result of investigation carried out by me in the School of Chemistry, University of Hyderabad, India under supervision of Prof. Anunay Samanta.

With my signature I confirm:

- I have committed none of the forms of plagiarism.
- This thesis work is screened electronically for plagiarism check.
- I have documented all methods, data and processes truthfully.
- I have mentioned all persons who were significant contributors to this work.

University of Hyderabad, India

17th June, 2023

Sumanta Paul

Signature

Professor Anunay Samanta
School of Chemistry
University of Hyderabad
Hyderabad-500046, India

Phone: +91-40-2313 4813
FAX: +91-40-2301 1594
Email: anunay@uohyd.ac.in

Certificate

This is to certify that the thesis entitled ***"Deciphering Photoluminescence and Charge Carrier Recombination Dynamics of the Lead Halide Perovskite Nanocrystals at the Single-Particle and Ensemble Level"*** submitted by **Mr. Sumanta Paul** bearing the registration number 17CHPH43 in partial fulfilment of the requirements for the award of Doctor of Philosophy (Ph.D.) in the School of Chemistry, University of Hyderabad, India under my supervision and guidance. This thesis is free from plagiarism and has not been submitted previously in part or full to this or other University/Institution for any degree or diploma. Further, the student has following publications before submission of the thesis for adjudication and has produced evidences for the same in the form of reprints.

Parts of this thesis have been published in following publications:

1. **S. Paul** and A. Samanta, *ACS Energy Lett.* **2020**, *5*, 64−69 **(Chapter 3)**
2. **S. Paul,** T. Ahmed, S. Das and A. Samanta, *J. Phys. Chem. C* **2021**, *125*, 23539−23547 **(Chapter 4)**
3. **S. Paul** and A. Samanta, *J. Phys. Chem. Lett.* **2022,** *13,* 5742−5750 **(Chapter 5)**
4. **S. Paul,** G. Kishore and A. Samanta, *J. Phys. Chem. C 2023*, *127,* 10207−10214 **(Chapter 6)**

The student have made presentations in the following conferences:

1. 15th Trombay Symposium on Radiation and Photochemistry (TSRP-2020), Bhabha Atomic Research Centre (BARC), Mumbai, India, January 5-9, 2020. **(Poster presentation)**
2. National Workshop on Fluorescence and Raman Spectroscopy (FCSXIII-2022), IISER Trivandrum, Trivandrum, India, January 6-11, 2023. **(Poster presentation)**
3. Special Satellite meeting Celebrating 50 Years of Fluorescence Correlation Spectroscopy (FCS@50) Kovalam, Trivandrum, India, January 11-14, 2023. **(Poster presentation)**
4. 17th Annual In-House Symposium of the School of Chemistry (Chemfest-2020), University of Hyderabad, Hyderabad, India, February, 2021. **(Oral Presentation)**

Further, the student has passed the following courses:

1. CY801- Research Proposal (4 credit)
2. CY805- Instrument Methods-A (4 credit)
3. CY806- Instrument Methods-B (4 credit)

Anunay Samanta

Thesis Supervisor

PROF. ANUNAY SAMANTA
SCHOOL OF CHEMISTRY
UNIVERSITY OF HYDERABAD
HYDERABAD - 500 046

22/06/2023

Dean

School of Chemistry, UoH

Dean
SCHOOL OF CHEMISTRY
University of Hyderabad
Hyderabad-500 046

PUBLICATIONS

1. **Paul, S**.; Samanta, A. N-Bromosuccinimide as Bromide Precursor for Direct Synthesis of Stable and Highly Luminescent Green-Emitting Perovskite Nanocrystals. *ACS Energy Lett.* **2020,** *5*, 64−69.
2. **Paul, S.**; Ahmed, T.; Das, S.; Samanta, A. Effect of Lead:Halide Precursor Ratio on the Photoluminescence and Carrier Dynamics of Violet- and Blue-Emitting Lead Halide Perovskite Nanocrystals. *J. Phys. Chem. C* **2021,** *125*, 23539−23547.
3. **Paul, S.**; Samanta, A. Phase-Stable and Highly Luminescent $CsPbI_3$ Perovskite Nanocrystals with Suppressed Photoluminescence Blinking. *J. Phys. Chem. Lett.* **2022,** *13*, 5742−5750.
4. **Paul, S.**; Kishore, G.; Samanta, A. Photoluminescence Blinking of Quantum Confined $CsPbBr_3$ Perovskite Nanocrystals: Influence of Size. *J. Phys. Chem. C* **2023,** *127*, 10207-10214.
5. Ahmed T.; **Paul, S.**; Samanta, A. Photoluminescence Blinking Revealing Static and Dynamic Heterogeneity of the Hole Transfer Process in Phenothiazine-Adsorbed $FAPbBr_3$ Single Nanocrystals. *J. Phys. Chem. C* **2022,** *126*, 9109-9116.
6. Ahmed T.; De, A.; **Paul, S.**; Samanta, A. Individual Particle-Level Picture of Charge Carrier Recombination in Bi-Doped $CsPbBr_3$ Nanocrystals. *J. Phys. Chem. C* **2021,** *125*, 2156-2162.
7. Mondal, N.; De, A.; Das, S.; **Paul, S.;** Samanta, A. Ultrafast Carrier Dynamics of Metal Halide Perovskite Nanocrystals and Perovskite-Composites. *Nanoscale* **2019**, *11*, 9796−9818.
8. Mondal, N.; De, A.; Seth, S.; Ahmed, T.; Das, S.; **Paul, S.**; Gautam, R. K.; Samanta, A. Dark Excitons of the Perovskites and Sensitization of Molecular Triplets. *ACS Energy Lett.* **2021**, *6*, 588− 597.
9. Mondal, S.; Bobbili, K. B.; **Paul, S.;** Swamy, M. J. DSC and FCS Studies Reveal the Mechanism of Thermal and Chemical Unfolding of CIA17, a Polydisperse Oligomeric Protein from Coccinia Indica. *J. Phys. Chem. B* **2021**, *125*, 7117−7127.
10. Mondal, S.; Das, S.; **Paul, S.;** Barik, S.; Swamy, M. J. Low pH Molten Globule-Like Form of CIA17, a Chitooligosaccharide Specific Lectin from the Phloem Exudate of Coccinia indica, Retains Carbohydrate Binding Ability. *J. Phys. Chem. B* **2022,** *126*, 4049− 4060.

PRESENTATIONS

1. "Near Unity Photoluminescence Quantum Efficiency for Blue and Green Emitting Perovskites Nanocrystals". 15th Trombay Symposium on Radiation and Photochemistry (TSRP-2020), Bhabha Atomic Research Center (BARC), Mumbai, India, January 5-9, 2020. **(Poster presentation)**

2. "The Size-Effect on Photoluminescence Blinking of the Quantum Confined $CsPbBr_3$ Nanocrystals". National Workshop on Fluorescence and Raman Spectroscopy (FCSXIII-2022), IISER Trivandrum, Trivandrum, January 6-11. **(Poster presentation)**

3. "Individual Particle-Level Picture of Charge Carrier Recombination in Bi-Doped $CsPbBr_3$ Nanocrystals" Special Satellite meeting Celebrating 50 Years of Fluorescence Correlation Spectroscopy (FCS@50) (FCSXIII-2022), IISER Trivandrum, Trivandrum, January 11-14. **(Poster presentation)**

4. "**Phase Stabilization and Near-Complete Suppression of Photoluminescence Blinking of $CsPbI_3$ Nanocrystals". National Workshop on Fluorescence and Raman Spectroscopy (FCSXII-2021),** IISER Trivandrum, Trivandrum, November 27- December 2. **(Oral Presentation)**

5. "**Mechanistic Investigation of Photoluminescence Blinking of Red-Emitting Perovskite ($CsPbI_3$) Nanocrystals". 17thAnnual In-House Symposium of the School of Chemistry (Chemfest-2020),** University of Hyderabad, Hyderabad, India, February, 2021. **(Oral Presentation) (Best Oral)**

Acknowledgements

This thesis is the results of five years of hard work, which wouldn't have been possible without some very important figures.

I would like to express my heartfelt gratitude to my research supervisor Prof. Anunay Samanta, for his constant support, kind guidance and patience. I am very grateful to him for giving me the scientific freedom to pursue my interests and modulating me into an independent researcher. He has been quite helpful to me in both academic and personal fronts.

I would like to thank the former and present Dean, School of Chemistry, for their constant support, inspiration and for available facilities. I am extremely appreciative individually to all the faculty members (especially my doctoral committee members, Prof. M.J. Swamy & Prof. S. Pal) of the School for their help, cooperation and encouragement at various stages.

Financial assistance from University Grant Commission (UGC) is greatly acknowledged. Special thanks are due to UGC for providing me a five year research fellowship.

I would like to acknowledge Prof. K. George. Thomas and Prof. Mahesh Hariharan , Indian Institute of Science Education & Research for giving me access to Time-Resolved Confocal Microscope setup for photon antibunching measurement. I also thank Visnu EK, Philippe Daniel Marate and Devika Rajan for assisting me during this measurement.

I also acknowledge Mr. Durga Prasad and Mr. Sunil, Mr. Rajesh for the special care during TEM and EDX measurements.

I express my heartfelt gratitude to dedicated teachers I came by different stages of my life. During my school life teaching Manabendranath Biswas, Kalyan Chatterjee, Asit kumar Nath , Chandra bhanu Chakraborty, Arun Pramanik, Gautam Pal, Adhir ranjan Maitra, Prashanta Das, Dipak Saha and Lipika Biswas made me more passionate about science and made me more inclined to chemistry. I still enjoy the happy moments and unforgettable memories; I had with Shreyasi, Rajib, Siddhan, Rahul, Binoy, Ratul, Jyoti, Nikkon, Deba, Rathin, Sourav,. During my B.Sc. days I got extremely good professor like Safallya kr. Ghosh, Sanjoy Nath, Arijit De, Partha Majumder, Subhash De and their lectures helped me understand fundamental aspects of Chemistry. I am fortunate enough to have great teachers like Prof. Anunay Samanta, Prof. M. Durga Prasad, Prof. T.P. Radhakrishnan, Prof. Susanta Mahapatra, Prof. KC kumar Swamy, Prof. S.Pal, Prof. A.K. Sahoo. Prof. D.B. Ramachary Prof. Debashis Barik. I express my sincere gratitude Prof. Susanta Mahapatra, Prof. M. Durga

Prasad and Prof. Debashis Barik for their encouraging lectures on physical chemistry which helped me to grow interest in spectroscopy.

I am grateful for the valuable friendship of my college friends (Prabir, Subhasis, Debu, Sudipto, Abhyuday, Bhola, Bishal, Imdadul, Motahar, Abdul, Ahad, Gargi,) and hostel mates (Insan, Nurul, Fleming, Utpal Da, Rakesh Da, Rakesh Bhai, Najir, Kadir, Apurba, Kumaresh, Baloram, Animesh, Prasenjit, Samirul, Mominur……..) for all sweet memories.

I feel fortunate to have friends like Abhishek (Sharmaji), Gautam, Karan (KP) Deepshikha, Avinaba, Goon da, Saptarshi, Sagnik, Sayan, Rana pratap, Souradip, Anwesha from my M.Sc. time.

I feel myself lucky for being a part of this AS lab. I am fortunate to have a senior like Navendu da, who has always motivated me and has been always there for any kind of help. I really enjoyed any kind of discussions with you which has been always fruitful. It was an amazing experience to work with Sudipta Da. I will always be grateful to you for teaching me everything in lab, starting from synthesis of perovskite nanocrystals to handling all the instruments. I really enjoyed all the discussions with you and learnt a lot from you. Sneha di has been an excellent senior. I am thankful for your help and support in several occasions. I really admire your presentation and communication skills, which I always tried to adopt. I really lucky to have supportive seniors like Saddam da, Apurba da, Tasnim di, Somnath da. I really enjoyed all the academic and non-academic discussions with you and will cherish all the leg pulling of each other. I have always appreciated Saddam da for his positive attitude and maintaining a cheerful environment in the lab. It was a nice experience to work with Tasnim di, I cannot mention how much I have learnt from you. I am fortunate having batch mates like Somnath, Rajesh and Alila. I feel myself lucky for being able to work with such wonderful people. I thank all my lab mates for keeping a healthy atmosphere in lab.

I cherish my bonding with my batch mates and juniors like Vamsi, Vinoy, Vinod, Surya, Rabiul, Nitai, Shyam, Debu, Somratan, Debojyoti. I enjoyed the time we spent together during the organization of PhD freshers' party, Chemfest, and playing cricket and badminton tournaments. I value my bonding with Surya and Rabiul.

I am really lucky having company of Suman da, Shubham da, Alamgir, Anupam da, Nilu da, Soutrick da, Kuntal Da, Bappa da, Arijit da, Soumen, Alim vai in hostel and department. I really miss those Saturday night parties. Our Warangal trip in bike was awesome. I am lucky to be part of the nairit kone group. Without the cheerful company of all these people the campus life would have been boring and difficult to survive. I treasure the moments shared with Sugata da, Rudra da, Kuntal Da and Debikadi.

I believe that no words or actions would suffice to express my feeling about or even acknowledge my parents', sister's and brother's contribution in my life. I would like to express my gratitude to my parents, sister and brother who have been the pillars of immense love and strength throughout my life. I also wish to thank my grandmother for her adoration and love. I also thank my father and mother in law for their constant supports.

Finally, I reserve my deepest gratitude to my dearest friend; my wife ***Shreyasi*** *for her selfless love, unwavering tolerance and understanding and* ***co-authoring my long term projects****. I am eternally grateful for your unconditional sacrifice, support for me and always cheering me up.*

Hyderabad, June 23, 2023 *Sumanta*

Contents

List of Abbreviations

ADC	Analog to Digital Converter
CBM	Conduction Band Minima
CFD	Constant Fraction Discriminator
EDX	Energy Dispersive X-ray
FESEM	Field Emission Scanning Electron Microscopy
EPR	Electronic Paramagnetic Resonance
ESA	Excited State Absorption
FTIR	Fourier-Transform Infrared Spectroscopy
GSB	Ground State Bleach
HR-TEM	High Resolution Transmission Electron Microscopy
HOMO	Highest Occupied Molecular Orbital
LED	Light Emitting Diode
LUMO	Lowest Unoccupied Molecular Orbital
MCA	Multi Channel Analyzer
MCP	Micro-Channel Plate
NCs	Nanocrystals
OPA	Optical Parametric Amplifier
OA	Oleic acid
OLA	Oleylamine
PMT	Photomultiplier Tube
PLQY	Photoluminescence Quantum Yield
PXRD	Powder X-ray Diffraction
QDs	Quantum Dots
RT	Room Temperature
SE	Stimulated Emission

Thesis Layout

The thesis consists of seven chapters. ***Chapter 1*** starts with a brief discussion on semiconductor NCs and their size dependent optical properties and carrier recombination processes. Then the lead halide perovskites, one of the most celebrated semiconductor materials in recent time, are introduced. Their crystal structure and composition dependent optical properties are discussed. The synthesis method, nucleation and growth processes, surface chemistry and photophysical properties are briefly discussed. In ***Chapter 2***, we have described the synthesis and purification methods of the LHP NCs used in this project work. Basic principles of different spectroscopic techniques used for our studies, like steady state UV-Vis absorption and emission, time correlated single-photon counting, PL blinking, fluorescence correlation spectroscopy, femtosecond pump-probe spectroscopy have been discussed. The working chapters begin from ***Chapter 3***, in which a general methodology for obtaining all bromide-based LHP NCs with unparalleled PLQY and stability employing N-bromosuccinimide as a new bromide precursor is described. In ***Chapter 4***, we have extended this method to develop violet- and blue-emitting LHP NCs using N-halophthalimides and N-halosuccinimide as halide precursors. The effect of lead:halide precursor ratio on the PL and carrier dynamics of these NCs is then discussed. In ***Chapter 5,*** we have described a strategy for achieving phase stable and highly luminescent $CsPbI_3$ NCs with suppressed PL blinking. We have also thoroughly investigated the mechanism of PL fluctuation of these NCs. In ***Chapter 6,*** the effect of size on PL blinking of the quantum confined $CsPbBr_3$ NCs has been discussed. By analyzing the PL blinking data, the rate of carrier trapping processes in these NCs is assessed. In ***Chapter 7***, a summary of these findings is presented, and the future scope of investigation is highlighted.

CHAPTER 1

Introduction

Overview

In this chapter, relevant concepts and theories necessary for understanding of the research work presented in this thesis are provided. The origin of band structures, charge carrier recombination processes, and quantum confinement effect in semiconductors are described. The discussion is then focused on newly emerged perovskite NCs, which are one of the most celebrated semiconductor NCs in recent time and around which this thesis work evolves. A brief discussion on the methods of synthesis, nucleation and growth mechanism, and strategies for shape and size control of this important class of materials is presented. Specific attention is given to the defects, surface termination and ligand binding mechanism of these systems. PL blinking of the perovskite single NCs and processes, which contribute to this phenomenon, are discussed.

1.1. Preface

In the last 20 years the world has witnessed tremendous advancement in technology, energy, and medicine. These advances are driven by materials, which are thousand times smaller than a single strand of hair known as nanocrystals (NCs). The size of a NC usually ranges from 1 to 100 nm. Significant efforts have been made in developing the NCs and associated technologies in recent years. Nanotechnology has already made a huge impact in bio-imaging and sensing capabilities in medicine, drug delivery and gene therapy. The applications of the NCs extended from the biological sphere to energy solution including photovoltaics devices, light emitting diodes and water splitting catalyst.[1] Recently, Samsung used semiconductor NCs for making of QLED television display. NCs offer both energy efficiency and color gamut advantages over other existing screen technologies, such as organic LEDs. NCs can also be used as potential single photon emitter in quantum technologies.[2] Their application breadth and success is due to the tunability of the physical, chemical, and biological properties, coupled with ease of their processing.

Semiconducting NCs, known as quantum dots, are of particular interest in photovoltaics and optoelectronics due to their interesting physical and electronic properties. Cadmium based metal chalcogenide quantum dots were first used in these applications. Due to the toxicity issue of the Cd based NCs, indium phosphide based NCs were introduced later as an alternative. Despite making it to the market, these are still limited in their performance due to the lack of color tunability, size restrictions and defect intolerance. From last decade, lead halide perovskites (LHPs) with chemical formula $APbX_3$, where A is an inorganic or organic cation, and X is the halide anion, burst on to the photovoltaic research as a replacement of the dyes in typical dye-sensitized solar cell.[3] Since then, LHPs have set up its own field of research for photovoltaics and other optoelectronic applications, such as LEDs, photo detectors, and single photon emitter, and photocatalysis. A tremendous rise in photovoltaic efficiency with records 25.7% for single junction and 29.8% for perovskite silicon tandem solar cell have been observed.[4] Research on LHPs NCs has been built on the foundations of traditional quantum dots. The bridging of these two research fields, alongside the remarkable properties of perovskite NCs, has allowed the field to rapidly grow and develop in a short span of time. To give a glimpse, more than 2500 papers on metal halide perovskite have been published by only ACS journals and earned nearly 120,000 citations within 10 years.[5] The application of the LHP NCs in photovoltaics and LEDs is of particular interest. Their broad absorption spectra, high absorption coefficient, bright emission, narrow line widths, and bandgap

tunability made them suitable contender for these applications.[6] Despite vast growth in application-orientated research of the perovskites, the understanding of several fundamental aspects of the LHPs remains unclear till date. Specifically, in NCs' research, there remains several questions regarding surface passivation, obtaining near-unity photoluminescence efficiency across different compositions, sizes, and understanding of the charge carrier dynamics at the single particle and ensemble level. Targeting these areas is quite challenging for these systems because of their compositional breadth and diversity in chemistry for different compositions. For the proper utilization of the perovskite NCs in photovoltaics, LEDs and other optoelectronic applications, their synthesis, surface passivation and charge carrier dynamics must be well understood. With this aim, this thesis contributes by introducing a new synthetic route for perovskite NCs using unique precursors and unveil some interesting photophysical behavior by probing them at the single particle and ensemble level.

1.2. Background and Theory

1.2.1. Semiconductors and Band Structure

Solids are categorized into three classes based on their electrical conductivity: metal, semiconductor, and insulator. Semiconductors are a class of materials that sit between a metal and an insulator. There are two schools of thought for understanding the electronic structure of bulk solids in general and the principles are laid out in solid-state physics, and in the chemistry-based atomic and molecular orbital approach. In molecular orbital (MO) theory, electrons are considered to be spread in the entire molecule, and the MO where these electrons reside, made up by linear combination of atomic orbitals. Combination of N number atomic orbitals generates N number molecular orbitals in a molecule. A solid can be considered as a collection of infinite number of molecules and the combination of MO eventually gives rise to a continuum of states. The highest occupied MO (HOMO) evolves into the valence band (VB) whereas the lowest unoccupied MO (LUMO) into the conduction band (CB) (Figure 1.1.a). The energy separation between the edge of VB and CB is the bandgap energy of a material. In case of insulators VB occupied by electron and empty CB is separated by large bandgap (>4eV). However, for semiconductors, the band structure is more or less similar to the insulator but the bandgap is low. Due to the low bandgap (e.g. 0.67 eV for germanium, 1.43 eV for gallium arsenide) of the semiconductors, the electrons can be easily excited to CB from VB by thermal or light energy. Further, the semiconductors can be classified into (i) direct bandgap semiconductor, (ii) indirect bandgap semiconductor based on their band structures (Figure 1.1.b). In direct bandgap semiconductors, maxima and minima of the CB and VB possess same wave

vector (k), while the indirect one has different k. The Indirect bandgap semiconductors exhibit most often very weak transition probability of radiative emission, while direct band gap materials exhibit strong transition probability of radiative emission.

Density of state (DoS) is the possible number of states an electron (or hole), can occupy per unit volume when excited. It has been observed that DoS is not uniform over a band due to uneven spread of energy levels across the band. The DoS is zero at the bandgap whereas in the VB and CB a curved distribution is observed, shown in Figure 1.1.c. It should be noted that the DoS in semiconductor NCs depends on the shape of the NCs (vide infra).

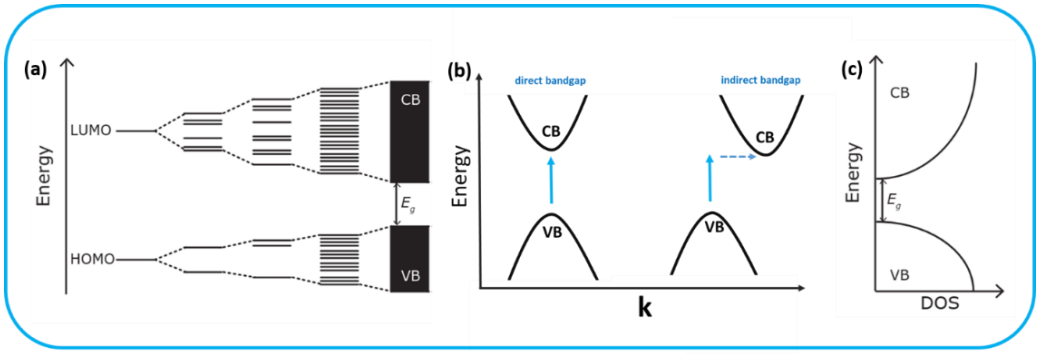

Figure 1.1. (a) Schematic illustration of the formation of band from molecular orbital, (b) direct and indirect band gap semiconductor and (c) density of states of a semiconductor.

1.2.2. Charge Carrier Recombination in Semiconductor

In a semiconductor, bandgap can be overcome by a photon, which excites an electron to the CB and leaves a hole in VB. The electron and hole always feel some level of binding interaction and the strength of this interaction determines if the electrons and holes are viewed as an exciton (high binding energy) or free charge carriers (low binding energy). In the case of exciton forming, the columbic interaction between them lowers the total energy of the system. There are two types of excitons: Frenkel and Wannier-Mott. In Frenkel exciton, electron and hole pair are bound to their parent atom and this kind of exciton (binding energy ~0.1 – 1 eV) is mainly observed in organic molecules. While, in case of Wannier-Mott exciton (binding energy ~10 – 100 meV), the electron and hole pair are delocalized throughout the lattice, which is mainly observed in inorganic semiconductors.

In a semiconductor, the exciton can recombine radiatively and/or non-radiatively. Photons are emitted in radiative recombination, whereas in non-radiative recombination, phonons are emitted.[7] These

two processes are not mutually exclusive and they can occur at the same time as competing processes. The rate equation of these competing processes is summarized in equation 1.1.

$$\frac{dn}{dt} = -k_3 n^3 - k_2 n^2 - k_1 n \qquad \text{---------- 1.1}$$

Here n is the density of charge carriers in a semiconductor at time t. k_1 represents the rate constant of unimolecular recombination, e.g. trap-assisted recombination. A trap-state is an electronic energy state, which arises due to the defects in semiconductor that traps the charge carriers before they recombine radiatively. k_2 corresponds to the rate constant of bimolecular recombination of the electron and hole. This recombination usually occurs from the conduction band minima, and is called band edge excitonic recombination. k_3 represents the rate constant of Auger recombination. Auger recombination is a many-body process, involving at least three particles. In this process, the recombination energy of the electron and hole is transferred to another carrier (electron or hole). These processes are shown in Figure 1.2.a-c, respectively.

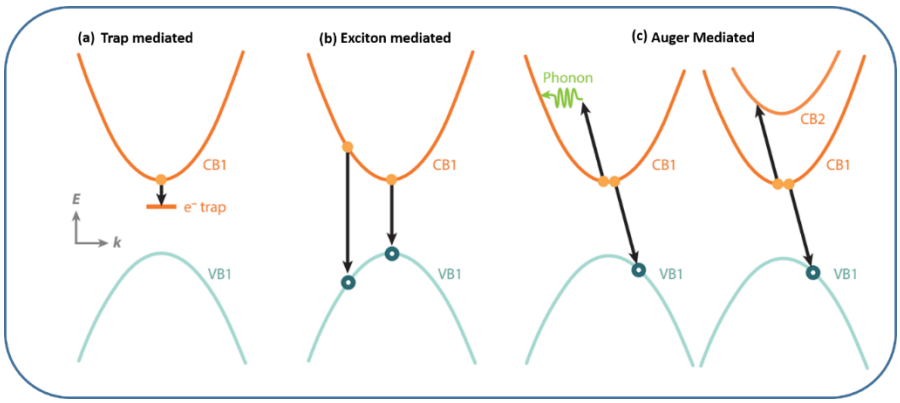

Figure 1.2. Schematic diagram of different recombination mechanisms in semiconductors (a) Trap-assisted recombination, (b) bimolecular recombination between electron and hole, (c) Auger recombination involving at least three particles (adapted from reference 7).

Practically, photoluminescence quantum yield (PLQY) of a material gives an idea about the relative contribution of the radiative and non-radiative recombination processes. PLQY of system is the ratio of number of photons emitted against photons absorbed (equation 1.2). If in a material only radiative recombination occurs, a unity PLQY is observed. However, for the majority of semiconductors this is not the case; trapping of the charge carriers causes deviation from near-unity PLQY.

$$PLQY(\phi) = \frac{no.\ of\ photons\ emitted}{no.\ of\ photons\ absorbed} \quad \text{----------1.2}$$

Exciton recombination lifetime (τ_{exc}) is the average time taken to recombine and is typically measured by time-resolved photoluminescence spectroscopy (TRPL) (described in detail in chapter 2). To measure the lifetime for nonradiative processes (e.g. trapping process and Auger process) ultrafast transient absorption spectroscopy is generally used (details in chapter 2).

1.2.3. Nanocrystals and Quantum Confinement

A NC sits between a molecule with defined discrete energy levels and a bulk crystallite sample with continuous bands. Electronic energy states of a nanoparticle directly depend on the size of that particle, known as quantum confinement.[8] Quantum confinement can be described by examining a particle in a sphere (PIS), which is nothing but an extension of the particle in a box. PIS model was first developed by Brus (Brus, 1984) to characterize the band edge absorption feature of small semiconductor crystallites.[9] In this model, a sphere of radius **a** is considered which is homogenous medium of arbitrary dielectric constant with no point charges or potential, and outside the sphere, there is infinite potential. Inside the sphere, there is a non-zero solution to the wavefunction, whereas outside the sphere the wavefunction is zero. The exciton can be compared with the hydrogen atom. The H atom has a nucleus (single proton) and single electron. This is why, the wave function of exciton has similarity with the H atom wavefunction and can be described as

$$\psi(\theta, \phi, r) = Y_l^m(\theta, \phi)\beta_{nl} \text{ ----------1.3}$$

Where $Y_l^m(\theta, \phi))$ and β_{nl} are the spherical harmonics and radial Bessel function, respectively. Only a certain number of non-zero solutions exist for this system which gives rise to some allowed quantum energy states. After solving the Schrodinger equation using parabolic approximation, the discrete energy levels for an electron confined in a sphere are obtained.

$$E_{nl} = \frac{\hbar^2 \chi_{nl}^2}{2m^* a^2} \text{ ----------1.4}$$

Here χ_{nl} represents roots of the Bessel functions and their absolute values depend on the principal and azimuthal quantum numbers, n and l respectively, and m* is the effective mass of the electron/hole. The value of l depends on n (l≤n-1, and if l=0, 1, 2 the s, p, d) for H atom. However, unlike H atom l has no

restriction for particle in sphere as the potential energy different from the H atom which results exciton energy levels sequence of 1S, 1P, 1D and then 2S.

From equation 1.4, it is evident that with decreasing size of the NCs, the energy of the electron/hole levels increases thus the energy corresponds the band edge transition is also increased (Figure 1.3.a). The Columbic interaction between the electron and hole also needs to be considered as they are confined in the same NC volume. Columbic force is inversely proportional to the radius and dielectric constant (ε). The Columbic interaction for this system can be represented by equation 1.5.

$$E_{Couloumb} = -\frac{1.786e^2}{\epsilon a} \text{ ----------1.5}$$

The total energy of the nanoparticle is a combination of the bandgap of the bulk system (E_g), coulombic energy (E_{cou}), quantization energy (Enl).

$$E_{total} = E_g + E_{nl} + E_{cou} \text{ ----------1.6}$$

Coulombic attraction is proportional to 1/a, whereas the quantization energy is proportional to $1/a^2$. The extent of quantum confinement is depends on the size of the NCs and its relative size in comparison to the radius of the Bohr exciton. The Bohr exciton radius (a_B) is the radius of the sphere in which the exciton resides, and is presented in Equation 1.7, where μ is the reduced mass of the exciton.

$$a_B = \frac{\epsilon\hbar^2}{\mu e^2} \text{ ---------- 1.7}$$

The Bohr exciton radius is characteristic of a material and in general it ranges from 2 - 50 nm.[10] For example a_B is 3.5 nm for $CsPbBr_3$ NCs, while it is 7 nm for $CsPbI_3$ NCs.[11] In the weak confinement regime (larger NCs), where $a>>a_B$, Coulombic interaction has a larger effect on the band gap as coulombic energy proportional to 1/a (equation 1.6), whereas for strong confinement regime (smaller NCs), where $a>>a_B$, the total energy mainly depends on the quantum confinement energy. In $CsPbBr_3$ NCs, a good correlation between experimental and theoretical results for the change in band gap energy in weak, strong and intermediate quantum confinement regimes has been found by Butkus et al.[12] (Figure 1.3.b). While a sphere is considered here, the degree of quantum confinement can be different across three dimensions. As a particle in a sphere is three dimensional extension of a particle in a one-dimensional box, each dimension can undergo a quantum confinement and that can influence the density of states of

the NCs. When the exciton is confined in all three directions, a quantum dot is formed. Two-dimensional confinement leads to a quantum wire, and one-dimensional to a quantum well (Figure 1.3.c).

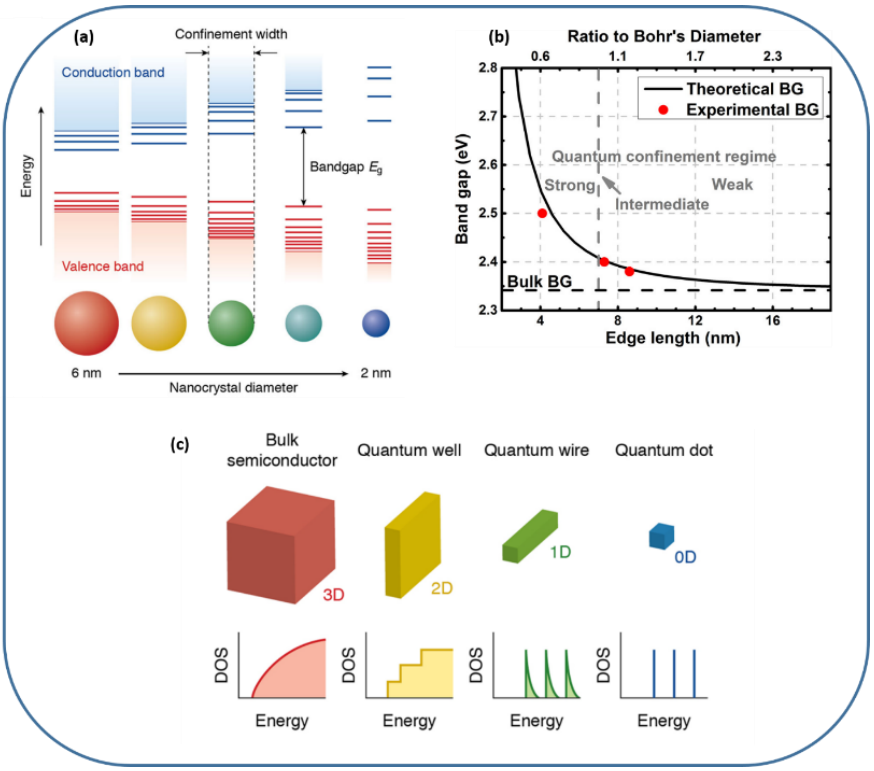

Figure 1.3. (a) Schematic representation of the effect of quantum confinement on band structure of a semiconductor nanoparticle. Panel (b) shows dependence of the bandgap on the size of the $CsPbBr_3$ NCs due to quantum confinement. (c) Density of states of a semiconductor NC of different shapes. Panels a and c are reproduced from reference 8 and panel b from reference 12.

1.3. Lead Halide Perovskites

1.3.1 Background

A perovskite is a mineral compound, $CaTiO_3$, and the name also can be used for other compounds of same structure and general formula of ABX_3. LHPs are a subset of this class of materials. They follow a structure of perovskite lattice (Figure 1.4.a), where the cation A^+ resides in the cavity formed by the eight corner-sharing $[PbX_6]^{4-}$ octahedra. The 'A' cation can be cesium (Cs^+) for all inorganic perovskites, and methyl ammonium ($CH_3NH_3^+$) (MA) or formamidinium ($CH(NH_2)^{2+}$) (FA) for hybrid perovskites and the anion X^- is either a single or mixture of halides: I^-, Br^- or Cl^-. While Pb based perovskites are

extensively studied, Sn based perovskites, which are less toxic compared to Pb, can also be used as an alternative.[13, 14] However, the major problem for the Sn halide perovskites is their longevity as these exhibit very poor phase stability.[15] However, several variants on perovskite structure also can be possible with different stoichiometry and octahedral tilting leading to formation of "perovskite-related" structures.[6, 16-18]

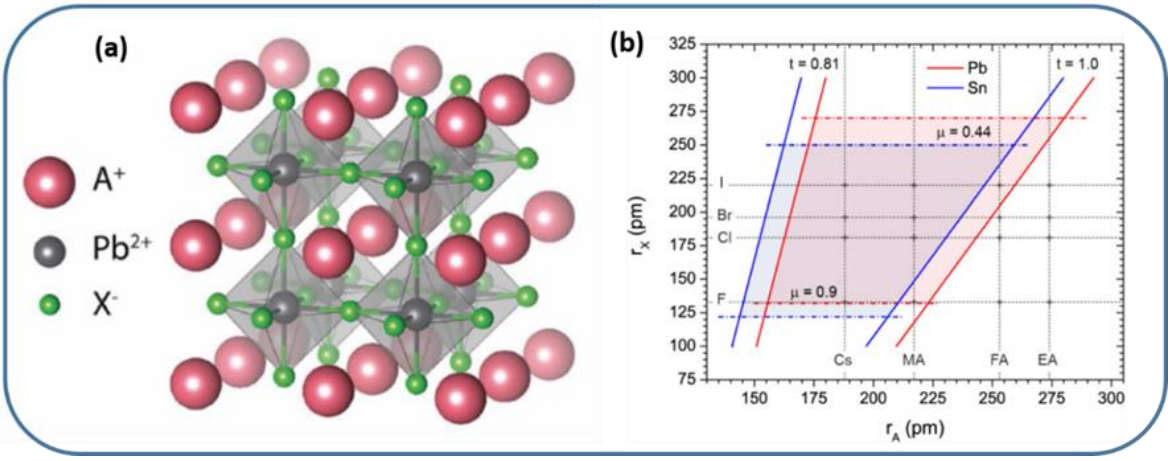

Figure 1.4. (a) Schematic representation of LHP crystal structure. Adapted from reference 18 (b) Formidability of the perovskite structure as a function of r_A and r_X. The area between the red and blue lines corresponds to Pb and Sn, respectively. Reproduced from reference 22.

One of the major advantages of the LHP family is compositional tuning. Mixing of cations, metals and anions offers tuning of the optical properties for device application.[18] While there are plenty of compositional possibilities, there are limitations too on whether the composition will be in the perovskite phase or not. This formidability of perovskite structure can be explained by Goldsmith tolerance factor (t).[19]

$$t = \frac{r_A + r_X}{\sqrt{2}(r_B + r_X)} \text{ ---------- 1.8}$$

r_A, r_B, and r_X correspond to the ionic radii of each lattice site constituent. Empirical knowledge shows that for stable cubic perovskite phase 't' usually falls into the range of 0.8−1.0.[20-22] The formidability of the BX_6 octahedra also depends on another factor that is octahedral factor (μ) expressed as:

$$\mu = \frac{r_B}{r_x} \text{.....1.9}$$

For stable perovskites, μ should be 0.442-0.895.[20] Both t and μ are used to predict the stability of perovskite structure (Figure 1.4.b).

What makes lead halide perovskites stand out, and has been the cause for the generation of a new research field, is their outstanding optoelectronic properties. To understand these features the physics and chemistry of these materials must be discussed. The rest of this chapter shall focus on the perovskite NCs; synthesis methods, surface properties, photophysical properties. As an enormous amount of research on the LHP NCs is currently underway, there are many excellent reviews for further reading.[6, 23-28]

1.3.2. Influence of A Cation and X Anion on Optical Properties of LHPs

The band structure of LHPs mainly depends on the $[PbX_6]^{4-}$ octahedral units. The VB maximum comprises Pb 6s and X 3/4/5p orbitals, while the CB minimum is constituted majorly by Pb 6p orbitals. As halides have direct influence on the bandgaps, the color of emission in LHPs is mainly determined by the halides. $CsPbI_3$ NCs emit in the red, $CsPbBr_3$ in the green, and $CsPbCl_3$ in the blue region. Mixing of halides (Br_xCl_{1-x}; Br_xI_{1-x}) allows fine-tuning of the emission peaks across the entire visible region (Figure 1.5.a-b).[11] However, mixing of I^- and Cl^- is a difficult task due to large size difference and also it does not affect band gap much.[11]

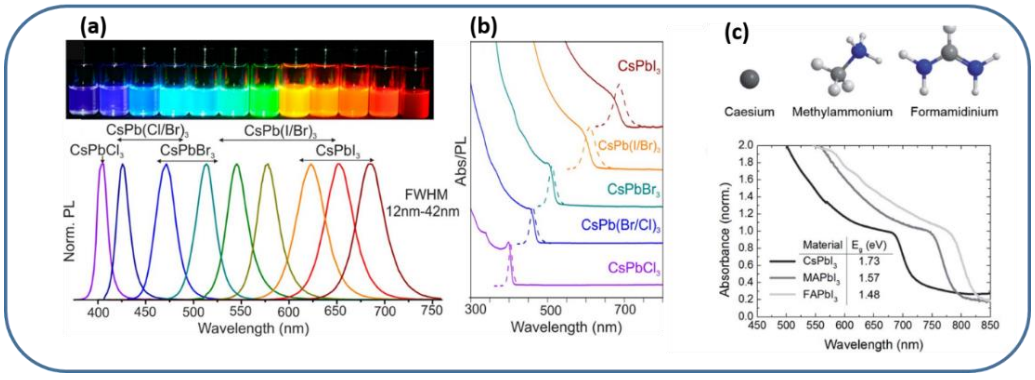

Figure 1.5. (a) Colloidal solution of $CsPbX_3$ NCs showing halide dependent emission comprising entire visible region of the spectrum and (b) tunable absorption and emission spectra of $CsPbX_3$ NCs with variation of X. Panel (a) and (b) reproduced from reference 11. (c) Effect of variation of A cation on the bandgap (reproduced from reference 29).

However, electronic structure calculation shows that A cation has no direct effect on the bandgap of the perovskites, can influence the bandgap to some extent. As mentioned earlier, A cation must be fit into the cuboctahedral cavity, a change in A cation can expand or contract the lattice which gives rise to disturbance in the $[PbX_6]^{4-}$ units. This result in variation of the Pb-X-Pb bond angles and Pb-X bond length and changes the bandgap. Hence, the indirect influence of A-cation size on the bandgap is the following. With increase in ionic radius of the A cation (FA>MA>Cs), the lattice expands, which causes decrease in bandgap energy thus a red-shift in the absorption onset (Figure 1.5.c.).[29]

1.3.3. Synthesis Methods

Semiconductor NCs are synthesized broadly by two different approaches: top-down and bottom up. In top-down method, a readymade material is fragmented into smaller pieces either chemically (e.g. chemical exfoliation[30]) or mechanically (e.g. ball milling[31]), whereas in bottom-up method, the nanoparticles are generated by stitching molecules or atoms together. These approaches are further divided depending on the synthesis phase: vapor, solid, liquid. Among these procedures, the liquid phase bottom up approach is found to be most effective for the synthesis of LHPs NCs.[26, 32]

Here we will discuss the two most studied liquid phase bottom-up synthesis method of the LHP NCs: hot injection (HI) and ligand assisted reprecipitation (LARP) methods. Schematic diagram of these methods is depicted in figure 1.6. The fundamental concept of the LARP method is known for centuries.[16, 33] In this method, first, precursors are dissolved in a solvent and then the solution is moved to a supersaturated state. This can be achieved through several ways: decreasing the temperature of the solution or evaporating the solvent or introducing another miscible solvent in which ions have poor solubility. The formation and growth of crystals can be controlled down to the nanoscale by adding ligands in this method, which is why this method is termed as LARP.

To prepare LHPs following LARP method, first PbX_2 and AX are to be dissolved in a suitable polar solvent, typically dimethylsulfoxide (DMSO) or dimethylformamide (DMF). This mixture is then thrown into a non-polar solvent (hexane or toluene) in the presence of ligands. This mixing induces supersaturation and initiates nucleation and growth of the NCs. Employing this method a wide variety of compositions of the LHP NCs comprising different halides (Cl, Br, and I) and cations (FA, MA, and Cs) can be synthesized.[34-38] This method is also useful for obtaining NCs of different shapes and sizes. This synthesis is often carried out in open atmosphere and readily scalable.[39]

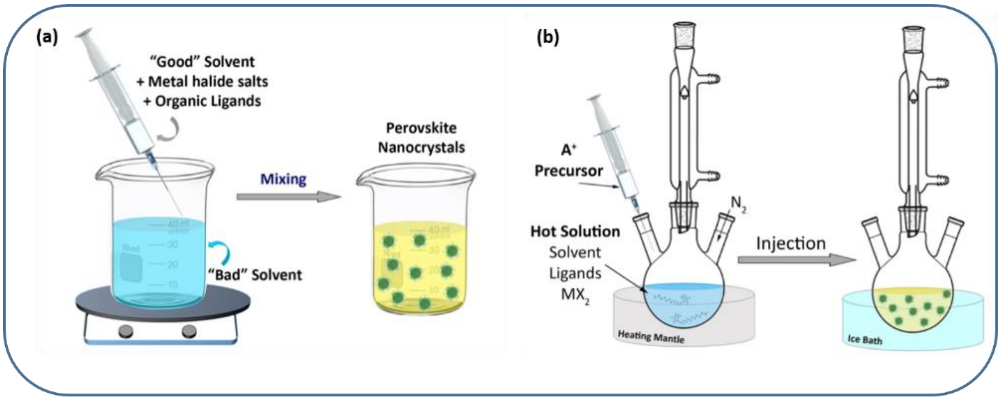

Figure 1.6. Schematics of the (a) LARP and (b) HI synthesis methods of the LHP NCs. Panel (a) and (b) reproduced from reference 16.

HI synthesis is another popular method of synthesis of the semiconductor NCs since its first success in the preparation of cadmium chalcogenides.[40] In this method, a precursor is injected into the remaining precursors and ligands dissolved in a high boiling solvent (1.6.b). The HI method is very effective in producing uniform sized NCs because it consists separate nucleation and growth steps.[41, 42] After achieving the required growth, the reaction is quenched usually through a rapid change of temperature by plunging the reaction flask into an ice bath. These reactions are most often carried out under inert atmosphere and require long degassing steps to remove all air and moisture from the reaction flask. The key parameters that control shape and size-distribution of colloidal NCs in this method are (i) the ratio of the surfactants to the precursors; (ii) the injection temperature (iii) the reaction time and (iv) the concentration of the precursors.

$CsPbX_3$ NCs were first prepared via HI method by Protesescu et al.[11]There are several other HI methods for preparation of the LHPs that are developed recently.[20, 43, 44] We have also developed a generic synthesis method for obtaining LHP NCs,[45] which is discussed in detail in chapter 3 and 4. It is important to note that in both LARP and HI methods, the nucleation and growth of the NCs are vital for achieving control in the synthesis. Each synthesis method offers size and shape control, as well as engineering of the surface of the resulting NCs. Indeed, these have been achieved successfully for LHP NCs.

1.3.4. Nucleation and Growth of the NCs

Nucleation and growth are the two most important steps in the formation of the NCs. Synthesis of any NC begins with the precursors and once the concentration of the precursors in solvent is above the nucleation

threshold, they start aggregation and form small nuclei, or seeds, which act as a basis for crystal growth. The interaction with the remaining precursors in solution and each other helps small nuclei to grow to particle. Growth of the nanoparticle mainly depends on the particle surface and diffusion of the monomer to the surface. When particles overcome a critical radius, they grow further and form NCs, and below which they dissolve again. The size distribution of the NCs dispersion depends on the time in which the nuclei form and by size focusing effects or ripening. These two processes can be explained classically using theories of thermodynamics and kinetics, and a detailed overview of the mathematics behind these processes is reported by Thanh et al.[46] It should be noted that new nuclei can be formed during the growth of NCs that often broadens size distribution of the NCs. In order to obtain monodisperse NCs, these two processes must be well separated. This was conceptually introduced by LaMer in the 1950,[47] showing that a discrete nucleation must be followed by a slow and controlled growth, Figure 1.7. This is achieved in HI method where rapid addition of precursor increases the concentration above the nucleation threshold, and a burst nucleation occurs to mitigate the super-saturation. These nuclei grow continuously with rapid depletion of the monomers and ideally no nuclei. This growth usually follows Ostwald ripening process, where the dissolution of smaller particles helps the larger particles to grow further, leading to size defocusing. [47, 48]

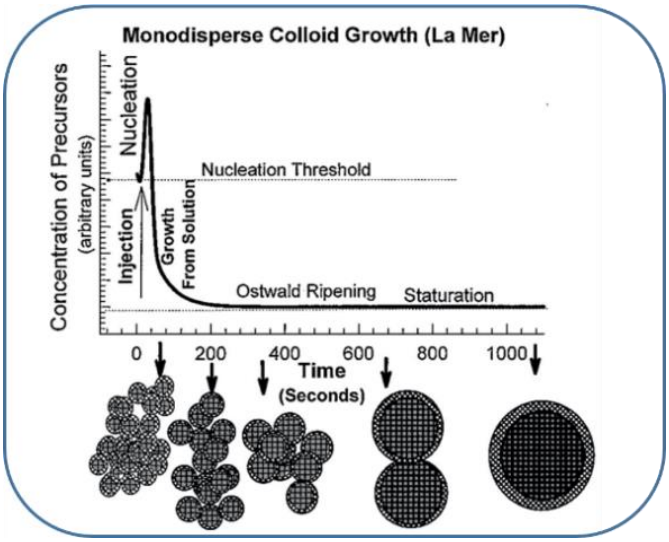

Figure 1.7. Schematic depiction of the nucleation and growth stages for the synthesis of monodisperse NCs in the framework of LaMer model (adapted from reference 48).

Since the first report of HI synthesis of the $CsPbX_3$ NCs there have been several attempts to find the nucleation and growth mechanism of the LHP NCs. Liganos et al. employed microfluidic reactors coupled with in-situ optical spectroscopy to form droplets of the NCs and determine their nucleation and growth dynamics.[49] Monitoring the *in situ* absorption and PL they showed that both processes happened in the initial 1−5 s of the reaction, indicating that these NCs have extremely fast reaction kinetics. Alternatively, transmission electron microscopy (TEM) studies have been used by Koolyk et al. to understand these processes. They reported a size focusing regime lasting for 20 seconds in $CsPbI_3$ NCs, whereas $CsPbBr_3$ NCs undergoes a defocusing from the beginning of the reaction with continuous broadening of the size distribution which lasted for 40 seconds.[50] These reports indicate that lack of unified picture for these key processes in LHP NCs. The major challenge for investigation of the nucleation and growth kinetics for this system is the incredibly fast reaction kinetics.

1.3.5. Surfaces and Ligands

The most important factor in growth, optical properties, and stability of the NCs is the ligand shell. The ligands for a NC consist of tethering head group that interacts with the NCs surface, and a long hydrocarbon tail. In principle, longer chain ligands are better for colloidal stability and interaction between the surface and anchoring head group. Ligand-NC interaction is classified using the framework of covalent bond classification in organometallic chemistry in which every bond is treated as a covalent 2-centre-2-electron interaction.[51] Ligands are classified into three types based on the number of electrons that the ligand contributes in the metal-ligand bond. These are L-, X-, and Z-type and they contribute 2, 1, and 0 electrons to the metal to form a bond, respectively. L-type ligands are usually Lewis base that typically coordinates to the surface metal ions. Z-type ligands are generally Lewis acids, which coordinate to the non-metal atoms, whereas the X-type ligands bind with either metal or nonmetal atom depending on their affinity of each. A schematic representation of the binding motif of L-, X- and Z-type ligands with a NC is presented in figure 1.8.a.[52] Uncoordinated surface atoms with dangling bonds lead to appearance of electronic levels in the bandgap which act like a defect site. Bonding between NC and ligands creates new MO with bonding and antibonding character and a good covalent interaction removes these mid-gap states by drifting the energies of bonding and antibonding orbitals outside of the bandgap, effectively cleaning up the trap states.

For perovskite NCs, the most used ligand head groups are primary ammonium (OLA^+) and carboxylate (OA^-) ions. These ligands have been known for long time since the synthesis of traditional

quantum dots. The surface of a LHP NC can be viewed as series of vacancy defects and it can be either PbX_2 terminated, or AX terminated. De Roo et al. showed that OA and OLA form dynamically bound ligand shell on the surface of $CsPbX_3$ NCs.[53] From NMR study they showed that OLA^+ ion mainly binds to the surface of the NCs as OLA^+Br^- and then interacts with other species such as OA^- or OLA in equilibrium (1.8.b). This complex equilibrium can be detrimental to the stability and optical properties of the NC if not balanced properly. If the equilibrium is moved away from the surface of the NC, colloidal stability is lost along with luminescence quenching. Indeed, $CsPbX_3$ NCs most often degrades during washing with polar solvents due to the striping of OLA^+ from the sutface.[52] However, it is difficult for the OLA^+ to detach as a discrete solvated ion in a non-polar solvent like hexane/toluene therefore, they most often pull out the surface halides and oleates to maintain charge-neutrality.[54] The binding motif between ligand and NC not only depends on the ligand tethering head, but also the surface of the NCs itself. The surface termination of a NC is very important as it regulates how ligands will interact with the surface atoms, and what is best for PLQY and stability. This was investigated for $CsPbBr_3$ NCs in detail by Bodnarchuk et al.[52] These NCs can be represented as $[CsPbX_3](PbX_2)\{AX'\}$, [55] in which core $CsPbX_3$ terminated with a PbX_2 inner shell and then a capping layer of AX′ in the outer shell (1.8.c). Here, A is the monovalent cation (Cs^+ and/or alkylammonium) and X′ is the monovalent anion (halide and/or oleate). The steric hindrance and equilibria existing between the NCs surface and solution determine the proportion of long chain ions in AX′ shell. Alternatively, outer layer PbX'_2 termination i.e. $[CsPbX_3](CsX)\{PbX'_2\}$, also can be possible and to achieve colloidal stabilization X′ must be OA^- However, formation of $\{PbX'_2\}$ outer layer is highly unfavorable because 2.5 times denser ligand packing is required in this case that leads to steric hindrance and it also breaks the octahedral coordination of the Pb^{2+}. Therefore, $[CsPbX_3](PbX_2)\{AX'\}$ is the most stable surface termination for the $CsPbX_3$ NCs. They also pointed out that halide rich surface with complete $PbBr_6$ octahedra are key to achieving minimal surface traps and high PLQY, and long chain ligands are required in the outer surface for colloidal stabilization (1.8.d). Indeed, they showed that post-synthetic treatment of the $CsPbBr_3$ NCs with lead bromide and didodecyldimethyl-ammonium bromide leads to enhancement of PLQY from 30-40% to 90-100% and colloidal stability against washing with polar solvents. It is noteworthy that, most of the studies on defect formation and surface chemistry of perovskite NCs have been focused on $CsPbBr_3$ due to its ease of synthesis and phase stability. However, there is very little research on perovskite with other A cations and other halides.[54, 56] Compositional variation will undoubtedly influence the surface of the NCs and binding nature to different ligands, call for an extensive study on surface chemistry of these NCs.

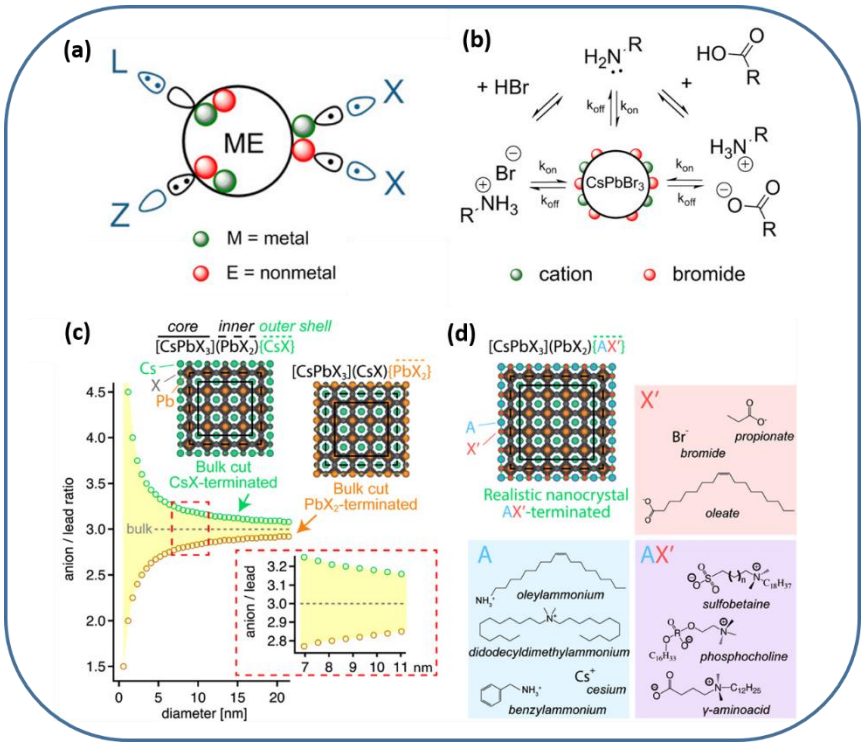

Figure 1.8. (a) Ligand binding motifs in NCs according to covalent bond classification. (b) Schematicdepiction of dynamic surface passivation by oleylammonium bromide oleylammonium oleate, oleylamine. Panel a and b reproduced from reference 53 (c) Schematic representation of possible surface termination of $CsPbX_3$ NCs. (d) Realistic surface termination for obtaining colloidal stability of $CsPbX_3$ NCs with the common cationic and anionic surface ligands. Panel c and d adapted from reference 52.

1.3.6. Defects in Perovskite NCs

Defects have always been an indigenous part of the semiconductor NCs, influencing their electronic and optical properties. However popularity of the LHP NCs in several optoelectronic applications stems from their defect-tolerant nature, photophysical properties and stability of these materials are still controlled by the defects.[24,23]These materials exhibit a high density of point defects, like vacancy defects (e.g. halide vacancies), which have low formation energy. The interstitial and antisite defects, which have much higher formation energy, are almost absent in these systems as the ions in the perovskite crystal are difficult to misplace.[57, 58] Vacancy defects are shallow in energy due to the unique bonding characteristics in LHPs; antibonding character of valance bond maxima and spin-orbit effects in the conduction band

(Figure 1.9.a). However, that the LHP NCs are not entirely free of deep traps is evident from sub-unity PLQY of these NCs.[59, 60] Nenon et al. have shown that the impact of halide vacancies on the electronic properties of LHP NCs depends on the halide constituent.[54] The deleterious effect of halide-vacancies on PLQY is much more pronounced in case of $CsPbCl_3$ NCs compared to $CsPbBr_3$ and $CsPbI_3$ NCs (Figure 1.9.b). In $CsPbCl_3$ NCs, chloride-vacancies (V_{Cl}) lead to the formation of highly localized deep trap-states,[54, 61] while the V_{Br} and V_I in $CsPbBr_3$ and $CsPbI_3$ NCs lead to formation of shallow trap-states. This explains why the $CsPbCl_3$ NCs exhibit a PLQY of 1-10%, whereas it is above 60% for both $CsPbBr_3$ and $CsPbI_3$ NCs.[62]

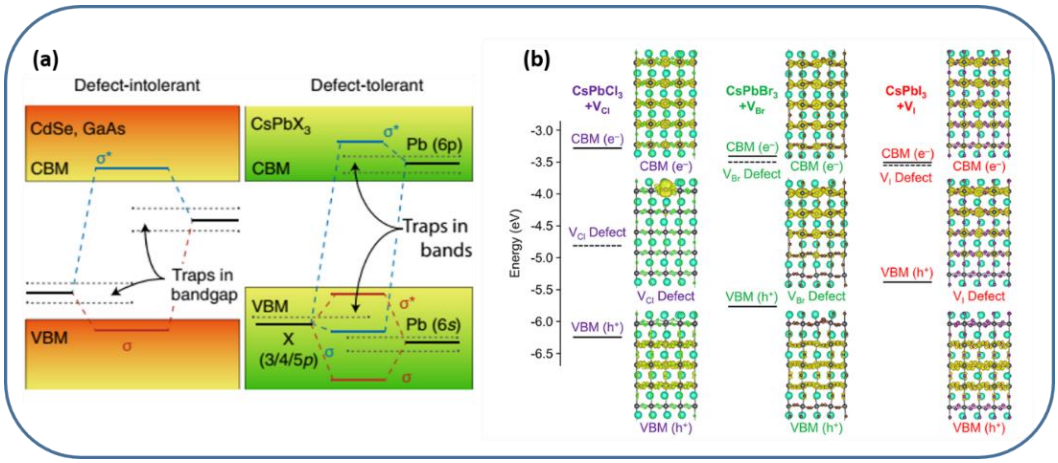

Figure 1.9. (a) Schematic representation of electronic band structure of traditional semiconductors and LHPs. In traditional semiconductors (eg CdSe) the bandgap is formed between bonding (σ) and antibonding (σ) orbitals, whereas for LHPs between two antibonding orbitals. (b) Electronic structure and charge density of LHP NCs in presence of halide vacancies. Panel (a) and (b) are reproduced from reference 23 and 54, respectively.*

Structural disorder in LHP NCs also generates defect states.[62, 63] In $CsPbI_3$ NCs, due to the large ionic radius of I^-, $[PbI_6]^{4-}$ octahedral units create large void for Cs^+. This size mismatch imparts slight tilting of the $[PbI_6]^{4-}$ octahedral units to hold the 3D structure.[21] This octahedral tilting is one of the key reasons for poor stability and low PLQY of this system. Again, in $CsPbCl_3$ NCs, halide vacancies and uncoordinated Pb atoms create short range disorder in crystal structure, which is another reason for poor optical properties of this system.[64]

1.3.7. Defect Passivation Strategy

It is evident from the above discussion that defects originate in this system due to dynamic nature of binding of OLA and OA in the surface and halide vacancies. In this regard several other ligands with a wide variety of functionalities are explored by several groups to provide better surface protection.[54, 60, 65] Krieg et al. showed that zwitterionic capping ligands such as sulfobetaines, phosphocolines, and γ-aminoacids are favorable ligands for preparation of stable and highly luminescent $CsPbBr_3$ NCs (1.10.a-b).[66] Recently, Kovalenko and coworkers showed that natural lecithin, a phospholipid, can be used as an effective surface capping agent for obtaining ultra-stable $CsPbX_3$ NCs. These ligands are free from mutual or external neutralization through acid-base equilibria, and their chelation ability is highly beneficial for stability. Alvisatos and coworkers showed that the X-type soft ligands can also effectively passivate surface defects. The soft Lewis bases (e.g.,hexylphosphonate, benzoate, etc.) strongly bind with under-coordinated lead atoms (soft Lewis acid) and yield defect-free NCs of $CsPbBr_3$ with nearly single-exponential PL decay. [54]

To tackle defects arising from halide vacancies, the three-precursor hot injection methods are found to be very effective, where separate Pb and X precursors are used instead of a common precursor, PbX_2. [45, 67, 68] In traditional synthesis, where PbX_2 is used as a source of both Pb and X, the Pb:X molar ratio of 1:2 in the reaction 1:2 is much less than the stoichiometric ratio of 1:3. In three precursor HI method, separate Pb and X precursors offers tunability of the Pb:X ratio. We have developed a three-precursor HI method using N-haloimides as an halide precursor for the preparation of high quality LHP NCs. Several groups have been used other halide precursor to obtain stable and highly luminescent NCs of these materials.[45, 55] Plenty of reports showed that post-synthetic or *in situ* treatment of metal halide salts (e.g.) can efficiently remove halide vacancies in these NCs (1.10.c).[69, 70] Structural disorder in these NCs can be removed by partial substitution (doping) of smaller sized metal cations in place of lead.[63, 64] As defect passivation is one of the main theme of this thesis work, this is discussed further as the thesis progresses.

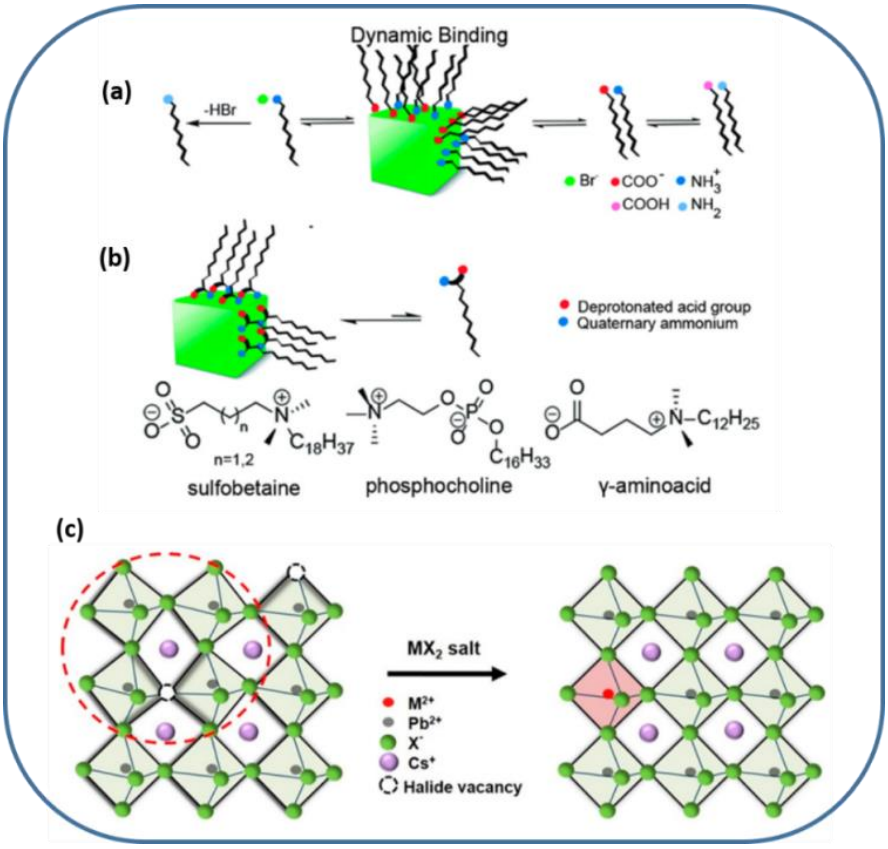

Figure 1.10. (a) The net effect of two possible sets of equilibria is facile ligand (oleic acid and oleylamine) desorption during purification. (b) Examples of capping with long-chain sulfobetaines, phosphocholines, and γ-amino acids are depicted left to right (n = 1): 3-(N,N-dimethyloctadecylammonio)-propanesulfonate, N-hexadecylphosphocholine, and N,N-dimethyldodecylammoniumbutyrate. (c) Schematic representation of elimination of halide vacancies by post-synthetic treatment of MX_2 salt. Panel (a) and (b) are adapted from reference 66 and panel c reproduced from reference 62.

1.3.8. Single Particle Photoluminescence Blinking

Under constant illumination, almost all colloidal semiconductor NCs synthesized till now exhibit intermittency in their PL, which is called PL blinking. However, at ensemble level such fluctuation of PL is smoothed out, thus undetectable. PL blinking was first reported for single NCs of CdSe with or without ZnS shell by Nirmal et al. in 1996.[71]

PL blinking is observable for a large variety of single fluorophore comprising dyes and fluorescent proteins prior to discovery in semiconductor NCs.[72] In simple fluorophores, PL blinking arises due to intersystem crossing (ISC) to long-lived triplet states leading to a single blinking rate. While for more complex single emitters, including semiconductor NCs, a wide distribution of blinking rates is generally observed, resulting occurrence of high fluorescence (ON) and low fluorescence (OFF) states lasting from hundreds of microseconds to hundreds of seconds (Figure 1.11). Apart from the OFF-state, a low-intensity gray state can be observed during the blinking process.[73] The widely distributed blinking kinetics indicates a static or dynamic distribution of the trapping and detrapping rates. Although PL blinking was initially described for very small quantum dots, afterwards it has been studied for many morphologies including nanocubes, nanowires, nanoplates and nanorods.[74, 75]

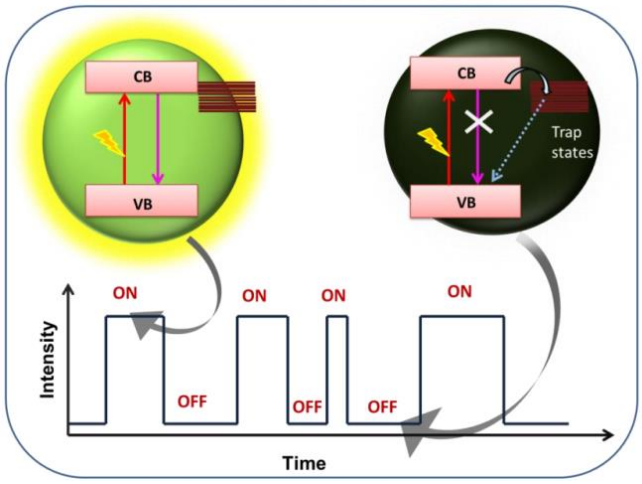

Figure 1.11. Schematic illustration of blinking of a semiconductor NC due to competing radiative and nonradiative recombination through trapping of a charge carrier.

While it is mostly accepted that PL blinking occurs due to trapping of the charge carries, details of the underlying mechanism are still highly debated. Several models have been set forth to explain PL blinking mechanism, and among them, a charging model[76, 77] and multiple recombination center (MRC) model[78] are the most featured ones. When one of the charge carriers is trapped for a longer duration, the NCs become charged. The absorption of another photon by a charged NC when produces an exciton, the system becomes a trion. The trion can recombine nonradiative way by Auger recombination or/and radiative way at a much faster rate (twice the neutral exciton recombination rate). PL blinking arising

from trion-mediated recombination is known as Auger or A-type blinking (1.12.a). Duration of the off-states in this case is usually depends on time spent by the carriers in the trap states.

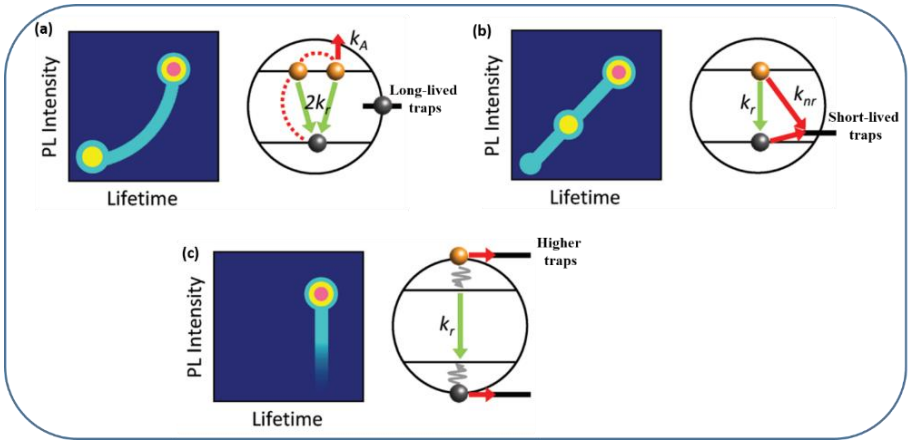

Figure 1.12. Schematic depiction of different types of blinking mechanism. Left side of each panel represents fluorescence lifetime intensity distribution which is represented by false color coding and the corresponding recombination processes of the photoexcited charge carriers in the right side. Green arrows indicate the radiative processes, whereas the red arrows indicate nonradiative processes (adapted from reference 86).

Trapping of charge carrier in a short-lived trap states can facilitate its instant relaxation by a nonradiative pathway. Random activation and deactivation of these trap states results in a constantly changing nonradiative rate constant. This time dependent fluctuation of the nonradiative rate constant leads to PL blinking, which is termed as band-edge carrier (BC)-blinking when trapping of the charge carriers takes place from the band-edge states (1.12.b).[79] Blinking can also be caused by trapping of the hot carriers (HC-blinking).[80] Trapping of the hot carriers allows their rapid relaxation through a nonradiative recombination route, and one observes a large drop of PL intensity without any noticeable change in lifetime (1.12.c). As both BC- and HC-blinking arise from the activation and deactivation of the trap states, these two types of blinking are often referred to as B-type blinking.

Estimation of ratio of radiative rates (k_r) of the different PL intensity states helps to find out underlying blinking mechanism. The following relationship is used to estimate the radiative contribution, τ_r, to the fluorescence lifetime (τ).

$$I \propto PLQY = \frac{k_r}{k_r + k_{nr}} = \tau k_r = \frac{\tau}{\tau_r} \text{.....1.10}$$

Here I and k_{nr} represent the PL intensity and nonradiative recombination rate, respectively. For trion blinking ratio of kr between two different intensity state is ~2.0 whereas it is 1.0 for BC blinking. Fluorescence lifetime intensity distribution (FLID) measurement is also found to be an effective method for the investigation of blinking mechanism. The FLID trajectory of the Auger blinking is typically a curved line (Figure1.12) whereas a linear FLID pattern is observable for BC-blinking. In HC-blinking, fluorescence lifetime is almost constant irrespective of the large change in PL intensity. The LHP NCs most often show multistate blinking events without clear separation of the ON and OFF states[2, 81-83] due to coexistence of multiple PL blinking mechanism.[82, 84-86]

The above discussion shows that blinking is linked to the nonradiative recombination of the charge carriers through short-lived trap states (BC blinking and HC blinking) and charging of the NCs due to the trapping of charge carrier in long lived trap states (Auger blinking). Hence, by eliminating these traps states one can achieve non-blinking NCs. In the case of traditional QDs, blinking can be eliminated by growing very thick shell outside the NCs forming a trap free core-shell structure. [87, 88]As far as the LHP NCs are concerned, till now this is not an effective approach for elimination of blinking. Recently, blinking in $CsPbBr_3$ NCs is suppressed by modifying the surface using tetrafluoroborate salts.[84] We have also shown an effective approach for suppression of blinking in $CsPbI_3$ NCs and that will be discussed in chapter 5.

1.4 Outline of the thesis

This thesis contributes to the design high quality perovskite NCs and understanding their charge carrier recombination dynamics. Among the emerging semiconductors, lead halide perovskites have found ubiquitous use in photovoltaics and optoelectronics because of their high photoluminescence quantum yield (PLQY), narrow and tunable PL covering a broad visible spectral range (400–800 nm).[6, 11] Even though high resistivity of these substances toward defect formation endows compelling optical properties and their manifestation in device applications, these are not free from defects, and these NCs often exhibit subunity PLQY and low stability in ambient atmosphere.[54, 62] In this study, we have ventured to enumerate the factors responsible for these detrimental properties of the NCs and designed new methods to obtain NCs with high PL and stability. Efficiency of an optoelectronic device made of these materials depends on the fate of the charge carriers. Hence, understanding of the nature of trap states and dynamics

of different competitive radiative and nonradiative charge carrier recombination processes is essential for proper utilization of these materials.

This thesis consists of seven chapters and among them **Chapter 3-6** are actual working chapters. In Chapter 1, 2 and 7 introduction, experimental methods and conclusion of this study are outlined, respectively.

Chapter 3: N-Bromosuccinimide as Bromide Precursor for Direct Synthesis of Stable and Highly Luminescent Green-Emitting Perovskite Nanocrystals[45]

Stable green-emitting perovskite NCs, exhibiting high PLQY, narrow bandwidth and adjustable PL in the 510-535 nm region are coveted materials for optoelectronic applications. A generic method of obtaining both hybrid and all-inorganic bromide based perovskite NCs with the desired characteristics is, however, lacking. In conventional two-precursor hot-injection method, $APbBr_3$ NCs were synthesized by using $PbBr_2$ as the precursor for both lead and bromine, which gave a Br:Pb molar precursor ratio of only 2 in the reaction system (less than the required value of 3). It has been also found that $PbBr_2$ is not a quite effective precursor for obtaining the organometal LHPs ($FAPbBr_3$ and $MAPbBr_3$). For example, $FAPbBr_3$ NCs obtained by this method exhibit a broader size distribution and poor optical properties. Even for $CsPbBr_3$ NCs, the PLQY obtained by this method is typically 60−80% or even lower due to nonradiative deactivation induced by the bromide vacancies. In order to overcome these issues we have introduced a three-precursor hot-injection method employing N-bromosuccinimide (NBS), a widely used source of bromine in organic synthesis, as the bromide precursor. Reaction of NBS with organic acids generates HBr, which reacts with oleylamine to form oleylammonium bromide; the latter serves as the active bromide source in the synthesis. The method, which is found to be highly reproducible, yields brightly luminescent (PLQY ~90-99%) extremely uniform sized cubes of nanodimension for all three systems. These NCs exhibit exceptional phase stability and photostability in ambient atmosphere. These NCs also show resistant against degradation by polar solvents. The exceptional characteristics of these NCs, which are attributed to the formation of oleylammonium lead bromide-terminated surfaces, in which A^+ are partially replaced by oleylammonium ions.

Chapter 4: Effect of Lead:Halide Precursor Ratio on the Photoluminescence and Carrier Dynamics of Violet- and Blue-Emitting Lead Halide Perovskite Nanocrystals[89]

Highly luminescent violet- and blue-emitting $CsPbCl_3$ and $CsPb(Cl/Br)_3$ NCs are promising materials for a number of optoelectronic applications like LEDs, and other display technologies. However, low PLQY of these large bangap NCs is an obstacle to the development of blue-and white-emitting LEDs. In this work, we show that these NCs with high PLQY can be obtained directly employing an appropriate halide precursor and by optimizing the Pb:X precursor ratio. Specifically, employing N-halophthalimides and N-halosuccinimides as halide precursorss and by varying the Pb:X precursor ratio, we have obtained stable and highly luminescent (PLQY 80 - 99%) perovskite NCs emitting in the blue-violet region extending to green by direct synthesis. Time-resolved PL and ultrafast pump-probe studies of these systems reveal the effect of Pb:X precursor ratio on the carrier recombination processes. Rapid carrier trapping is found to be the dominant process that impairs the PLQY of the NCs obtained using a stoichiometric (1:3) Pb:X precursor ratio. This trapping of carriers is effectively alleviated by using a higher Pb:X precursor ratio during the preparation of the NCs. The results brighten potential utility of these high-quality perovskite NCs emitting in the blue-violet region in optical applications.

Chapter 5: Phase-Stable and Highly Luminescent $CsPbI_3$ Perovskite Nanocrystals with Suppressed Photoluminescence Blinking[82]

Despite their low bandgap, the usage of the $CsPbI_3$ NCs in solar photovoltaic and optoelectronic applications is very limited due to their phase instability and single-particle PL intermittency. Herein we show that phase-pure, mono-dispersed, stable, highly luminescent $CsPbI_3$ NCs can be obtained by tweaking conventional hot-injection method using NH_4I as an additional precursor. Single-particle studies on these NCs show significant suppression of PL blinking and 60% of all NCs investigated are found to exhibit only high intensity ON-states (bright) with narrow distribution of intensity levels. A much wider distribution of intensity levels with significant contribution of low intensity OFF-states (dim) are observed for the remaining 40% NCs due to band-edge recombination through trap states and Auger recombination. Excellent characteristics of these $CsPbI_3$ NCs are shown to be the outcome of NH_4^+ replacing some surface Cs^+ of an iodide-rich surface of the NCs. These phase-stable, highly luminescent $CsPbI_3$ NCs with significantly suppressed PL blinking can be useful single photon emitter and promising materials for optoelectronic and solar photovoltaic applications.

Chapter 6: Photoluminescence Blinking of Quantum Confined $CsPbBr_3$ Perovskite Nanocrystals: Influence of Size[90]

Quantum confined $CsPbBr_3$ NCs with adjustable PL in the range of 470 - 500 nm are particularly desirable for applications in LEDs and many quantum technologies. Exploration of full potential of these perovskite NCs requires an understanding of the random fluctuation of their PL at the single particle level, commonly termed as blinking. In this work, we study the PL blinking of quantum confined single NCs of $CsPbBr_3$ of three different sizes between 3.80 and 5.90 nm in immobilized and fluid conditions to understand the recombination pathways and dynamics of the photogenerated charge carriers. In the immobilized state, the PL intensity trajectories and PL lifetime-intensity distributions of these single NCs reveal the contributions of both Auger recombination and trapping of hot carriers to the PL fluctuation. The results suggest a higher carrier trapping rate constant for smaller NCs. The fluorescence correlation spectroscopy measurements on freely diffusing NCs show a higher off-state fraction and lower per-particle brightness of the smaller NCs. It is concluded that a larger trap depth and higher probability density of the carriers at the surface in smaller NCs make the trapping process more feasible and detrapping more difficult. The results provide first information on the effect of size on PL blinking of the quantum confined $CsPbBr_3$ NCs, and this knowledge is expected to be useful in better designing photoluminescent samples of this class for optoelectronic applications.

Bibliography

1. Kovalenko, M. V.; Manna, L.; Cabot, A.; Hens, Z.; Talapin, D. V.; Kagan, C. R.; Klimov, V. I.; Rogach, A. L.; Reiss, P.; Milliron, D. J.; Guyot-Sionnnest, P.; Konstantatos, G.; Parak, W. J.; Hyeon, T.; Korgel, B. A.; Murray, C. B.; Heiss, W., Prospects of Nanoscience with Nanocrystals. *ACS Nano* **2015,** 9, 1012-1057.
2. Park, Y.-S.; Guo, S.; Makarov, N. S.; Klimov, V. I., Room Temperature Single-Photon Emission from Individual Perovskite Quantum Dots. *ACS Nano* **2015,** 9, 10386–10393.
3. Lee, M. M.; Teuscher, J.; Miyasaka, T.; Murakami, T. N.; Snaith, H. J., Efficient Hybrid Solar Cells Based on Meso-Superstructured Organometal Halide Perovskites. *Science* **2012,** 338, 643-647.
4. National Renewable Energy Laboratory NREL. https://www.nrel.gov/pv/cell-efficiency.html (accessed on December 01, 2022).
5. Kamat, P. V., ACS Journals Celebrate 10 Years of Perovskite Photovoltaics. *ACS Energy Lett.* **2019,** 4, 1055-1056.
6. Dey, A.; Ye, J.; De, A.; Debroye, E.; Ha, S. K.; Bladt, E.; Kshirsagar, A. S.; Wang, Z.; Yin, J.; Wang, Y., State of the Art and Prospects for Halide Perovskite Nanocrystals. *ACS Nano* **2021,** 15, 10775–10981.
7. Herz, L. M., Charge-Carrier Dynamics in Organic-Inorganic Metal Halide Perovskites. *Annual Review of Physical Chemistry* **2016,** 67, 65-89.
8. Rabouw, F. T.; Donega, C. d. M., Excited-State Dynamics in Colloidal Semiconductor Nanocrystals. *Top Curr Chem* **2016,** 374, 58.
9. Brus, L. E., Electron–electron and electron-hole interactions in small semiconductor crystallites: The size dependence of the lowest excited electronic state. *J. Chem. Phys.* **1984,** 80, 4403.

10. Alivisatos, A. P., Lead halide perovskites are a subset of this class of materials and adhere to the perovskite structure. *J. Phys. Chem.* **1996,** 100, 13226–13239.
11. Protesescu, L.; Yakunin, S.; Bodnarchuk, M. I.; Krieg, F.; Caputo, R.; Hendon, C. H.; Yang, R. X.; Walsh, A.; Kovalenko, M. V., Nanocrystals of Cesium Lead Halide Perovskites ($CsPbX_3$, X = Cl, Br, and I): Novel Optoelectronic Materials Showing Bright Emission with Wide Color Gamut. *Nano Lett.* **2015,** 15, 3692–3696.
12. Butkus, J.; Vashishtha, P.; Chen, K.; Gallaher, J. K.; Prasad, S. K. K.; Metin, D. Z.; Laufersky, G.; Gaston, N.; Halpert, J. E.; Hodgkiss, J. M., The Evolution of Quantum Confinement in $CsPbBr_3$ Perovskite Nanocrystals. *Chem. Mater.* **2017,** 29, 3644−3652.
13. Yang, W.-F.; Igbari, F.; Lou, Y.-H.; Wang, Z.-K.; Liao, L.-S., Tin Halide Perovskites: Progress and Challenges. *Adv. Energy Mater.* **2020,** 10, 1902584.
14. Jellicoe, T. C.; Richter, J. M.; Glass, H. F. J.; Tabachnyk, M.; Brady, R.; Dutton, S. E.; Rao, A.; Friend, R. H.; Credgington, D.; Greenham, N. C.; Böhm, M. L., Synthesis and Optical Properties of Lead-Free Cesium Tin Halide Perovskite Nanocrystals. *J. Am. Chem. Soc.* **2016,** 138, 2941−2944.
15. Ricciarelli, D.; Meggiolaro, D.; Ambrosio, F.; Angelis, F. D., Instability of Tin Iodide Perovskites: Bulk p-Doping versus Surface Tin Oxidation. *ACS Energy Lett.* **2020,** 5, 2787–2795.
16. Shamsi, J.; Urban, A. S.; Imran, M.; Trizio, L. D.; Manna, L., Metal Halide Perovskite Nanocrystals: Synthesis, Post-Synthesis Modifications, and Their Optical Properties. *Chem. Rev.* **2019,** 119, 3296–3348.
17. Khalfin, S.; Bekenstein, Y., Advances in lead-free double perovskite nanocrystals, engineering band-gaps and enhancing stability through composition tunability. *Nanoscale* **2019,** 11, 8665–8679.
18. Prato, M.; Stasio, F. D., Lead Halide Perovskite Nanocrystals - A New Promise for Light Emitting Devices. *LED Professional* **2017**, 46-53.
19. Goldschmidt, V. M. D., Gesetze der Krystallochemie. *Naturwissenschaften* **1926,** 14, 477−485.
20. Protesescu, L.; Yakunin, S.; Kumar, S.; Bar, J.; Bertolotti, F.; Masciocchi, N.; Guagliardi, A.; Grotevent, M.; Shorubalko, I.; Bodnarchuk, M. I.; Shih, C.-J.; Kovalenko, M. V., Dismantling the "Red Wall" of Colloidal Perovskites: Highly Luminescent Formamidinium and Formamidinium−Cesium Lead Iodide Nanocrystals. *ACS Nano* **2017**, 3119−3134.
21. Dutta, A.; Pradhan, N., Phase-Stable Red-Emitting $CsPbI_3$ Nanocrystals: Successes and Challenges. *ACS Energy Lett.* **2019,** 4, 709–719.
22. Manser, J. S.; Christians, J. A.; Kamat, P. V., Intriguing Optoelectronic Properties of Metal Halide Perovskites. *Chem. Rev.* **2016,** 116, 12956–13008.
23. Akkerman, Q. A.; Rainò, G.; Kovalenko, M. V.; Manna, L., Genesis, challenges and opportunities for colloidal lead halide perovskite nanocrystals. *Nat. Mater.* **2018,** 17, 394–405.
24. Huang, H.; Bodnarchuk, M. I.; Kershaw, S. V.; Kovalenko, M. V.; Rogach, A. L., Lead Halide Perovskite Nanocrystals in the Research Spotlight: Stability and Defect Tolerance. *ACS Energy Lett.* **2017,** 2, 2071–2083.
25. Polavarapu, L.; Nickel, B.; Feldmann, J.; Urban, A. S., Advances in Quantum-Confined Perovskite Nanocrystals for Optoelectronics. *Adv. Energy Mater.* **2017,** 7, 1700267.
26. Wang, N.; Liu, W.; Zhang, Q., Perovskite-Based Nanocrystals: Synthesis and Applications beyond Solar Cells. *Small Methods* **2018,** 2, 1700380.
27. Mondal, N.; De, A.; Das, S.; Paul, S.; Samanta, A., Ultrafast carrier dynamics of metal halide perovskite nanocrystals and perovskite-composites. *Nanoscale* **2019,** 11, 9796–9818.
28. Yang, D.; Li, X.; Zeng, H., Surface Chemistry of All Inorganic Halide Perovskite Nanocrystals: Passivation Mechanism and Stability. *Adv. Mater. Interfaces* **2018,** 5, 1701662.

29. Eperon, G. E.; Stranks, S. D.; Menelaou, C.; Johnston, M. B.; Herza, L. M.; Snaith, H. J., Formamidinium lead trihalide: a broadly tunable perovskite for efficient planar heterojunction solar cells. *Energy Environ. Sci.* **2014,** 7, 982-988.
30. Hintermayr, V. A.; Richter, A. F.; Ehrat, F.; Döblinger, M.; Vanderlinden, W.; Sichert, J. A.; Tong, Y.; Polavarapu, L.; Feldmann, J.; Urban, A. S., Tuning the Optical Properties of Perovskite Nanoplatelets through Composition and Thickness by Ligand-Assisted Exfoliation. *Adv. Mater.* **2016,** 28, 9478– 9485.
31. Protesescu, L.; Yakunin, S.; Nazarenko, O.; Dirin, D. N.; Kovalenko, M. V., Low-Cost Synthesis of Highly Luminescent Colloidal Lead Halide Perovskite Nanocrystals by Wet Ball Milling. *ACS Appl. Nano Mater.* **2018,** 1, 1300– 1308,.
32. de Weerd, C.; Gregorkiewicz, T.; Gomez, L., All-Inorganic Perovskite Nanocrystals: Microscopy Insights in Structure and Optical Properties. . *Adv. Opt. Mater* **2018,** 6, 1800289.
33. Zhao, Y. S.; Fu, H.; Peng, A.; Ma, Y.; Xiao, D.; Yao, J., Low-Dimensional Nanomaterials Based on Small Organic Molecules: Preparation and Optoelectronic Properties. 6. *Adv. Mater.* **2008**, 2859– 287.
34. Zhao, Y.; Xu, X.; You, X., Colloidal Organometal Halide Perovskite ($MAPbBr_xI_{3-x}$, $0 \le x \le 3$) Quantum Dots: Controllable Synthesis and Tunable Photoluminescence. *Sci. Rep.* **2016,** 6, 35931.
35. Levchuk, I.; Herre, P.; Brandl, M.; Osvet, A.; Hock, R.; Peukert, W.; Schweizer, P.; Spiecker, E.; Batentschuka, M.; Brabeca, C. J., Ligand-assisted thickness tailoring of highly luminescent colloidal $CH_3NH_3PbX_3$ (X = Br and I) perovskite nanoplatelets. *Chem. Commun.* **2017,** 53, 244-247.
36. Sun, S.; Yuan, D.; Xu, Y.; Wang, A.; Deng, Z., Ligand-Mediated Synthesis of Shape-Controlled Cesium Lead Halide Perovskite Nanocrystals via Reprecipitation Process at Room Temperatur. *ACS Nano* **2016,** 10, 3648–3657.
37. Levchuk, I.; Osvet, A.; Tang, X.; Brandl, M.; Perea, J. D.; Hoegl, F.; Matt, G. J.; Hock, R.; Batentschuk, M.; Brabec, C. J., Brightly Luminescent and Color-Tunable Formamidinium Lead Halide Perovskite $FAPbX_3$ (X = Cl, Br, I) Colloidal Nanocrystals. *Nano Lett.* **2017,** 17, 2765−2770.
38. Minh, D. N.; Kim, J.; Hyon, J.; Sim, J. H.; Sowlih, H. H.; Seo, C.; Nam, J.; Eom, S.; Suk, S.; Lee, S.; Kim, E.; Kang, Y., Room-Temperature Synthesis of Widely Tunable Formamidinium Lead Halide Perovskite Nanocrystals. *Chem. Mater.* **2017,** 29, 5713−5719.
39. Seth, S.; Samanta, A., A Facile Methodology for Engineering the Morphology of $CsPbX_3$ Perovskite Nanocrystals under Ambient Condition. *Sci. Rep.* **2016,** 6, 37693.
40. Murray, C. B.; Norris, D. J.; Bawendi, M. G., Synthesis and characterization of nearly monodisperse CdE (E = sulfur, selenium, tellurium) semiconductor nanocrystallites. *J. Am. Chem. Soc.* **1993,** 115, 8706–8715.
41. Chang, J.; Waclawik, E. R., Colloidal semiconductor nanocrystals: controlled synthesis and surface chemistry in organic media. *RSC Adv.* **2014,** 4, 23505-23527.
42. Yin, Y.; Alivisatos, A. P., Colloidal nanocrystal synthesis and the organic–inorganic interface. *Nature* **2005,** 437, 664–670.
43. Protesescu, L.; Yakunin, S.; Bodnarchuk, M. I.; Bertolotti, F.; Masciocchi, N.; Guagliardi, A.; Kovalenko, M. V., Monodisperse Formamidinium Lead Bromide Nanocrystals with Bright and Stable Green Photoluminescence. *J. Am. Chem. Soc.* **2016,** 138, 14202–14205.
44. Vybornyi, O.; Yakunin, S.; Kovalenko, M. V., Polar-solvent-free colloidal synthesis of highly luminescent alkylammonium lead halide perovskite nanocrystals. *Nanoscale* **2016,** 8, 6278-6283.
45. Paul, S.; Samanta, A., N-Bromosuccinimide as Bromide Precursor for Direct Synthesis of Stable and Highly Luminescent Green-Emitting Perovskite Nanocrystals. *ACS Energy Lett.* **2020,** 5, 64–69.

46. Thanh, N. T. K.; Maclean, N.; Mahiddine, S., Mechanisms of Nucleation and Growth of Nanoparticles in Solution. *Chem. Rev.* **2014,** 114, 7610–7630.
47. LaMer, V. K.; Dinegar, R. H., Theory, Production and Mechanism of Formation of Monodispersed Hydrosols. *J. Am. Chem. Soc.* **1950,** 72, 4847–4854

48. Murray, C. B.; Kagan, C. R.; Bawendi, M. G., Synthesis and Characterization of Monodisperse Nanocrystals and Close-Packed Nanocrystal Assemblies. *Annu. Rev. Mater. Sci.* **2000,** 330, 545–610.
49. Lignos, I.; Stavrakis, S.; Nedelcu, G.; Protesescu, L.; deMello, A. J.; Kovalenko, M. V., Synthesis of Cesium Lead Halide Perovskite Nanocrystals in a Droplet-Based Microfluidic Platform: Fast Parametric Space Mapping. *Nano Lett.* **2016,** 16, 1869–1877.
50. Koolyk, M.; Amgar, D.; Aharona, S.; Etgar, L., Kinetics of cesium lead halide perovskite nanoparticle growth; focusing and de-focusing of size distribution *Nanoscale* **2016,** 8, 6403-6409.
51. Boles, M. A.; Ling, D.; Hyeon, T.; Talapin, D. V., The surface science of nanocrystals. *Nat. Mater.* **2016,** 15, 141–153.
52. Bodnarchuk, M. I.; Boehme, S. C.; Brinck, S. t.; Bernasconi, C.; Shynkarenko, Y.; Krieg, F.; Widmer, R.; Aeschlimann, B.; Günther, D.; Kovalenko, M. V.; Infante, I., Rationalizing and Controlling the Surface Structure and Electronic Passivation of Cesium Lead Halide Nanocrystals. *ACS Energy Lett.* **2019,** 4, 63-74.
53. Roo, J. D.; Ibáñez, M.; Geiregat, P.; Nedelcu, G.; Walravens, W.; Maes, J.; Martins, J. C.; Driessche, I. V.; Kovalenko, M. V.; Hens, Z., Highly Dynamic Ligand Binding and Light Absorption Coefficient of Cesium Lead Bromide Perovskite Nanocrystals. *ACS Nano* **2016,** 10, 2071–2081.
54. Nenon, D. P.; Pressler, K.; Kang, J.; Koscher, B. A.; Olshansky, J. H.; Osowiecki, W. T.; Koc, M. A.; Wang, L.-W.; Alivisatos, A. P., Design Principles for Trap-Free $CsPbX_3$ Nanocrystals: Enumerating and Eliminating Surface Halide Vacancies with Softer Lewis Bases. *J. Am. Chem. Soc.* **2018,** 140, 17760–17772.
55. Pradhan, N., Alkylammonium Halides for Facet Reconstruction and Shape Modulation in Lead Halide Perovskite Nanocrystals. *Acc. Chem. Res.* **2021,** 54, 1200-1208.
56. Pan, J.; Shang, Y.; Yin, J.; Bastiani, M. D.; Peng, W.; Dursun, I.; Sinatra, L.; El-Zohry, A. M.; Hedhili, M. N.; Emwas, A.-H.; Mohammed, O. F.; Ning, Z.; Bakr, O. M., Bidentate Ligand-Passivated $CsPbI_3$ Perovskite Nanocrystals for Stable Near-Unity Photoluminescence Quantum Yield and Efficient Red Light-Emitting Diodes. *J. Am. Chem. Soc.* **2018,** 140, 562–565.
57. Brandt, R. E.; Stevanovic, V.; Ginley, D. S.; Buonassisi, T., Identifying defect-tolerant semiconductors with high minority-carrier lifetimes: beyond hybrid lead halide perovskites. *MRS Commun.* **2015,** 5, 265–275.
58. Kang, J.; Wang, L.-W., High defect tolerance in lead halide perovskite $CsPbBr_3$. *J. Phys. Chem. Lett.* **2017,** 8, 489–493
59. Koscher, B. A.; Swabeck, J. K.; Bronstein, N. D.; Alivisatos, A. P., Essentially Trap-Free $CsPbBr_3$ Colloidal Nanocrystals by Postsynthetic Thiocyanate Surface Treatment. *J. Am. Chem. Soc.* **2017,** 139, 6566–6569.
60. Ahmed, T.; Seth, S.; Samanta, A., Boosting the Photoluminescence of $CsPbX_3$ (X = Cl, Br, I) Perovskite Nanocrystals Covering a Wide Wavelength Range by Postsynthetic Treatment with Tetrafluoroborate Salts. *Chem. Mater.* **2018,** 30, 3633–3637.
61. Lai, R.; Wua, K., Picosecond electron trapping limits the emissivity of $CsPbCl_3$ perovskite nanocrystals. *J. Chem. Phys.* **2019,** 151, 194701.

62. Seth, S.; Ahmed, T.; De, A.; Samanta, A., Tackling the Defects, Stability, and Photoluminescence of $CsPbX_3$ Perovskite Nanocrystals. *ACS Energy Lett.* **2019,** 4, 1610–1618.
63. Swarnkar, A.; Mir, W. J.; Nag, A., Can B-Site Doping or Alloying Improve Thermal- and Phase-Stability of All-Inorganic $CsPbX_3$ (X = Cl, Br, I) Perovskites? *ACS Energy Lett.* **2018,** 3, 286–289.
64. Yong, Z.-J.; Guo, S.-Q.; Ma, J.-P.; Zhang, J.-Y.; Li, Z.-Y.; Chen, Y.-M.; Zhang, B.-B.; Zhou, Y.; Shu, J.; Gu, J.-L.; Zheng, L.-R.; Bakr, O. M.; Sun, H.-T., Doping-Enhanced Short-Range Order of Perovskite Nanocrystals for Near-Unity Violet Luminescence Quantum Yield. *J. Am. Chem. Soc.* **2018,** 140, 9942–9951.
65. Shynkarenko, Y.; Bodnarchuk, M. I.; Bernasconi, C.; Berezovska, Y.; Verteletskyi, V.; Ochsenbein, S. T.; Kovalenko, M. V., Direct Synthesis of Quaternary Alkylammonium-Capped Perovskite Nanocrystals for Efficient Blue and Green Light-Emitting Diodes. *ACS Energy Lett.* **2019,** 4, 2703–2711.
66. Krieg, F.; Ochsenbein, S. T.; Yakunin, S.; Brinck, S. t.; Aellen, P.; Süess, A.; Clerc, B.; Guggisberg, D.; Nazarenko, O.; Shynkarenko, Y.; Kumar, S.; Shih, C.-J.; Infante, I.; Kovalenko, M. V., Colloidal $CsPbX_3$ (X = Cl, Br, I) Nanocrystals 2.0: Zwitterionic Capping Ligands for Improved Durability and Stability. *ACS Energy Lett.* **2018,** 3, 641–646.
67. Wei, S.; Yang, Y.; Kang, X.; Wang, L.; Huang, L.; Pan, D., Room-temperature and gram-scale synthesis of $CsPbX_3$ (X = Cl, Br, I) perovskite nanocrystals with 50–85% photoluminescence quantum yields. *Chem. Commun.* **2016,** 52, 7265-7268.
68. Imran, M.; Caligiuri, V.; Wang, M.; Goldoni, L.; Prato, M.; Krahne, R.; Trizio, L. D.; Manna, L., Benzoyl Halides as Alternative Precursors for the Colloidal Synthesis of Lead-Based Halide Perovskite Nanocrystals. *J. Am. Chem. Soc.* **2018,** 140, 2656–2664.
69. Li, F.; Liu, Y.; Wang, H.; Zhan, Q.; Liu, Q.; Xia, Z., Postsynthetic Surface Trap Removal of $CsPbX_3$ (X = Cl, Br, or I) Quantum Dots via a ZnX_2/Hexane Solution toward an Enhanced Luminescence Quantum Yield. *Chem. Mater.* **2018,** 30, 8546–8554.
70. De, A.; Das, S.; Mondal, N.; Samanta, A., Highly Luminescent Violet- and Blue-Emitting Stable Perovskite Nanocrystals. *ACS Materials Lett.* **2019,** 1.
71. Nirmal, M.; Dabbousi, B. O.; Bawendi, M. G.; Macklin, J. J.; Trautman, J. K.; Harris, T. D.; Brus, L. E., Fluorescence intermittency in single cadmium selenide nanocrystals. *Nature* **1996,** 383, 802–804
72. F.Cichos; Borczyskowski, C. v.; M.Orrit, Power-law intermittency of single emitters. *Curr. Opin. Colloid Interface Sci.* **2007,** 12, 272–284.
73. Gao, F.; Bajwa, P.; Nguyen, A.; Heyes, C. D., Shell-Dependent Photoluminescence Studies Provide Mechanistic Insights into the Off–Grey–On Transitions of Blinking Quantum Dots. *ACS Nano* **2017,** 11, 2905–2916.
74. Knappenberger, K. L.; Jr.; Wong, D. B.; Xu, W.; Schwartzberg, A. M.; Wolcott, A.; Zhang, J. Z.; Leone, S. R., Excitation-Wavelength Dependence of Fluorescence Intermittency in CdSe Nanorods. *ACS Nano* **2008,** 2, 2143–2153.
75. Cordones, A. A.; Leone, S. R., Mechanisms for charge trapping in single semiconductor nanocrystals probed by fluorescence blinking. *Chem. Soc. Rev.* **2013,** 42, 3209-3221.
76. Efros, A. L.; Rosen, M., Random Telegraph Signal in the Photoluminescence Intensity of a Single Quantum Dot. *Phys. Rev. Lett.* **1997,** 78, 1110--1113.
77. Krauss, T. D.; Brus, L. E., Charge, Polarizability, and Photoionization of Single Semiconductor Nanocrystals. *Phys. Rev. Lett.* **2000,** 83, 4840--4843.

78. Frantsuzov, P. A.; Volkán-Kacsó, S.; Jankó, B., Model of Fluorescence Intermittency of Single Colloidal Semiconductor Quantum Dots Using Multiple Recombination Centers. *Phys. Rev. Lett.* **2009,** 103, 207402.
79. Yuan, G.; Gómez, D. E.; Kirkwood, N.; Boldt, K.; Mulvaney, P., Two Mechanisms Determine Quantum Dot Blinking. *ACS Nano* **2018,** 12, 3397–3405.
80. Galland, C.; Ghosh, Y.; Steinbrück, A.; Sykora, M.; Hollingsworth, J. A.; Klimov, V. I.; Htoon, H., Two types of luminescence blinking revealed by spectroelectrochemistry of single quantum dots. *Nature* **2011,** 479, 203-207.
81. Seth, S.; Ahmed, T.; Samanta, A., Photoluminescence Flickering and Blinking of Single $CsPbBr_3$ Perovskite Nanocrystals: Revealing Explicit Carrier Recombination Dynamics. *J. Phys. Chem. Lett.* **2018,** 9, 7007–7014.
82. Paul, S.; Samanta, A., Phase-Stable and Highly Luminescent $CsPbI_3$ Perovskite Nanocrystals with Suppressed Photoluminescence Blinking. *J. Phys. Chem. Lett.* **2022,** 13, 5742–5750.
83. Gibson, N. A.; Koscher, B. A.; Alivisatos, A. P.; Leone, S. R., Excitation Intensity Dependence of Photoluminescence Blinking in $CsPbBr_3$ Perovskite Nanocrystals. *J. Phys. Chem. C* **2018,** 122, 12106–12113.
84. Ahmed, T.; Seth, S.; Samanta, A., Mechanistic Investigation of the Defect Activity Contributing to the Photoluminescence Blinking of $CsPbBr_3$ Perovskite Nanocrystals. *ACS Nano* **2019,** 13, 13537–13544.
85. Trinh, C. T.; Minh, D. N.; Ahn, K. J.; Kang, Y.; Lee, K.-G., Verification of Type-A and Type-B-HC Blinking Mechanisms of Organic–Inorganic Formamidinium Lead Halide Perovskite Quantum Dots by FLID Measurements. *Sci. Rep.* **2020,** 10, 2172.
86. Kim, T.; Jun, S. I.; Ham, S.; Chung, H.; Kim, D., Elucidation of Photoluminescence Blinking Mechanism and Multiexciton Dynamics in Hybrid Organic–Inorganic Perovskite Quantum Dots. *Small* **2019,** 5, 1900355.
87. Chen, O.; Zhao, J.; Chauhan, V. P.; Cui, J.; Wong, C.; Harris, D. K.; Wei, H.; Han, H.-S.; Fukumura, D.; Jain, R. K.; Bawendi, M. G., Compact high-quality CdSe–CdS core–shell nanocrystals with narrow emission linewidths and suppressed blinking. *Nat. Mater* **2013,** 12, 445-451.
88. Qin, H.; Niu, Y.; Meng, R.; Lin, X.; Lai, R.; Fang, W.; Peng, X., Single-Dot Spectroscopy of Zinc-Blende CdSe/CdS Core/Shell Nanocrystals: Nonblinking and Correlation with Ensemble Measurements. *J. Am. Chem. Soc.* **2014,** 136, 179-187.
89. Paul, S.; Ahmed, T.; Das, S.; Samanta, A., Effect of Lead:Halide Precursor Ratio on the Photoluminescence and Carrier Dynamics of Violet- and Blue-Emitting Lead Halide Perovskite Nanocrystals. *J. Phys. Chem. C* **2021,** 125.
90. Paul, S.; Kishore, G.; Samanta, A., Photoluminescence Blinking of Quantum Confined $CsPbBr_3$ Perovskite Nanocrystals: Influence of Size. *J. Phys. Chem. C* **2023,** 127, 10207–10214.

CHAPTER 2

Materials and Methods

Overview

In this chapter, details of synthesis of perovskite NCs used for this study and their optical and structural characterization methods have been discussed. Starting materials used for our studies are enlisted here. Basic principles of the instrument setups used for these studies have been discussed briefly. We have elaborated fundamental concepts of single molecule PL measurements including sample preparations. The experimental details of time-resolved confocal fluorescence microscope are described, especially for the intensity time-trace and fluorescence correlation spectroscopy measurements. Basic principle of time-correlated single photon counting and femtosecond transient absorption setup is outlined. The experimental details of UV-Vis absorption, photoluminescence and quantum yield measurements are described. Furthermore, instrument details for different structural characterization methods such as TEM, PXRD, EDX, NMR, FTIR, XPS etc. have been outlined.

2.1. Synthesis Methods

2.1.1. Materials

Cesium carbonate (99.9%), formamidinium acetate (99%), methylamine, lead oxide (99%), lead chloride (99.999%), lead iodide (99%), lead bromide (99.999%),zinc bromide (99%), ammonium iodide (99%), N-bromosuccinimide (NBS, 99%), N-chlorophthalimide (NCP, 96%), 1-octadecene (ODE, 90%), oleic acid (OA, 90%), oleylamine (OLA, 70%), toluene (anhydrous), hexane (anhydrous), were procured from Sigma-Aldrich. We have used these materials in the synthesis without any purification.

2.1.2. Preparation of cesium-oleate (Cs-oleate)

Cs-oleate was prepared by following a reported method with slight modification.[1] In this method, 0.195 g of Cs_2CO_3, 9 mL of ODE and 1 mL of OA were taken in a 50 mL two-necked round-bottom (RB) flask. Then this mixture was degassed for 10 min at room-temperature and heated under vacuum at 120°C for 1 h. Then the reaction mixture is kept under N_2 atmosphere with constant heating until all Cs_2CO_3 reacted with OA to form a transparent solution of Cs-oleate complex. To avoid precipitation at room-temperature, it is preheated at 120°C before using.

2.1.3. Preparation of formamidinium-oleate (FA-oleate)

Formamidinium acetate (0.26 g) was taken into a 50 mL double-necked RB flask along with 10 mL of OA and then heated under N_2 atmosphere at 100ºC until the entire solution becomes clear indicating the formation of FA-oleate.[2] The resultant solution was then dried at 50ºC under vacuum for 30 min to remove moistures.

2.1.4. Preparation of methylammonium-oleate (MA-oleate)

Preparation of MA-oleate is quite simple as in this case high temperature is not required. It is prepared by thoroughly mixing 250 µL of methylamine (2M in tetrahydrofuran) with 2.5 mL of OA at room temperature.

2.1.5. Synthesis of $CsPbBr_3$ NCs using NBS as bromide precursor

PbO (44 mg) and NBS (108 mg) were loaded into a two-neck 50 mL round-bottom flask along with 5 ml ODE. The reaction mixture was kept under vacuum at 120°C for 15 min and then transferred in N_2 atmosphere at the same temperature. Subsequently, 1 mL OA and 1 mL OLA were injected into the

reaction mixture and keep it same temperature up to 30 min to dissolve everything in the reaction mixture. The temperature of the reaction mixture was increased to 200°C and 0.5 ml of preheated Cs-oleate solution was swiftly injected into it. After 15 s the reaction was quenched by using an ice-water bath. Then 8 mL of Me-OAc was added to the crude product and it was centrifuged at 7000 rpm for 6 min. After centrifugation, the supernatant solution was discarded and the bright green precipitate ($CsPbBr_3$ NCs) was dispersed in hexane. The hexane dispersion of the NCs was again centrifuged at 12000 rpm for 10 min. The precipitate was discarded and the supernatant solution containing the NCs was stored. Lastly, 25 µL of OLA and 25 µl OA mixture was added into the NCs solution and it was stored for future studies.

2.1.6. Synthesis of $FAPbBr_3$ NCs

To obtain $FAPbBr_3$ NCs, PbO (44 mg) and NBS (108 mg) were loaded into a 50 ml two-neck round-bottom flask along with 5 mL ODE. The reaction mixture was kept under vacuum at 140°C for 15 min and then transferred under N_2 atmosphere at same temperature. Then, 0.3 mL of OLAM and 0.5 ml of OA was injected. After confirming everything dissolved in ODE, the temperature of the reaction system was raised to 165°C and 2.5 mL of FA-oleate solution was injected smoothly. Subsequently, the reaction system was immediately cooled by using an ice-water bath. Then 3 mL of MeOAc was added to the crude product and it was centrifuged for 7000 rpm for 6 min. Then the supernatant liquid was discarded and bright green precipitate ($FAPbBr_3$ NCs) was dispersed in hexane. After 30 min, it was again centrifuged at 12000 rpm for 10 min, the precipitate was discarded and the supernatant liquid containing the NCs was stored for future studies.

2.1.7. Synthesis of $MAPbBr_3$ NCs

$MAPbBr_3$ NCs were prepared following a protocol similar to that used for $FAPbBr_3$ except for the preparation of the MA-oleate solution.

2.1.8. Synthesis of $CsPbI_3$ NCs using NH_4I as an additional precursor

0.2 mmol (92 mg) PbI_2, 0.25 mmol (36 mg) NH_4I, 5 mL ODE, 0.8 mL OA and 0.8 mL OLA were loaded into a 50 mL double-neck round-bottom flask. The mixture was kept under vacuum for 15 min at room temperature and then heated at 120°C in N_2 atmosphere until the formation of clear orange colour solution. The reaction temperature was then increased to 160- 165°C and 0.5 mL of Cs-oleate solution (pre-heated at 100°C) was swiftly injected (under nitrogen atmosphere). Immediately after injection, the reaction mixture was cooled in an ice-water bath to obtain the crude product. The crude product was

centrifuged for 3 min at 2500 rpm following which the precipitate was discarded and the supernatant liquid was again centrifuged at 7800 rpm for 12 min. Then, the supernatant liquid was discarded and the precipitate was dispersed in hexane. The dispersed solution was again centrifuged for 12 min at 7500 rpm. The supernatant bright red dispersion of the NCs was stored for measurements and the precipitate, if any, was discarded.

2.1.9. Synthesis of Quantum Confined $CsPbBr_3$ NCs

These NCs of different sizes were synthesized by hot injection method following a reported procedure with minor changes in the reaction conditions.[39] In the first step, Cs-oleate was prepared from its precursors. For this purpose, 0.25 g Cs_2CO_3, 0.9 mL oleic acid (OA), and 9 mL 1-octadecene (ODE) were loaded into a 50 mL 2-neck round-bottom flask and dried under vacuum for 1 h at 120 °C. The mixture was then heated under N_2 atmosphere to 150 ºC until Cs_2CO_3 dissolved completely. The Cs-oleate solution was then kept at 100 ºC to prevent precipitation of Cs-oleate. For preparation of the $CsPbBr_3$ NCs, in another 50 mL 2-neck round-bottom flask, 75 mg $PbBr_2$ and $ZnBr_2$ (250 mg) were dissolved in a mixture of ODE (5 mL), oleic acid (3 mL), and oleylamine (3 mL) at 120°C in vacuum. Then 0.4 mL Cs-oleate was injected swiftly into the reaction mixture at preset reaction temperature (in N_2 atmosphere). The reaction temperature used for synthesis of the NCs of three different sizes were 80°C, 140°C and 180°C, respectively. The reaction was quenched after 120 s by cooling the system in an ice bath. Once cooled to room temperature, the crude product was centrifuged at 3500 rpm for 20 min to remove the unreacted salt. Two different cleaning methods were used depending on whether the reaction was conducted at high (140-180 °C) or low temperatures (80°C). For reactions conducted at higher temperatures (140-180 °C), less unreacted salt remained in solution from a greater reaction yield. In this case, ~8 mL of methyl acetate was directly added into the supernatant to precipitate the NCs followed by centrifuging at 7000 rpm for 8 min. The precipitants were collected and dissolved in ~1 mL of hexane. For reactions conducted at lower temperature (80°C), a larger amount of unreacted salt remained in the supernatant after centrifuging. In this case, the supernatant was left on the bench top under ambient conditions for ~ 2 hours until the salt precipitated. Then the mixture was centrifuged again. This procedure was repeated until the supernatant became clear. Then ~ 8 mL of methyl acetate was slowly added to the supernatant solution until the mixture became turbid. Then this turbid solution was centrifuged at 7000 rpm for 8 min and the precipitate was collected and dissolved in ~1 mL of hexane and stored for the measurements.

2.2. Optical Characterization

2.2.1. Steady State Measurements

UV-Vis absorption and photoluminescence spectra were recorded using Varian CARY100 spectrophotometer and Horiba Jobin Yvon FluoroLog-3 spectrofluorimeter, respectively. These measurements were carried out by taking very dilute (optical density of <0.10 at excitation wavelength in 1 cm path length cuvette) colloidal solution of NCs.

2.2.2 Measurement of Photoluminescence Quantum Yield (PLQY)

The PLQY of the NCs were estimated using the following equation,

$$QY_S = QY_R \times (I_S/I_R) \times (OD_R/OD_S) \times (n_S^2/n_R^2) \quad \ldots\ldots 2.1$$

Where, I corresponds to the area under the emission spectrum, OD is the optical density at the excitation wavelength and n is the refractive index of the medium. The subscripts S and R designated for sample and reference, respectively. 9,10-diphenylanthracene (ϕ_f = 0.93 in hexane[4]), coumarin 153 (ϕ_f = 0.54 in ethanol[5]), Rhodamine 6G (PLQY of 0.95 in water[6]) were used as the standard for blue, green, red emitting NCs, respectively.

2.2.3. Time Correlated Single Photon Counting (TCSPC)

Fluorescence lifetime (100s of ps to ~10s of ns) is measured by TCSPC technique. [7] In this measurement, the excitation laser starts a timer, which is terminated upon detection of a light emitted by the fluorophore or vice versa. The important components of a TCSPC unit are shown in figure 2.1. A mode-locked laser (pulse width, picosecond or femtosecond) with high repetition rate is commonly used as an excitation source and a microchannel plate (MCP) photomultiplier tube (PMT) as detector in this technique. Ultrashort laser pulse excites the sample and forwards a signal to the constant fraction discriminator (CFD1) to measure arrival time of the pulse. Then the signal is directed to a time-to-amplitude converter (TAC), which triggers a voltage ramp that is a voltage which increases linearly with time. The photons emitted by the sample after sending through a polarizer (optional) and monochromator are detected by a PMT and then passed to another CFD2. Then CFD2 sends a signal to end the voltage ramp in TAC. The final voltage in the TAC is proportional to time duration between start and stop pulses (Δt). The output voltage from the TAC is amplified by a programmable gain amplifier (PGA) and then an analog-to-digital converter (ADC) is used to convert the analog signal to a digital signal. These numerical values are

processed as a single photon event in the multi-channel analyzer (MCA). To obtain a histogram of fluorescence intensity versus time many such photon events are measured.

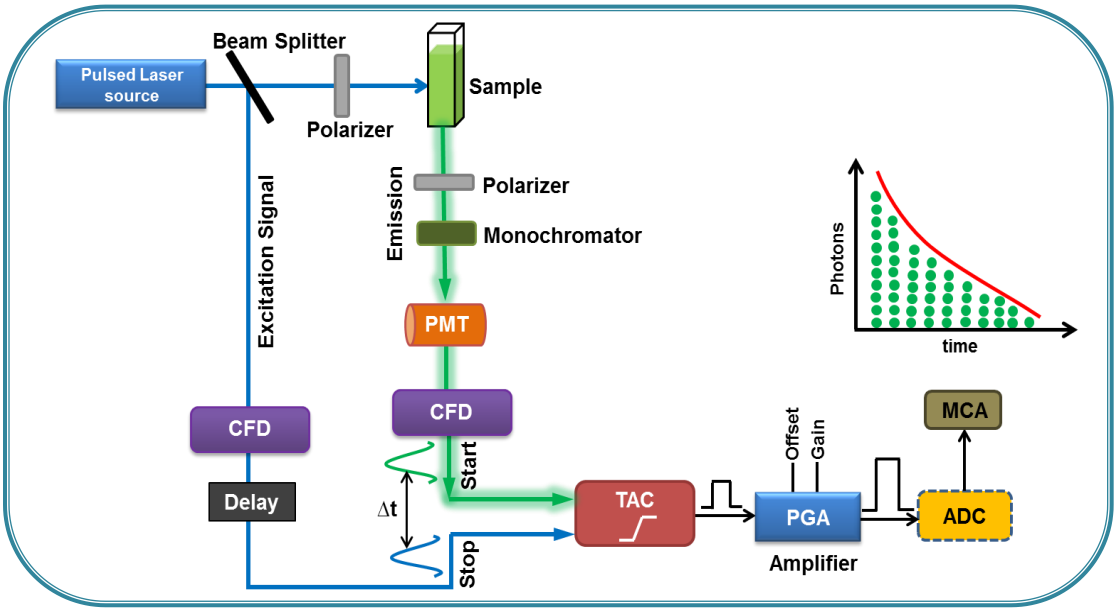

Figure 2.1. Schematic diagram of the working principle and main components of a TCSPC.

The above described operating mode of a TCSPC is called forward mode. Because of high repetition rate of excitation source, forward mode of TCSPC measurement show a major problem. The TAC needs to be reset and set to zero before receiving each start signal, which requires finite time duration. Hence, the TAC can stay in reset mode always if the start signals reach too rapidly. The emission signals appear much rarely than the excitation pulses (1 emission signal per 100 excitation pulses).To avoid this problem TCSPC measurements are generally carried out in the reverse mode where the fluorescence act as the START pulse and the excitation pulse as the STOP pulse.

2.2.4. Fluorescence Lifetime Measurements

Photoluminescence lifetime was measured by a time-correlated single photon counting instrument (Horiba Jobin Yvon IBH). A diode laser (λ_{exc} = 376 nm, 405 nm, 485 nm) and an MCP photomultiplier (Hamamatsu R3809U-50) were used as the excitation source and detector, respectively. Instrument response was measured by recording the excitation profile by placing a scatterer solution (ludox in water) in place of the sample. Decay profiles were analysed by nonlinear least-squares iteration procedure using

IBH DAS6 (version 2.2) decay analysis software. The photoluminescence decay curves were fitted to the following equation,

$$I(t) = \sum_{i=1}^{n} \alpha_i \exp(-t/\tau_i) \ldots\ldots\ldots\ldots\ldots\ldots 2.2$$

here τ_i and α_i represent amplitude and lifetime of the i^{th} component respectively. Fractional contribution of i^{th} lifetime (a_i) to the steady-state PL intensity is given as

$$a_i = \frac{\alpha_i \tau_i}{\sum_{i=1}^{n} \alpha_i \tau_i} \ldots\ldots\ldots\ldots\ldots\ldots\ldots\ldots 2.3$$

and the average fluorescence lifetimes were enumerated using following equation.

$$\boldsymbol{\tau_{av} = \sum_{i=1}^{n} a_i \tau_i} \ldots\ldots\ldots\ldots\ldots 2.4$$

2.2.5. Single molecule Spectroscopy

Single molecule spectroscopy emerged as one of the most advanced techniques due to its sensitivity up to a single molecule and helped to find several longstanding questions in physics, chemistry and biology.[8-10] Single molecule spectroscopy gives access to statistical distributions and correlations of microscopic parameters of molecules, and also their temporal fluctuations, which are not visible in ensemble measurements. Single molecule spectroscopy earned great attention since 1990s with the pioneering works of Michel Orrit and W. E. Moerner and currently stand out as one of the most powerful techniques for the study of physical and chemical properties of single molecule.[10] At the beginning time, the main challenges for this technique were isolation of a single molecule and recording of signal with high signal to noise (S/N) ratio. However, these problems are solved with upgradation of lasers, optics and detectors, and now signals with good S/N ratios can be recorded from highly dilute sample (pM – nM) with infinitesimal excitation volume (fL). The spatial resolution of a microscope is 'diffraction-limited' and given by Abbe's formula.[11]

$$d = \lambda / 2NA \ldots\ldots\ldots\ldots\ldots 2.5$$

$$NA = n \sin\theta \ldots\ldots\ldots\ldots\ldots 2.6$$

Where d is the minimum separable distance, λ and NA correspond to wavelength of light and numerical aperture of the lens, respectively. n and θ represent refractive index of the lens and half angle of the cone of light entering or leaving the lens.

2.2.6. Confocal Fluorescence Microscope

We have used time resolved confocal microscope for the study of single particle fluorescence signal. Confocal fluorescence microscopy offers several advantages compared to conventional wide-field microscopy, including the ability to control depth of field, elimination of background information, and the capability of collection of serial optical sections from thick specimens. The basic principle of the confocal microscopy is the use of spatial filtering technique to eliminate out of focus light and which is done by using very small pinhole at the confocal plane in the optical path. For this study a time resolved confocal fluorescence microscope setup (MicroTime 200, PicoQuant[12]) comprising of an inverted microscope (Olympus IX71) equipped with a piezo scanning stage is used (Figure 2.2). Photons are collected by a water immersion objective (UplanSApo 60× NA 1.2). We have used three picosecond diode lasers sources: 405, 485 and 640 nm as excitation sources. The repetition rate of the lasers can be tuned from 1 – 80 MHz. The output of the diode laser is passed to the main optical unit (MOU) through single mode optical fiber and guided by a dichroic mirror. The excitation light was then focused on the sample placed on a coverslip and mounted on a movable piezo scanning stage using the water immersion objective. A photodiode has been used to measure excitation power. The same objective is also used to collect the emission from the sample. A long-pass or band pass filter is used to spectral filtration of photons. To eliminate out of focus light a 50μm diameter pinhole was used in the confocal plane. Single photon avalanche photo diodes (SPAD) used as detectors in this instrument because they have high detection efficiencies in the visible range and very small active area (50-100 μm) to reduce the dark counts. SPAD signal is subjected to TCSPC electronics (PicoHarp 300) to get the timing information of the photons.

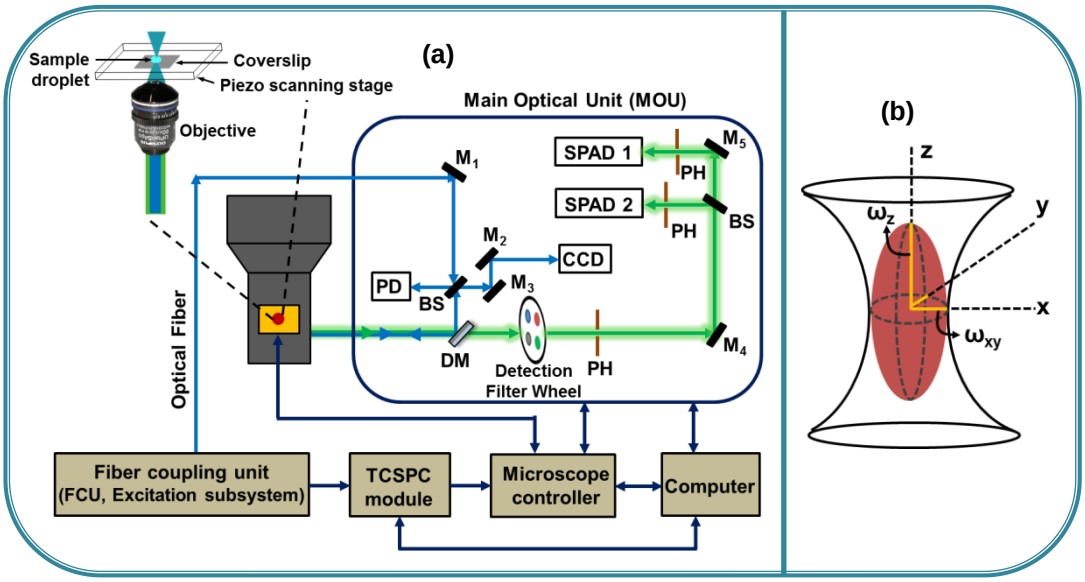

Figure 2.2. (a) Schematic depiction of the time resolved confocal microscope setup. Mi = Mirror, BS = Beam splitter, DM = Dichroic mirror, PH = Pinhole and PD = Photodiode. (b) Ellipsoidal observation volume in a confocal microscope setup.

2.2.6. Intensity Time-Trace and Photon Antibunching Measurement:

We have used time tagged time resolved (TTTR, T3) method to measure the PL intensity time traces. Fluorescence lifetime is generally measured by TCSPC instrument and which is discussed in the subsection 2.2.2. To get insight on PL dynamics of single NCs, TTTR method is used for measuring PL intensity-time traces. In this technique each emitted photon is tagged with both its absolute arrival time (relative to the start of the experiment) and the delay time relative to excitation pulse so that PL intensity traces and PL decays can be measured at the same time for a given NC. The major advantage of this method is that one can study excited state dynamics as a function of PL intensity for a given interval.

The photon-antibunching or single photo purity is characterized by the second-order intensity correlation function,

$$g^{(2)}(t) = \frac{\langle I_1(t) I_2(t+\tau) \rangle}{\langle I_1(t) \rangle \langle I_2(t+\tau) \rangle} \quad \ldots\ldots\ldots\ldots\ldots\ldots\ldots 2.7$$

as a function of the delay time τ between the two photon detection events. Here, $I_1(t)$ is the emission intensity at time t in detector 1, and $I_2(t+\tau)$ is the intensity after a time delay of τ at detector 2. For a single particle, $g^{(2)}(0)$ is expected to be 0 as it cannot emit more than one photon at any given time. For this measurement, spectrally and spatially filtered photons were passed through a 50:50 beam splitter and focused onto two identical SPADs arranged in the Hanbury Brown−Twiss configuration. The detector signal was processed using PicoHarp300 TCSPC unit. The TCSPC unit was operated in time-tagged (T2) mode. The recording and analysis of the data were done by using the SymPhoTime software.

2.2.7. Calculation of number of excitons (N) generated per pulse

The number of excitons (N) generated per pulse was calculated using the formula: $N= J_p \times \sigma$ where J_p is per-pulse photon fluence and σ is the absorption cross section. J_p is calculated by using the formula:

$$J_P = \frac{P}{f \times E(\lambda)} \text{.....2.8}$$

Where P, f and E(λ) are power density of centre of the focused excitation spot, repetition rate of laser and energy of a photon, respectively.[13, 14]

2.2.8. Calculation of the intensity-lifetime scaling parameter

PL intensity (or quantum yield (QY)) of a system is linearly proportional to the PL lifetime (τ) and radiative rate (k_r) as follows.

$$I \propto QY = k_r / (k_r + k_{nr}) = \tau k_r \text{.....2.9.}$$

k_r and k_{nr} represent the rate constant of the nonradiative decay process. Intensity-lifetime scaling (η) is the ratio of the radiative rates of two different intensity levels (1 and 2) and can be shown as,

$$\eta = kr(1): kr(2) = I_1/\tau_1 : I_2/\tau_2 \text{.....2.10}$$

2.2.9. Calculation of probability density distribution of ON (P_{ON}) and OFF (P_{OFF}) events

The on- and off- events were distinguished in the PL intensity time-trace by applying a threshold, which was typically 10 times the maximum intensity of the background noise. Probability densities of the on- and off-events, $P_{on}(t)$ and $P_{off}(t)$, were then calculated using the following equation,[14, 15]

$$P_i(t) = \frac{N_i}{N_{i,total}} 1/\Delta t_{avg}$$

where i is the on- or off-events, N_i representing the number of on- or off-events with duration time of t, N_{total} is the total number of on- or off-events, and Δt_{avg} is the average of the time intervals between the nearest neighboring events. Data are analyzed by using PYTHON Jupyter Notebook script developed by our research group.

2.2.10. Fluorescence Correlation and Fluorescence Lifetime Correlation Spectroscopy

FCS used as powerful technique for the quantification of molecular dynamics through correlation study of the intensity fluctuation of fluorophore in and out of observation volume.[7, 16, 17] One can measure accurately local concentration, hydrodynamic radius, diffusion coefficient, and the interaction of other molecules, etc. of a sample in this technique. FCS can show higher sensitivity up to a single-molecule level and it can identify the process occurring at ns to ms timescale. Because of these advantages PL blinking behavior of a single molecule can be studied in this technique.[17] For this measurement we have used same time resolved confocal fluorescence microscopy setup which was used for PL intensity time trace measurements (Figure 2.4). The occupancy of fluorophores in the detection volume is best described by Poisson distribution as fluorophores diffuse in and out of the detection volume randomly.

The fluctuation of fluorescence intensity is quantified by the temporal autocorrelation analysis (Figure 2.3). The autocorrelation function for the fluorescence fluctuations δF(t) of the signal F (t) is expressed as

$$G(\tau) = \frac{\langle \delta F(t) \delta F(t+\tau) \rangle}{\langle F(t) \rangle^2} \quad \text{.....2.11}$$

Where $\delta F(t) = F(t) - \langle F(t) \rangle$

$$\delta F(t+\tau) = F(t+\tau) - \langle F(t) \rangle$$

If the fluctuation of fluorescence intensity arises only due to the diffusion of molecule in three-dimensions in and out of the observation volume, G(τ) is given by

$$G(\tau) = \frac{1}{N}\left(1 + \frac{\tau}{\tau_D}\right)^{-1}\left[1 + \left(\frac{\omega_{xy}}{\omega_z}\right)^2 \left(\frac{\tau}{\tau_D}\right)\right]^{-1/2} \quad \text{.....2.12}$$

N is number of fluorescent molecules in the detection volume, τ_D is the diffusion time.

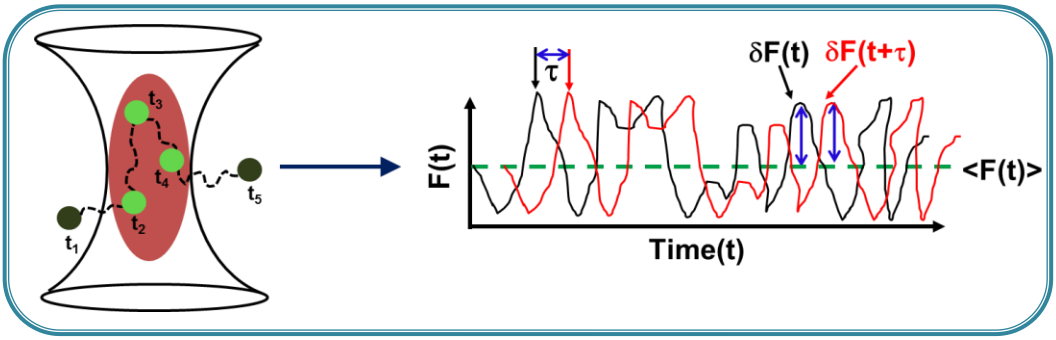

Figure 2.3. Representative scheme of basic working principle of FCS.

However, the fluorophore also can show PL intensity fluctuation due to the transition between bright and dark which is much faster than diffusion. In such case G(τ) can be represented as

$$G(\tau) = G(\tau)_{diffusion} \times G(\tau)_{fast\ process}$$

Molecules can show several fast processes for example intersystem crossing, conformational dynamics, complexation, charge carrier trapping etc. Expression of the $G(\tau)_{fast\ process}$ depend on the process responsible for the fluctuation of PL intensity.

While the FCS measures only macroscopic arrival time of each detected photon (τ, with resolution μs) with respect to the beginning of the experiment, the fluorescence Lifetime Correlation Spectroscopy (FLCS) additionally measures the microscopic delay time (t, with ps resolution) of the detected photons relative to the excitation pulse. Hence, FLCS is a variant of FCS, which uses differences in PL decay to distinct contributions of different emitter properties in a FCS signal.

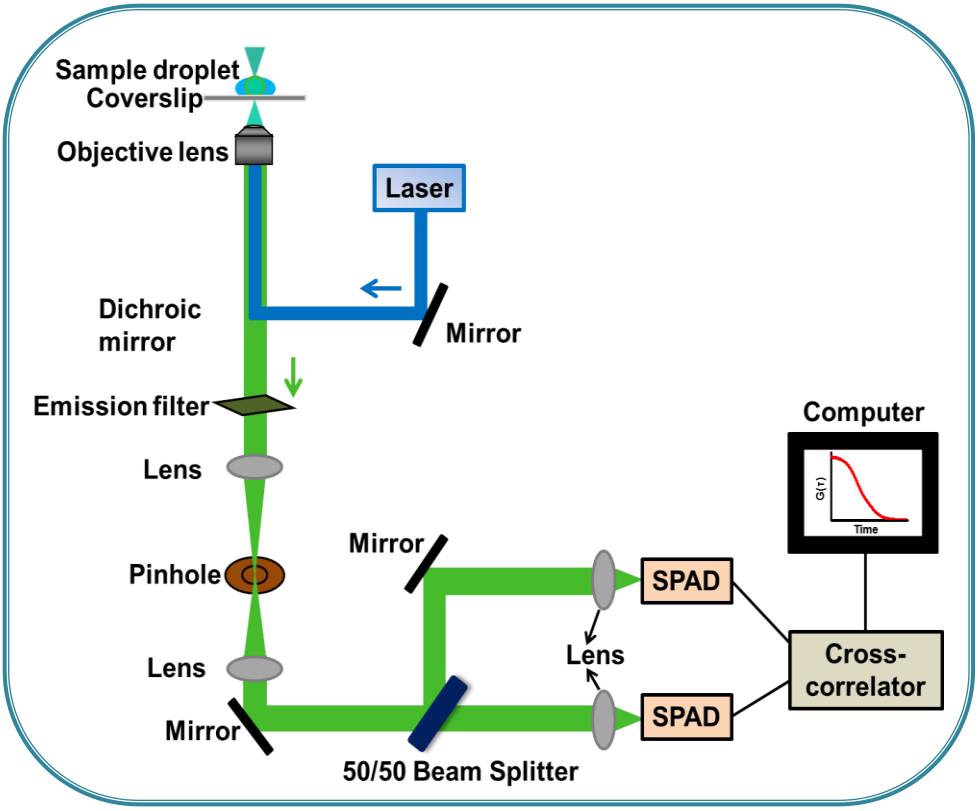

Figure 2.4. Schematic representation of instrument setup used for FCS measurement. Here two detectors are used at a time to cross-correlation of the data.

2.2.11. Femtosecond Optical Spectroscopy

Femtosecond transient absorption spectroscopy (TA) allows measurement of charge carrier dynamics occurring in the ultrafast timescale (10^{-12} s-10^{-15} s) which cannot be measured in the TSCPC technique that has ps to ns time resolution.[18] In TA spectroscopy, the sample is excited by intense laser (optical pump) and the processes occurring in the excited (transient) species is identified by using a broad band probe pulse. Timing information of the molecular processes obtained by using variable delay time between pump and probe pulse. Thanks to speed of light which offers fs-ps time resolution in this technique. This technique is also known as pump-probe measurement.[19]

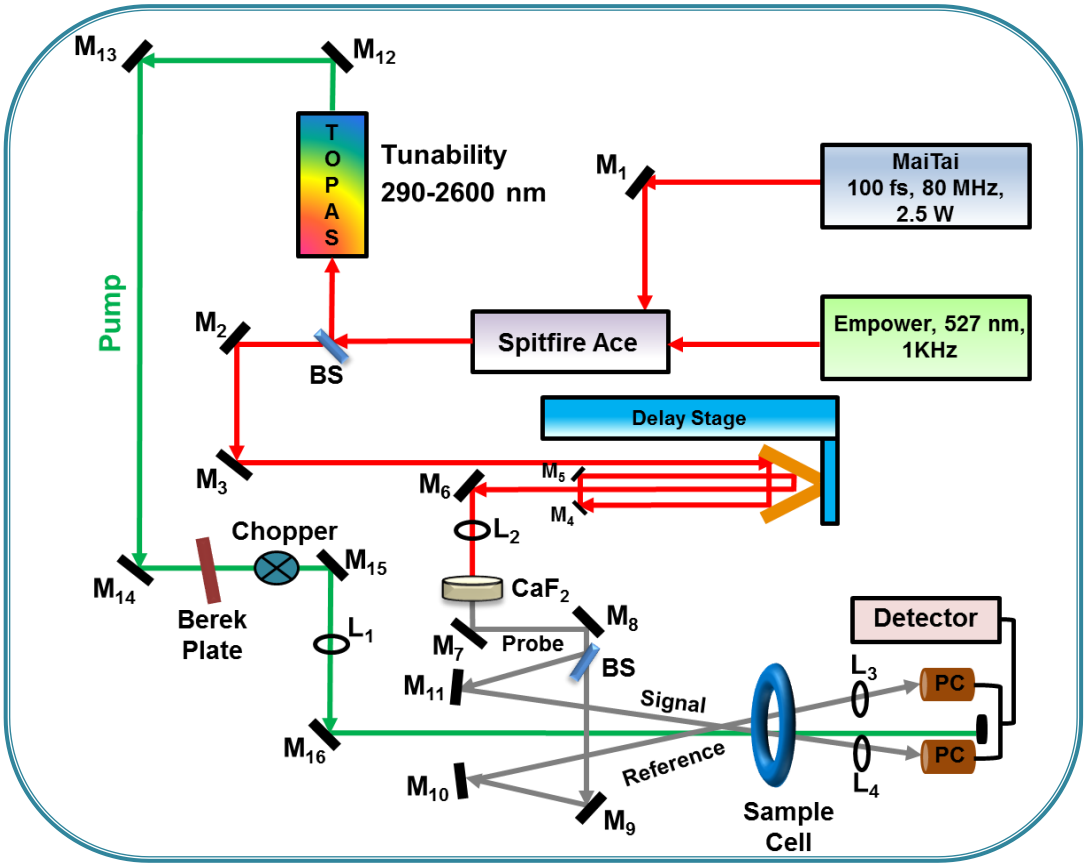

Figure 2.5. Schematic demonstration of the femtosecond pump-probe setup. Mi = Mirror, Li = Lens, PC = Polychromator, BS = Beam splitter.

Femtosecond pulses are generally generated by a process called 'mode-locking' in which longitudinal modes present inside the laser cavity subjected to constructive interference by maintaining fixed phase to produce short pulse. The pulse width of short pulse can be expressed as $\tau = 1/N\Delta\nu$, where $\Delta\nu$ is the frequency difference between two modes and N corresponds to total number of modes. Hence one can generate short pulses by increasing the frequency spacing between modes and decreasing the cavity length of laser or employing a gain medium with large band-width that increases the number of longitudinal modes. Ti:sapphire laser due to its large gain band-width of its active medium and broad absorption (peak maximum ~500 nm) and a broad emission (690 – 1040 nm with maxima at~800 nm) has become ideal for tunable femtosecond laser.

In this study, TA measurements were performed in a setup (Figure 2.5) consisting of femtosecond laser sources from a Spectra-Physics, USA, and a spectrometer from CDP Systems, Russia. The seed laser output from MaiTai (800 nm, <100 fs, 80 MHz) was directed into a Ti:sapphire regenerative amplifier, which was pumped by the second harmonic (532 nm) of an Nd:YLF laser. A portion of the amplified output (800 nm, <120 fs, 1 kHz) was passed through an optical parametric amplifier to generate the pump wavelength (350 nm) for the excitation of the NCs. The remaining portion of the output was passed through a variable optical delay line of 4 ns and then directed to a rotating CaF_2 crystal to generate the probe white light. The probe beam was divided into two parts to use as signal and reference beams. The pump and signal beams were focused onto a rotating sample cell. The transmitted signal and reference beams were received by a multichannel photodiode array through a polychromator and further processed to record difference in absorbance (ΔA) as a function of wavelength and pump–probe delay. All TA spectra were chirp-corrected, and the instrumental resolution was ~100 fs. Data were analyzed using ExciPro (CDP system) and Igor Pro software. The differential absorption is given as:

$$\Delta A(\lambda, t) = A_{pump\ on}(\lambda, t) - A_{pump\ off}(\lambda) = A_{excited}(\lambda, t) - A_{ground}(\lambda)$$

$$\Delta A(\lambda, t) = log\left(\frac{I_{0,excited}(\lambda)}{I_{excited}(\lambda,t)}\right) - log\left(\frac{I_{0,ground}(\lambda)}{I_{ground}(\lambda)}\right) = log\left(\frac{I_{ground}(\lambda)}{I_{excited}(\lambda,t)}\right) \quad \text{.....2.13}$$

where A_{ground} and $A_{excited}$ are the absorbance of the ground and excited state species and I_0 and I_t represent the incident and transmitted intensities of the probe. The intensity of the probe pulse is kept low in comparison to the pump pulse to eliminate multiphoton processes.

A TA spectrum mainly exhibits contributions from three processes: ground state bleach (GSB), excited state absorption (ESA), and stimulated emission (SE) (Figure 2.6).[20] The Pump pulse excites a fraction of molecules in the sample, therefore, the probe pulse experience lesser number of molecule in the ground state in the pump on condition compared to pump-off (unexcited) condition. This results a negative ΔA signal (GSB) in the spectral region of the ground-state absorption of the sample. The excited molecule (pump-on) can be further excited to higher energy states by probe light that leads to absorption of the probe light at specific wavelength regions (ESA) which results lower probe transmitted intensity in pump-on condition than in pump-off and positive ΔA values observed in these spectral regions. Lastly, the probe pulse also can bring back photo excited sample (pump on) to ground state through stimulated emission that increase number of photon in the direction of the probe. This lead to a negative ΔA signal (SE) in the spectral region corresponding to the emission of the sample.

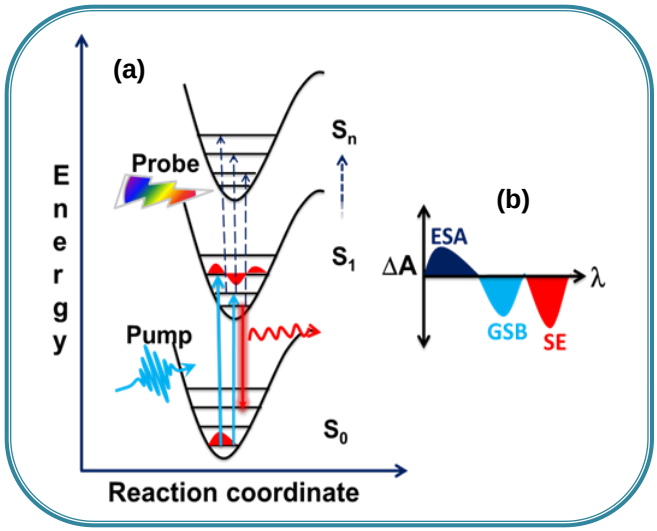

Figure 2.6. (a) Diagram representing excitation of molecule by a femtosecond pump pulse and probing of the excited state by a broadband femtosecond probe pulse. (B) Observed spectral features in a typical pump-probe measurement.

2.3 Structural Characterization

2.3.1. Powder X-ray diffraction (PXRD) measurement

PXRD patterns of the samples were recorded using Cu-Kα X-ray radiation (λ=1.5406 A^0) generated by Bruker AXS D8 X-ray diffractometer. A concentrated film of the NCs was used for this measurement which was prepared by drop casting a concentrated solution of the NCs.

2.3.2. Transmission electron microscopy (TEM) measurement

TEM images were captured using JEOL JEM-F200 and Tecnai G2 FE1 F12 transmission electron microscope. These instruments were operated at an accelerating voltage of 200 kV. The samples were prepared by drop casting a dilute solution of the NCs on a carbon-coated copper grid. Grids were kept in a vacuum before use.

2.3.2. X-ray photoelectron spectroscopy (XPS) measurement

XPS spectra of our samples were measured using Thermo-Scientific K-Alpha spectrometer consisting with a micro-focused monochromatic X-ray source (Al Kα, spot size ~400 μm) which was operated at 70 W. The energy resolution of the spectrometer was set at 0.5 eV at pass energy of 50 eV. Throughout

measurement a 5×10^{-5} torr base pressure was maintained inside the analysis chamber. Samples were prepared by drop casting a concentrated solution of the NCs and kept under vacuum for overnight for drying.

2.3.3. Energy dispersive X-ray spectroscopy

Energy dispersive X-ray spectra were measured by Oxford instruments X-MaxN SDD (50 mm^2) system and INCA analysis software. Samples were prepared by drop casting the NCs solution on cover slips.

Bibliography

1. Protesescu, L.; Yakunin, S.; Bodnarchuk, M. I.; Krieg, F.; Caputo, R.; Hendon, C. H.; Yang, R. X.; Walsh, A.; Kovalenko, M. V., Nanocrystals of Cesium Lead Halide Perovskites ($CsPbX_3$, X = Cl, Br, and I): Novel Optoelectronic Materials Showing Bright Emission with Wide Color Gamut. *Nano Lett.* **2015,** 15, 3692–3696.
2. Protesescu, L.; Yakunin, S.; Bodnarchuk, M. I.; Bertolotti, F.; Masciocchi, N.; Guagliardi, A.; Kovalenko, M. V., Monodisperse Formamidinium Lead Bromide Nanocrystals with Bright and Stable Green Photoluminescence. *J. Am. Chem. Soc.* **2016,** 138, 14202–14205.
3. Dong, Y.; Qiao, T.; Kim, D.; Parobek, D.; Rossi, D.; Son, D. H., Precise Control of Quantum Confinement in Cesium Lead Halide Perovskite Quantum Dots via Thermodynamic Equilibrium. *Nano Lett.* **2018,** 18, 3716-3722.
4. A.Maciejewski; R.P.Steer, Spectral and photophysical properties of 9,10-diphenylanthracene in perfluoro-n-hexane: the influence of solute—solvent interactions. *Journal of Photochemistry* **1986,** 35, 59-69.
5. Rurack, K.; Spieles, M., Fluorescence Quantum Yields of a Series of Red and Near-Infrared Dyes Emitting at 600−1000 nm. *Anal. Chem.* **2011,** 83, 1232–1242.
6. R.F.Kubin; A.N.Fletcher, Fluorescence quantum yields of some rhodamine dyes. *Journal of Luminescence* **1982,** 27, 455-462.
7. Lakowicz, J. R., *Principles of Fluorescence Spectroscopy*, Springer, New York, USA, 2006.
8. Moerner, W. E.; Fromm, D. P., Methods of single-molecule fluorescence spectroscopy and microscopy. *Rev.Sci. Instrum.* **2003,** 74, 3597-3619.
9. Moerner, W. E.; Kador, L., Optical detection and spectroscopy of single molecules in a solid. *Phys. Rev. Lett.* **1989,** 62, 2535-2538.
10. Orrit, M.; Bernard, J., Single pentacene molecules detected by fluorescence excitation in a p-terphenyl crystal. *Phys. Rev. Lett.* **1990,** 65, 2716-2719.
11. Born, M.; Wolf, E., *Principles of Optics,* 4th edn., Pergamon Press, Oxford, U.K., 1970.
12. https://www.picoquant.com/images/uploads/downloads/microtime200brochure.pdf.
13. Qin, H.; Niu, Y.; Meng, R.; Lin, X.; Lai, R.; Fang, W.; Peng, X., Single-Dot Spectroscopy of Zinc-Blende CdSe/CdS Core/Shell Nanocrystals: Nonblinking and Correlation with Ensemble Measurements. *J. Am. Chem. Soc.* **2014,** *136*, 179-187.
14. Vishnu, E. K.; Nair, A. A. K.; Thomas, K. G., Core-Size-Dependent Trapping and Detrapping Dynamics in CdSe/CdS/ZnS Quantum Dots. *J. Phys. Chem. C* **2021,** *125*, 25706–25716.

15. Seth, S.; Ahmed, T.; Samanta, A., Photoluminescence Flickering and Blinking of Single $CsPbBr_3$ Perovskite Nanocrystals: Revealing Explicit Carrier Recombination Dynamics. *J. Phys. Chem. Lett.* **2018,** *9*, 7007-7014.
16. Magde, D.; Elson, E.; Webb, W. W., Thermodynamic Fluctuations in a Reacting System—Measurement by Fluorescence Correlation Spectroscopy. *Phys. Rev. Lett.* **1972,** 29, 705--708.
17. Haustein, E.; Schwille, P., Fluorescence Correlation Spectroscopy: Novel Variations of an Established Technique. *Annu. Rev. Biophys. Biomol. Struct.* **2007,** 36, 151-169.
18. Abramczyk, H., *Introduction to Laser Spectroscopy,* ELSEVIER B.V., AE Amsterdam, 2005.
19. Mondal, N.; Samanta, A., Complete ultrafast charge carrier dynamics in photo-excited all-inorganic perovskite nanocrystals ($CsPbX_3$). *Nanoscale* **2017,** 9, 1878-1885.
20. Berera, R.; Grondelle, R. v.; Kennis, J. T. M., Ultrafast transient absorption spectroscopy: principles and application to photosynthetic systems. *Photosynth Res* **2009,** 101, 105–118.

CHAPTER 3

N-Bromosuccinimide as Bromine Precursor for Direct Synthesis of Stable and Highly Luminescent Green-Emitting Perovskite Nanocrystals

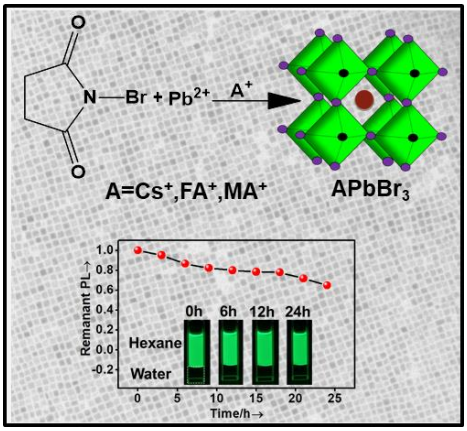

Overview

Stable green-emitting perovskite nanocrystals (NCs) with general formula, **A**$PbBr_3$, exhibiting high photoluminescence quantum yield (PLQY), narrow bandwidth and adjustable PL in the 510-535 nm region are coveted materials for optoelectronic applications. A generic method of obtaining both hybrid and all-inorganic perovskite NCs with the desired characteristics is, however, lacking. Herein, we report a methodology for the synthesis of $CsPbBr_3$, **FA**$PbBr_3$ and **MA**$PbBr_3$ NCs employing N-bromosuccinimide as bromide precursor. The NCs show uniform size distribution, PL maxima between 512 and 531 nm, near-unity PLQY with FWHM of 18-22 nm and remarkable stability in ambient condition, in presence of water and under UV irradiation. These exceptional characteristics of the NCs not only indicate their high potential in real applications, but, this new methodology may also open new vistas for direct synthesis of other perovskites with high PLQY and stability without resorting to any additional post-synthesis treatment.

3.1. Introduction

The lead halide-based perovskite NCs with general formula **A**PbX_3, where **A** = Cs^+, $CH_3NH_3^+$ (**MA**), $CH(NH_2)_2^+$ (**FA**) and X = Cl, Br, I, are in the forefront of research in optoelectronics and photovoltaics for nearly a decade for their impressive optical properties, such as high PLQY, narrow PL bandwidth, composition-tunable band gap and high absorption coefficient.[1-9] Among the perovskites, the bromide-based ones (**A**$PbBr_3$) with bright green PL and narrow full-width at half-maximum (FWHM) of <25 nm are most desirable for television displays and green-emitting LEDS.[10-13] These NCs are obtained by hot-injection or ligand-asisted reprecipitation (LARP) methods.[11, 14-16] The two-precursor hot-injection method, in which $PbBr_2$ is used as precursor for both lead and bromine, and which is commonly used for the synthesis of $CsPbBr_3$ NCs, is not quite effective for the organometallic (**FA**$PbBr_3$ and **MA**$PbBr_3$) perovskites.[13, 16, 17] For example, **FA**$PbBr_3$ NCs obtained by this method exhibit a broader size distribution and poor optical properties.[13] Even for $CsPbBr_3$ NCs, the PLQY obtained by this method is typically 60-80%,[11] or even lower due to nonradiative deactivation induced by the bromide vacancies.[18-21] This is why most often an *in situ* or a post-synthetic treatment with bromide salt, [22-25] or other reagents is necessary to improve the PLQY of these NCs.[26-28]

Kovalenko and coworkers synthesized **FA**$PbBr_3$ NCs by a three-precursor hot-injection method, wherein oleylammonium bromide was employed as the bromide source.[13] Pradhan and coworkers recently synthesized $CsPbX_3$ (X = Cl, Br, I) with 97% PLQY following this approach (i.e. using oleylammonium halides as halide precursor).[29] Although the three-precursor hot-injection method gives reasonably good quality $CsPbBr_3$ NCs and **FA**$PbBr_3$ NCs, the **MA**$PbBr_3$ NCs are still obtained by LARP mehod and they exhibit poor optical properties.[16] Except for the work of Manna and coworkers, who could succeed in obtaining all three green-emitting perovskites with 92% PLQY using benzoyl bromide as bromide precursor, we are not aware of any other work reporting synthesis of $CsPbBr_3$, **FA**$PbBr_3$ and **MA**$PbBr_3$ following a given protocol.[30] A point to note here is that, while the **A**$PbBr_3$ NCs obtained by this only method are highly luminescent, no stability data of these NCs is available. As bright green-emitting **A**$PbBr_3$ NCs with adjustable PL maxima in the 510-535 nm range and FWHM of <25 nm are very much

essential for most optoelectronic applications (considering NTSC and most recent rec.2020 colour standard), but no direct method of obtaining stable all-three NCs with these characteristics is yet to be available, we have been working towards developing a general protocol for the synthesis of all three green-emitting NCs with high stability, monodispersity, narrow PL bandwith and near-unity PLQY. We propose here a new three precursor hot-injection hot-injection method employs N-bromo succinimide (NBS), a widely used source of bromine in organic synthesis, as bromide precursor.[31] The **A**$PbBr_3$ NCs that were prepared using this protocol are characterized by their near-unity PLQYs, and exceptional air and photo stability.

3.2. Results

3.2.1 Reaction Conditions

Reaction of NBS with organic acids generates HBr,[32] which reacts with oleylamine to form oleylammonium bromide, the latter serves as active bromide source in the synthesis (Scheme 3.1 and AI.1). In our method, (PbO) and NBS were dissolved in octadecene in presence of oleic acid and oleyl amine at 120°C-140°C in vacuum. The reaction temperature was then set to 200°C for $CsPbBr_3$ and 165°C for both **MA**$PbBr_3$ and **FA**$PbBr_3$ in N_2 atmosphere, and desired amount of the oleate salt of the respective **A** cation (which was prepared separately) was injected swiftly (details are in the chapter 2). The method, which is found to be highly reproducible (Figure AI.1), yields brightly luminescent extremely uniform sized cubes of nano-dimension (Figure 3.1.a-c and AI.2).

Scheme 3.1*. Reaction scheme of the NBS mediated synthesis of* ***A****$PbBr_3$ NCs*

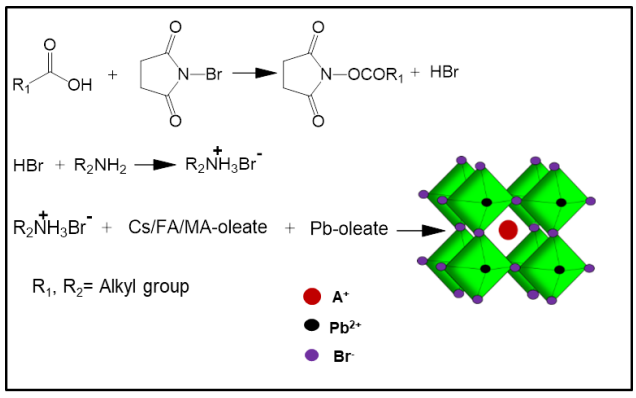

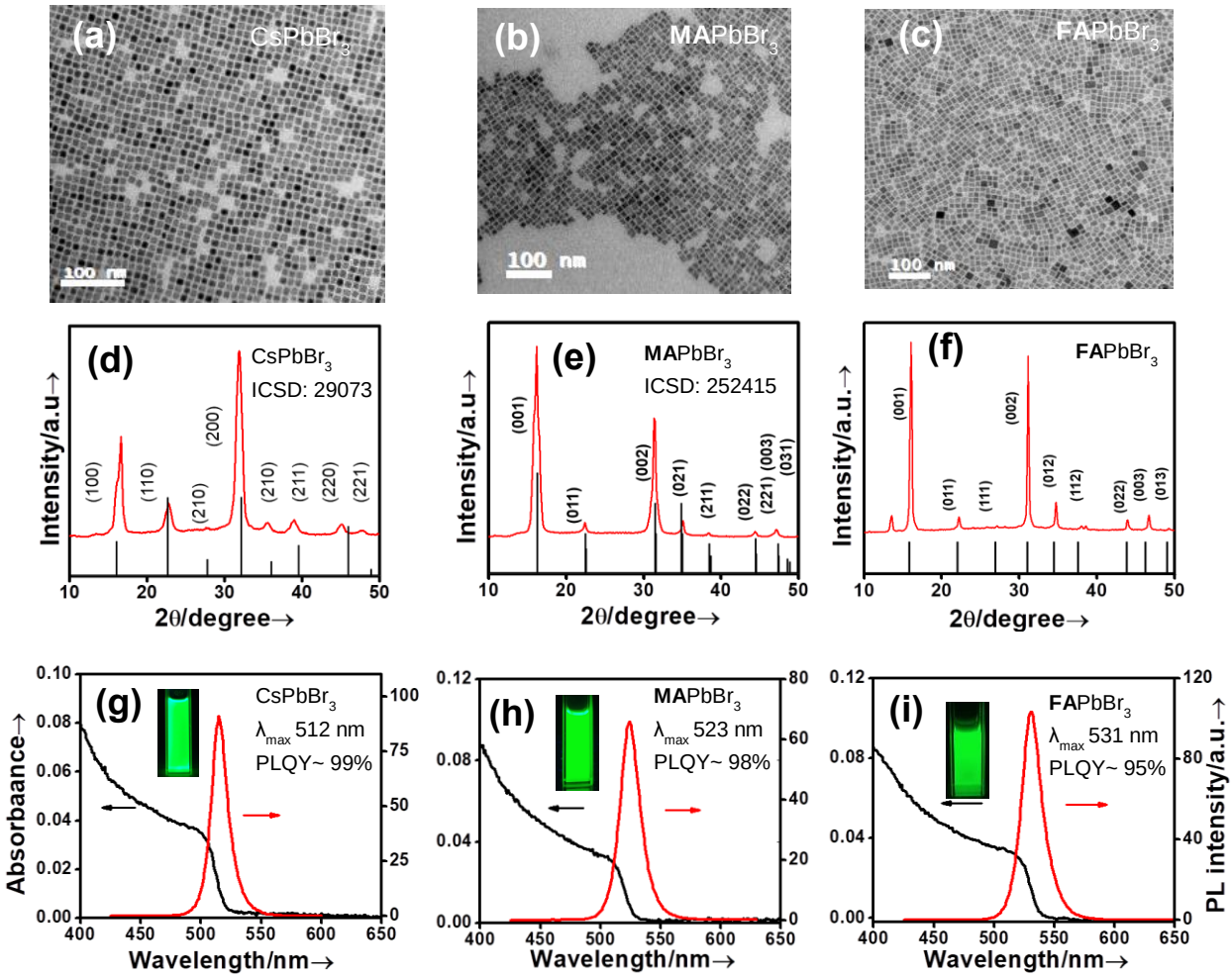

Figure 3.1. *Bright field TEM images of (a) $CsPbBr_3$ (b) **MA**$PbBr_3$ (c) **FA**$PbBr_3$ NCs. Scale bar is 100 nm in all the cases. PXRD pattern of (d) $CsPbBr_3$ (e) **MA**$PbBr_3$ and (f) **FA**$PbBr_3$ NCs along with corresponding references for bulk cubic phases. In case of **FA**$PbBr_3$ NCs, the PXRD patterns are compared with the reported crystal structure.[33] UV-Vis absorption and emission spectra of (g) $CsPbBr_3$ NCs (h) **MA**$PbBr_3$ and (i) **FA**$PbBr_3$ NCs. The excitation wavelength is 405 nm in all cases. The insets show respective NCs under UV light excitation.*

The quality of the NCs, as determined by their PLQY and size distribution, was found to be quite sensitive to the reaction conditions; particularly, the reaction temperature and Pb:Br precursor ratio. For $CsPbBr_3$ NCs, it was found that at temperatures below 200°C, a mixture of

2D nanoplates and cubes was formed (Figure AI.4) with consequent increase in PL bandwidth, appearance of multiple peaks (Figure AI.5) and low PLQY (e.g. PLQY 40% at 130°C) (Table AI.2). A low PLQY of the NCs was also observed for lower Pb:Br precursor ratio (69% for a Pb:Br ratio of 1:2.5) (Figure AI.6, Table AI.2). The **MA**$PbBr_3$ NCs, when synthesized below 165°C, exhibited broad PL spectra and at temperatures <150°C, multiple emission peaks indicating a heterogeneous distribution of the size and morphology of the NCs (Figure AI.7.a) and significant drop in PLQY were observed (Table AI.3). The **FA**$PbBr_3$ NCs obtained at temperature below 165°C, showed lower PLQY, larger FWHM and blue shift of the PL peak (Figure AI.7.b, Table AI.3). A Pb:Br precursor molar ratio of 1:3 and a temperature of 200°C for $CsPbBr_3$ NCs, 165°C for both **MA**$PbBr_3$ and **FA**$PbBr_3$ NCs were found to be the optimum reaction conditions for obtaining NCs with near-unity PLQY, uniform size distribution, and high stability.

3.2.2. Structural Characterization

Bright field TEM images indicate the cubic shape and narrow size distribution of the NCs (Figure 3.1.a-c,AI.2). The measured edge lengths for the $CsPbBr_3$, **MA**$PbBr_3$, and **FA**$PbBr_3$ NCs are 8.4±0.62, 14.2±1.2 and 11.9±1 nm, respectively. The PXRD patterns nicely match with the cubic perovskite structures of $CsPbBr_3$ ICSD code 29073 and **MA**$PbBr_3$ ICSD code 252415 (Figure 3.1.d-f). For **FA**$PbBr_3$ NCs, the PXRD pattern matches with that reported by Zhumekenov et al.[33] No secondary phases are observed in the PXRD pattern.

3.2.3. Photoluminescence Properties

Excellent PL properties of the NCs are exemplified by narrow FWHM of 18 nm for $CsPbBr_3$, 21 nm for **MA**$PbBr_3$ and 20 nm for **FA**$PbBr_3$ NCs and PLQY between 95 and 99% (Figure 3.1.g-i). The PL decay profiles of the NCs are recorded to understand the photo-physical processes involved. $CsPbBr_3$ NCs exhibits bi-exponential decay (Figure 3.2.a, Table 3.1) with 5.49 ns (80%) and 15.68 (20%) ns lifetime components. The major 5.49 ns component is clearly due to excitonic recombination.[34] The absence of any sub-ns lifetime component indicates that the

$CsPbBr_3$ NCs are largely free from surface traps. This is corroborated by the fact that an additional short lifetime component (1.65 ns) is indeed observed for the $CsPbBr_3$ NCs, which are obtained using a lower Pb:Br ratio of 1:2.5 (Figure AI.8 and Table 3.1). **MA**$PbBr_3$ and **FA**$PbBr_3$ NCs also exhibit biexponential PL decay behaviour with lifetimes of 11.78 ns (71%) and 30.17 ns (29%) for the former and 10.00 ns (80%) and 31.18 ns (20%) for the latter (Figure 3.2.b,c and Table 3.1). In both cases, the shorter lifetime component, which has major contribution, is assigned to excitonic recombination based on literature. [34, 35]

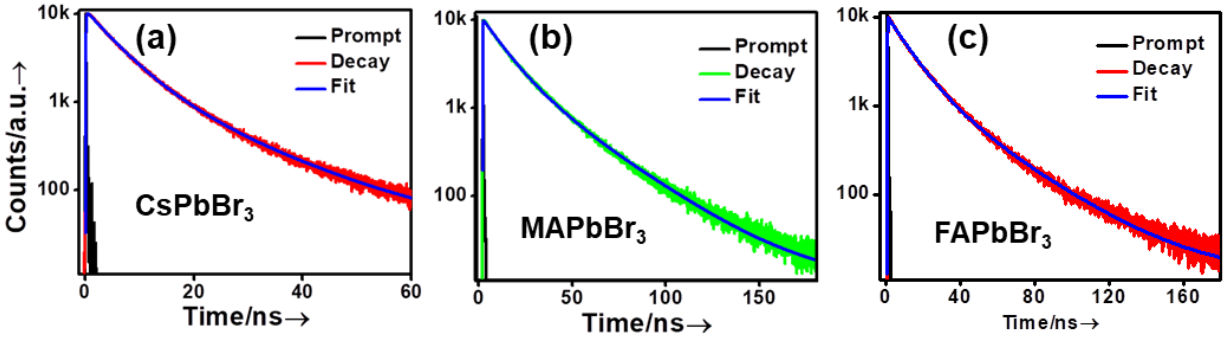

Figure 3.2*. Time-resolved PL decay of (a) $CsPbBr_3$ (b)* ***MA****$PbBr_3$ NCs. Excitation wavelength monitored at 405 nm in both the cases. PL is monitored at 512 nm and 523 nm in (a) and (b) respectively.*

Table 3.1. Photoluminiscence decay parameters of different ***A****$PbBr_3$ NCs.*

System	$\tau_1(A_1)$ **ns**	$\tau_2(A_2)$ **ns**	$\tau_3(A_3)$ **ns**	τ_{av} **ns**
$CsPbBr_3$(1:2.5)	6.53(0.46)	17.44(0.14)	1.65(0.40)	10.36
$CsPbBr_3$(1:3)	5.49(0.80)	15.68(0.20)		9.73
MA$PbBr_3$	11.78(0.71)	30.17(0.29)		21.18
FA$PbBr_3$	11.58(0.80)	31.18(0.20)		19.46

3.2.4. Stability of the NCs

Perhaps the biggest problem with the perovskite NCs is their poor stability towards polar solvents (including water) and light.[1, 2] The structural integrity of the $CsPbBr_3$ NCs is lost during

purification with polar solvent and on ageing.[18, 19] The stability of the organometallic halide perovskites, particularly for **MA**$PbBr_3$ NCs, is a major issue.[2, 36] Methods such as providing an inert protection layer,[37, 38] doping or alloying with heteroatoms,[20, 39] changing ligands[40-42] and post-synthetic treatments etc.[21, 26, 27, 43] have been attempted to impart stability to the NCs. However, none of these methods yields **A**$PbBr_3$ NCs with the desired stability. Interestingly, all the NCs obtained by our method show exceptional stability. For example, $CsPbBr_3$ NCs retain 90% PLQY even after three months of storage in ambient condition (Figure 3.3.a and Figure AI.10). PXRD pattern of these NCs recorded after 3 month of storage and TEM images obtained after 60 days of storage show that the cubic shape with uniform size distribution of these NCs is retained for a long duration in ambient atmospheric condition (Figure 3.3.b-c).

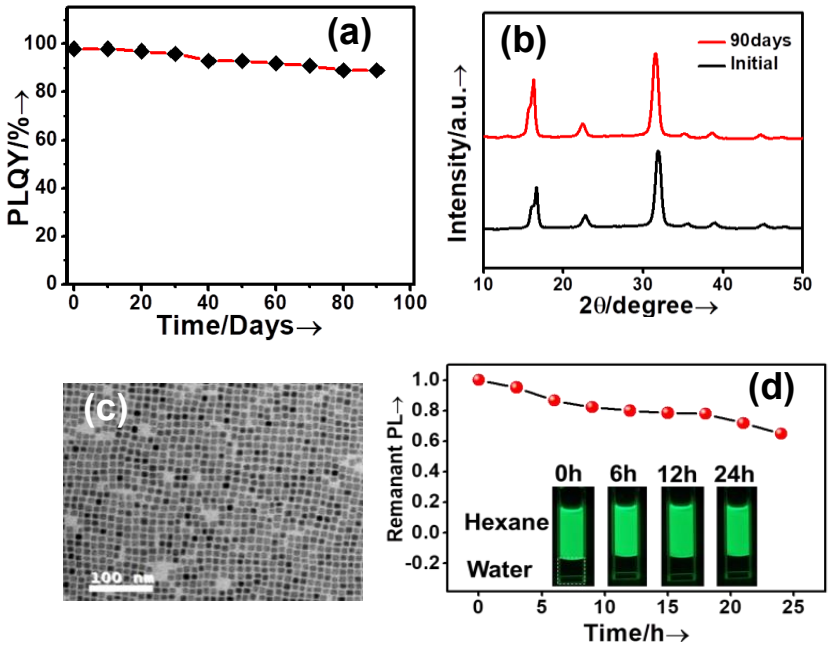

Figure 3.3. *(a) Air stability of $CsPbBr_3$ NCs under storage in ambient atmosphere (b) PXRD patterns after 90 days. (c) TEM image after 60 days. (d) Photo-stability of $CsPbBr_3$ NCs under continuous illumination of 365 nm, 8 W UV lamp in presence of water. Photographs at different time intervals under UV illumination are shown in the inset.*

Excellent photo-stability of these NCs is evident from the fact that 81% of initial PL of our $CsPbBr_3$ NCs is retained even after 24 h of continuous illumination with an 8 W, 365 nm UV

light (Figure AI.11). Water treatment of the $CsPbBr_3$ NCs generally results in rapid degradation of the NCs with loss of PLQY. However, remarkable stability of our $CsPbBr_3$ NCs is evident from the fact that nearly 70% of the initial PL is retained even 36 h after mixing 2.5 mL dispersed NCs in hexane with 1.5 mL water (Figure AI.12). The stability of the NCs towards UV irradiation in presence of water is evident from the fact that 65% of initial PL can be observed even after 24 h of continuous illumination (Figure 3.3.d and AI.13). Table 3.1, which presents a comparison of PLQY and stability of our $CsPbBr_3$ NCs with those obtained by other methods so far, highlights superior characteristics of our $CsPbBr_3$ NCs.

Table 3.1. Comparison of stability and PLQY of $CsPbBr_3$ NCs obtained by different methods

Synthesis method	PLQY	Air stability	Photo-stability
Zwitterionic ligands as capping agent[18]	90%	50 days (90%)	NA
Oleylammonium bromide as bromide precursor[29]	97%	NA	NA
Benzoyl bromide as bromide precursor[30]	92%	NA	NA
L type ligand assisted synthesis[40]	100%	NA	1 h (80%)
NBS as bromide precursor(this work)	99%	90 days (90%)	24 h(81% in hexane, 65% in hexane water mixture)

The stability of **FA**$PbBr_3$ and **MA**$PbBr_3$ NCs is also quite impressive. Nearly 85% of the initial PL of both **FA**$PbBr_3$ and **MA**$PbBr_3$ is retained after 60 days of storage in ambient atmosphere (Figure AI.14-AI.15). Photo-stability of **MA**$PbBr_3$ NCs has been a major issue as these NCs undergo rapid photo-degradation with continuous PL peak shift.[36] However, retention

of 75% of the initial PL without any change of PL peak position and FWHM (Figure 3.4.a-b) demonstrates much better photo-stability of our **MA**$PbBr_3$ NCs. **FA**$PbBr_3$ NCs also exhibit distinctive photo-stability. 80% of the initial PL is retained even after 24 h of continuous illumination (Figure AI.16). The PXRD pattern of **FA**$PbBr_3$ and **MA**$PbBr_3$ recorded after 60 days of storage reveal that the cubic crystal structure is retained without formation of secondary phase (Figure AI.17). Table AI.5, which summarizes the PL properties and stability data of a variety of green-emitting perovskite NCs obtained by different approaches, clearly highlights better optical properties and stability of the NCs obtained by our method of synthesis.

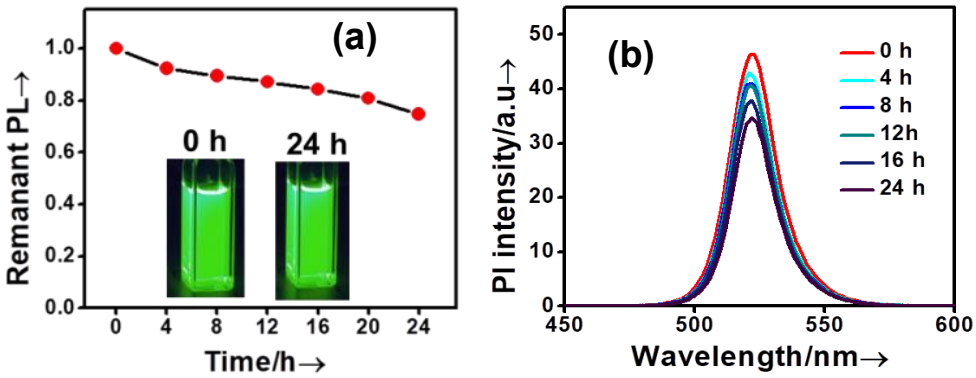

Figure 3.4. *(a) Photostability of* ***MA****$PbBr_3$ NCs on continuous illumination of 365 nm, 8 W UV lamp. Photographs at different time intervals under UV illumination are shown in the inset. b) PL emission spectra of* ***MA****$PbBr_3$ NCs at different time interval on continuous UV light illumination.*

3.3. Discussion

The factor(s) contributing to the exceptional stability and optical properties of these **A**$PbBr_3$ NCs can be understood considering that the $CsPbBr_3$ NCs obtained using a Pb:Br precursor ratio of 1:3 exhibit much improved stability and optical properties compared to those prepared using a lower Pb:Br ratio (Figure AI.18). As the EDX measurements confirm that the former samples are indeed bromide-rich (Cs:Pb:Br = 0.9:1:3.66) (Figure 3.5 and AI.19), it is evident that a bromide-rich environment helps providing better stability and PL of the NCs. This observation is consistent with current literature.[20] A second factor also needs to be considered in this context. It

is well known that alkylammonium ions enhance the stability of the $CsPbBr_3$ NCs by replacing the surface Cs^+. It is therefore very likely that oleylammonium bromide formed during our reaction replaces some surface Cs^+ forming an oleylammonium lead-bromide terminated surface, which provides necessary stability to the NCs.[44] To confirm the binding of oleylammonium cation on the surface of the NCs, we have measured the NMR and FTIR spectra of the NCs (Figure AI.21-AI.22). The NMR spectra of MeOAc-washed $CsPbBr_3$ NCs exhibit broad peak at 6.7 ppm and 3.6 ppm characteristics of the oleylammonium cation corresponding to an α-proton (NH_3^+) and β-proton (CH_2-N) respectively,[45] confirming the presence of oleylammonium cation on the surface of the NCs. The FTIR spectrum of the $CsPbBr_3$ NCs shows peaks at 1641 and 1540 cm^{-1} due to the asymmetric and symmetric bending of N^+-H bond of the oleylammonium cation[46] and reconfirms the binding of oleylammonium cation on the surface of the NCs. Hence, the superb stability and optical properties of our **A**$PbBr_3$ NCs are the outcome of formation of an oleylammonium lead-bromide terminated surface.

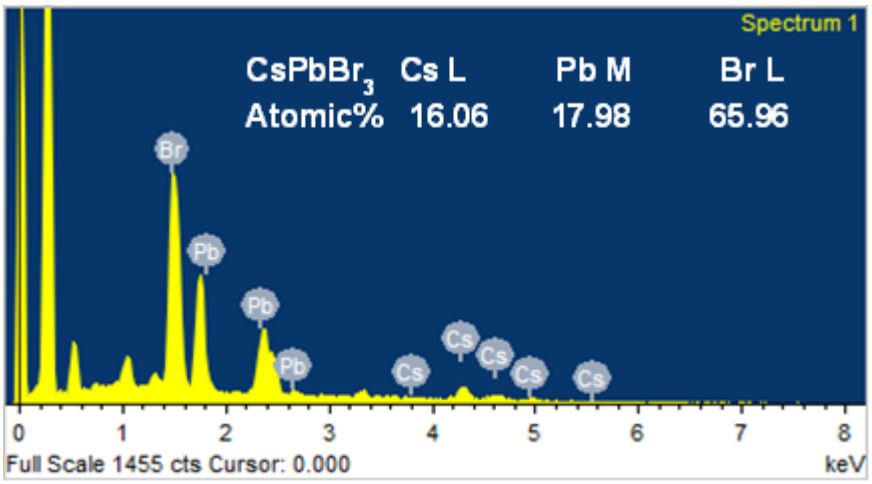

Figure 3.5. *EDX spectrum of the $CsPbBr_3$ NCs obtained using a Pb:Br precursor ratio of 1:3 in the synthesis.*

3.4. Conclusion

In conclusion, a generic method for synthesis of three commonly used green-emitting $APbBr_3$ NCs, with narrow size distribution, low PL bandwidth, near-unity PLQY and remarkable

stability under different conditions is reported for the first time employing NBS as the bromide precursor. The exceptional characteristics of these NCs, which are attributed to the formation of oleylammonium lead-bromide terminated surfaces, indicate high potential of these materials in real applications. As preliminary studies indicate applicability of this method to other halide-based perovskites using corresponding N-haloimide, the present protocol opens up new avenues for synthesis of a wide variety of perovskite NCs with high PL and stability.

3.4. Bibliography

1. Akkerman, Q. A.; Rainò, G.; Kovalenko, M. V.; Manna, L., Genesis, challenges and opportunities for colloidal lead halide perovskite nanocrystals. *Nature Materials* **2018,** 17, 394-405.

2. Huang, H.; Bodnarchuk, M. I.; Kershaw, S. V.; Kovalenko, M. V.; Rogach, A. L., Lead Halide Perovskite Nanocrystals in the Research Spotlight: Stability and Defect Tolerance. *ACS Energy Lett.* **2017,** 2, 2071-2083.

3. Zhang, F.; Zhong, H.; Chen, C.; Wu, X.-g.; Hu, X.; Huang, H.; Han, J.; Zou, B.; Dong, Y., Brightly Luminescent and Color-Tunable Colloidal $CH_3NH_3PbX_3$ (X = Br, I, Cl) Quantum Dots: Potential Alternatives for Display Technology. *ACS Nano* **2015,** 9, 4533-4542.

4. He, X.; Qiu, Y.; Yang, S., Fully Inorganic Trihalide Perovskite Nanocrystals: A New Research Frontier of Optoelectronic Materials. *Adv.Mater.* **2017,** 29, 1700775.

5. Manser, J. S.; Christians, J. A.; Kamat, P. V., Intriguing Optoelectronic Properties of Metal Halide Perovskites. *Chem. Rev.* **2016,** 116, 12956-13008.

6. Ono, L. K.; Juarez-Perez, E. J.; Q, Y., Progress on Perovskite Materials and Solar Cells with Mixed Cations and Halide Anions. *ACS Appl. Mater. Interfaces* **2017,** 9, 30197-30246.

7. Kovalenko, M. V.; Protesescu, L.; Bodnarchuk, M. I., Properties and potential optoelectronic applications of lead halide perovskite nanocrystals. *Science* **2017,** 358, 745-750.

8. Bai, S.; Yuana, Z.; Gao, F., Colloidal metal halide perovskite nanocrystals: synthesis, characterization, and applications. *J. Mater. Chem. C* **2016,** 4, 3898-3904.

9. Adjokatse, S.; Hong-HuaFang; Loi, M. A., Broadly tunable metal halide perovskitesfor solid-state light-emission applications. *Materials Today* **2017,** 20, 413-424.

10. Zhang, X.; Lin, H.; Huang, H.; Reckmeier, C.; Zhang, Y.; Choy, W. C. H.; Rogach, A. L., Enhancing the Brightness of Cesium Lead Halide Perovskite Nanocrystal Based Green Light-Emitting Devices through the Interface Engineering with Perfluorinated Ionomer. *Nano Lett.* **2016,** 16, 1415-1420.

11. Protesescu, L.; Yakunin, S.; Bodnarchuk, M. I.; Krieg, F.; Caputo, R.; Hendon, C. H.; Yang, R. X.; Walsh, A.; Kovalenko, M. V., Nanocrystals of Cesium Lead Halide Perovskites ($CsPbX_3$, X = Cl, Br, and I): Novel Optoelectronic Materials Showing Bright Emission with Wide Color Gamut. *Nano Lett.* **2015,** 15, 3692-3696.

12. Shynkarenko, Y.; Bodnarchuk, M. I.; Bernasconi, C.; Berezovska, Y.; Verteletskyi, V.; Ochsenbein, S. T.; Kovalenko, M. V., Direct Synthesis of Quaternary Alkylammonium-Capped Perovskite Nanocrystals for Efficient Blue and Green Light-Emitting Diodes. *ACS Energy Lett.* **2019,** 4, 2703-2711.

13. Protesescu, L.; Yakunin, S.; Bodnarchuk, M. I.; Bertolotti, F.; Masciocchi, N.; Guagliardi, A.; Kovalenko, M. V., Monodisperse Formamidinium Lead Bromide Nanocrystals with Bright and Stable Green Photoluminescence. *J. Am. Chem. Soc.* **2016,** 138, 14202-14205.

14. Amgar, D.; Aharon, S.; Etgar, L., Inorganic and Hybrid Organo-Metal Perovskite Nanostructures: Synthesis, Properties, and Applications. *Adv. Funct.Mater.* **2016,** 26, 8576-8593.

15. Koolyk, M.; Amgar, D.; Aharon, S.; Etgar, L., Kinetics of cesium lead halide perovskite nanoparticle growth; focusing and de-focusing of size distribution. *Nanoscale* **2016,** 8, 6403-6409.

16. Vybornyi, O.; Yakunina, S.; Kovalenko, M. V., Polar-solvent-free colloidal synthesis of highly luminescent alkylammonium lead halide perovskite nanocrystals. *Nanoscale* **2016,** 8, 6278-6283.

17. Pradhan, N., Tips and Twists in Making High Photoluminescence Quantum Yield Perovskite Nanocrystals. *ACS Energy Lett.* **2019,** 4, 1634-1638.

18. Krieg, F.; Ochsenbein, S. T.; Yakunin, S.; Brinck, S. t.; Aellen, P.; Süess, A.; Clerc, B.; Guggisberg, D.; Nazarenko, O.; Shynkarenko, Y.; Kumar, S.; Shinh, C.-J.; Infante, I.; Kovalenko, M. V., Colloidal $CsPbX_3$ (X = Cl, Br, I) Nanocrystals 2.0: Zwitterionic Capping Ligands for Improved Durability and Stability. *ACS Energy Lett.* **2018,** 3, 641-646.

19. Bodnarchuk, M. I.; Boehme, S. C.; Brinck, S. t.; Bernasconi, C.; Shynkarenko, Y.; Krieg, F.; Widmer, R.; Aeschlimann, B.; Günther, D.; Kovalenko, M. V.; Infante, I., Rationalizing and Controlling the Surface Structure and Electronic Passivation of Cesium Lead Halide Nanocrystals. *ACS Energy Lett.* **2019,** 4, 63-74.

20. Woo, J. Y.; Kim, Y.; Bae, J.; Kim, T. G.; Kim, J. W.; Lee, D. C.; Jeong, S., Highly Stable Cesium Lead Halide Perovskite Nanocrystals through in Situ Lead Halide Inorganic Passivation. *Chem. Mater.* **2017,** 29, 7088-7092.

21. Nenon, D. P.; Pressler, K.; Kang, J.; Koscher, B. A.; Olshansky, J. H.; Osowiecki, W. T.; Koc, M. A.; Wang, L.-W.; Alivisatos, A. P., Design Principles for Trap-Free $CsPbX_3$ Nanocrystals: Enumerating and Eliminating Surface Halide Vacancies with Softer Lewis Bases. *J. Am. Chem. Soc.* **2018,** 140, 17760-17772.

22. Liu, P.; Chen, W.; Wang, W.; Xu, B.; Wu, D.; Hao, J.; Cao, W.; Fang, F.; Li, Y.; Zeng, Y.; Pan, R.; Chen, S.; Cao, W.; Sun, X. W.; Wang, K., Halide-Rich Synthesized Cesium Lead Bromide Perovskite Nanocrystals for Light-Emitting Diodes with Improved Performance. *Chem. Mater.* **2017,** 29, 5168-5173.

23. Stasio, F. D.; Christodoulou, S.; Huo, N.; Konstantatos, G., Near-Unity Photoluminescence Quantum Yield in $CsPbBr_3$ Nanocrystal Solid-State Films via Postsynthesis Treatment with Lead Bromide. *Chem. Mater.* **2017,** 29, 7663-7667.

24. Bohn, B. J.; Tong, Y.; Gramlich, M.; Lai, M. L.; Döblinger, M.; Wang, K.; Hoye, R. L. Z.; Müller-Buschbauz, P.; Stranks, S. D.; Urban, A. S.; Polavarapu, L.; Feldmann, J., Boosting Tunable Blue Luminescence of Halide Perovskite Nanoplatelets through Postsynthetic Surface Trap Repair. *Nano Lett.* **2018,** 18, 5231-5238.

25. Li, F.; Liu, Y.; Wang, H.; Zhan, Q.; Liu, Q.; Xia, Z., Postsynthetic Surface Trap Removal of $CsPbX_3$ (X = Cl, Br, or I) Quantum Dots via a ZnX_2/Hexane Solution toward an Enhanced Luminescence Quantum Yield. *Chem. Mater.* **2018,** 30, 8546-8554.

26. Zheng, X.; Hou, Y.; Sun, H.-T.; Mohammed, O. F.; Sargent, E. H.; Bakr, O. M., Reducing Defects in Halide Perovskite Nanocrystals for Light Emitting Applications. *J. Phys. Chem. Lett.* **2019,** 10, 2629-2640.

27. Seth, S.; Ahmed, T.; De, A.; Samanta, A., Tackling the Defects, Stability, and Photoluminescence of $CsPbX_3$ Perovskite Nanocrystals. *ACS Energy Lett.* **2019,** 4, 1610-1618.

28. Ahmed, T.; Seth, S.; Samanta, A., Boosting the Photoluminescence of $CsPbX_3$ (X = Cl, Br, I) Perovskite Nanocrystals Covering a Wide Wavelength Range by Postsynthetic Treatment with Tetrafluoroborate Salts. *Chem. Mater.* **2018,** 30, 3633-3637.

29. Dutta, A.; Behera, R. K.; Pal, P.; Baitalik, S.; Pradhan, N., Near-Unity Photoluminescence Quantum Efficiency for All $CsPbX_3$(X=Cl, Br, and I) Perovskite Nanocrystals: A Generic Synthesis Approach. *Angew. Chem. Int. Ed.* **2019,** 58, 5552-5556.

30. Imran, M.; Caligiuri, V.; Wang, M.; Goldoni, L.; Prato, M.; Krahne, R.; Trizio, L. D.; Manna, L., Benzoyl Halides as Alternative Precursors for the Colloidal Synthesis of Lead-Based Halide Perovskite Nanocrystals. *J. Am. Chem. Soc.* **2018,** 140, 2656-2664.

31. Saikia, n.; Borah, A. J.; Phukan, P., Use of Bromine and Bromo-Organic Compounds in Organic Synthesis. *Chem. Rev.* **2016,** 116, 6837-7042.

32. Xue, H.; Tan, H.; Wei, D.; Wei, Y.; Lin, S.; Liang, F.; Zhao, B., N-Bromosuccinimide–carboxylic acid combination: mild and efficient access to dibromination of unsaturated carbonyl compounds. *RSC Adv.* **2013,** 3, 5382-5385.

33. Zhumekenov, A. A.; Saidaminov, M. I.; Haque, M. A.; Alarousu, E.; Sarmah, S. P.; Murali, B.; Dursun, I.; Miao, X.-H.; Abdelhady, A. L.; Wu, T.; Mohammed, O. F.; Bakr, O. M., Formamidinium Lead Halide Perovskite Crystals with Unprecedented Long Carrier Dynamics and Diffusion Length. *ACS Energy Lett.* **2016,** 1, 32-37.

34. Mondal, N.; De, A.; Das, S.; Paul, S.; Samanta, A., Ultrafast carrier dynamics of metal halide perovskite nanocrystals and perovskite composites. *Nanoscale* **2019,** 11, 9796-9818.

35. Mondal, N.; Samanta, A., Complete ultrafast charge carrier dynamics in photo-excited all-inorganic perovskite nanocrystals ($CsPbX_3$). *Nanoscale* **2017,** 9, 1878-1885.

36. Liu, L.; Deng, L.; Huang, S.; Zhang, P.; Linnros, J.; Zhong, H.; Sychugov, I., Photodegradation of Organometal Hybrid Perovskite Nanocrystals: Clarifying the Role of Oxygen by Single-Dot Photoluminescence. *J. Phys. Chem. Lett.* **2019,** 10, 864-869.

37. Sun, C.; Zhang, Y.; Ruan, C.; Yin, C.; Wang, X.; Wang, Y.; Yu, W. W., Efficient and Stable White LEDs with Silica-Coated Inorganic Perovskite Quantum Dots. *Adv. Mater.* **2016,** 28, 10088-10094.

38. Wang, H.-C.; Lin, S.-Y.; Tang, A.-C.; Singh, B. P.; Tong, H.-C.; Chen, C.-Y.; Lee, Y.-C.; Tsai, T.-L.; Liu, R.-S., Mesoporous Silica Particles Integrated with All-Inorganic $CsPbBr_3$ Perovskite Quantum-Dot Nanocomposites (MP-PQDs) with High Stability and Wide Color Gamut Used for Backlight Display. *Angew.Chem.Int.Ed.* **2016,** 55, 7924-7929.

39. Stam, W. v. d.; Geuchies, J. J.; Altantzis, T.; Bos, K. H. W. v. d.; Meeldijk, J. D.; Aert, S. V.; Bals, S.; Vanmaekelbergh, D.; Donega, C. d. M., Highly Emissive Divalent-Ion-Doped Colloidal $CsPb_{1-x}M_xBr_3$ Perovskite Nanocrystals through Cation Exchange. *J. Am. Chem. Soc.* **2017,** 139, 4087-4097.

40. Zhong, Q.; Cao, M.; Xu, Y.; Li, P.; Zhang, Y.; Hu, H.; Yang, D.; Xu, Y.; Wang, L.; Li, Y.; Zhang, X.; Zhang, Q., L-Type Ligand-Assisted Acid-Free Synthesis of $CsPbBr_3$

Nanocrystals with Near-Unity Photoluminescence Quantum Yield and High Stability. *Nano Lett.* **2019,** 19, 4151-4157.

41. Almeida, G.; Ashton, O. J.; Goldoni, L.; Maggioni, D.; Petralanda, U.; Mishra, N.; Akkerman, Q. A.; Infante, I.; Snaith, H. J.; Manna, L., The Phosphine Oxide Route toward Lead Halide Perovskite Nanocrystals. *J. Am. Chem. Soc.* **2018,** 140, 14878-14886.

42. Imran, M.; Ijaz, P.; Baranov, D.; Goldoni, L.; Petralanda, U.; Akkerman, Q.; Abdelhady, A. L.; Prato, M.; Bianchini, P.; Infante, I.; Mann, L., Shape-Pure, Nearly Monodispersed $CsPbBr_3$ Nanocubes Prepared Using Secondary Aliphatic Amines. *Nano Lett.* **2018,** 18, 7822-7831.

43. Mondal, N.; De, A.; Samanta, A., Achieving Near-Unity Photoluminescence Efficiency for Blue-Violet-Emitting Perovskite Nanocrystals. *ACS Energy Lett.* **2019,** 4, 32-39.

44. Ravi, V. K.; Santra, P. K.; Joshi, N.; Chugh, J.; Singh, S. K.; Rensmo, H.; Ghosh, P.; Nag, A., Origin of the Substitution Mechanism for the Binding of Organic Ligands on the Surface of $CsPbBr_3$ Perovskite Nanocubes. *J. Phys. Chem. Lett.* **2017,** 8, 4988-4994.

45. Roo, J. D.;˜ez, M. I.; Geiregat, P.; Nedelcu, G.; Walravens, W.; Maes, J.; Martins, J. C.; Driessche, I. V.; Kovalenko, M. V.; Hens, Z., Highly Dynamic Ligand Binding and Light Absorption Coefficient of Cesium Lead Bromide Perovskite Nanocrystals. *ACS Nano* **2016,** 10, 2071-2081.

46. Dutta, A.; Dutta, S. K.; Adhikari, S. D.; Pradhan, N., Phase-Stable $CsPbI_3$ Nanocrystals: The Reaction Temperature Matters. *Angew. Chem. Int. Ed.* **2018,** 57, 9083-9087.

CHAPTER 4

Effect of Lead:Halide Precursor Ratio on the Photoluminescence and Carrier Dynamics of Violet- and Blue-Emitting Lead Halide Perovskite Nanocrystals

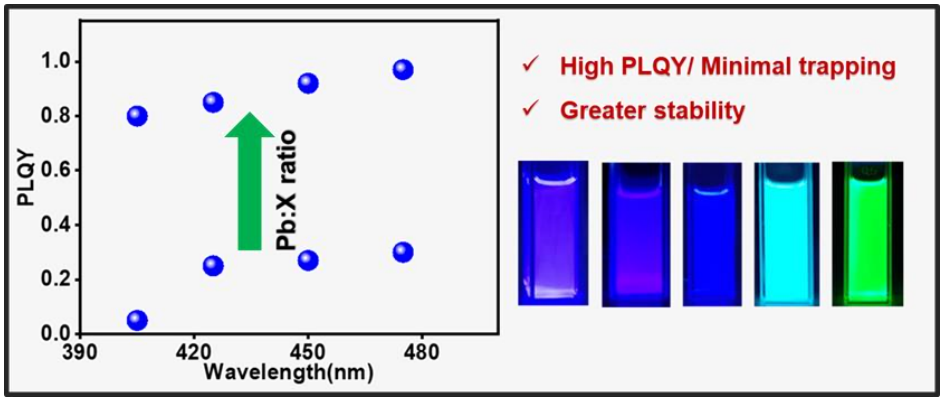

Overview

Highly luminescent caesium lead halide ($CsPbX_3$, X = Cl, Br, I) perovskite nanocrystals (NCs) are promising materials for a number of optoelectronic applications like LEDs, and other display technologies. However, low photoluminescence (PL) quantum yield (QY) of the large-bandgap violet- and blue-emitting $CsPbCl_3$ and $CsPb(Cl/Br)_3$ NCs is an obstacle to the development of blue- and white-emitting LEDs. In this work, we show that these NCs with high PLQY can be obtained directly employing an appropriate halide precursor and by optimizing the Pb:X precursor ratio. Specifically, employing N-chloro- and N-bromo-phthalimides as halide precursors and by varying the Pb:X precursor ratio, we have obtained stable and highly luminescent (PLQY 80 - 99%) perovskite NCs emitting in the blue-violet region extending to green by direct synthesis. Time-resolved PL and ultrafast pump-probe studies of these systems reveal the effect of Pb:X precursor ratio on the carrier recombination processes. Rapid carrier trapping is found to be the dominant process that impairs the PLQY of the NCs obtained using a stoichiometric (1:3) Pb:X precursor ratio. This trapping of carriers is effectively alleviated by using a higher Pb:X precursor ratio during the preparation of the NCs. The results brighten potential utility of these high-quality perovskite NCs emitting in the blue-violet region in optical applications.

4.1. Introduction

Because of their great potential in diverse applications like in photovoltaics, LEDs, display technologies, lasing, etc., the caesium lead halide ($CsPbX_3$, X = Cl, Br, I) perovskite NCs continue to receive great attention of the researchers.[1-13] High PLQY and ease of tunability of the PL band position across the entire visible region make these substances quite attractive for optoelectronic applications.[8-11, 14, 15] In this family of perovskites, $CsPbCl_3$ and $CsPb(Cl/Br)_3$ NCs are considered indispensable due to their violet and blue emission, which are essential color components for fabrication of white LEDs.[16-20] Unlike the conventional metal chalcogenide semiconductor NCs, the halide perovskites generally exhibit high PLQY due to their defect-tolerant nature.[5, 21-23] However, compared to their green- and red-emitting counterparts, $CsPbBr_3$ and $CsPbI_3$, the large-bandgap perovskites such as violet- and blue-emitting $CsPbCl_3$ and $CsPb(Cl/Br)_3$ NCs most often exhibit much lower PLQY due to competing nonradiative recombination of the photo-generated charge carriers through the deep trap states generated by halide vacancies and distorted $[PbX_6]^{4-}$ octahedral units.[9, 22, 24-26] Since the first synthesis of these NCs by hot-injection (HI) method,[9] several methodologies have been developed for the preparation of violet- and blue-emitting $CsPCl_3$ and $CsPb(Cl/Br)_3$ NCs with higher PLQY.[17, 22, 27, 28-36] Doping with different bivalent metal ions[16, 18, 19, 28, 29, 31, 33, 37, 38] and a variety of post-synthetic treatments of the as-synthesized NCs[17, 24, 32, 35, 36, 39, 40] are the most common practices for improving the PLQY of these NCs. Considering that in the first synthesis of the $CsPbX_3$ NCs,[9] PbX_2 was used as precursor for both lead and halogen, which gave X:Pb molar precursor ratio of only 2 in the reaction system (less than the required value of 3), Manna and coworkers used separate precursor for each constituent and succeeded in obtaining highly luminescent perovskite NCs in direct synthesis.[30] They could obtain $CsPbCl_3$ NCs with PLQY of 65% using benzoyl chloride as chloride precursor.[30] Pradhan and coworkers recently prepared $CsPbCl_3$ NCs with very high PLQY (~97%) using oleylammonium chloride as the chloride source.[34] However, the blue-emitting $CsPb(Cl/Br)_3$ NCs were not reported.[34]

As halide precursor is an important element in direct synthesis of the NCs, many recent studies are directed towards finding the right candidate for this purpose. Recently, we found N-

bromosuccinimide (**NBS**) as an excellent bromide precursor using which highly luminescent green-emitting $CsPbBr_3$ NCs could be obtained in direct synthesis.[41] This success prompted us to explore the efficacy of structurally related other haloimides for the preparation of quality violet- and blue-emitting NCs, which can perhaps be used in optoelectronic applications. These studies led to the identification of two phthalimide derivatives, N-chlorophthalimide (**NCP**) and N-bromophthalimide (**NBP**), as halide precursors, for obtaining high quality NCs emitting in blue-violet, extending even to the green region. As halide vacancies lead to the formation of the mid-bandgap states, which facilitate nonradiative recombination of the photo-generated carriers and decrease the PLQY of the NCs, the PL properties of these systems are also expected to depend on Pb:X precursor ratio during the reaction. For this reason, we have prepared different samples of each system by varying the Pb:X precursor ratios, determined the optimized conditions for obtaining these systems with high PL efficiency and examined the influence of the Pb:X ratio on carrier recombination processes by time-resolved PL and pump-probe studies.

4.2. Results

4.2.1 Structural Characterization

We prepared three different samples of violet-emitting $CsPbCl_3$ NCs using molar Pb:Cl precursor ratios of 1:3, 1:6 and 1:9. For the blue (420-480 nm) region, we prepared mixed halide NCs, $CsPbCl_2Br$, $CsPbCl_{1.5}Br_{1.5}$ and $CsPbClBr_2$, and for each system, two different samples were prepared using Pb:X (Cl and Br) molar precursor ratios of 1:3 and 1:6. For each sample, the molar Pb:X precursor ratio is indicated in the bracket after the formula of the system. We also prepared green-emitting $CsPbBr_3$ NCs using stoichiometric Pb:Br ratio of 1:3 for comparative purpose. Bright field TEM images (Figure 4.1 and AII.1) indicate cubic shape of the NCs obtained under optimized conditions. The average edge lengths of the $CsPbCl_3$(1:3), $CsPbCl_3$(1:6) and $CsPbCl_3$(1:9) NCs are found to be 10±2.0, 9.0±2.0 and 8.0±1.0 nm, respectively (Figure 4.1.A-C and AII.2). A decrease in size and improved mono-dispersity of the NCs with increase in the amount of the chloride precursor (NCP) is similar to the trend observed for $CsPbBr_3$ NCs.[43] The $CsPbCl_2Br$(1:6), $CsPbCl_{1.5}Br_{1.5}$(1:6) and $CsPbClBr_2$(1:6) NCs obtained

under the optimized condition show average size of 9.0±1.5, 8.5±1.0 and 8.0±1.5 nm, respectively (Figure 4.1. D-F and AII.2.). For these systems also a decrease in average size (by 1.5-2.5 nm) and a narrower size distribution is observed for 1:6 Pb:X precursor ratio. Powder X-ray diffraction (PXRD) patterns suggest orthorhombic crystal structure of the NCs (Figure AII.3.) with no evidence of any secondary phases. For higher bromide content, the PXRD peaks shift towards lower angle indicating lattice expansion due to larger ionic radii of Br^- compared to Cl^-

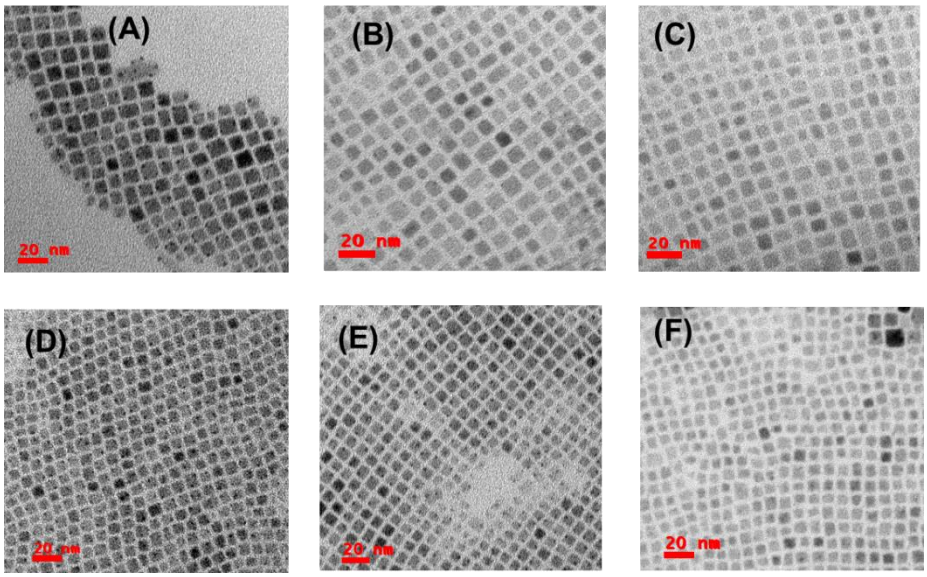

Figure 4.1. *TEM images of the* ***(A)*** *$CsPbCl_3$(1:3),* ***(B)*** *$CsPbCl_3$(1:6),* ***(C)*** *$CsPbCl_3$(1:9),* ***(D)*** *$CsPbCl_2Br$(1:6)* ***(E)*** *$CsPbCl_{1.5}Br_{1.5}$(1:6) and* ***(F)*** *$CsPbClBr_2$(1:6) NCs. The scale bar is 20 nm in all cases.*

4.2.2. Photoluminescence and Carrier Relaxation Dynamics

The UV-vis absorption and fluorescence spectra of some representative samples are shown in Figure 4.2.A and 4.2.B, respectively. A summary of the spectral data and PLQY values of all samples (including $CsPbBr_3$ NCs) are collected in Table 4.1. The PL of the $CsPbCl_3$ NCs is characterized by a peak between 404-407 nm and a narrow full width at half maximum (FWHM) of 9-12 nm. With increasing Pb:Cl molar precursor ratio a small (2-3 nm) blue shift of the PL maximum and slight (by 2-3 nm) decrease in FWHM is observed (Figure 4.2.C). For the mixed

halide perovskite NCs, $CsPbCl_2Br$, $CsPbCl_{1.5}Br_{1.5}$ and $CsPbClBr_2$, the PL maxima appear at 430±5, 451±6 and 473±5 nm with FWHM of 14-15, 15-17 and 17-18 nm, respectively (Figure 4.2.B). For these systems, no noticeable change in PL peak position and spectral bandwidth is observed with change in Pb:X precursor ratio. Though the spectral features of the systems show small/negligible dependence on the Pb:X precursor ratio, the PLQY values change drastically depending on this ratio. As can be seen from Table 4.1, the PLQY changes from 5 to 80% for $CsPbCl_3$, 25 to 85% for $CsPbCl_2Br$, 27 to 92% for $CsPbCl_{1.5}Br_{1.5}$ and 30 to 97% for $CsPbClBr_2$ NCs (Figure 4.2.C, 4.2.D and AII.4).

An important point to note here is that $CsPbBr_3$ NCs with near-unity (~99%) PLQY is obtained using a stoichiometric (1:3) Pb:Br precursor ratio, however, for all other systems, an excess amount of halide precursor is necessary for obtaining the most luminescent sample. For the mixed halide systems, $CsPbCl_2Br$, $CsPbCl_{1.5}Br_{1.5}$ and $CsPbClBr_2$ NCs, most luminescent system is obtained for a Pb:X precursor ratio of 1:6; however, for $CsPbCl_3$ NCs, 1:9 Pb:Cl ratio yielded the most luminous sample (PLQY of 80%). To find out the cause of significant dependence of PLQY on the Pb:X precursor ratio we have determined the Pb:X ratio in the prepared samples by energy dispersive X-ray (EDX) measurements. These measurements reveal that actual Pb:Cl ratios in $CsPbCl_3$(1:3), $CsPbCl_3$(1:6) and $CsPbCl_3$(1:9) NCs are 1:2.90, 1:3.24 and 1:3.45 respectively (Figure AII.5 and Table AII.2). The actual ratios in the prepared mixed halide perovskite NCs were also determined (Figure II.5 and Table AII.2). The Pb:X ratios in $CsPbCl_{1.5}Br_{1.5}$ NCs synthesized using 1:3 and 1:6 Pb:X precursor ratio are found to be 1:2.98 and 1:3.53, respectively. Interestingly, the EDX data of $CsPbBr_3$ NCs prepared by stoichiometric Pb:Br precursor ratio indicated a halide rich surface with actual Pb:Br ratio of 1:3.36 (Table AII.2). A much higher Pb:X precursor ratio required for obtaining most photo-luminescent sample of $CsPbCl_3$ is a reflection of greater halide vacancy in these NCs, as indicated by the EDX data (Table AII.2).

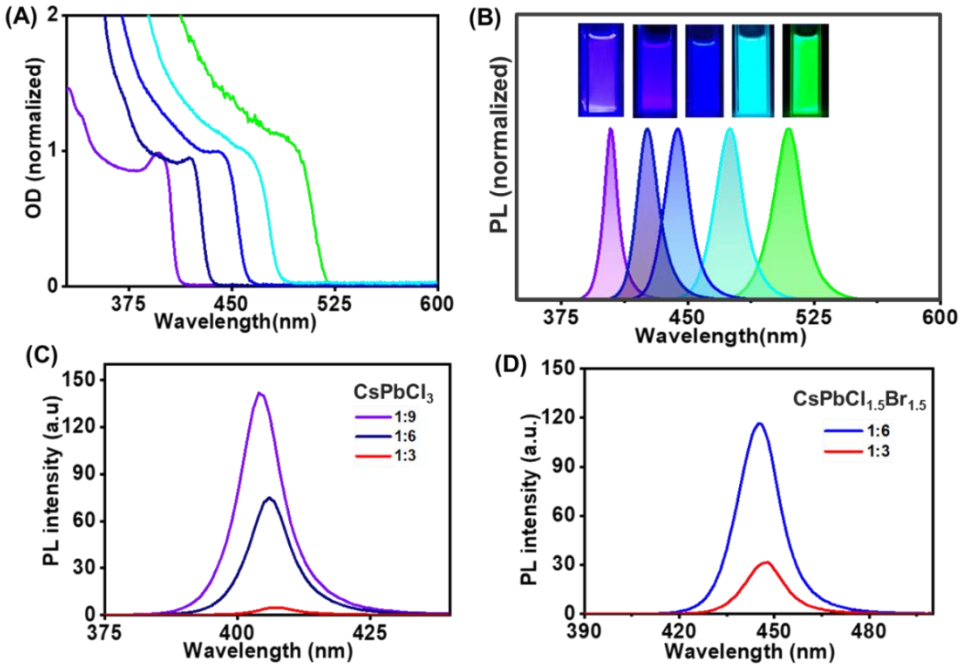

Figure 4.2.: *Normalized absorption* ***(A)*** *and* ***(B)*** *PL spectra (λ_{ex} = 350 nm) of dilute colloidal solutions of $CsPbCl_3$(1:9), $CsPbCl_2Br$(1:6), $CsPbCl_{1.5}Br_{1.5}$(1:6), $CsPbClBr_2$(1:6) and $CsPbBr_3$ NCs, respectively in hexane. Panel* ***(B)*** *also shows digital photographs of the colloidal solutions of the $CsPbCl_3$(1:9), $CsPbCl_2Br$(1:6), $CsPbCl_{1.5}Br_{1.5}$(1:6), $CsPbClBr_2$(1:6) and $CsPbBr_3$ nanocrystals under illuminations (365 nm). Panel* ***(C)*** *and* ***(D)*** *show the dependence of PL spectra of $CsPbCl_3$ and $CsPbCl_{1.5}Br_{1.5}$ NCs, respectively on the Pb:X (Cl and Br) precursor ratio.*

As stated before that choice of N-halophthalimide as halide precursor was guided by our earlier work where we have used N-bromosuccinimide as bromide precursor for the synthesis of green emitting perovskite NCs.[39] Herein, we prepared these violet-blue emitting NCs also using N-chlorosuccinimide and N-bromosuccinimide as halide precursors. We found that N-chlorosuccinimide and N-bromosuccinimide leads to a maximum PLQY of 70%, 80%, 85%, 95% for $CsPbCl_3$(1:9), $CsPbCl_2Br$(1:6), $CsPbCl_{1.5}Br_{1.5}$(1:6) and $CsPbClBr_2$(1:6) NCs, respectively (Figure AII.3). These data suggest that highly luminescent violet and blue emitting perovskite NCs can be prepared by using N-halosuccinimide when it is dealt with appropriate Pb:X ratio.

Table 4.1. *PL parameters of different samples of the $CsPbCl_3$, $CsPb(Cl/Br)_3$ and $CsPbBr_3$ NCs obtained by using N-halophthalimide as halide precursor.*

System	Pb:X precursor ratio	PLQY (%)	λ_{max} (nm)	FWHM (nm)
$CsPbCl_3$	1:3	5	407	12
	1:6	40	406	10
	1:9	80	404	9
$CsPbCl_2Br$	1:3	25	426	15
	1:6	85	428	14
$CsPbCl_{1.5}Br_{1.5}$	1:3	27	447	17
	1:6	92	447	15
$CsPbClBr_2$	1:3	30	474	18
	1:6	97	475	17
$CsPbBr_3$	1:3	99	510	20

To understand the influence of Pb:X ratio on carrier recombination processes of the NCs we have studied the PL decay behavior and transient absorption (TA) spectra of these systems. Except for the $CsPbBr_3$ NCs, PL decay profiles of all the samples (Figure 4.3) are found to be tri-exponential. The PL decay parameters of the samples are collected in Table 4.2. As can be seen, for $CsPbCl_3$(1:3) NCs, the PL decay consists of two short components, 70 (0.52) and 490 ps (0.28), which are much faster than the radiative lifetime of $CsPbCl_3$ NCs,[9, 16, 19] and hence, can be attributed to the trap state mediated recombination processes. The long 5.28 ns component with 20% contribution clearly represents direct excitonic recombination process. The $CsPbCl_3$(1:6) and $CsPbCl_3$(1:9) NCs are characterized by a short PL decay component (0.6-0.7 ns), a long component (11.90-21.60 ns) and a third component with lifetime of 2.97-5.50 ns. The short component is assigned to trap state mediated recombination,[9, 16, 19] the intermediate component (2.97-5.50 ns) to direct excitonic recombination from the band-edge and the long component (11.90-21.60 ns) to band-edge recombination after trapping and de-trapping of the cariers.[19, 44] The contribution of the trapping component decreases from 36% in $CsPbCl_3$(1:6) to 20% in $CsPbCl_3$(1:9). Unlike in $CsPbCl_3$(1:3) NCs, no trapping component with time constant of

<100 ps could be observed for the $CsPbCl_2Br$(1:3), $CsPbCl_{1.5}Br_{1.5}$(1:3) and $CsPbClBr_2$(1:3) NCs; however, a sub-ns trapping component with time constant between 0.40-0.92 ns can be found. For samples with higher Pb:X precursor ratio, for example, for $CsPbCl_{1.5}Br_{1.5}$(1:6) and $CsPbCl_2Br$ NCs(1:6), the contribution of the trapping component is significantly lower (<10%) and for the $CsPbClBr_2$(1:6) NCs, no <1 ns lifetime component could be observed. The contribution of the direct excitonic recombination component (2.4-7.6 ns) increases significantly with increase in Pb:X precursor ratio from 1:3 to 1:6 for these mixed halide NCs. The nonradiative rate constant (k_{nr}), estimated from the measured PLQY and average PL lifetime (Table 4.2), is found to decrease from 7.77×10^8 s^{-1} in $CsPbCl_3$(1:3) NCs to 1.6×10^7 s^{-1} in $CsPbCl_3$(1:9) NCs. The k_{nr} values for the $CsPbCl_2Br$, $CsPbCl_{1.5}Br_{1.5}$ and $CsPbClBr_2$ NCs decrease by factors of 10, 17 and 23, respectively on increasing the Pb:X precursor ratio from 1:3 to 1:6. No sub-ns trapping component could be observed for the $CsPbBr_3$ NCs (Figure AII.6. and Table 4.2) obtained using stoichiometric (1:3) Pb:Br precursor ratio and this observation is consistent with its near-unity PLQY. Lower PLQY, shorter PL lifetime and higher nonradiative recombination rate of the $CsPbCl_3$ and $CsPb(Cl/Br)_3$ NCs obtained by using stoichiometric Pb:X (1:3) precursor ratio confirm that halide deficiencies in these NCs serve as major carrier trapping centers.

Due to limited time resolution (~54 ps) of our TCSPC setup, faster trapping process (if any) cannot be precisely estimated using this setup. For this reason, we have examined the transient absorption (TA) behavior of the $CsPbCl_3$ NCs using pump-probe technique with femto-second time resolution (λ_{exc} = 350 nm, pump power of 4-5 $\mu J/cm^2$). The TA-spectra of the $CsPbCl_3$ NCs are characterized by a sharp negative signal at 403 nm and positive signal on both sides of it (Figure 4.4.4A and 4.4.B). The negative (bleach) signal is induced by state filling of the electron and hole in the band edges.[45-47] The bleach recovery kinetics of the $CsPbCl_3$(1:3) NCs is characterized by two fast components , 4 (16%) and 41 ps (55%), and a much slower component (>750 ps (29%)) (Figure 4.4.C and Table 4.3), the exact value of which cannot be estimated accurately in this setup as it falls beyond the time-window of this femtosecond setup.

The fast components are attributed to carrier trapping and the long component to direct band-edge carrier recombination.[19, 31, 46, 47]

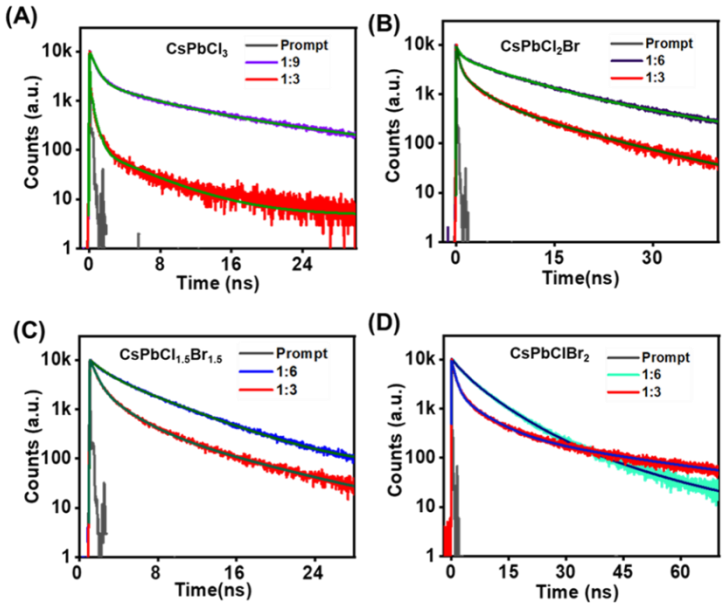

Figure 4.3.: *Dependence of the PL decay profile of the* ***(A)*** *$CsPbCl_3$* ***(B)*** *$CsPbCl_2Br$,* ***(C)*** *$CsPbCl_{1.5}Br_{1.5}$ and* ***(D)*** *$CsPbClBr_2$ NCs on the Pb:X precursor ratio.*

Table 2: *PL decay parameters of different samples of $CsPbCl_3$, $CsPb(Cl/Br)_3$ and $CsPbBr_3$ NCs.*

System	τ_1/ ns (a_1)	τ_2/ ns (a_2)	τ_3/ ns (a_3)	$<\tau_{ins}>$/ ns	$^{a}k_{nr}$($\times10^8 s^{-1}$)
$CsPbCl_3$(1:3)	0.07 (0.52)	0.49 (0.28)	5.28 (0.20)	1.23	7.77
$CsPbCl_3$(1:6)	0.60 (0.36)	2.97 (0.32)	11.90 (0.32)	4.97	1.20
$CsPbCl_3$(1:9)	0.70 (0.20)	5.50 (0.34)	21.60 (0.46)	11.95	0.16
$CsPbCl_2Br$(1:3)	0.40 (0.16)	2.86 (0.33)	11.88 (0.51)	7.06	1.06
$CsPbCl_2Br$(1:6)	0.60 (0.04)	7.60 (0.48)	22.08 (0.48)	14.27	0.105
$CsPbCl_{1.5}Br_{1.5}$(1:3)	0.62 (0.30)	2.40 (0.40)	8.17 (0.30)	3.60	2.03
$CsPbCl_{1.5}Br_{1.5}$(1:6)	1.1 (0.07)	4.64 (0.68)	12.50 (0.25)	6.36	0.12
$CsPbClBr_2$(1:3)	0.92 (0.37)	6.22 (0.26)	32.00 (0.37)	13.80	0.51
$CsPbClBr_2$(1:6)	2.48 (0.2)	6.78 (0.53)	35.40 (0.27)	13.64	0.022
$CsPbBr_3$	2.70 (0.51)	9.73 (0.49)	----	6.13	0.016

$^{a}k_{nr}=(1-PLQY)/<\tau_{ins}>$

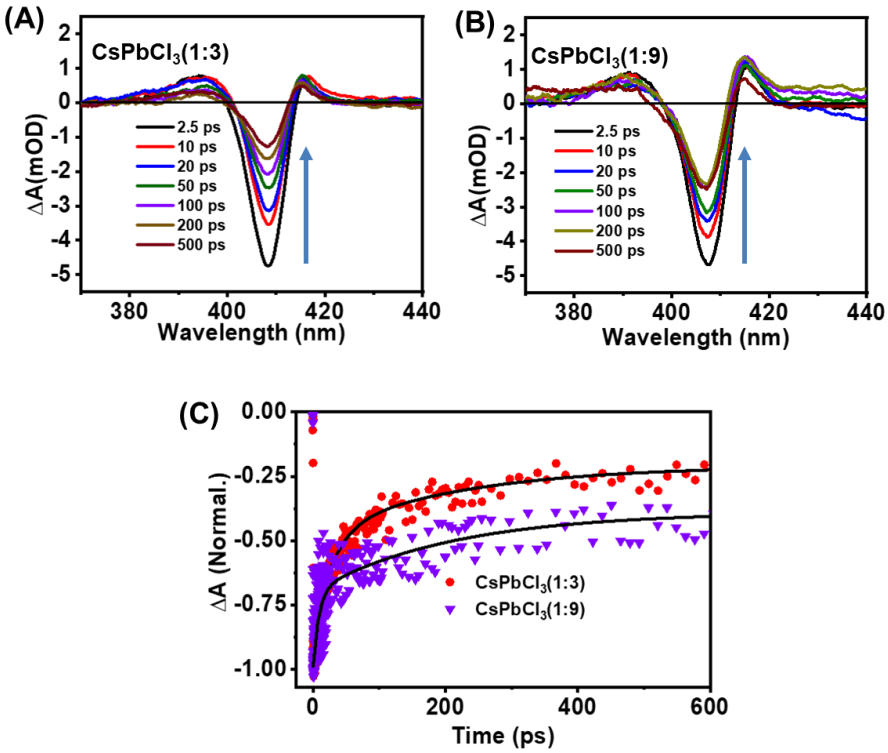

Figure 4.4. *Panels* ***(A)*** *and* ***(B)*** *depict the TA spectra of the $CsPbCl_3$(1:3) and $CsPbCl_3$(1:9) NCs at different delay times. Panel* ***(C)*** *compares the bleach recovery kinetics of the two samples monitored at bleach maximum position.*

The observed 41 ps time component of the bleach recovery kinetics is comparable to the 70 ps PL component of similar origin. As can be seen, the carrier trapping component is suppressed (from 71% to 41%) with increase in Pb:X precursor ratio from 1:3 to 1:9 (Figure 4.4.C and Table 4.3). This reconfirms that halide deficiency in these NCs leads to the formation of trap states and trapping of the carriers occurs in picosecond timescale. One important point to note in this context is that the bleach recovery kinetics of the $CsPbCl_3$(1:9) NCs still comprises 41% of a fast trapping component (~4.73 ps). This suggests that in addition to the halide vacancies, other factor like structural distortion of the octahedral $[PbX_6]^{4-}$ contribute to the defect states in these NCs, as shown recently by Sun and coworkers.[16]

Table 4.3. *Kinetic parameters of the bleach recovery dynamics of $CsPbCl_3$ NCs.*

System	τ_1/ ps (a_1)	τ_2/ ps (a_2)	τ_3/ ps (a_3)
$CsPbCl_3$(1:3)	4.0±0.15 (0.16)	41.05±2.8 (0.55)	>750 (0.29)
$CsPbCl_3$(1:9)	4.73±1.2 (0.41)	----	>750 (0.59)

4.2.3. Stability of the NCs

In addition to high PLQY, the NCs obtained by our method exhibit very good stability. For example, when kept under ambient condition, 85% of initial PL of a dilute (~10 nM) colloidal solution of $CsPbCl_3$(1:9) NCs in hexane is retained after 14 days with no change in PL peak position (Figure 4.5.5A and AII.7). Under similar condition, only 30% of initial PL intensity of $CsPbCl_3$(1:3) NCs is retained (Figure 4.5.A). Mixed halide perovskite NCs generally exhibit low stability due to phase segregation,[48, 49] but these NCs also show impressive stability. For example, $CsPbCl_{1.5}Br_{1.5}$(1:6) NCs retain 75% of its initial PL intensity without any change in PL peak position after 14 days of storage in ambient condition, whereas, for $CsPbCl_{1.5}Br_{1.5}$(1:3) NCs, only 25% of initial PL is retained (Figure 4.5.B and AII.7).

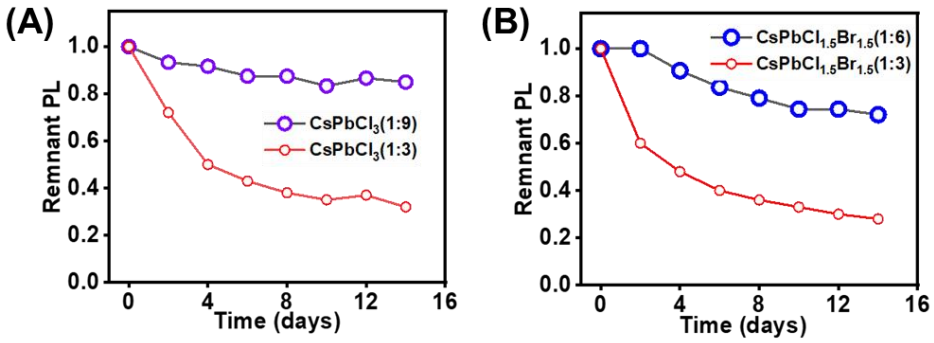

Figure 5.1. *Air stability of different samples of* ***(A)*** *$CsPbCl_3$ NCs and* ***(B)*** *$CsPbCl_{1.5}Br_{1.5}$ NCs under ambient condition. Stability was checked using dilute (~10 nM) NCs solution in hexane.*

4.3. Discussion

The $CsPbCl_3$ and $CsPb(Cl/Br)_3$ NCs obtained using a stoichiometric Pb:X precursor ratio are halide-deficient having a large density of the trap states, which facilitate nonradiative deactivation of the charge carriers and decrease the PLQY of the systems. However, the NCs obtained using higher Pb:X precursor

ratios possess halide-rich surface with fewer trap states arising only from the inherent structural distortion in these systems. This is pictorially illustrated in Scheme 1. As the alkylammonium ions are known to enhance the stability of the $CsPbX_3$ NCs by replacing the surface Cs^+, it is quite likely that oleylammonium halide formed during the reaction (Scheme S1) also contributes to the stability of the systems by forming an oleylammonium halide-terminated surface. A comparison of the PLQY and stability of $CsPbCl_3$ and $CsPb(Cl/Br)_3$ NCs obtained so far by direct synthesis (Table AII.3) reveals high quality of our samples. Our violet-emitting $CsPbCl_3$ NCs with 80% PLQY are the second best and blue-emitting $CsPb(Cl/Br)_3$ NCs with 85-97% PLQY are by far the best directly prepared samples as far as the PL efficiency is concerned. In terms of stability also, the present samples stand out.

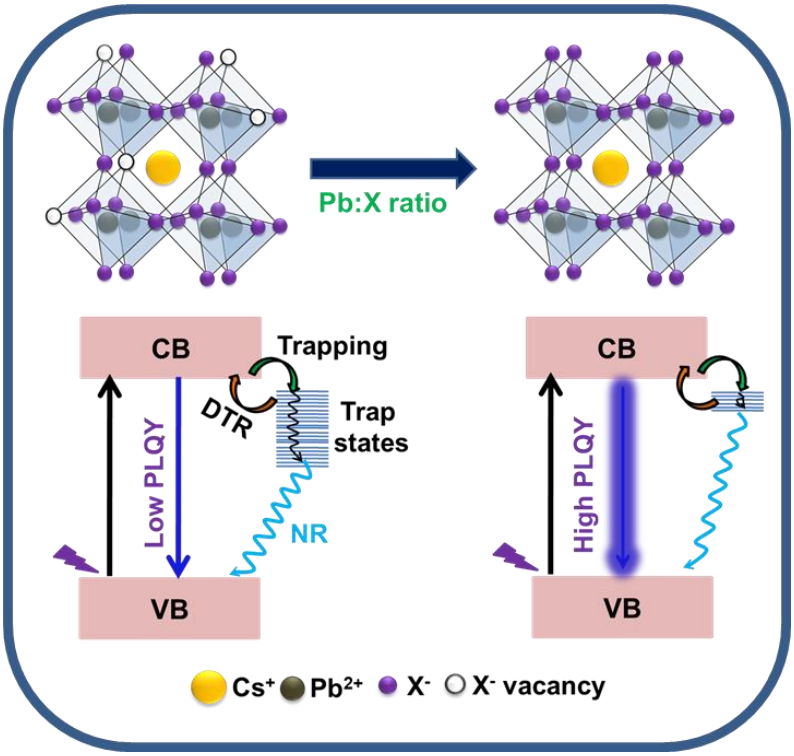

Scheme 4.1. *Schematic illustration of the influence of an increasing Pb:X precursor ratio on the PL properties of the $CsPbCl_3$ and $CsPb(Cl/Br)_3$ NCs. NR and DTR represent nonradiative recombination and detrapping processes, respectively.*

4.4. Conclusion

Highly luminescent (PLQY~80-99%) and stable $CsPbCl_3$, $CsPb(Cl/Br)_3$ and $CsPbBr_3$ NCs with narrow size distribution emitting in the violet, blue, and green region (405-510 nm) have been obtained by direct synthesis employing N-halophthalimides as halide precursor and by optimizing the Pb:X precursor ratio. The results show that when the key issue, halide-deficiency of the surface of the NCs, is dealt with using an effective halide precursor and appropriate Pb:X precursor ratio, it is indeed possible to directly obtain highly luminescent and stable NCs even for the blue-violet region. The time-resolved PL and ultrafast pump-probe measurements show dependence of the carrier trapping processes on the Pb:X precursor ratio and that carrier trapping is greatly suppressed when these NCs are prepared using higher than stoichiometric Pb:X precursor ratio.

4.4. Bibliography

1. Dey, A.; Ye, J.; De, A.; Debroye, E.; Ha, S. K.; Bladt, E.; Kshirsagar, A. S.; Wang, Z.; Yin, J.; Wang, Y.; et al. State of the Art and Prospects for Halide Perovskite Nanocrystals. *ACS Nano* **2021,** *15,* 10775-10981.

2. Kojima, A.; Teshima, K.; Shirai, Y.; Miyasaka, T. Organometal Halide Perovskites as Visible-Light Sensitizers for Photovoltaic Cells. *J. Am. Chem. Soc.* **2009,** *131,* 6050-6051.

3. Heo, J. H.; Im, S. H.; Noh, J. H.; Mandal, T. N.; Lim, C.-S.; Chang, J. A.; Lee, Y. H.; Kim, H.-J.; Sarkar, A.; Nazeeruddin, M. K.; et al. Efficient Inorganic–Organic Hybrid Heterojunction Solar Cells Containing Perovskite Compound and Polymeric Hole Conductors. *Nat. Photonics* **2013,** *7,* 486-491.

4. Lee, M. M.; Teuscher, J.; Miyasaka, T.; Murakami, T. N.; Snaith, H. J. Efficient Hybrid Solar Cells Based on Meso-Superstructured Organometal Halide Perovskites. *Science* **2012,** *338,* 643-647.

5. Kovalenko, M. V.; Protesescu, L.; Bodnarchuk, M. I. Properties and Potential Optoelectronic Applications of Lead Halide Perovskite Nanocrystals. *Science* **2017,** *358,* 745-750.

6. Correa-Baena, J.-P.; Abate, A.; Saliba, M.; Tress, W.; Jacobsson, T. J.; Gratzel, M.; Hagfeldt, A. The Rapid Evolution of Highly Efficient Perovskite Solar Cells. *Energy Environ. Sci.* **2017,** *10,* 710-727.

7. Sanehira, E. M.; Marshall, A. R.; Christians, J. A.; Harvey, S. P.; Ciesielski, P. N.; Wheeler, L. M.; Schulz, P.; Lin, L. Y.; Beard, M. C.; Luther, J. M. Enhanced Mobility $CsPbI_3$ Quantum Dot Arrays for Record-Efficiency, High-Voltage Photovoltaic Cells. *Sci. Adv.* **2017,** *3,* eaao4204.

8. Sutherland, B. R.; Sargent, E. H. Perovskite Photonic Sources. *Nat. Photonics* **2016,** *10,* 295-302.

9. Protesescu, L.; Yakunin, S.; Bodnarchuk, M. I.; Krieg, F.; Caputo, R.; Hendon, C. H.; Yang, R. X.; Walsh, A.; Kovalenko, M. V. Nanocrystals of Cesium Lead Halide Perovskites ($CsPbX_3$, X = Cl, Br, and I): Novel Optoelectronic Materials Showing Bright Emission with Wide Color Gamut. *Nano Lett.* **2015,** *15,* 3692-3696.

10. Yakunin, S.; Protesescu, L.; Krieg, F.; Bodnarchuk, M. I.; Nedelcu, G.; Humer, M.; Luca, G. D.; Fiebig, M.; Heiss, W.; Kovalenko, M. V. Low-Threshold Amplified Spontaneous Emission and Lasing from Colloidal Nanocrystals of Caesium Lead Halide Perovskites. *Nat. Commun.* **2015,** *6,* 8056.

11. Akkerman, Q. A.; Gandini, M.; Stasio, F. D.; Rastogi, P.; Palazon, F.; Bertoni, G.; Ball, J. M.; Prato, M.; Petrozza, A.; Manna, L. Strongly Emissive Perovskite Nanocrystal Inks for High-Voltage Solar cells. *Nat. Energy* **2017,** *2,* 16194.

12. Mondal, N.; De, A.; Seth, S.; Ahmed, T.; Das, S.; Paul, S.; Gautam, R. K.; Samanta, A. Dark Excitons of the Perovskites and Sensitization of Molecular Triplets. *ACS Energy Lett.* **2021,** *6,* 588-597.

13. Ahmed, T.; De, A.; Paul, S.; Samanta, A. Individual Particle-Level Picture of Charge Carrier Recombination in Bi-Doped $CsPbBr_3$ Nanocrystals. *J. Phys. Chem. C* **2021,** *125,* 2156-2162.

14. Tong, Y.; Bladt, E.; Aygüler, M. F.; Manzi, A.; Milowska, K. Z.; Hintermayr, V. A.; Docampo, P.; Bals, S.; Urban, A. S.; Polavarapu, L.; et al. Highly Luminescent Cesium Lead

Halide Perovskite Nanocrystals with Tunable Composition and Thickness by Ultrasonication. *Angew.Chem. Int.Ed.* **2016,** *55*, 13887-13892.

15. Shamsi, J.; Urban, A. S.; Imran, M.; Trizio, L. D.; Manna, L. Metal Halide Perovskite Nanocrystals: Synthesis, Post-Synthesis Modifications, and Their Optical Properties. *Chem. Rev.* **2019,** *119*, 3296-3348.

16. Yong, Z.-J.; Guo, S.-Q.; Ma, J.-P.; Zhang, J.-Y.; Li, Z.-Y.; Chen, Y.-M.; Zhang, B.-B.; Zhou, Y.; Shu, J.; Gu, J.-L.; et al. Doping-Enhanced Short-Range Order of Perovskite Nanocrystals for Near-Unity Violet Luminescence Quantum Yield. *J. Am. Chem. Soc.* **2018,** *140*, 9942-9951.

17. Shynkarenko, Y.; Bodnarchuk, M. I.; Bernasconi, C.; Berezovska, Y.; Verteletskyi, V.; Ochsenbein, S. T.; Kovalenko, M. V. Direct Synthesis of Quaternary Alkylammonium-Capped Perovskite Nanocrystals for Efficient Blue and Green Light-Emitting Diodes. *ACS Energy Lett.* **2019,** *4*, 2703-2711.

18. Hou, S.; Gangishetty, M. K.; Quan, Q.; Congreve, D. N. Efficient Blue and White Perovskite Light-Emitting Diodes via Manganese Doping. *Joule* **2018,** *2*, 2421-2433.

19. Mondal, N.; De, A.; Samanta, A. Achieving Near-Unity Photoluminescence Efficiency for Blue-Violet-Emitting Perovskite Nanocrystals. *ACS Energy Lett.* **2019,** *4*, 32-39.

20. Ahmed, G. H.; El-Demellawi, J. K.; Yin, J.; Pan, J.; Velusamy, D. B.; Hedhili, M. N.; Alarousu, E.; Bakr, O. M.; Alshareef, H. N.; Mohammed, O. F. Giant Photoluminescence Enhancement in $CsPbCl_3$ Perovskite Nanocrystals by Simultaneous Dual-Surface Passivation. *ACS Energy Lett.* **2018,** *3*, 2301-2307.

21. Akkerman, Q. A.; Rainò, G.; Kovalenko, M. V.; Manna, L. Genesis, Challenges and Opportunities for Colloidal Lead Halide Perovskite Nanocrystals. *Nat. Mater.* **2018**, *17*, 394-405.

22. Seth, S.; Ahmed, T.; De, A.; Samanta, A. Tackling the Defects, Stability, and Photoluminescence of $CsPbX_3$ Perovskite Nanocrystals. *ACS Energy Lett.* **2019,** *4*, 1610-1618.

23. Ghosh, S.; Mandal, S.; Mukherjee, S.; De, C. K.; Samanta, T.; Mandal, M.; Roy, D.; Mandal, P. K. Near-Unity Photoluminescence Quantum Yield and Highly Suppressed Blinking in a Toxic-Metal-Free Quantum Dot. *J. Phys. Chem. Lett.* **2021,** *12*, 1426-1431.

24. Behera, R. K.; Adhikari, S. D.; Dutta, S. K.; Dutta, A.; Pradhan, N. Blue-Emitting $CsPbCl_3$ Nanocrystals: Impact of Surface Passivation for Unprecedented Enhancement and Loss of Optical Emission. *J. Phys. Chem. Lett.* **2018,** *9*, 6884-6891.

25. Zheng, X.; Hou, Y.; Sun, H.-T.; Mohammed, O. F.; Sargent, E. H.; Bakr, O. M. Reducing Defects in Halide Perovskite Nanocrystals for Light Emitting Applications. *J. Phys. Chem. Lett.* **2019,** *10*, 2629-2640.

26. Mandal, S.; Ghosh, S.; Mukherjee, S.; De, C. K.; Roy, D.; Samanta, T.; Mandal, P. K. Unravelling Halide-Dependent Charge Carrier Dynamics in $CsPb(Br/Cl)_3$ Perovskite Nanocrystals. *Nanoscale* **2021,** *13*, 3654-3661.

27. Kumawat, N. K.; Liu, X.-K.; Kabra, D.; Gao, F. Blue Perovskite Light-Emitting Diodes: Progress, Challenges and Future Directions. *Nanoscale* **2019,** *11*, 2109-2120.

28. Naresh, V.; Lee, N. Zn(II)-Doped Cesium Lead Halide Perovskite Nanocrystals with High Quantum Yield and Wide Color Tunability for Color-Conversion Light-Emitting Displays. *ACS Appl. Nano Mater.* **2020,** *3*, 7621-7632.

29. Chen, J.-K.; Ma, J.-P.; Guo, S.-Q.; Chen, Y.-M.; Zhao, Q.; Zhang, B.-B.; Li, Z.-Y.; Zhou, Y.; Hou, J.; Kuroiwa, Y.; et al. High-Efficiency Violet-Emitting All-Inorganic Perovskite Nanocrystals Enabled by Alkaline-Earth Metal Passivation. *Chem. Mater.* **2019,** *31*, 3974-3983.

30. Imran, M.; Caligiuri, V.; Wang, M.; Goldoni, L.; Prato, M.; Krahne, R.; Trizio, L. D.; Manna, L. Benzoyl Halides as Alternative Precursors for the Colloidal Synthesis of Lead-Based Halide Perovskite Nanocrystals. *J. Am. Chem. Soc.* **2018,** *140*, 2656-2664.

31. De, A.; Das, S.; Mondal, N.; Samanta, A. Highly Luminescent Violet- and Blue-Emitting Stable Perovskite Nanocrystals. *ACS Materials Lett.* **2019,** *1*, 116-122.

32. Li, F.; Liu, Y.; Wang, H.; Zhan, Q.; Liu, Q.; Xia, Z. Postsynthetic Surface Trap Removal of $CsPbX_3$ (X = Cl, Br, or I) Quantum Dots via a ZnX_2/Hexane Solution toward an Enhanced Luminescence Quantum Yield. *Chem. Mater.* **2018,** *30*, 8546-8554.

33. Das, S.; De, A.; Samanta, A. Ambient Condition Mg^{2+} Doping Producing Highly Luminescent Green- and Violet-Emitting Perovskite Nanocrystals with Reduced Toxicity and Enhanced Stability. *J. Phys. Chem. Lett.* **2020,** *11*, 1178-1188.

34. Dutta, A.; Behera, R. K.; Pal, P.; Baitalik, S.; Pradhan, N. Near-Unity Photoluminescence Quantum Efficiency for All $CsPbX_3$(X = Cl, Br, and I) Perovskite Nanocrystals: A Generic Synthesis Approach. *Angew. Chem. Int. Ed.* **2019,** *58,* 5552-5556.

35. Ahmed, T.; Seth, S.; Samanta, A. Boosting the Photoluminescence of $CsPbX_3$ (X = Cl, Br, I) Perovskite Nanocrystals Covering a Wide Wavelength Range by Postsynthetic Treatment with Tetrafluoroborate Salts. *Chem. Mater.* **2018,** *30,* 3633-3637.

36. Wang, S.; Wang, Y.; Zhang, Y.; Zhang, X.; Shen, X.; Zhuang, X.; Lu, P.; Yu, W. W.; Kershaw, S. V.; Rogach, A. L. Cesium Lead Chloride/Bromide Perovskite Quantum Dots with Strong Blue Emission Realized via a Nitrate-Induced Selective Surface Defect Elimination Process. *J. Phys. Chem. Lett.* **2019,** *10,* 90-96.

37. Bi, C.; Wang, S.; Li, Q.; Kershaw, S. V.; Tian J.; Rogach, A. L. Thermally Stable Copper(II)-Doped Cesium Lead Halide Perovskite Quantum Dots with Strong Blue Emission. *J. Phys. Chem. Lett.* **2019,** *10,* 943-952.

38. Ahmed, G. H.; Yin, J.; Bakr, O. M.; Mohammed, O. F. Near-Unity Photoluminescence Quantum Yield in Inorganic Perovskite Nanocrystals by Metal-Ion Doping. *J. Chem. Phys.* **2020,** *152,* 020902.

39. Nenon, D. P.; Pressler, K.; Kang, J.; Koscher, B. A.; Olshansky, J. H.; Osowiecki, W. T.; Koc, M. A.; Wang, L.-W.; Alivisatos, A. P. Design Principles for Trap-Free $CsPbX_3$ Nanocrystals: Enumerating and Eliminating Surface Halide Vacancies with Softer Lewis Bases. *J. Am. Chem. Soc.* **2018,** *140,* 17760-17772.

40. Mamgain, S.; Kunnathodi, V.; Yella, A. Humidity-Mediated Synthesis of Highly Luminescent and Stable $CsPbX_3$ (X = Cl, Br, I) Nanocrystals. *Energy Technol.* **2019,** *8,* 1900890.

41. Paul, S.; Samanta, A. N-Bromosuccinimide as Bromide Precursor for Direct Synthesis of Stable and Highly Luminescent Green-Emitting Perovskite Nanocrystals. *ACS Energy Lett.* **2020,** *5,* 64-69.

42. Grabolle, M.; Spieles, M.; Lesnyak, V.; Gaponik, N.; Eychmuller, A.; Resch-Genger, U. Determination of the Fluorescence Quantum Yield of Quantum Dots: Suitable Procedures and Achievable Uncertainties. *Anal. Chem.* **2009,** *81,* 6285-6294.

43. Dong, Y.; Qiao, T.; Kim, D.; Parobek, D.; Rossi, D.; Son, D. H. Precise Control of Quantum Confinement in Cesium Lead Halide Perovskite Quantum Dots via Thermodynamic Equilibrium. *Nano Lett.* **2018,** *18,* 3716-3722.

44. Guo, T.; Bose, R.; Zhou, X.; Gartstein, Y. N.; Yang, H.; Kwon, S.; Kim, M. J.; Lutfullin, M.; Sinatra, L.; Gereige, I.; et al. Delayed Photoluminescence and Modified Blinking Statistics in Alumina-Encapsulated Zero-Dimensional Inorganic Perovskite Nanocrystals. *J. Phys. Chem. Lett.* **2019,** *10,* 6780-6787.

45. Mondal, N.; Samanta, A. Complete Ultrafast Charge Carrier Dynamics in Photo-excited All-Inorganic Perovskite Nanocrystals ($CsPbX_3$). *Nanoscale* **2017,** *9,* 1878-1885.

46. Mondal, N.; De, A.; Das, S.; Paul, S.; Samanta, A. Ultrafast Carrier Dynamics of Metal Halide Perovskite Nanocrystals and Perovskite-Composites. *Nanoscale* **2019,** *11,* 9796-9818.

47. Lai, R.; Wu, K. Picosecond Electron Trapping Limits the Emissivity of $CsPbCl_3$ Perovskite Nanocrystals. *J. Chem. Phys.* **2019,** *151,* 194701.

48. Karlsson, M.; Yi, Z.; Reichert, S.; Luo, X.; Lin, W.; Zhang, Z.; Bao, C.; Zhang, R.; Bai, S.; Zheng, G.; et al. Mixed Halide Perovskites for Spectrally Stable and High-Efficiency blue Light-Emitting Diodes. *Nat. Commun.* **2021,** *12,* 361.

49. Abdi-Jalebi, M.; Andaji-Garmaroudi, Z.; Cacovich, S.; Stavrakas, C.; Philippe, B.; Richter, J. M.; Alsari, M.; Booker, E. P.; Hutter, E. M.; Pearson, A. J.; et al. Maximizing and Stabilizing Luminescence from Halide Perovskites with Potassium Passivation. *Nature* **2018,** *555,* 497-501.

CHAPTER 5

Phase-Stable and Highly Luminescent $CsPbI_3$ Perovskite Nanocrystals with Suppressed Photoluminescence Blinking

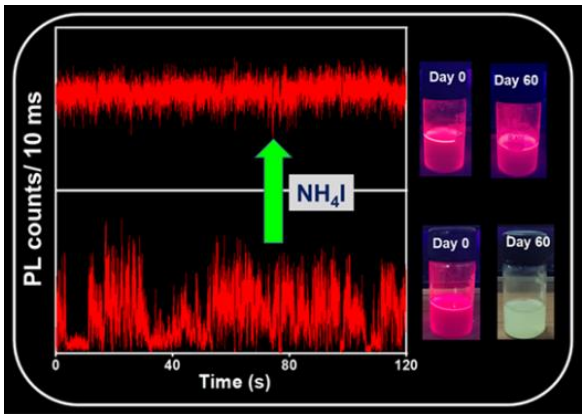

Overview

Despite their low bandgap, the usage of the $CsPbI_3$ nanocrystals (NCs) in solar photovoltaic and optoelectronic applications is very limited due to their phase instability and single-particle photoluminescence (PL) intermittency. Herein we show that phase-pure, mono-dispersed, stable, highly luminescent $CsPbI_3$ NCs can be obtained by tweaking conventional hot-injection method using NH_4I as an additional precursor. Single-particle studies on these NCs show significant suppression of PL blinking and 60% of all NCs investigated are found to exhibit only high intensity ON-states (bright) with narrow distribution of intensity levels. A much wider distribution of intensity levels with significant contribution of low intensity OFF-states (dim) are observed for the remaining 40% NCs due to band-edge recombination through trap states and Auger recombination. Excellent characteristics of these $CsPbI_3$ NCs are shown to be the outcome of NH_4^+ replacing some surface Cs^+ of an iodide-rich surface of the NCs. These phase-stable, highly luminescent $CsPbI_3$ NCs with significantly suppressed PL blinking can be useful single photon emitter and promising materials for optoelectronic and solar photovoltaic applications.

5.1. Introduction

Among the cesium lead halide ($CsPbX_3$ with X= Cl, Br and I) perovskite nanocrystals (NCs), the $CsPbI_3$ NCs, because of their low bandgap, are the most promising candidates for solar photovoltaic and various optoelectronic applications.[1-13] However, poor phase-stability of these NCs even under ambient condition is a major obstacle to these applications.[14-17] Apart from the stability related issues, photoluminescence (PL) blinking of the single NCs is another factor, which restricts the applications of the $CsPbI_3$ NCs as single photon emitter and other light emitting applications.[18-26] PL blinking is indeed an issue for all single emitters. Among different models invoked for explaining the PL blinking of semiconductor NCs, charging model based on trapping of the carrier in long-lived trap-states[19, 27-39] and multiple recombination center (MRC) model based on trapping of the carrier in short-lived trap states [36, 40-43] are the most common ones. In charging model, the NCs are emissive (ON), when in their neutral state, but are non-emissive (OFF), when in their charged state due to Auger recombination. This ON-OFF PL fluctuation is known as Auger-blinking or trion-blinking. Here, the OFF-state duration is determined by the lifetime of the carrier residing in the long-lived trap state. In MRC model, the ON-OFF PL fluctuation is the result of transformation of the trap states between the active and inactive forms. This blinking arising from time dependent fluctuations of the carrier trapping rate is termed as BC-blinking. In addition, interception of the hot carriers (HC) by trap states can also contribute to PL blinking, which is known as HC-blinking.[44-47] Mulvaney and co-workers observed both Auger-blinking and BC-blinking in single CdSe QD.[36] Ahmed et al. recently found Auger blinking, BC blinking and HC blinking in a single $CsPbBr_3$ NC.[48] PL blinking of the $CsPbI_3$ NCs was attributed to charging and discharging of the NCs by Klimov and coworkers, [19] but later Yuan et al. showed that it arises due to activation and deactivation of the trap-states.[18]

Obtaining phase-stable red-emitting $CsPbI_3$ NCs with high PL efficiency and suppressed blinking, which is necessary for many optoelectronic applications, is a challenging task.[15] Phase-instability and deteriorating PL properties of these NCs arise from surface iodide vacancies, poor surface capping by the coordinating ligands and intrinsic disorder of the $[PbI_6]^{4-}$ units.[9, 14, 49] The nature of the surface of the NCs depends largely on their method of preparation.[14, 50-57] The widely used two-precursor method,[3] in which PbI_2 is used as precursor for both lead and halide, yields NCs of poor quality primarily due to halide

vacancies on the surface. Use of additional iodide precursors during synthesis is known to improve the phase stability and PL of the NCs.[54, 55, 58, 59] Doping of metal ions[60-65] and surface treatment by coordinating ligands[9, 11, 66-68] are also effective approaches for obtaining highly luminescent and stable $CsPbI_3$ NCs. However, despite intense investigations, phase-stable, highly luminescent $CsPbI_3$ NCs with suppressed PL blinking are still not known. In this work, we show that phase-stable, highly luminescent $CsPbI_3$ NCs with significantly suppressed PL blinking can be obtained by the most widely used method of synthesis of perovskite NCs[3] using optimum amount of NH_4I as an additional reagent, which is chosen considering that a second source of I^- provides a halide-rich synthesis condition and surface capping by NH_4^+ enhances the PLQY and colloidal stability of the NCs.[66]

5.2. Results

5.2.1 Reaction Condition

The $CsPbI_3$ NCs were prepared as follows. 0.2 mmol of PbI_2, 0.25 mmol of NH_4I, 5 mL of 1-octadecene, 0.8 mL of oleic acid (OA) and 0.8 mL of oleylamine (OLA) were taken in a 50 mL round-bottom flask and stirred under vacuum for 15 min at room temperature. The reaction mixture was then heated at 120°C in N_2 atmosphere until formation of a clear orange color solution. The temperature was then raised to 160-165°C, 0.5 mL of cesium-oleate was injected into it, and the reaction mixture was quenched immediately in an ice bath. The obtained NCs were purified (details in experimental section in supporting information (SI)) and dispersed in hexane for all measurements. We also prepared $CsPbI_3$ NCs following conventional method[3] (i.e. without using NH_4I, details in SI) for comparative purpose. The $CsPbI_3$ NCs obtained by our method are labelled as $CsPbI_3$(I), and the conventional ones as $CsPbI_3$(II) throughout the manuscript.

5.2.2 Ensemble Photoluminescence Properties

The bright field transmission electron microscope (TEM) images show uniform cubic shape of the $CsPbI_3$(I) NCs with a narrow size distribution and average edge length of 9.0±1.0 nm (Figures 5.1.a and AIII.1.a). In contrast, the $CsPbI_3$(II) NCs exhibit much wider size distribution and larger average edge length (12.5±2.0 nm) (Figures 5.1.b and AII.1.b). High resolution TEM (HRTEM) images show an inter-planar distance (d_{100}) of 0.62 nm for both samples (insets of Figures 5.1.a and 5.1.b) indicating that the crystal parameters are not affected due to use of NH_4I during synthesis. A decrease in size and improved mono-

dispersity of the $CsPbI_3$(I) NCs is similar to that observed in the case of $CsPbBr_3$ NCs obtained in halide rich synthesis condition.[69] The UV-vis absorption and emission spectra of these samples are shown in Figures 5.1.c and 5.1.d, respectively. The first excitonic peak (in absorption) and the PL maximum of $CsPbI_3$(I) NCs are blue shifted (by 6-8 nm) compared with the respective peaks of the $CsPbI_3$(II) NCs due to the smaller size of the former sample. The PL quantum yield (QY) of the $CsPbI_3$(I) NCs (90±3%) is found to be much higher than that of the $CsPbI_3$(II) NCs (60±5%) (Figure 5.1.d). The high PLQY (90±3%) is observed for $CsPbI_3$(I) NCs only when an optimum molar ratio of PbI_2:NH_4I (1:1.25) is used during the synthesis and for higher or lower ratio, this NCs exhibited lower PLQY values (Figure AIII.2).

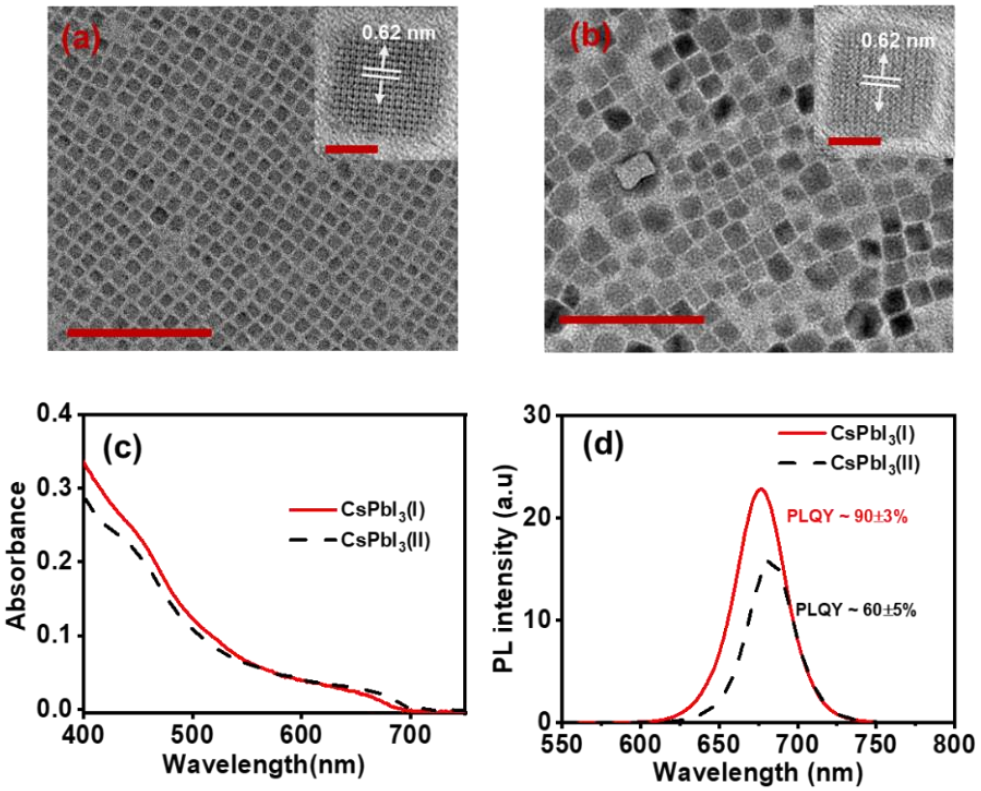

Figure 5.1. *Bright field TEM images of the* ***(a)*** *$CsPbI_3$(I) and* ***(b)*** *$CsPbI_3$(II) NCs with scale bar of 100 nm. Insets show HRTEM image of the NCs (scale bar 5 nm) with inter-planar spacing corresponding to the (100) planes.* ***(c)*** *UV-vis absorption and* ***(d)*** *PL spectra of the $CsPbI_3$(I) and $CsPbI_3$(II) NCs.*

5.2.3. Stability of the NCs

The $CsPbI_3$(I) NCs are also found to display much improved stability compared to the $CsPbI_3$(II) NCs. This is evident from the fact that the PL of a freshly prepared colloidal solution of the $CsPbI_3$(I) NCs decreases only by 4% after 30 days of storage under ambient

condition with humidity 50-60% and temperature 25±5°C in cuvette, whereas 95% PL of the $CsPbI_3$(II) NCs is lost similar conditions (Figures 5.2.2.a-b and AIII.3). The $CsPbI_3$(I) NCs stored in a sealed reagent bottle retain almost its original PL intensity after 60 days in contrast to the $CsPbI_3$(II) NCs, which become non-luminescent during this period (Figure AII.4). High photo-stability of our samples is evident from the fact that after continuous UV illumination (365 nm, 8W) of a colloidal solution of the $CsPbI_3$(I) NCs (taken in a quartz cuvette) for a test period of 24 h, nearly 92% of the original PL is retained, whereas for $CsPbI_3$(II) NCs, PL decreases to 28% under similar conditions (Figures 5.2.c and AIII.5). The powder X-ray diffraction (PXRD) patterns of these samples (monitored for 20 days) show that $CsPbI_3$(II) film starts degrading to δ-$CsPbI_3$ phase within 2 days, and a complete transition is noticed within 20 days (Figure 5.2.d). However, no noticeable degradation of the $CsPbI_3$(I) film could be observed (Figure 5.2.e). The sample stays in its α-phase even after 20 days under ambient condition.

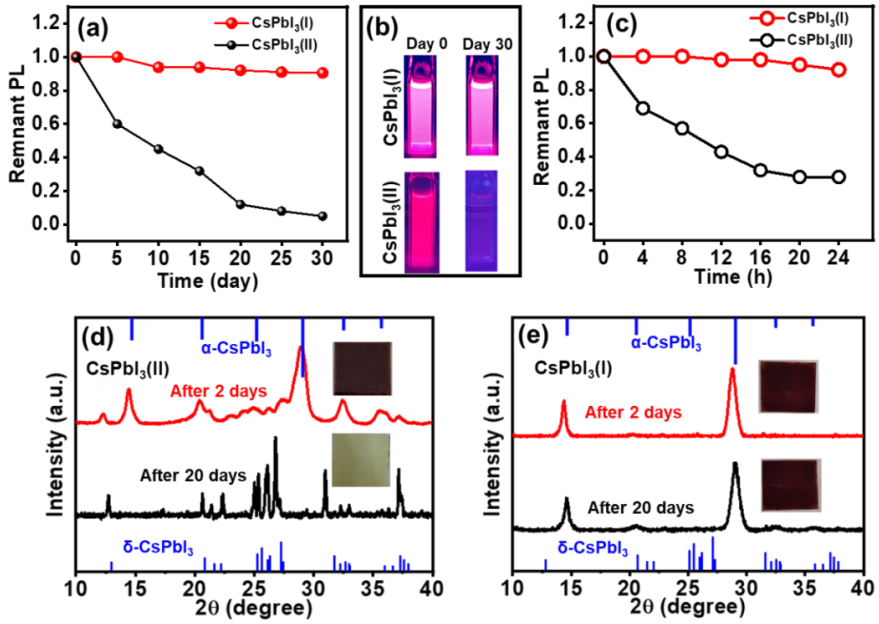

Figure 5.2. ***(a)*** *Air stability of the colloidal dispersions of $CsPbI_3$(I) and $CsPbI_3$(II) NCs under ambient condition.* ***(b)*** *Digital images (under UV illumination) of these samples at different time intervals stored under ambient condition.* ***(c)*** *Photo-stability of $CsPbI_3$(I) and $CsPbI_3$(II) NCs under continuous UV illumination (365 nm, 8W).* ***(d)*** *and* ***(e)*** *PXRD patterns of these samples at different time periods. Insets of the* ***(d)*** *and* ***(e)*** *show the digital images of the film used for the PXRD measurements.*

5.2.4. Single-Particle Photoluminescence Properties

As already mentioned, random fluctuation of the PL intensity at the single particle level is one of the biggest problems for the $CsPbI_3$ NCs. High PLQY and excellent stability of our samples of $CsPbI_3$(I) NCs allow us to study the PL properties of these NCs at the single particle level. We carried out these studies by drop-casting a very dilute solution (pM, in hexane) of the NCs on a cover glass and obtaining a film by drying under vacuum. The film of the NCs was excited by a pulsed laser at 485 nm (pulsed width ~144 ps, repetition rate 4 MHz and power 0.1 μW) (details in SI). The low laser power was used to avoid any nonlinear processes. Under our experimental condition, the number of excitons generated in each NC per pulse is 0.06.

The confocal PL microscopy image of a film of $CsPbI_3$(I) NCs is shown in Figure 5.3.a. We have examined the PL blinking behavior of 66 individual single NCs of $CsPbI_3$(I) (Figures 5.3.b, AIII.6 and AIII.7), among which 40 single NCs show complete suppression of PL blinking indicating the presence of only the ON-states (bright-states) with a narrow distribution of intensity. A representative time-trace of one single NC of this type is depicted in Figure 5.3.b (and in AIII.6). Single-exponential decay of the PL intensity indicates that the photogenerated charge carriers recombine only through the radiative excitonic recombination process (Figures 5.3.d). Fluorescence-lifetime-intensity-distribution (FLID) plot also shows the presence of only the high intensity ON-sates (Figure 5.3.e). Complete elimination of the low intensity OFF-states for majority of the single NCs of $CsPbI_3$(I) is consistent with the sample's bulk PL properties.

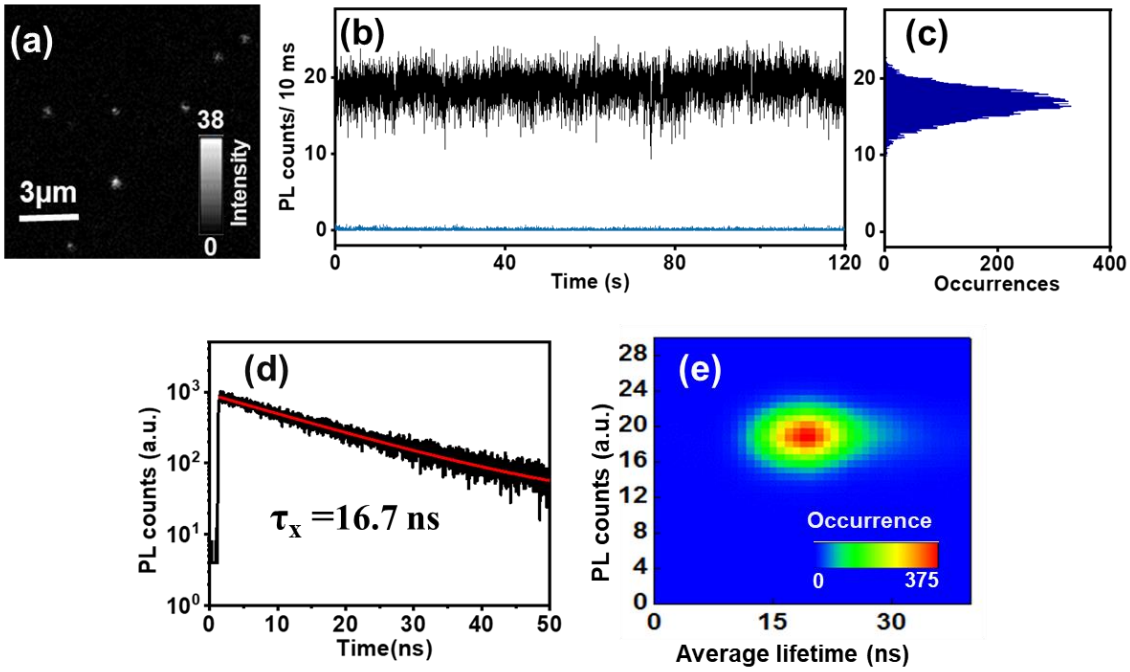

Figure 5.3. ***(a)*** *PL intensity image of a film of $CsPbI_3$(I) NCs.* ***(b)*** *PL intensity time-trace of a given single $CsPbI_3$(I) NC among the 40 NCs, which show complete suppression of blinking. Background signal is shown in cyan-blue color trace.* ***(c)*** *Distribution of PL intensities and occurrence.* ***(d)*** *PL decay profile of the trace.* ***(e)*** *A false color representation of FLID obtained from the analysis of intensity and lifetime of the PL intensity time-trace shown in panel* ***b****.*

The PL intensity time-trace of a representative single NC belonging to the remaining 26 NCs is shown in Figure 5.4.a. The PL intensity fluctuation in this case is much wider with no clear separation of the ON and OFF-states (Figure 5.4.b). To understand the mechanism of PL blinking of these NCs we have examined the PL decay behavior of five different intensity levels (R1 to R5) for each NC. While the PL decay is single exponential for the high intensity levels (R1 to R3), the decay profile is biexponential for the bottom two intensity levels (R4 to R5) (Figure 5.4.c). The highest intensity level (R1), which is characterized by a lifetime of 9.80 ns for the representative NCs, is due to radiative excitonic recombination. The PL lifetime of the highest intensity state, when averaged for all ~26 NCs studied, is ~13.28 ±2.65 ns (Figure A.III.8). The lifetime decreases gradually with lowering of the PL intensity (Table 5.1). The intensity-lifetime scaling parameter (η) (details in SI) for first three intensity levels is

$$\eta = k_{R1} : k_{R2} : k_{R3} = I_1/\tau_1 : I_2/\tau_2 : I_3/\tau_3 = 1.00 : 0.93 : 0.74$$

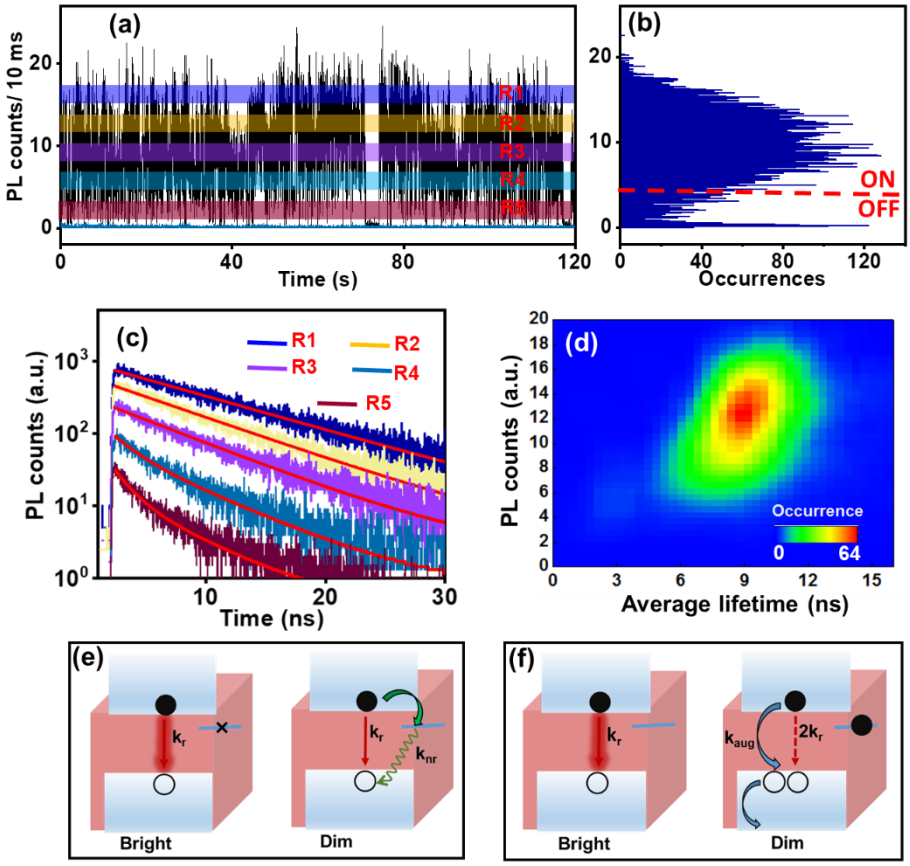

Figure 5.4. ***(a)*** *PL intensity time-trace of a given single NC of $CsPbI_3$(I) NC (among 26 NCs exhibiting similar blinking behavior). The trace is divided into five intensity levels (R1 to R5).* *Background signal is shown in the cyan-blue color trace.* ***(b)*** *Distribution of the intensities with occurrence. Threshold is shown by the red dashed line.* ***(c)*** *PL decay profiles for levels R1 to R5 and* ***(d)*** *FLID pattern of the PL intensity time-trace shown in panel* ***a****. Schematic illustration of* ***(e)*** *BC-blinking and* ***(f)*** *Auger-blinking. k_r, k_{nr} and k_{aug} represent rate constants of the radiative, nonradiative and Auger-recombination, respectively.*

A near-unity ratio of the radiative recombination rates of two high intensity levels indicates the competition between a fixed radiative rate and variable nonradiative rates in the NC. This is typical of BC blinking arising from trapping and de-trapping of the charge carrier in/from short lived trap-states.[36] The deviation of the η value from near-unity from R3 level onward indicates involvement of additional competing recombination process (es). These levels are associated with a second lifetime component (between 1.30 and 1.70 ns) and the

contribution of this component increases from R4 to R5 level. This short-lived component must be arising from trion recombination as multi-excitonic recombination is ruled out in our experimental condition.[19, 30] The involvement of two simultaneously occurring processes is not very clear in the FLID pattern (Figure 5.4.d) due to low occurrences of the OFF states. BC-blinking and Auger-blinking occurring in these samples are represented schematically in Figures 5.4.e and 5.4.f, respectively.

Table 5.1. *PL Lifetime components (τ_i) and their weightages (α_i) of different PL intensity levels of the PL intensity time-trace of $CsPbI_3$(I) NC shown in Figure 5.4.a.*

Region [Intensity (counts/10 ms)]	τ_1 (α_1) [ns]	τ_2(α_2) [ns]
R1 (17.00)	9.80	
R2 (13.00)	8.10	
R3 (9.00)	7.01	
R4 (5.50)	5.97 (0.63)	1.71 (0.37)
R5 (2.00)	4.99 (0.43)	1.33 (0.57)

It was difficult to investigate the single-particle PL properties of the $CsPbI_3$(II) NCs due to their poor-stability.[12, 18, 19] We observed that several single NCs often degrade within a minute during recording the PL intensity-time traces (Figure AIII.9). However, we could manage to record the PL blinking traces of 53 NCs up to 60 s (Figures 4.5.a and AIII.10), during which no significant photo-degradation could be observed. A representative PL blinking trace of these NCs, depicted in Figure 5.5.a, show a broad distribution of intensity levels with no clear separation between the ON and OFF-states (Figure 5.5.b). To determine the origin of PL blinking of this system, PL intensity trace is marked for five different intensity regions, P1 to P5 (Figure 5a), and their PL decay behavior studied (Figures 5.5.c and Table AIII.1). The intensity-lifetime scaling parameter (η) for the first three intensity levels is

$$\eta = k_{P1} : k_{P2} : k_{P3} = I_1/\tau_1 : I_2/\tau_2 : I_3/\tau_3 = 1.00 : 0.92 : 0.75$$

A near-unity ratio of the radiative recombination rates of the two high intensity levels indicates BC-blinking arising from fluctuating trapping rate of the carriers.[36] The deviation of the η value from near-unity from P3 level onward and appearance of a short lifetime component for levels P4 and P5 indicate Auger-blinking or trion-blinking in these NCs. The FLID plot shows a combination of linear and curvature behavior confirming both Auger- and

BC-blinking in the same NC (Figure 5.5.d). The competition between the fixed radiative and fluctuating nonradiative relaxations leads to the linear behavior in FLID pattern, whereas trion recombination leads to non-linearity in the FLID pattern.

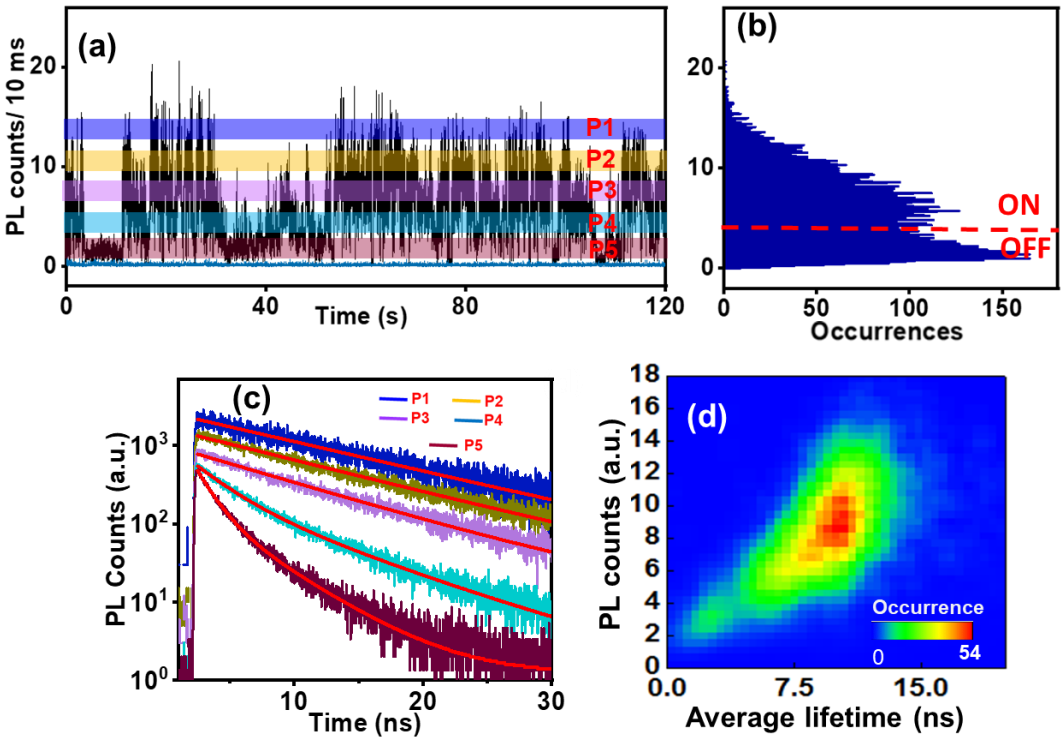

Figure 5.5. ***(a)*** *PL Blinking trace of a single $CsPbI_3$(II) NC. The trace is divided into five intensity levels (P1 to P5).* ***Background signal*** *is shown in cyan-blue color trace.* ***(b)*** *Distribution of the intensities observed in the blinking trace. Threshold is shown by the red dashed line.* ***(c)*** *PL decay profiles for the levels P1 to P5.* ***(d)*** *FLID patterns of the PL blinking trace shown in panel* ***(a)*** *with false color representation.*

To shed additional light on the nature of the trap states and their effect on carrier recombination, we have analyzed blinking statistics by constructing the probability distributions of the ON- and OFF-events (Figure 5.6). Although the ON- and OFF-events are not so well separated, we have used a threshold of five times the maximum background noise level (red dashed line in Figure 5.4.b) for calculation of the probability distributions of ON- and OFF-events. The probability distributions of the OFF-events is best represented by a power-law function of the form, $P_{OFF}(t) \propto t^{\alpha OFF}$; however, for the ON state, it follows a truncated power-law behavior, $P_{ON}(t) \propto t^{\alpha ON} \exp(-t/\tau_c)$ (details in SI). Here, α and τ_c indicate

power law exponent and truncation time, respectively. The power-law behavior indicates a dispersive kinetics of carrier trapping and detrapping arising from the (i) difference in static distribution of trap states, (ii) energetic diffusion of barrier between core and surface trap states for charge tunneling and (iii) difference in the number of time-fluctuating active trap sites.[34, 40, 70] A larger value of the power-law exponent for the OFF-state and a smaller value for the ON-state of the $CsPbI_3$(I) NCs compared to the $CsPbI_3$(II) NCs indicates a much longer ON-durations of the former sample (Figures 5.6.a-d and Table AIII.2).

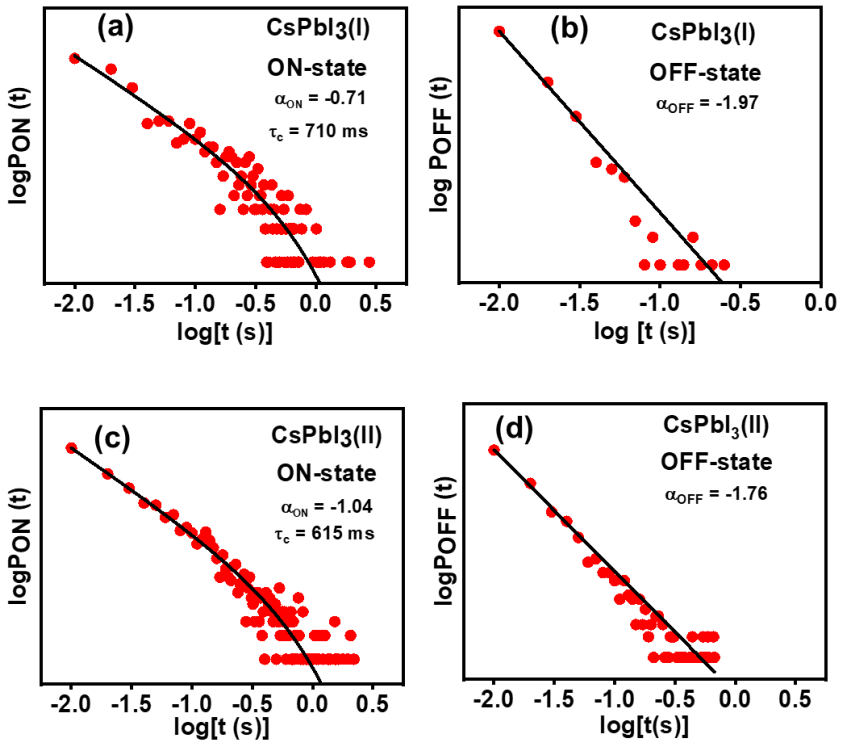

Figure 5.6. *Log–log distributions of* ***(a, c)*** *ON-time and* ***(b, d)*** *OFF-time probability of representative NCs of $CsPbI_3$(I) and $CsPbI_3$(II).*

The average time fraction spent by the NCs in their ON-state, calculated both for $CsPbI_3$(I) and $CsPbI_3$(II) NCs from individual PL blinking trace (up to 60 s) and corresponding distributions, are shown in Figures 5.7.a and 5.7.b, respectively. The $CsPbI_3$(I) NCs show an average ON-state fraction of 0.945±0.09, which is quite remarkable. Also important to note here is that 60% of these NCs exhibit an average ON-state fraction of ~1.0.

Whereas, in the case of the $CsPbI_3$(II) NCs, the average ON-state fraction is much lower (0.676 ±0.11).

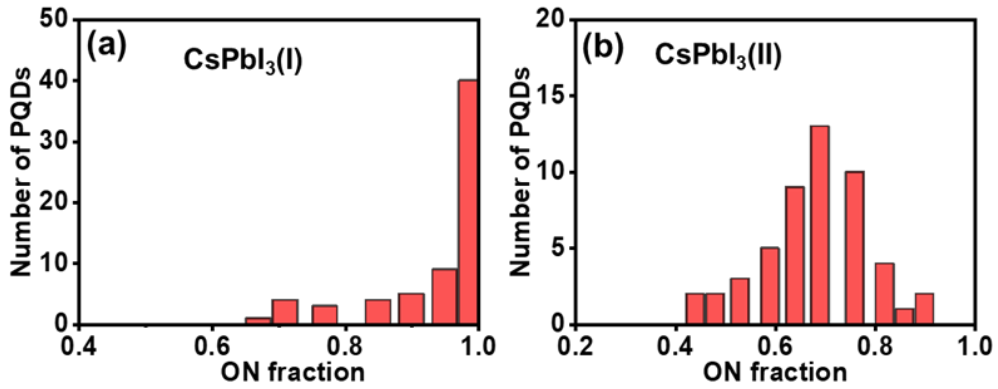

Figure 5.7. *Distribution of the ON-state fraction of* ***(a)*** *$CsPbI_3$(I) and* ***(b)*** *$CsPbI_3$(II) NCs.*

5.3. Discussion

The factors contributing to the exceptional phase stability and PL properties of the $CsPbI_3$(I) NCs compared to the $CsPbI_3$(II) NCs can be understood by comparing the XPS spectra of the two samples (Figures 5.8 and AIII.11). First, the areas under the spectral bands (considering the atomic sensitivity factor[71]) of the constituting elements show a Cs:Pb:I atomic percentage ratio of 0.83:1.00:3.33 and 0.90:1.00:2.89 in $CsPbI_3$(I) and $CsPbI_3$(II) NCs, respectively (Figure 5.8.a and Table AIII.3) indicating a halide-rich surface of the former sample. Second, inspection of the atomic percentage of Cs and N indicates a decrease in Cs-content and an increase in N-content for the $CsPbI_3$(I) NCs (Figure 5.8.a). This indicates replacement of some surface Cs^+ by NH_4^+.[72] Third, the N 1s core level XPS spectrum for $CsPbI_3$(I) NCs is seen to be broader and blue-shifted compared to $CsPbI_3$(II) NCs (Figure 5.8.b). This reflects the presence of two different types of ammonium cations, namely, NH_4^+ and OLA^+ and a higher binding energy of NH_4^+ compared to OLA^+. Fourth, a higher binding energy of I^- $3d_{3/2}$ and $3d_{5/2}$ electrons in the $CsPbI_3$(I) NCs compared with the corresponding signals in $CsPbI_3$(II) (**Figure 5.**8.c) implies a stronger binding of the surface I^- with NH_4^+ in the former sample. Fifth, a decrease in binding energy of the Pb $4f_{7/2}$ and Pb $4f_{5/2}$ levels (Figure 5.8.d) indicates weakening of the Pb-I bond because of stronger interaction between NH_4^+ and I^-. It is thus evident that improved phase stability and significant suppression of PL blinking of the $CsPbI_3$(I) NCs arises from the replacement of some surface Cs^+ by NH_4^+ of an iodide-rich surface of the NCs (Scheme 1).

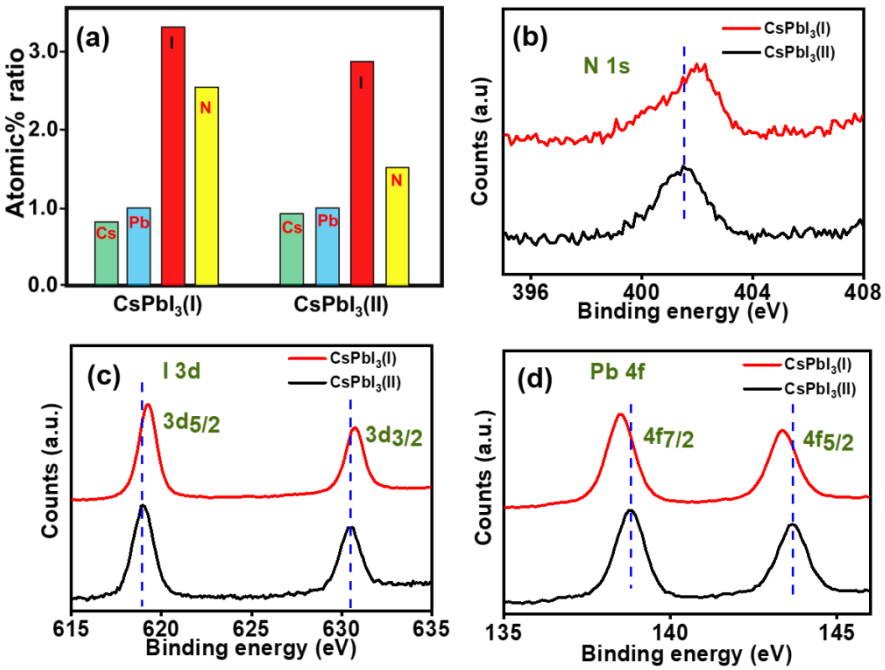

Figure 5.8. (a) *Atomic % ratio (with respect to Pb) of the constituting elements of the $CsPbI_3$(I) and $CsPbI_3$(II) NCs calculated using high resolution XPS data. High resolution XPS spectra of* ***(b)*** *N 1s,* ***(c)*** *I 3d ($3d_{5/2}$, $3d_{3/2}$) and* ***(d)*** *Pb 4f ($4f_{5/2}$, $4f_{7/2}$) of these samples.*

5.4. Conclusion

In short, focusing on the core issue of phase instability and PL blinking of the $CsPbI_3$ nanocrystals that restricts the utility of these low bandgap substances in photovoltaic, light emitting and single photonic applications, it is shown that exceptionally phase stable and highly luminescent $CsPbI_3$ NCs with significantly suppressed PL blinking can be obtained by tweaking the conventional hot-injection method of synthesis employing NH_4I as an additional reagent. The PL blinking characteristics of a large number of single $CsPbI_3$ NCs reveal an average ON-state fraction of 0.945 with 60% of them exhibiting complete suppression of PL blinking. Remaining 40% NCs exhibit OFF-states due to both Auger recombination of trion and trap induced recombination of the band-edge carrier. The extraordinary features of these NCs are attributed to NH_4I serving both as halide precursor and surface capping agent. This work, which provides a simple approach to obtaining high quality $CsPbI_3$ NCs hitherto unknown, is expected to be of great significance in photovoltaic, light emitting and single photonic applications.

Scheme1: *Schematic illustration of surface passivation of the $CsPbI_3$ NCs by NH_4I.*

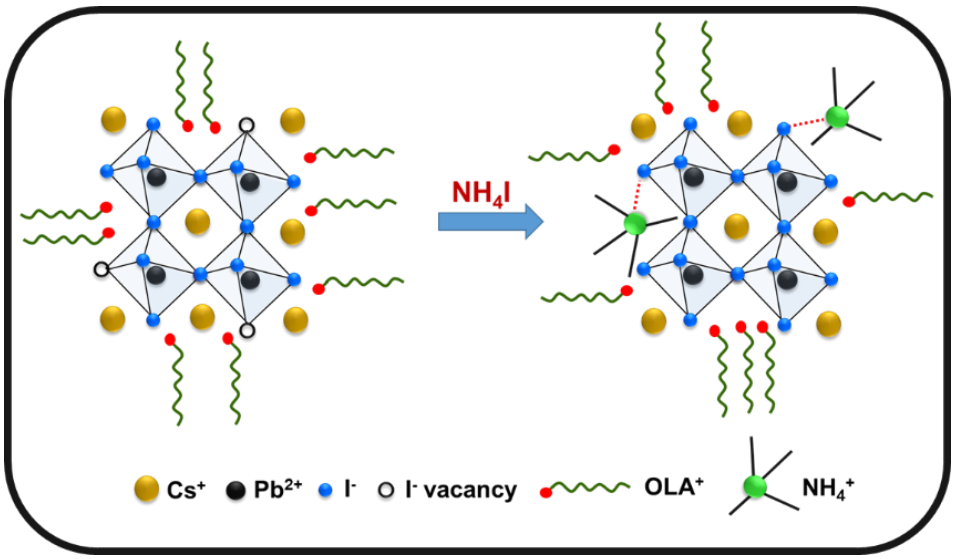

5.4. Bibliography

(1) Sanehira, E. M.; Marshall, A. R.; Christians, J. A.; Harvey, S. P.; Ciesielski, P. N.; Wheeler, L. M.; Schulz, P.; Lin, L. Y.; Beard, M. C.; Luther, J. M. Enhanced Mobility $CsPbI_3$ Quantum Dot Arrays for Record-Efficiency, High-Voltage Photovoltaic Cells. *Sci. Adv.* **2017,** *3*, eaao4204.

(2) Swarnkar, A.; Marshall, A. R.; Sanehira, E. M.; Chernomordik, B. D.; Moore, D. T.; Christians, J. A.; Chakrabarti, T.; Luther, J. M. Quantum Dot–Induced Phase Stabilization of α-$CsPbI_3$ Perovskite for High-Efficiency Photovoltaics. *Science* **2016,** *354*, 92-95.

(3) Protesescu, L.; Yakunin, S.; Bodnarchuk, M. I.; Krieg, F.; Caputo, R.; Hendon, C. H.; Yang, R. X.; Walsh, A.; Kovalenko, M. V. Nanocrystals of Cesium Lead Halide Perovskites ($CsPbX_3$, X = Cl, Br, and I): Novel Optoelectronic Materials Showing Bright Emission with Wide Color Gamut. *Nano Lett.* **2015,** *6*, 3692-3696.

(4) Bai, S.; Yuan, Z.; Gao, F. Colloidal Metal Halide Perovskite Nanocrystals: Synthesis, Characterization, and Applications. *J. Mater. Chem. C* **2016,** *4*, 3898-3904.

(5) Huang, H.; Polavarapu, L.; Sichert, J. A.; Susha, A. S.; Urban, A. S.; Rogach, A. L. Colloidal Lead Halide Perovskite Nanocrystals: Synthesis, Optical Properties and Applications. *NPG Asia Mater.* **2016,** *8*, e328.

(6) Zhang, J.; Yang, X.; Deng, H.; Qiao, K.; Farooq, U.; Ishaq, M.; Yi, F.; Liu, H.; Tang, J.; Song, H. Low-Dimensional Halide Perovskites and Their Advanced Optoelectronic Applications. *Nano-Micro Lett.* **2017,** *9*, 36.

(7) Huang, H.; Bodnarchuk, M. I.; Kershaw, S. V.; Kovalenko, M. V.; Rogach, A. L. Lead Halide Perovskite Nanocrystals in the Research Spotlight: Stability and Defect Tolerance. *ACS Energy Lett.* **2017,** *2*, 2071-2083.

(8) Mondal, N.; De, A.; Seth, S.; Ahmed, T.; Das, S.; Paul, S.; Gautam, R. K.; Samanta, A. Dark Excitons of the Perovskites and Sensitization of Molecular Triplets. *ACS Energy Lett.* **2021,** *6*, 588-597.

(9) Pan, J.; Shang, Y.; Yin, J.; Bastiani, M. D.; Peng, W.; Dursun, I.; Sinatra, L.; El-Zohry, A. M.; Hedhili, M. N.; Emwas, A.-H.; et al. Bidentate Ligand-Passivated $CsPbI_3$ Perovskite Nanocrystals for Stable Near-Unity Photoluminescence Quantum Yield and Efficient Red Light-Emitting Diodes. *J. Am. Chem. Soc.* **2018,** *140*, 562-565.

(10) Chen, K.; Jin, W.; Zhang, Y.; Yang, T.; Reiss, P.; Zhong, Q.; Bach, U.; Li, Q.; Wang, Y.; Zhang, H.; et al. High Efficiency Mesoscopic Solar Cells Using $CsPbI_3$ Perovskite Quantum Dots Enabled by Chemical Interface Engineering. *J. Am. Chem. Soc.* **2020,** *142*, 3775-3783.

(11) Lan, Y.-F.; Yao, J.-S.; Yang, J.-N.; Song, Y.-H.; Ru, X.-C.; Zhang, Q.; Feng, L.-Z.; Chen, T.; Song, K.-H.; Yao, H.-B. Spectrally Stable and Efficient Pure Red $CsPbI_3$ Quantum Dot Light-Emitting Diodes Enabled by Sequential Ligand Post-Treatment Strategy. *Nano Lett.* **2021,** *21*, 8756-8763.

(12) Dey, A.; Ye, J.; De, A.; Debroye, E.; Ha, S. K.; Bladt, E.; Kshirsagar, A. S.; Wang, Z.; Yin, J.; Wang, Y; et al. State of the Art and Prospects for Halide Perovskite Nanocrystals. *ACS Nano* **2021,** *15*, 10775-10981.

(13) Tang, X.; Yang, J.; Li, S.; Liu, Z.; Hu, Z.; Hao, J.; Du, J.; Leng, Y.; Qin, H.; Lin, X.; et al. Single Halide Perovskite/Semiconductor Core/Shell Quantum Dots with Ultrastability and Nonblinking Properties. *Adv. Sci.* **2019,** *6*, 1900412.

(14) Dutta, A.; Pradhan, N. Phase-Stable Red-Emitting $CsPbI_3$ Nanocrystals: Successes and Challenges. *ACS Energy Lett.* **2019,** *4*, 709-719.

(15) Protesescu, L.; Yakunin, S.; Kumar, S.; Bar, J.; Bertolotti, F.; Masciocchi, N.; Guagliardi, A.; Grotevent, M.; Shorubalko, I.; Bodnarchuk, M. I.; et al. Dismantling the “Red Wall” of

Colloidal Perovskites: Highly Luminescent Formamidinium and Formamidinium−Cesium Lead Iodide Nanocrystals. *ACS Nano* **2017,** *11*, 3119-3134.

(16) Matuhina, A.; Grandhi, G. K.; Liu, M.; Smatt, J.-H.; Viswanath, N. S. M.; Ali-Löytty, H.; Lahtonen, K.; Vivo, P. Octahedral Distortion Driven by $CsPbI_3$ Nanocrystal Reaction Temperature – the Effects on Phase Stability and Beyond. *Nanoscale* **2021,** *13*, 14186–14196.

(17) Straus, D. B.; Guo, S.; Abeykoon, A. M.; Cava, R. J. Understanding the Instability of the Halide Perovskite $CsPbI_3$ through Temperature-Dependent Structural Analysis. *Adv. Mater.* **2020,** *32*, 2001069.

(18) Yuan, G.; Ritchie, C.; Ritter, M.; Murphy, S.; Gomez, D. E.; Mulvaney, P. The Degradation and Blinking of Single $CsPbI_3$ Perovskite Quantum Dots. *J. Phys. Chem. C* **2018,** *122*, 13407-13415.

(19) Park, Y.-S.; Guo, S.; Makarov, N. S.; Klimov, V. I. Room Temperature Single-Photon Emission from Individual Perovskite Quantum Dots. *ACS Nano* **2015,** *9*, 10386-10393.

(20) Hu, F.; Yin, C.; Zhang, H.; Sun, C.; Yu, W. W.; Zhang, C.; Wang, X.; Zhang, Y.; Xiao, M. Slow Auger Recombination of Charged Excitons in Nonblinking Perovskite Nanocrystals without Spectral Diffusion. *Nano Lett.* **2016,** *16*, 6425-6430.

(21) Hsu, B.-W.; Chuang Y.-T.; Cheng, C.-Y.; Chen, C.-Y.; Chen, Y.-J.; Brumberg, A.; Yang, L.; Huang, Y.-S.; Schaller, R. D.; Chen, L.-J.; et al. Very Robust Spray-Synthesized $CsPbI_3$ Quantum Emitters with Ultrahigh Room-Temperature Cavity-Free Brightness and Self-Healing Ability. *ACS Nano* **2021,** *15*, 11358–11368.

(22) Bose, R.; Zhou, X.; Guo, T.; Yang, H.; Yin, J.; Mishra, A.; Slinker, J. D.; Bakr, O. M.; Mohammed, O. F.; Malko, A. V. Single-Particle Spectroscopy as a Versatile Tool to Explore Lower-Dimensional Structures of Inorganic Perovskites. *ACS Energy Lett.* **2021,** *6*, 3695-3708.

(23) Mandal, S.; Roy, D.; De, C. K.; Ghosh, S.; Mandal, M.; Das, A.; Mandal, P. K. Instantaneous, Room-Temperature, Open-Air Atmosphere, solution-Phase Synthesis of Perovskite Quantum Dots Through Halide Exchange Employing Non-Metal Based Inexpensive HCl/HI: Ensemble and Single Particle Spectroscopy. *Nanoscale Adv.* **2019,** *1*, 3506–3513.

(24) Halder, A.; Pathoor, N.; Chowdhury, A.; Sarkar, S. K. Photoluminescence Flickering of Micron-Sized Crystals of Methylammonium Lead Bromide: Effect of Ambience and Light Exposure. *J. Phys. Chem. C* **2018,** *122*, 15133–15139.

(25) Rainò, G.; Nedelcu, G.; Protesescu, L.; Bodnarchuk, M. I.; Kovalenko, M. V.; Mahrt, R. F.; Stöferle, T. Single Cesium Lead Halide Perovskite Nanocrystals at Low Temperature: Fast Single-Photon Emission, Reduced Blinking, and Exciton Fine Structure. *ACS Nano* **2016,** *10*, 2485–2490.

(26) Zhang, A.; Dong, C.; Ren, J. Tuning Blinking Behavior of Highly Luminescent Cesium Lead Halide Nanocrystals through Varying Halide Composition. *J. Phys. Chem. C* **2017,** *121*, 13314–13323.

(27) Efros, A. L.; Rosen, M. Random Telegraph Signal in the Photoluminescence Intensity of a Single Quantum Dot. *Phys. Rev. Lett.* **1997,** *78*, 1110.

(28) Krauss, T. D.; Brus, L. E. Charge, Polarizability, and Photoionization of Single Semiconductor Nanocrystals. *Phys. Rev. Lett.* **1999,** *83*, 4840-4843.

(29) Yarita, N.; Tahara, H.; Saruyama, M.; Kawawaki, T.; Sato, R.; Teranishi, T.; Kanemitsu, Y. Impact of Postsynthetic Surface Modification on Photoluminescence Intermittency in Formamidinium Lead Bromide Perovskite Nanocrystals. *J. Phys. Chem. Lett.* **2017,** *8*, 6041-6047.

(30) Kanemitsu, Y. Trion Dynamics in Lead Halide Perovskite Nanocrystals. *J. Chem. Phys.* **2019,** *151*, 170902.

(31) Yumoto, G.; Tahara, H.; Kawawaki, T.; Saruyama, M.; Sato, R.; Teranishi, T.; Kanemitsu, Y. Hot Biexciton Effect on Optical Gain in $CsPbI_3$ Perovskite Nanocrystals. *J. Phys. Chem. Lett.* **2018,** *9*, 2222–2228

(32) Vishnu, E. K.; Nair, A. A. K.; Thomas, K. G. Core-Size-Dependent Trapping and Detrapping Dynamics in CdSe/CdS/ZnS Quantum Dots. *J. Phys. Chem. C* **2021,** *125*, 25706–25716.

(33) Chouhan, L.; Ito, S.; Thomas, E. M.; Takano, Y.; Ghimire, S.; Miyasaka, H.; Biju, V. Real-Time Blinking Suppression of Perovskite Quantum Dots by Halide Vacancy Filling. *ACS Nano* **2021,** *15*, 2831-2838.

(34) Cordones, A. A.; Leone, S. R. Mechanisms for Charge Trapping in Single Semiconductor Nanocrystals Probed by Fluorescence Blinking. *Chem. Soc. Rev.* **2013,** *42*, 3209-3221.

(35) Li, B.; Huang, H.; Zhang, G.; Yang, C.; Guo, W.; Chen, R.; Qin, C.; Gao, Y.; Biju, V. P.; Rogach, A. L.; et al. Excitons and Biexciton Dynamics in Single $CsPbBr_3$ Perovskite Quantum Dots. *J. Phys. Chem. Lett.* **2018,** *9*, 6934-6940.

(36) Yuan, G.; Gomez, D. E.; Kirkwood, N.; Bold, K.; Mulvaney, P. Two Mechanisms Determine Quantum Dot Blinking. *ACS Nano* **2018,** *12*, 3397-3405.

(37) Gibson, N. A.; Koscher, B. A.; Alivisatos, A. P.; Leone, S. R. Excitation Intensity Dependence of Photoluminescence Blinking in $CsPbBr_3$ Perovskite Nanocrystals. *J. Phys. Chem. C* **2018,** *122*, 12106–12113.

(38) Trinh, C. T.; Minh, D. N.; Ahn, K. J.; Kang, Y.; Lee, K.-G. Organic–Inorganic $FAPbBr_3$ Perovskite Quantum Dots as a Quantum Light Source: Single-Photon Emission and Blinking Behaviors. *ACS Photonics* **2018,** *5*, 4937–4943

(39) Park, Y.-S.; Bae, W. K.; Pietryga, J. M.; Klimov, V. I. Auger Recombination of Biexcitons and Negative and Positive Trions in Individual Quantum Dots. *ACS Nano* **2014,** *8*, 7288-7296.

(40) Frantsuzov, P. A.; Volkan-Kacso, S.; Janko, B. Model of Fluorescence Intermittency of Single Colloidal Semiconductor Quantum Dots Using Multiple Recombination Centers. *Phys. Rev. Lett.* **2009,** *103*, 207402.

(41) Frantsuzov, P. A.; Marcus, R. A. Explanation of Quantum Dot Blinking without the Long-Lived Trap Hypothesis. *Phys. Rev. B* **2005,** *72*, 155321.

(42) Gerhard, M.; Louis, B.; Frantsuzov, P. A.; Li, J.; Kiligaridis, A.; Hofkens, J.; Scheblykin, I. G. Heterogeneities and Emissive Defects in $MAPbI_3$ Perovskite Revealed by Spectrally Resolved Luminescence Blinking. *Adv.Optical Mater.* **2021,** *9*, 2001380.

(43) Seth, S.; Ahmed, T.; Samanta, A. Photoluminescence Flickering and Blinking of Single $CsPbBr_3$ Perovskite Nanocrystals: Revealing Explicit Carrier Recombination Dynamics. *J. Phys. Chem. Lett.* **2018,** *9*, 7007-7014.

(44) Galland, C.; Ghosh, Y.; Steinbruck, A.; Sykora, M.; Hollingsworth, J. A.; Klimov, V. I.; Htoon, H. Two Types of Luminescence Blinking Revealed by Spectroelectrochemistry of Single Quantum Dots. *Nature* **2011,** *479*, 203-207.

(45) Kim, T.; Jung, S. I.; Ham, S.; Chung H.; Kim, D. Elucidation of Photoluminescence Blinking Mechanism and Multiexciton Dynamics in Hybrid Organic–Inorganic Perovskite Quantum Dots. *Small* **2019,** *15*, 1900355.

(46) Trinh, C.T.; Minh, D. N.; Ahn, K.J; Kang, Y.; Lee, K.-G. Verification of Type-A and Type B-HC Blinking Mechanisms of Organic–Inorganic Formamidinium Lead Halide Perovskite Quantum Dots by FLID Measurements. *Sci. Rep.* **2020,** *10*, 2172.

(47) Reid, K. R.; McBride, J. R.; Croix, A. D. L.; Freymeyer, N. J.; Click, S. M.; Macdonald, J. E.; Rosenthal, S. J. Role of Surface Morphology on Exciton Recombination in Single Quantum Dot-in-Rods Revealed by Optical and Atomic Structure Correlation. *ACS Nano* **2018,** *12*, 11434–11445.

(48) Ahmed, T.; Seth, S.; Samanta, A. Mechanistic Investigation of the Defect Activity Contributing to the Photoluminescence Blinking of $CsPbBr_3$ Perovskite Nanocrystals. *ACS Nano* **2019,** *13*, 13537-13544.

(49) Seth, S.; Ahmed, T.; De, A.; Samanta, A. Tackling the Defects, Stability, and Photoluminescence of $CsPbX_3$ Perovskite Nanocrystals. *ACS Energy Lett.* **2019,** *4*, 1610-1618.

(50) Dutta, A.; Dutta, S. K.; Adhikari, S. D.; Pradhan, N. Phase-Stable $CsPbI_3$ Nanocrystals:The Reaction Temperature Matters. *Angew.Chem., Int.Ed.* **2018,** *57*, 9083-9087.

(51) Paul, S.; Samanta, A. N-Bromosuccinimide as Bromide Precursor for Direct Synthesis of Stable and Highly Luminescent Green-Emitting Perovskite Nanocrystals. *ACS Energy Lett.* **2020,** *5*, 64-69.

(52) Paul, S.; Ahmed, T.; Das, S.; Samanta, A. Effect of Lead:Halide Precursor Ratio on the Photoluminescence and Carrier Dynamics of Violet- and Blue-Emitting Lead Halide Perovskite Nanocrystals. *J. Phys. Chem. C* **2021,** *125*, 23539−23547.

(53) Pradhan, N. Tips and Twists in Making High Photoluminescence Quantum Yield Perovskite Nanocrystals. *ACS Energy Lett.* **2019,** *4*, 1634−1638.

(54) Imran, M.; Caligiuri, V.; Wang, M.; Goldoni, L.; Prato, M.; Krahne, R.; Trizio, L. D.; Manna, L. Benzoyl Halides as Alternative Precursors for the Colloidal Synthesis of Lead-Based Halide Perovskite Nanocrystals. *J. Am. Chem. Soc.* **2018,** *140*, 2656−2664.

(55) Dutta, A.; Behera, R. K.; Pal, P.; Baitalik, S.; Pradhan, N. Near-Unity Photoluminescence Quantum Efficiency for All $CsPbX_3$(X=Cl, Br, and I) Perovskite Nanocrystals: A Generic Synthesis Approach. *Angew. Chem., Int. Ed.* **2019,** *58*, 5552-5556.

(56) Liu, P.; Chen, W.; Wang, W.; Xu, B.; Wu, D.; Hao, J.; Cao, W.; Fang, F.; Li, Y.; Zeng, Y.; et al. Halide-Rich Synthesized Cesium Lead Bromide Perovskite Nanocrystals for Light-Emitting Diodes with Improved Performance. *Chem. Mater.* **2017,** *29*, 5168-5173.

(57) Park, J.; Kim, Y.; Ham, S.; Woo, J. Y.; Kim, T.; Jeong, S.; Kim, D. A Relationship Between the Surface Composition and Spectroscopic Properties of Cesium Lead Bromide ($CsPbBr_3$) Perovskite Nanocrystals: Focusing on Photoluminescence Efficiency. *Nanoscale* **2020,** *12*, 1563-1570.

(58) Cai, Y.; Wang, H.; Li, Y.; Wang, L.; Lv, Y.; Yang, X.; Xie, R.-J. Trimethylsilyl Iodine-Mediated Synthesis of Highly Bright Red-Emitting $CsPbI_3$ Perovskite Quantum Dots with Significantly Improved Stability. *Chem. Mater.* **2019,** *31*, 881-889.

(59) Das, S.; Samanta, A. Highly Luminescent and Phase-Stable Red/NIR-Emitting All-Inorganic and Hybrid Perovskite Nanocrystals. *ACS Energy Lett.* **2021,** *6*, 3780-3787.

(60) Yao, J.-S.; Ge, J.; Wang, K.-H.; Zhang, G.; Zhu, B.-S.; Chen, C.; Zhang, Q.; Luo, Y.; Yu, S.-H.; Yao, H.-B. Few-Nanometer-Sized α-$CsPbI_3$ Quantum Dots Enabled by Strontium Substitution and Iodide Passivation for Efficient Red-Light Emitting Diodes. *J. Am. Chem. Soc.* **2019,** *141*, 2069-2079.

(61) Shen, X.; Zhang, Y.; Kershaw, S. V.; Li, T.; Wang, C.; Zhang, X.; Wang, W.; Li, D.; Wang, Y.; Lu, M.; et al. Zn-Alloyed $CsPbI_3$ Nanocrystals for Highly Efficient Perovskite Light-Emitting Devices. *Nano Lett.* **2019,** *19*, 1552-1559.

(62) Akkerman, Q. A.; Meggiolaro, D.; Dang, Z.; Angelis, F. D.; Manna, L. Fluorescent Alloy $CsPbxMn_{1-x}I_3$ Perovskite Nanocrystals with High Structural and Optical Stability. *ACS Energy Lett.* **2017,** *2*, 2183-2186.

(63) Behera, R. K.; Dutta, A.; Ghosh, D.; Bera, S.; Bhattacharyya, S.; Pradhan, N. Doping the Smallest Shannon Radii Transition Metal Ion Ni(II) for Stabilizing α-$CsPbI_3$ Perovskite Nanocrystals. *J. Phys. Chem. Lett.* **2019,** *10*, 7916−7921.

(64) Chen, Z.; Zhou, B.; Yuan, J.; Tang, N.; Lian, L.; Qin, L.; Zhu, L.; Zhang, J.; Chen, R.; Zang, J. Cu^{2+}-Doped $CsPbI_3$ Nanocrystals with Enhanced Stability for Light Emitting Diodes. *J. Phys. Chem. Lett.* **2021,** *12*, 3038-3045.

(65) Shu, B.; Chang, Y.; Zhang, J.; Cheng, X.; Yu, D. Synthesis and Photoluminescence Kinetics of Ce^{3+}-Doped $CsPbI_3$ QDs with Near-Unity PLQY. *Nano Res.* **2021,** *14*, 3352-3357.

(66) Zhu, Y.; Zhao, J.; Yang, G.; Xu, X.; Pan, G. Ammonium Acetate Passivated $CsPbI_3$ Perovskite Nanocrystals for Efficient Red Light-Emitting Diodes. *Nanoscale* **2020,** *12*, 7712–7719.

(67) Lu, M.; Guo, J.; Lu, P.; Zhang, L.; Zhang, Y.; Dai, Q.; Hu, Y.; Colvin, V. L.; Yu, W. W. Ammonium Thiocyanate-Passivated $CsPbI_3$ Perovskite Nanocrystals for Efficient Red Light-Emitting Diodes. *J. Phys. Chem. C* **2019,** *123*, 22787-22972.

(68) Chen, Q.; Cao, S.; Xing, K.; Ning, M.; Zeng, R.; Wang, Y.; Zhao, J. Mg^{2+}-Assisted Passivation of Defects in $CsPbI_3$ Perovskite Nanocrystals for High-Efficiency Photoluminescence. *J. Phys. Chem. Lett.* **2021,** *12*, 11090-11097.

(69) Dong, Y.; Qiao, T.; Kim, D.; Parobek, D.; Rossi, D.; Son, D. H. Precise Control of Quantum Confinement in Cesium Lead Halide Perovskite Quantum Dots via Thermodynamic Equilibrium. *Nano Lett.* **2018,** *18*, 3716-3722.

(70) Tang, J.; Marcus, R. A. Mechanisms of Fluorescence Blinking in Semiconductor Nanocrystal Quantum Dots. *J. Chem. Phys.* **2005,** *123*, 054704.

(71) Balakrishnan, S. K.; Kamat, P. V. Ligand Assisted Transformation of Cubic $CsPbBr_3$ Nanocrystals into Two-Dimensional $CsPb_2Br_5$ Nanosheets. *Chem. Mater.* **2018,** *30*, 74-78.

(72) Ravi, V. K.; Santra, P. K.; Joshi, N.; Chugh, J.; Singh, S. K.; Rensmo, H.; Ghosh, P.; Nag, A., Origin of the Substitution Mechanism for the Binding of Organic Ligands on the Surface of $CsPbBr_3$ Perovskite Nanocubes. *J. Phys. Chem. Lett.* **2017,** *8*, 4998-4994.

CHAPTER 6

Photoluminescence Blinking of Quantum Confined $CsPbBr_3$ Perovskite Nanocrystals: Influence of Size

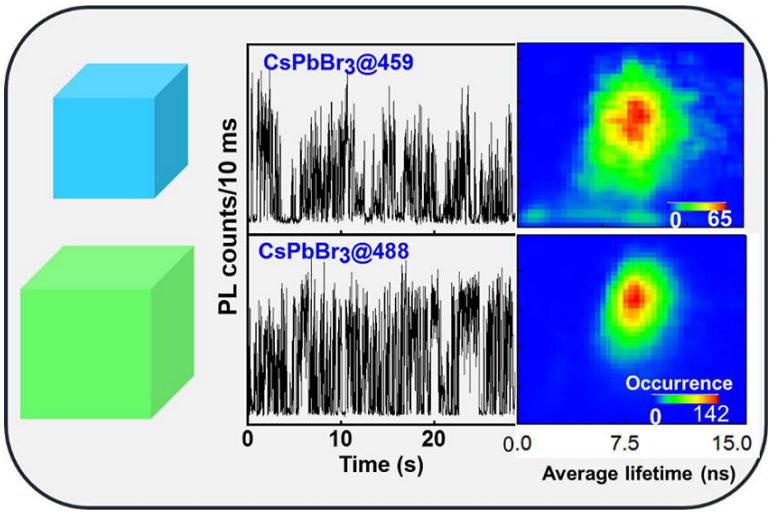

Overview

Quantum confined $CsPbBr_3$ nanocrystals (NCs) with adjustable photoluminescence (PL) in the range of 470 - 500 nm are particularly desirable for applications in light emitting diodes (LEDs) and many quantum technologies. Exploration of full potential of these perovskite NCs requires an understanding of the random fluctuation of their PL at the single particle level, commonly termed as blinking. In this work, we study the PL blinking of quantum confined single NCs of $CsPbBr_3$ of three different sizes between 3.80 and 5.90 nm in immobilized and fluid conditions to understand the recombination pathways and dynamics of the photogenerated charge carriers. In the immobilized state, the PL intensity trajectories and PL lifetime-intensity distributions of these single NCs reveal the contributions of both Auger recombination and trapping of hot carriers to the PL fluctuation. The results suggest a higher carrier trapping rate constant for smaller NCs. The fluorescence correlation spectroscopy (FCS) and fluorescence lifetime correlation spectroscopy (FLCS) measurements on freely diffusing NCs show a higher off-state fraction and lower per-particle brightness of the smaller NCs. It is concluded that a larger trap depth and higher probability density of the carriers at the surface in smaller NCs make the trapping process more feasible and detrapping more difficult. The results provide first information on the effect of size on PL blinking of the quantum confined $CsPbBr_3$ NCs, and this knowledge is expected to be useful in better designing photoluminescent samples of this class for optoelectronic applications.

6.1. Introduction

The Cesium lead halide ($CsPbX_3$) perovskite nanocrystals (NCs) continue to receive great attention owing to their potential applications in optoelectronic devices such as in light-emitting diodes [1-8] and single photon sources.[9-13] However, the fluctuation of photoluminescence (PL) of the single NCs of these substances between bright (on) and dark (off) states,[9, 12, 14-20] and sometimes, between the 'on' and a low intensity gray state,[16, 18, 21] is impediment to these applications. The PL fluctuation occurs over a rather broad timescale ranging from tens of microseconds to hundreds of seconds.[22, 23] While PL of these perovskite NCs originates from radiative recombination of the electron and hole produced on photoexcitation, the fluctuation of PL is caused by the involvement of various trap states in these systems. Several processes can contribute to the PL blinking of the semiconductor NCs.[9, 14, 17, 21, 22, 24] When one of the charge carriers is trapped for a longer duration, the NCs become charged. Absorption of another photon by a charged NC when produces an exciton, the system becomes a trion.[9, 21, 24-26] The trion can recombine nonradiatively by Auger recombination or/and radiatively at a much faster rate (twice the neutral exciton recombination rate).[9, 21, 24, 26] PL blinking arising from trion-mediated recombination is known as Auger or A-type blinking.[24] Trapping of charge carrier in a short-lived trap states can facilitate its instant relaxation by a nonradiative pathway.[16, 18, 19, 21, 27] Random activation and deactivation of these trap states results in a constantly changing nonradiative rate constant.[21, 22, 27] This time dependent fluctuation of the nonradiative rate constant leads to PL blinking, which is termed as band-edge carrier (BC)-blinking when trapping of the charge carriers takes place from the band-edge states.[21] Blinking can also be caused by trapping of the hot carriers (HC-blinking).[14, 22, 24, 28] Trapping of the hot carriers allows their rapid relaxation through a nonradiative recombination route, and one observes a large drop of PL intensity without any noticeable change in lifetime. As both BC- and HC-blinking arise from the activation and deactivation of the trap states, these two types of blinking are often referred to as B-type blinking.[24, 28] In many cases, more than one mechanism of blinking is observed.[16, 18, 19, 21, 24] The coexistence of Auger-, BC-and HC-blinking in single perovskite NCs has also been reported.[16, 29]

PL blinking studies on perovskite single NCs, excepting a few on $MAPbBr_3$ NCs,[14, 15] have been carried out on large systems (size range 6-20 nm) with no/weak quantum confinement.[9, 11, 14, 16-18, 30-38] One main reason for dearth of PL blinking studies on smaller particles was lack of any method of their preparation with uniform size distribution and control on size. A very recent report on synthesis of quantum confined $CsPbX_3$ NCs with uniform size distribution[39] has enabled photophysical studies on these smaller NCs.[40-42] These studies have revealed blue-shifted emission with larger Stokes shift,[39, 42] faster biexciton auger recombination rate,[40, 43, 44] intense dark exciton emission[41] and high single photon purity[11] of the quantum confined perovskite NCs compared to the non-quantum confined system. The smaller size NCs also have higher trion and biexciton binding energy because the Coulomb interaction between electrons and holes is enhanced as the NCs decrease in size.[45, 46] As size of the NCs plays an important role on the charge carrier trapping and detrapping processes,[14, 47, 48] an investigation of the PL blinking of quantum confined perovskite NCs of different size is expected to provide an understanding of the charge carrier trapping and detrapping processes in these substances, which may help unleashing these materials' full application potentials.

In order to study the PL blinking behavior of quantum confined perovskite NCs of different size, we have prepared $CsPbBr_3$ NCs with 3.80, 4.80 and 5.90 nm edge length and investigated their PL blinking by analyzing PL blinking traces, fluorescence lifetime intensity distribution (FLID) patterns and statistical distribution of the on- and off-events. PL blinking of freely diffusing NCs is also studied employing fluorescence correlation spectroscopy (FCS) and fluorescence lifetime correlation spectroscopy techniques.

6.2. Results

6.2.1. Structural Characterization and Ensemble PL Properties

The TEM images indicate an edge length of 3.80±0.24, 4.80±0.60 and 5.90±0.70 nm for the $CsPbBr_3$ NCs obtained at 80°C, 140°C and 180°C, respectively (Figure 6.1.a-c and AIV.1). The absorption and PL spectra of these NCs are shown in Figure 6.1.d-f. We have labelled these NCs

with numerical extension of their respective first excitonic peak position. The PL peaks of the $CsPbBr_3$@459, $CsPbBr_3$@478 and $CsPbBr_3$@488 NCs are observed at 470, 486 and 496 nm, respectively. Photoluminescence quantum yield (PLQY) of the $CsPbBr_3$@459, $CsPbBr_3$@478 and $CsPbBr_3$@488 NCs are estimated to be 0.45±0.03, 0.75±0.03 and 0.90±0.05, respectively.

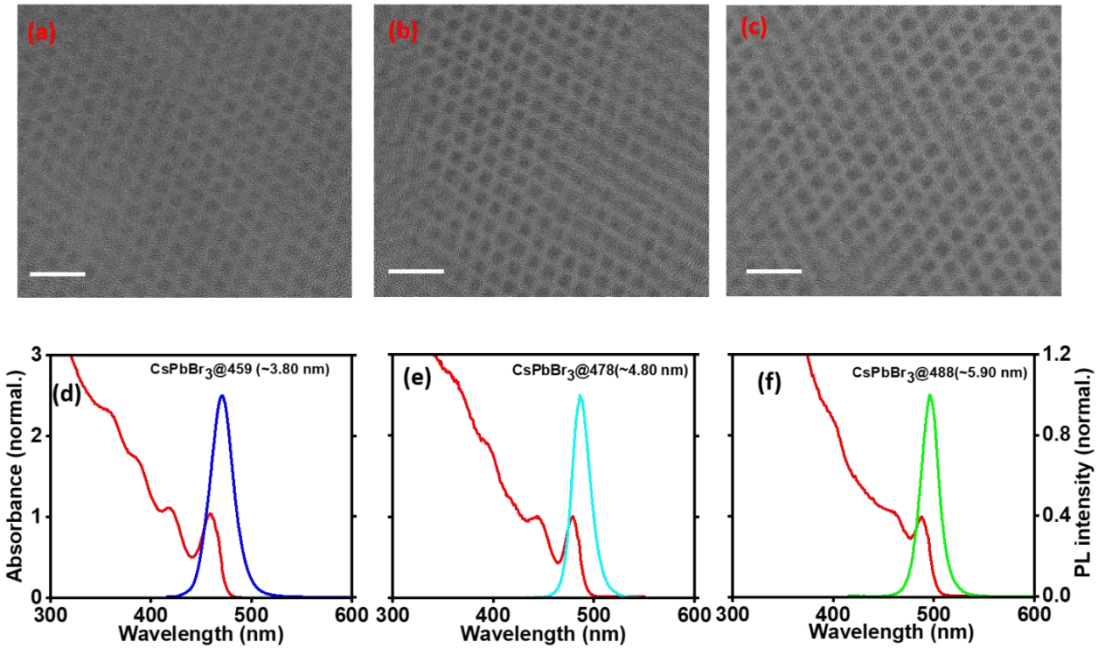

Figure 6.1. TEM images (top panel; a-c), and absorption and PL spectra (bottom panel; d-f) of the $CsPbBr_3$ NCs of different sizes. Scale bar is 20 nm for the TEM images. PL spectra were recorded by exciting colloidal dispersion of these NCs at 405 nm.

6.2.2. Single Particle Photoluminescence Properties

Before carrying out the PL blinking measurements on the immobilized NCs, we performed photon antibunching experiment to ensure that each fluorescent particle represents a single NC. The single-photon purity is characterized by the second-order intensity correlation function,

$$g^{(2)}(t) = \frac{\langle I_1(t) I_2(t+\tau) \rangle}{\langle I_1(t) \rangle \langle I_2(t+\tau) \rangle} \qquad (1)$$

as a function of the delay time τ between the two photon detection events, measured in a Hanbury Brown and Twiss (HBT) type setup (details in experimental section). Here, $I_1(t)$ is the emission intensity at time t in detector 1, and I_2 (t+ τ) is the intensity after a time delay of τ at detector 2. For a single particle, $g^{(2)}(0)$ is expected to be 0 as it cannot emit more than one photon at any given time. This implies that a dip at "zero" time in the correlation curves indicates photon antibunching. For our samples, as can be seen from Figure 6.2, $g^{(2)}(0)$ is not zero, but very small compared to the side peaks at other time delays. The non-zero value of $g^{(2)}(0)$ is attributed to biexciton, whose formation cannot be completely prevented even at low laser power.[9, 48, 51]

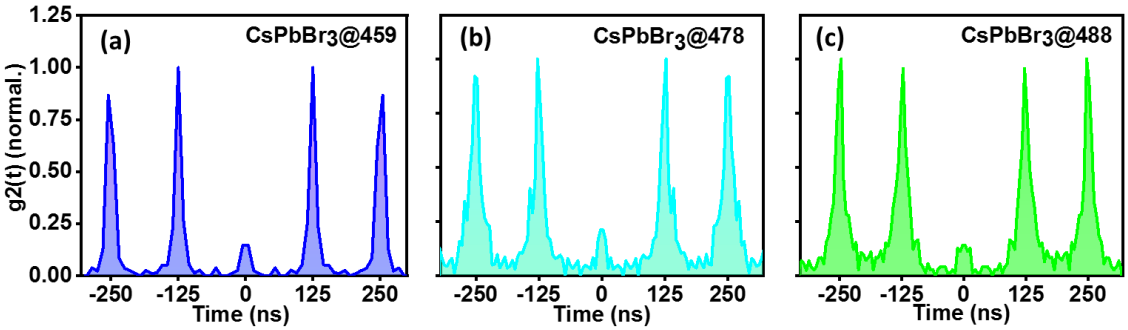

Figure 6.2. Second order photo-correlation plots of $CsPbBr_3$@459 (a), $CsPbBr_3$@478 (b) and $CsPbBr_3$@488 (c) NCs. Samples were excited at 405 nm using a pulsed laser with 8 MHz repetition rate.

PL blinking trajectories of the representative NCs of $CsPbBr_3$@459, $CsPbBr_3$@478 and $CsPbBr_3$@488 NCs, depicted in Figure 6.3.a-c (and also in AIV.2-4), show that PL of these NCs fluctuates over a range of intensity levels. The occurrence histograms (Figure 6.3.d-f) indicate no clear separation between the on- and off- PL intensity states. In order to understand the blinking mechanism, we have measured PL decay profiles of three different intensity regions (indicated by green, blue and violet shades) of the blinking traces (Figure 6.3.g-i). The high intensity level of these NCs is characterized by single exponential decay with lifetime around 8-9 ns (Table 6.1). The PL decay of the intermediate and low intensity levels are bi-exponential with one long (~8 ns) and a short component (~1 ns) (Table 6.1). The long 8-9 ns component of the highest intensity levels arises clearly from band-edge excitonic recombination. For the intermediate- and

low-intensity regions, a lifetime close to that of the high intensity region is possible only if the electron or hole is trapped prior to their relaxation to the band edge. Hence, this implies trapping of the hot carriers contributes to the PL fluctuation of these NC. The short component is attributed to Auger recombination of trion.[9,16, 26, 40]

The fluorescence lifetime intensity distribution (FLID) of these NCs also provides an understanding of the PL blinking mechanism. For the $CsPbBr_3$@459 NCs, the FLID plot (Figure 6.3.j) consists of (i) a high intensity-high lifetime, (ii) a low intensity-low lifetime and (iii) a low intensity-high lifetime component. The nonlinear nature of the FLID plot and low intensity-low lifetime component are reflection of Auger blinking,[9, 21, 24] and the low intensity-high lifetime component is an indicative of HC blinking.[16, 24, 28] For $CsPbBr_3$@478 and $CsPbBr_3$@488 NCs (Figure 6.3.k-l), both types of blinking are not clearly observable in the FLID plots due to low occurrence of the off-intensity levels. Coexistence of HC-blinking and Auger-blinking for each single NC indicates that these NCs have both short-lived and long-lived trap states.

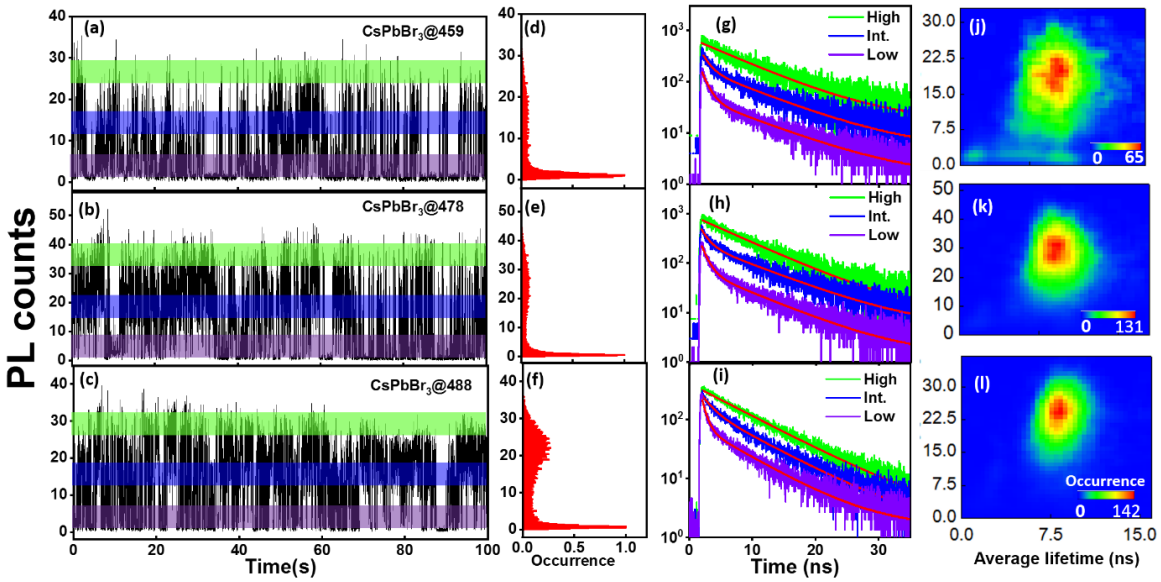

Figure 6.3. Representative PL intensity trajectories (a-c) (binning time 10 ms) and occurrence histograms (d-f) of the NCs of different sizes. Green, blue and violet shades indicate high, intermediate and low intensity regions, respectively, for which PL decay profiles were measured (g-i). FLID plots of these NCs are shown in panel j-l.

Table 6.1. PL lifetime components (τ_i) and their contributions (a_i) for different PL intensity levels of different samples of $CsPbBr_3$ NCs.

System	region	τ_1 /ns (a_1)	τ_2 /ns (a_2)
$CsPbBr_3$@459	high	8.56	
	intermediate	8.69 (0.44)	1.07 (0.56)
	low	7.70 (0.17)	0.82 (0.83)
$CsPbBr_3$@478	high	8.20	
	intermediate	8.40 (0.52)	1.37 (0.48)
	low	7.20 (0.30)	0.83 (0.70)
CsPbBr3@488	high	7.90	
	intermediate	7.60 (0.57)	1.60 (0.43)
	low	6.90 (0.42)	0.73 (0.58)

We have analyzed the probability density distribution (PDD) of the on- and off-events, P_{on} and P_{off}, to further understand the trapping and detrapping processes in these samples. For this purpose, we have sorted the data into on and off categories by assigning a threshold, above which the NCs are considered on and below which they are considered off. The PDD plots of the off-events (Figure 4) are best represented by a power law function (equation 2) indicating a widely distributed off→on switching rates. However, the PDD plots of the on events (Figure 6.4) are best represented by a truncated power-law (equation 3), indicating that the events which are power-law distributed at shorter times, become exponential at the longer times.

$$P_{off}(t) = t_{off}^{-m_{off}} \qquad (2)$$

$$P_{on}(t) = t_{ON}^{-m_{on}} exp - ({}^{t_{on}}/_{\tau_c^{on}}) \qquad (3)$$

Where, $m_{off/on}$ is the power-law exponent and τ_c^{on} represents the time corresponding to the exponential truncation of the power law. The exponential truncation of the on-events at long time implies that the on→off switching at long on-duration occurs at a single rate or the distributed rate process saturates at long on-duration.[22, 52, 53]

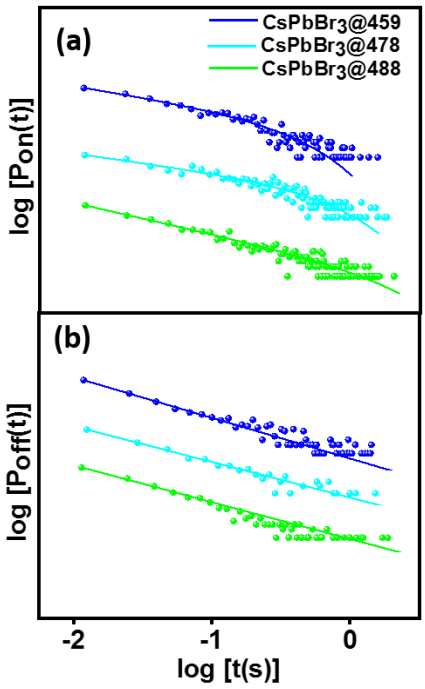

Figure 6.4. Probability density distribution of the on- and off-events (top and bottom panel) of the $CsPbBr_3$@459, $CsPbBr_3$@478 and $CsPbBr_3$@488 NCs.

A much higher m_{off} value of these NCs compared to their m_{on} value indicates that PL blinking is dominated by longer on-events and shorter off-events. A distinct variation of the truncation time with size of the NCs is observable (Figure 6.5.a and Table 6.2).With increase in size of the NCs, an increase in truncation time [0.31±0.15 s ($CsPbBr_3$@459), 0.51±0.28 s ($CsPbBr_3$@478) and 0.65±0.31 s ($CsPbBr_3$@488)] indicates a decrease in trapping rate constant (k_t).[48, 54-56] The average time fraction in the on-state (Figure 6.5.b) is estimated from measured blinking trajectory of nearly 100 NCs of a particular size. With increase in size of the NCs, this number increases as follows; 0.58±0.17 ($CsPbBr_3$@459), 0.69±0.15 ($CsPbBr_3$@478) and 0.77±0.16 ($CsPbBr_3$@488). A lower on-state fraction for the smaller $CsPbBr_3$ NCs is attributed to higher carrier trapping rate and lower detrapping rate in these systems. In larger NCs, charge carrier wave functions are localized in the core of the NCs, and with decrease in size of the NCs, the carrier probability density at the surface increases,[57] thus making the trapping process more

feasible. As $CsPbBr_3$ NCs possesses shallow trap states,[1, 8, 58] and the depth of these trap states decreases with increase in size of the NCs, the trapping process is more feasible and detrapping more difficult for smaller NCs.

Table 6.2. Power law exponents and truncation time for the $CsPbBr_3$ NCs of different sizes.

System	NCs size (nm)	m_{off}	m_{on}	τ_c^{on} (s)
$CsPbBr_3$@459	3.80±0.24	1.58±0.26	0.75±0.12	0.31±0.15
$CsPbBr_3$@478	4.80±0.60	1.78±0.32	0.71±0.13	0.51±0.28
$CsPbBr_3$@488	5.90±0.70	1.77±0.40	0.72±0.14	0.69±0.35

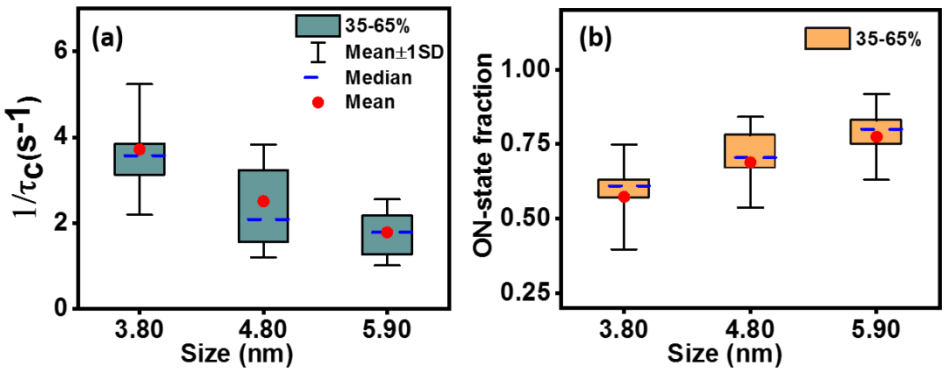

Figure 6.5. (a) Box plot of inverse of the truncation time ($1/\tau_c^{on}$) and (b) on-state fraction of the $CsPbBr_3$ NCs of different sizes. Interquartile range is equal to 35−65th percentile. Spheres indicate the mean. Whiskers indicate standard deviation from the mean. Dashed lines in the box indicate the median.

6.2.2. FCS and FLCS Measurement of the NCs

Additional insight on PL blinking of these NCs is obtained from the FCS and FLCS study of freely diffusing NCs. While the time resolution of PL blinking data discussed so far for the immobilized samples is limited by the binning time (10 ms here) of the measurement, the FCS and FLCS measurements can be used for extracting information on PL fluctuation occurring in μs timescale.[32, 59] In these techniques, one measures the fluctuations of PL intensity of a highly

dilute solution (nM) of the NCs in a small volume of the sample (typically ~1 fL) using a confocal fluorescence microscope (details in experimental section). While FCS experiment records only macroscopic arrival time of each detected photon (τ, with resolution μs) with respect to the beginning of the experiment, the FLCS additionally measures the microscopic delay time (t, with ps resolution) of the detected photons relative to the excitation pulse[60] which allowed us to study autocorrelation function of PL fluctuation of the neutral exciton (~8.5 ns) and trion (~1.6 ns) separately. The FCS and FLCS data of these NCs (Figure 6a, b and S5-S6) are best described by equation 5, which considers PL fluctuation due to (i) diffusion of the NCs in and out of the observation volume and (ii) trapping of the charge carriers, represented by a stretched exponential decay component. The amplitude of correlation at time τ, G(τ), is expressed as,

$$G(\tau) = [1 + \frac{T}{1-T}\exp(-\frac{\tau}{\tau_T})^{\beta}]\frac{1}{N}(1 + \frac{\tau}{\tau_D})^{-1}(1 + \frac{\tau}{k^2\tau_D})^{-\frac{1}{2}} \qquad (5)$$

where, N is the average number of particles undergoing reversible PL intensity fluctuation in the observation volume, τ_D is the diffusion time of the NCs, T is the fraction of the particles in their "off" state, and τ_T is the dark-state relaxation time or blinking time. β is the stretching exponent with a value between 0 and 1 and is related to the distribution of τ_T. κ (= ω_z/ω_{xy}) is the structure parameter of the observation volume; ω_z and ω_{xy} are the longitudinal and transverse radii of observation volume, respectively. The per-particle brightness (PPB) of the NCs is estimated by $I/\langle N\rangle$, where I is the average count rate of the PL intensity trace.

A close look at various parameters associated with PL fluctuation (Table 6.3), as obtained from analysis of the FCS and FLCS curves, reveals a large deviation of the β values from unity. This indicates a broadly distributed kinetics of PL blinking indicating the involvement of multiple trap states with varying carrier trapping and detrapping rates. The data also shows a decrease in off-state fraction with increase in size of the NCs (Table 6.3). While this trend is similar to that observed in the case of immobilized samples, the absolute values differ significantly in the two cases. The FCS and FLCS measurements provide a higher off-state

fraction compared to the blinking measurements on immobilized NCs simply because the former captures PL fluctuations at a faster timescale. As can be seen (Figure 6.6.c), the per-particle brightness (PPB) of these NCs increases with increase in size of the NCs: 1213.60±317.70 cps ($CsPbBr_3$@459), 1593.40±289.90 cps ($CsPbBr_3$@478) and 2131.50±421.70 cps (CsPbBr3@488). This trend is consistent with size dependent variation of the PLQY of the systems. A higher value of the off-state fraction and a lower PPB value of the smaller NCs reconfirms that with decrease in NCs size trapping become more feasible and detrapping difficult.

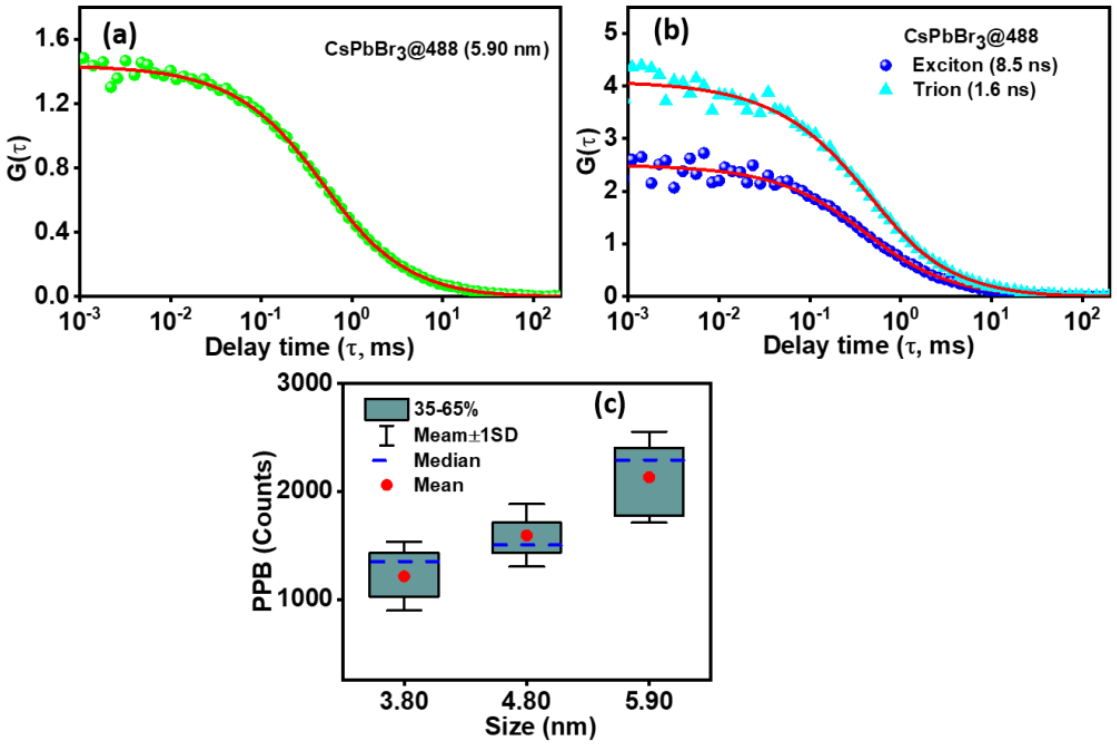

Figure 6.6. (a) Fluorescence correlation data (green dots) and the fit (red line) to the data of the $CsPbBr_3$@488 NCs in 1-octadecene. (b) Autocorrelation amplitudes of 8.5 ns (exciton) and 1.6 ns (trion) component as a function of delay time of this NCs. (c) Per-particle brightness of three different size NCs.

Table 6.3. Estimated values of the stretching exponent (β), off-state fraction (T) and off state relaxation time (τ_T).

System	Experiment	β	T	τ_T (ms)
$CsPbBr_3$@459	FCS	0.67±0.10	0.58±0.08	0.49±0.09
	FLCS (exciton)	0.65±0.12	0.63±0.09	0.43±0.05
	FLCS (trion)	0.53±0.08	0.68±0.12	0.44±0.05
$CsPbBr_3$@478	FCS	0.69±0.03	0.51±0.07	0.45±0.05
	FLCS (exciton)	0.71±0.10	0.55±0.07	0.37±0.06
	FLCS (trion)	0.63±0.09	0.57±0.11	0.40±0.08
$CsPbBr_3$@488	FCS	0.76±0.05	0.42±0.07	0.43±0.05
	FLCS (exciton)	0.79±0.11	0.46±0.06	0.42±0.06
	FLCS (trion)	0.65±0.08	0.47±0.07	0.35±0.05

6.3. Conclusion

PL blinking of three different size quantum confined single NCs of $CsPbBr_3$ has been studied. Both hot carrier trapping- and Auger-recombination are found to contribute to the PL fluctuations of the immobilized NCs indicating the presence of both short-lived and long-lived trap states. The results also suggest an increase in the trapping rate constant with decrease in size of the NCs. The FCS and FLCS measurements indicate a lower off-state fraction and higher per particle brightness for the bigger NCs. The observation is rationalized considering a smaller trap-depth, and localization of the charge-carrier wavefunction in the core region for large size NCs. The findings provide first insight into the charge carrier recombination pathway and dynamics of the quantum confined $CsPbBr_3$ NCs from PL blinking studies and the findings will be useful in the design and development of small size highly luminescent perovskite NCs for optoelectronic applications.

Bibliography

1. Protesescu, L.; Yakunin, S.; Bodnarchuk, M. I.; Krieg, F.; Caputo, R.; Hendon, C. H.; Yang, R. X.; Walsh, A.; Kovalenko, M. V. Nanocrystals of Cesium Lead Halide Perovskites ($CsPbX_3$, X = Cl, Br, and I): Novel Optoelectronic Materials Showing Bright Emission with Wide Color Gamut. *Nano Lett.* **2015,** *15*, 3692−3696.

2. Paul, S.; Ahmed, T.; Das, S.; Samanta, A. Effect of Lead:Halide Precursor Ratio on the Photoluminescence and Carrier Dynamics of Violet- and Blue-Emitting Lead Halide Perovskite Nanocrystal. *J. Phys. Chem. C* **2021,** *125*, 23539–23547.

3. Liu, X.-K.; Xu, W.; Bai, S.; Jin, Y.; Wang, J.; Friend, R. H.; Gao, F. Metal Halide Perovskites for Light-Emitting Diodes. *Nat. Mater.* **2021,** *20*, 10-21.

4. Fakharuddin, A.; Gangishetty, M. K.; Abdi-Jalebi, M.; Chin, S.-H.; Yusoff, A. R. b. M.; Congreve, D. N.; Tress, W.; Deschler, F.; Vasilopoulou, M.; Bolink, H. J. Perovskite Light-Emitting Diodes. *Nat. Electron.* **2022,** 5, 203-216.

5. Wei, Z.; Xing, J. The Rise of Perovskite Light-Emitting Diodes. *J. Phys. Chem. Lett.* **2019,** *10*, 3035-3042.

6. Ji, K.; Anaya, M.; Abfalterer, A.; Stranks, S. D. Halide Perovskite Light-Emitting Diode Technologies. *Adv. Optical Mater.* **2021,** *9*, 2002128.

7. Paul, S.; Samanta, A. N-Bromosuccinimide as Bromide Precursor for Direct Synthesis of Stable and Highly Luminescent Green-Emitting Perovskite Nanocrystals. *ACS Energy Lett.* **2020,** *5*, 64-69.

8. Dey, A.; Ye, J.; De, A.; Debroye, E.; Ha, S. K.; Bladt, E.; Kshirsagar, A. S.; Wang, Z.; Yin, J.; Wang, Y.; et al. State of the Art and Prospects for Halide Perovskite Nanocrystals. *ACS Nano* **2021,** *15*, 10775-10981.

9. Park, Y.-S.; Guo, S.; Makarov, N. S.; Klimov, V. I. Room Temperature Single-Photon Emission from Individual Perovskite Quantum Dots. *ACS Nano* **2015,** *9*, 10386–10393.

10. Rainò, G.; Yazdani, N.; Boehme, S. C.; Kober-Czerny, M.; Zhu, C.; Krieg, F.; Rossell, M. D.; Erni, R.; Wood, V.; Infante, I.; Kovalenko, M. V. Ultra-Narrow Room-Temperature Emission from Single $CsPbBr_3$ Perovskite Quantum Dots. *Nat. Commun.* **2022,** *13*, 2587.

11. Zhu, C.; Marczak, M.; Feld, L.; Boehme, S. C.; Bernasconi, C.; Moskalenko, A.; Cherniukh, I.; Dirin, D.; Bodnarchuk, M. I.; Kovalenko, M. V.; Rainò, G. Room-Temperature, Highly Pure Single-Photon Sources from AllInorganic Lead Halide Perovskite Quantum Dots. *Nano Lett.* **2022,** *22*, 3751-3760.

12. Feld, L. G.; Shynkarenko, Y.; Krieg, F.; Rainò, G.; Kovalenko, M. V. Perovskite Quantum Dots for Super-Resolution Optical Microscopy: Where Strong Photoluminescence Blinking Matters. *Adv.Optical Mater.* **2021,** *9*, 2100620.

13. Mir, W. J.; Alamoudi, A.; Yin, J.; Yorov, K. E.; Maity, P.; Naphade, R.; Shao, B.; Wang, J.; Lintangpradipto, M. N.; Nematulloev, S.; Emwas, A.-H.; Genovese, A.; Mohammed, O. F.; Bakr, O. M. Lecithin Capping Ligands Enable Ultrastable Perovskite-Phase CsPbI3 Quantum Dots for Rec. 2020 Bright-Red Light-Emitting Diodes. *J. Am. Chem. Soc.* **2022,** *144*, 13302–13310.

14. Kim, T.; Jung, S. I.; Ham, S.; Chung, H.; Kim, D. Elucidation of Photoluminescence Blinking Mechanism and Multiexciton Dynamics in Hybrid Organic–Inorganic Perovskite Quantum Dots. *Small* **2019,** *15*, 1900355.

15. Han, X.; Zhang, G.; Li, B.; Yang, C.; Guo, W.; Bai, X.; Huang, P.; Chen, R.; Qin, C.; Hu, J.; Ma, Y.; Zhong, H.; Xiao, L.; Jia, S. Blinking Mechanisms and Intrinsic Quantum-Confined Stark Effect in Single Methylammonium Lead Bromide Perovskite Quantum Dots. *Small* **2020,** *16*, 2005435.

16. Ahmed, T.; Seth, S.; Samanta, A. Mechanistic Investigation of the Defect Activity Contributing to the Photoluminescence Blinking of $CsPbBr_3$ Perovskite Nanocrystals. *ACS Nano* **2019,** *13*, 13537−13544.

17. Yarita, N.; Tahara, H.; Saruyama, M.; Kawawaki, T.; Sato, R.; Teranishi, T.; Kanemitsu, Y. Impact of Postsynthetic Surface Modification on Photoluminescence Intermittency in Formamidinium Lead Bromide Perovskite Nanocrystals. *J. Phys. Chem. Lett.* **2017,** *8*, 6041−6047.

18. Seth, S.; Ahmed, T.; Samanta, A. Photoluminescence Flickering and Blinking of Single $CsPbBr_3$ Perovskite Nanocrystals: Revealing Explicit Carrier Recombination Dynamics. *J. Phys. Chem. Lett.* **2018,** *9*, 7007−7014.

19. Paul, S.; Samanta, A. Phase-Stable and Highly Luminescent $CsPbI_3$ Perovskite Nanocrystals with Suppressed Photoluminescence Blinking. *J. Phys. Chem. Lett.* **2022,** *13*, 5742–5750.

20. Bose, R.; Zhou, X.; Guo, T.; Yang, H.; Yin, J.; Mishra, A.; Slinker, J. D.; Bakr, O. M.; Mohammed, O. F.; Malko, A. V. Single-Particle Spectroscopy as a Versatile Tool to Explore Lower-Dimensional Structures of Inorganic Perovskites. *ACS Energy Lett.* **2021,** *6*, 3695–3708.

21. Yuan, G.; Gomez, D. E.; Kirkwood, N.; Boldt, K.; Mulvaney, P. Two Mechanisms Determine Quantum Dot Blinking. *ACS Nano* **2018,** *12*, 3397-3405.

22. Cordones, A. A.; Leone, S. R. Mechanisms for Charge Trapping in Single semiconductor Nanocrystals Probed by Fluorescence Blinking. *Chem. Soc. Rev.* **2013,** *42*, 3209-3221.

23. Efros, A. L.; Nesbitt, D. J. Origin and Control of Blinking in Quantum Dots. *Nature Nanotechnol.* **2016,** *11*, 661–671.

24. Galland, C.; Ghosh, Y.; Steinbruck, A.; Sykora, M.; Hollingsworth, J. A.; Klimov, V. I.; Htoon, H. Two Types of Luminescence Blinking Revealed by Spectroelectrochemistry of Single Quantum Dots. *Nature* **2011,** *479*, 203-207.

25. Nirmal, M.; Dabbousi, B. O.; Bawendi, M. G.; Macklin, J. J.; Trautmant, J. K.; Harris, T. D.; Brus, L. E. Fluorescence Intermittency in Single Cadmium Selenide Nanocrystals. *Nature* **1996,** *383*, 802-804.

26. Kanemitsu, Y. Trion Dynamics in Lead Halide Perovskite Nanocrystals. *J. Chem. Phys.* **2019,** *151*, 170902.

27. Frantsuzov, P. A.; Volkan-Kacso, S.; Janko, B. Model of Fluorescence Intermittency of Single Colloidal Semiconductor Quantum Dots Using Multiple Recombination Centers. *Phys. Rev. Lett.* **2009,** *103*, 207402.

28. Trinh, C. T.; Minh, D. N.; Ahn, K. J.; Kang, Y.; Lee, K.-G. Verification of Type-A and Type B-HC Blinking Mechanisms of Organic–Inorganic Formamidinium Lead Halide Perovskite Quantum Dots by FLID Measurements. *Sci. Rep.* **2020,** *10*, 2172.

29. Park, J.; Kim, Y.; Ham, S.; Woo, J. Y.; Kim, T.; Jeong, S.; Kim, D. A Relationship Between the Surface Composition and Spectroscopic Properties of Cesium Lead Bromide ($CsPbBr_3$) Perovskite Nanocrystals: Focusing on Photoluminescence Efficiency. *Nanoscale* **2020,** *12*, 1563–1570

30. Yuan, G.; Ritchie, C.; Ritter, M.; Murphy, S.; Gomez, D. E.; Mulvaney, P. The Degradation and Blinking of Single $CsPbI_3$ Perovskite Quantum Dots. *J. Phys. Chem. C* **2018,** 122, 13407−13415.

31. Ahmed, T.; Paul, S.; Samanta, A. Photoluminescence Blinking Revealing Static and Dynamic Heterogeneity of the Hole Transfer Process in Phenothiazine-Adsorbed $FAPbBr_3$ Single Nanocrystals. *J. Phys. Chem. C* **2022,** *126*, 9109–9116.

32. Ahmed, T.; De, A.; Paul, S.; Samanta, A. Individual Particle-Level Picture of Charge Carrier Recombination in Bi-Doped $CsPbBr_3$ Nanocrystals. *J. Phys. Chem. C* **2021,** *125*, 2156-2162.

33. Mandal, S.; Ghosh, S.; Mukherjee, S.; Roy, D.; De, C. K.; Mukhuti, K.; Mandal, P. K. Near-Ergodic $CsPbBr_3$ Perovskite Nanocrystal with Minimal Statistical Aging. *J. Phys. Chem. Lett.* **2021,** *12*, 10169–10174.

34. Mandal, S.; Mukherjee, S.; De, C. K.; Roy, D.; Ghosh, S.; Mandal, P. K. Extent of Shallow/Deep Trap States beyond the Conduction Band Minimum in Defect-Tolerant $CsPbBr_3$ Perovskite Quantum Dot: Control over the Degree of Charge Carrier Recombination. *J. Phys. Chem. Lett.* **2020,** *11*, 1702-1707.

35. Li, B.; Huang, H.; Zhang, G.; Yang, C.; Guo, W.; Chen, R.; Qin, C.; Gao, Y.; Biju, V. P.; Rogach, A. L.; Xiao, L.; Jia, S. Excitons and Biexciton Dynamics in Single $CsPbBr_3$ Perovskite Quantum Dots. *J. Phys. Chem. Lett.* **2018,** *9*, 6934–6940.

36. Gibson, N. A.; Koscher, B. A.; Alivisatos, A. P.; Leone, S. R. Excitation Intensity Dependence of Photoluminescence Blinking in $CsPbBr_3$ Perovskite Nanocrystals. *J. Phys. Chem. C* **2018,** *122*, 12106-12113.

37. Trinh, C. T.; Minh, D. N.; Ahn, K. J.; Kang, Y.; Lee, K.-G. Organic−Inorganic $FAPbBr_3$ Perovskite Quantum Dots as a Quantum Light Source: Single-Photon Emission and Blinking Behaviors. *ACS Photonics* **2018,** *5*, 4937–4943.

38. Hou, L.; Zhao, C.; Yuan, X.; Zhao, J.; Krieg, F.; Tamarat, P.; Kovalenko, M. V.; Guo, C.; Lounis, B. Memories in the Photoluminescence Intermittency of Single Cesium Lead Bromide Nanocrystals. *Nanoscale* **2020,** *12*, 6795-6802.

39. Dong, Y.; Qiao, T.; Kim, D.; Parobek, D.; Rossi, D.; Son, D. H., Precise Control of Quantum Confinement in Cesium Lead Halide Perovskite Quantum Dots via Thermodynamic Equilibrium. *Nano Lett.* **2018,** *18*, 3716–3722.

40. Li, Y.; Luo, X.; Ding, T.; Lu, X.; Wu, K. Size- and Halide-Dependent Auger Recombination in Lead Halide Perovskite Nanocrystals. *Angew. Chem. Int. Ed.* **2020,** *59*, 14292 –14295.

41. Rossi, D.; Liu, X.; Lee, Y.; Khurana, M.; Puthenpurayil, J.; Kim, K.; Akimov, A. V.; Cheon, J.; Son, D. H. Intense Dark Exciton Emission from Strongly Quantum-Confined $CsPbBr_3$ Nanocrystals. *Nano Lett.* **2020,** *20*, 7321–7326.

42. Cheng, O. H.-C.; Qiao, T.; Sheldon, M.; Son, D. H. Size- and Temperature-Dependent Photoluminescence Spectra of Strongly Confined $CsPbBr_3$ Quantum Dots. *Nanoscale* **2020,** *12*, 13113–13118.

43. Dana, J.; Binyamin, T.; Etgar, L.; Ruhman, S. Unusually Strong Biexciton Repulsion Detected in Quantum Confined $CsPbBr_3$ Nanocrystals with Two and Three Pulse Femtosecond Spectroscopy. *ACS Nano* **2021,** *15*, 9039–9047.

44. Lubin, G.; Yaniv, G.; Kazes, M.; Ulku, A. C.; Antolovic, I. M.; Burri, S.; Bruschini, C.; Charbon, E.; Yallapragada, V. J.; Oron, D. Resolving the Controversy in Biexciton Binding Energy of Cesium Lead Halide Perovskite Nanocrystals through Heralded Single-Particle Spectroscopy. *ACS Nano* **2021,** *15*, 19581−19587.

45. Cho, K.; Yamada, T.; Tahara, H.; Tadano, T.; Suzuura, H.; Saruyama, M.; Sato, R.; Teranishi, T.; Kanemitsu, Y. Luminescence Fine Structures in Single Lead Halide Perovskite Nanocrystals: Size Dependence of the Exciton–Phonon Coupling. *Nano Lett.* **2021,** *21*, 7206−7212.

46. Cho, K.; Tahara, H.; Yamada, T.; Suzuura, H.; Tadano, T.; Sato, R.; Saruyama, M.; Hirori, H.; Teranishi, T.; Kanemitsu, Y. Exciton–Phonon and Trion–Phonon Couplings Revealed by Photoluminescence Spectroscopy of Single $CsPbBr_3$ Perovskite Nanocrystals. *Nano Lett.* **2022,** 22, 7674−7681.

47. Naghadeh, S. B.; Luo, B.; Pu, Y.-C.; Schwartz, Z.; Hollingsworth, W. R.; Lindley, S. A.; Brewer, A. S.; Ayzner, A. L.; Zhang, J. Z. Size Dependence of Charge Carrier Dynamics in Organometal Halide Perovskite Nanocrystals: Deciphering Radiative Versus Nonradiative Components. *J. Phys. Chem. C* **2019,** *123*, 4610–4619.

48. Vishnu, E. K.; Nair, A. A. K.; Thomas, K. G. Core-Size-Dependent Trapping and Detrapping Dynamics in CdSe/CdS/ZnS Quantum Dots. *J. Phys. Chem. C* **2021,** *46*, 25706–25716.

49. Puthenpurayil, J.; Cheng, O. H.-C.; Qiao, T.; Rossi, D.; Son, D. H. On the Determination of Absorption Cross Section of Colloidal Lead Halide Perovskite Quantum Dots. *J. Chem. Phys.* **2019,** *151*, 154706.

50. Qin, H.; Niu, Y.; Meng, R.; Lin, X.; Lai, R.; Fang, W.; Peng, X. Single-Dot Spectroscopy of Zinc-Blende CdSe/CdS Core/Shell Nanocrystals: Nonblinking and Correlation with Ensemble Measurements. *J. Am. Chem. Soc.* **2014,** *136*, 179-187.

51. Peterson, J. J.; Nesbitt, D. J. Modified Power Law Behavior in Quantum Dot Blinking: A Novel Role for Biexcitons and Auger Ionization. *Nano Lett.* **2009,** *9*, 338–345.

52. Tang, J.; Marcus, R. A. Diffusion-Controlled Electron Transfer Processes and Power-Law Statistics of Fluorescence Intermittency of Nanoparticles. *Phys. Rev. Lett.* **2005,** *95*, 107401.

53. Tang, J.; Marcus, R. A. Mechanisms of Fluorescence Blinking in Semiconductor Nanocrystal Quantum Dots. *J. Chem. Phys.* **2005,** *123*, 054704.

54. Roy, D.; Mandal, S.; De, C. K.; Kumara, K.; Mandal, P. K. Nearly Suppressed Photoluminescence Blinking of Small-Sized, Blue–Green–Orange–Red Emitting Single CdSe-Based Core/Gradient Alloy Shell/Shell Quantum Dots: Correlation between Truncation Time and Photoluminescence Quantum Yield. *Phys. Chem. Chem. Phys.* **2018,** *20*, 10332--10344.

55. Bixby, T. J.; Cordones, A. A.; Leone, S. R. CdSe/ZnS Qquantum Dot Intermittency in N,N'-Diphenyl-N,N'-Bis(3-Methylphenyl)-(1,1'-Biphenyl)-4,4'-Diamine (TPD). *Chemical Physics Letters* **2012,** *521*, 7-11.

56. Xu, Z.; Cotlet, M. Photoluminescence Blinking Dynamics of Colloidal Quantum Dots in the Presence of Controlled External Electron Traps. *Small* **2012,** *8*, 253-258.

57. Luo, X.; Lai, R.; Li, Y.; Han, Y.; Liang, G.; Liu, X.; Ding, T.; Wang, J.; Wu, K. Triplet Energy Transfer from $CsPbBr_3$ Nanocrystals Enabled by Quantum Confinement. *J. Am. Chem. Soc.* **2019,** *141*, 4186-4190.

58. Nenon, D. P.; Pressler, K.; Kang, J.; Koscher, B. A.; Olshansky, J. H.; Osowiecki, W. T.; Koc, M. A.; Wang, L.-W.; Alivisatos, A. P. Design Principles for Trap-Free $CsPbX_3$ Nanocrystals: Enumerating and Eliminating Surface Halide Vacancies with Softer Lewis Bases. *J. Am. Chem. Soc.* **2018,** *140*, 17760–17772.

59. Das, A.; Mishra, K.; Ghosh, S. Revealing Explicit Microsecond Carrier Diffusion from One Emission Center to Another in an All-Inorganic Perovskite Nanocrystal. *J. Phys. Chem. Lett.* **2021,** *12*, 5413–5422.

60. Kapusta, P.; Wahl, M.; Benda, A.; Hof, M.; Enderlein, J. Fluorescence Lifetime Correlation Spectroscopy. *J. Fluoresc.* **2007,** *17*, 43-48.

CHAPTER 7

Concluding Remarks and Future Scope

7.1. Overview

This thesis contributes to the design high quality perovskite NCs and understanding their charge carrier recombination dynamics. Because of high tendency of defect formation due to halide vacancies and dynamic nature of binding of the surface capping ligands (OLA and OA) to the ionic surface of this material, synthesis of highly luminescent perovskite NCs whilst maintaining uniform size distribution, high phase- and photo-stability is an onerous task. In this study, we have shown that stable green blue and violet emitting perovskite NCs with exceptional PL properties can be obtained by a three-precursor hot-injection method using N-haloimides as halide precursors. However, we found that the iodide analogue of this precursor is not quite effective reagent for the preparation of the red-emitting $CsPbI_3$ NCs. We found that phase-stable, highly luminescent $CsPbI_3$ NCs with suppressed PL blinking we have used NH_4I as an additional precursor during synthesis of this NCs following conventional synthesis method. A thorough understanding of the dynamics of the different competing radiative and nonradiative charge carrier recombination processes is essential for proper utilization of these substances in devices. We have employed time resolved confocal fluorescence microscopy, fluorescence correlation spectroscopy and transient absorption spectroscopy techniques to understand these processes in these NCs. As size plays a significant role on the charge carrier trapping and detrapping processes in the NCs, we have also studied charge carrier trapping and detrapping processes in different sized quantum confined $CsPbBr_3$ NCs.

In conventional two-precursor hot-injection method, the $APbBr_3$ NCs are synthesized by using $PbBr_2$ as a precursor for both lead and bromine, which gave a Br:Pb molar precursor ratio of only 2 in the reaction system (less than the required value of 3). It has also been found that $PbBr_2$ is not an effective precursor for synthesis of organometal lead halide perovskites ($FAPbBr_3$ and $MAPbBr_3$). For example, $FAPbBr_3$ NCs obtained by this method exhibit a much broader size distribution and poor optical properties. Even for $CsPbBr_3$ NCs, the PLQY of the samples obtained by this method is typically 60−80% or even lower due to nonradiative deactivation induced by the bromide vacancies. In order to overcome these issues we have introduced a three-precursor hot-injection method employing N-bromosuccinimide (NBS), a widely used source of bromine in organic synthesis, as the bromide precursor. Reaction of NBS with organic acids generates HBr, which reacts with

oleylamine to form oleylammonium bromide; the latter serves as the active bromide source in the synthesis. The method, which is found to be highly reproducible, yields brightly luminescent (PLQY ~90-99%) extremely uniform sized cubes of nanodimension for all three systems. These NCs exhibit exceptional phase stability and photostability at ambient atmosphere. These NCs also show resistant against degradation by polar solvents. The exceptional characteristics of these NCs, are attributed to the formation of oleylammonium lead bromide-terminated surfaces, in which A^+ are partially replaced by oleylammonium ions.

However, compared to their green-emitting counterparts, violet- and blue-emitting $CsPbCl_3$ and $CsPb(Cl/Br)_3$ NCs most often exhibit much lower PLQY due to competing nonradiative recombination of the photogenerated charge carriers through the deep trap states generated by halide vacancies and distorted $[PbX_6]^{4-}$ octahedral units. We found that when the key issue, halide deficiency of the surface of the NCs, is dealt with by using an effective halide precursor, N-halophthalimides and N-halosuccinimides, and appropriate Pb:X precursors ratio, it is indeed possible to directly obtain highly luminescent and stable NCs even for the blue-violet region. For the mixed halide systems, $CsPbCl_2Br$, $CsPbCl_{1.5}Br_{1.5,}$ and $CsPbClBr_2$ NCs, the most luminescent system (PLQY ~85-97%) is obtained for a Pb:X precursor ratio of 1:6; however, for $CsPbCl_3$ NCs, a 1:9 Pb:Cl ratio yielded the most luminous sample (PLQY~80%) using N-halophthalimides as halide precursor. The time-resolved PL and ultrafast pump−probe measurements show the dependence of the carrier trapping processes on the Pb:X precursor ratio and that carrier trapping is greatly suppressed when these NCs are prepared by using a higher than stoichiometric X:Pb precursor ratio.

Among the $CsPbX_3$ perovskite NCs, the $CsPbI_3$ NCs, because of its low band gap, is the most promising candidate for solar photovoltaic and various optoelectronic applications. However, poor phase stability of these NCs even under ambient condition is a major obstacle to these applications. Apart from the stability-related issues, photoluminescence (PL) blinking of the single NCs is another factor that restricts the applications of the $CsPbI_3$ NCs as single-photon emitters and other light-emitting applications. Here, by focusing on the core issues of phase instability and PL blinking of the $CsPbI_3$ NCs that restrict the utility of these NCs in above mentioned applications, it is shown that exceptionally phase-stable and highly luminescent $CsPbI_3$ NCs with significantly suppressed PL blinking can be obtained by

tweaking the conventional hot-injection method of synthesis employing NH_4I as an additional reagent. The PL blinking characteristics of a large number of single $CsPbI_3$ NCs reveal an average ON-state fraction of 0.945 with 60% of them exhibiting the complete suppression of PL blinking. The remaining 40% of the NCs exhibit OFF states due to both Auger recombination of the trion- and trap-induced recombination of the band-edge carrier. The extraordinary features of these NCs are attributed to NH_4I, which serve both a halide precursor and a surface capping agent.

As size of the NCs plays an important role on the charge carrier trapping and detrapping processes, we have studied PL blinking of three different size quantum confined single NCs of $CsPbBr_3$ to quantify these processes. Both hot carrier trapping- and Auger-recombination are found to contribute to the PL fluctuations of the immobilized NCs indicating the presence of both short-lived and long-lived trap states. The results also suggest an increase in the trapping rate constant with decrease in size of the NCs. The FCS and FLCS measurements indicate a lower off-state fraction and higher per particle brightness for the bigger NCs. This observation is rationalized considering a smaller trap-depth, and localization of the charge-carrier wavefunction in the core region for large size NCs. The findings provide first insight into the charge carrier recombination pathway and dynamics of the quantum confined $CsPbBr_3$ NCs from PL blinking studies and the findings will be useful in the design and development of small size highly luminescent perovskite NCs for optoelectronic applications.

7.2. Future scope

In the first two working chapters we have shown a method for obtaining green blue and violet emitting perovskite NCs employing N-halosuccinimide and N-halophthalimide as alternative halide precursors. In this method Pb and X amount can be tuned independently. While we succeeded in obtaining green emitting $CsPbBr_3$, $MAPbBr_3$, $FAPbBr_3$ NCs with near-unity PLQY, the blue emitting $CsPb(Br/Cl)_3$ and violet emitting $CsPbCl_3$ NCs exhibit PLQY of 80-95% and 70-80%, respectively. This suggested that the iodide analogues precursor is not effective for the synthesis of the highly luminescent and stable $CsPbI_3$ NCs. Hence, it calls for finding of efficient halide precursor for the synthesis of highly luminescent $CsPbCl_3$ and $CsPbI_3$ NCs. NCs surfaces are difficult to characterize due to both their spatial and temporal

heterogeneity. This problem is exacerbated by weak bonding on $CsPbX_3$ NCs surfaces, which creates a highly dynamic ligand shell. In this regard, more studies are required for clear understanding of surface properties of the NCs obtained by our method.

In chapter 5, we have described a method for obtaining phase stable highly luminescent red emitting $CsPbI_3$ NCs with suppressed photoluminescence blinking. This has been achieved by tweaking conventional method of synthesis using NH_4I as an additional reagent. Even though this method produces good quality $CsPbI_3$ NCs problems still remain for other iodide based perovskites which are $FAPbI_3$ and $MAPbI_3$ NCs. Clearly, there lies a huge scope of improving the properties of organometal halide perovskites ($FAPbI_3$ and $MAPbI_3$).

In chapter 6, we have studied the PL blinking behaviour of quantum confined $CsPbBr_3$ NCs. We have also investigated influence of size on carrier trapping and detrapping processes. Analysis of the blinking data reveal both hot carrier trapping- and Auger-recombination contribute to the PL fluctuations of these NCs indicating the presence of both short-lived and long-lived trap states. The probability density distribution of the on-events indicates an increase in trapping rate constant with decrease in size of the NCs leading to a lower on-state fraction for smaller NCs. In this regard, it will be interesting to study the blinking behaviour of strongly quantum confined NCs for other systems as of now most of the blinking studies has been done on non-quantum confined perovskite NCs. Nonblinking strongly quantum confined NCs is highly desirable for several emerging quantum technologies. Hence, methods for obtaining nonblinking NCs of these systems need to be developed. We have studied blinking of these NCs analysing intensity fluctuation data. However, one can also think of analysis of the blinking data in terms of lifetime fluctuation to extract more information about the systems.

The operating condition of the device fabricated from these NCs is completely separate from the spectroscopic measurement condition. In devices, these NCs are integrated with charge transport layers. Hence, investigation of charge carrier recombination processes with such charge transport layers is necessary to achieve maximum utility of these NCs.

Appendix I

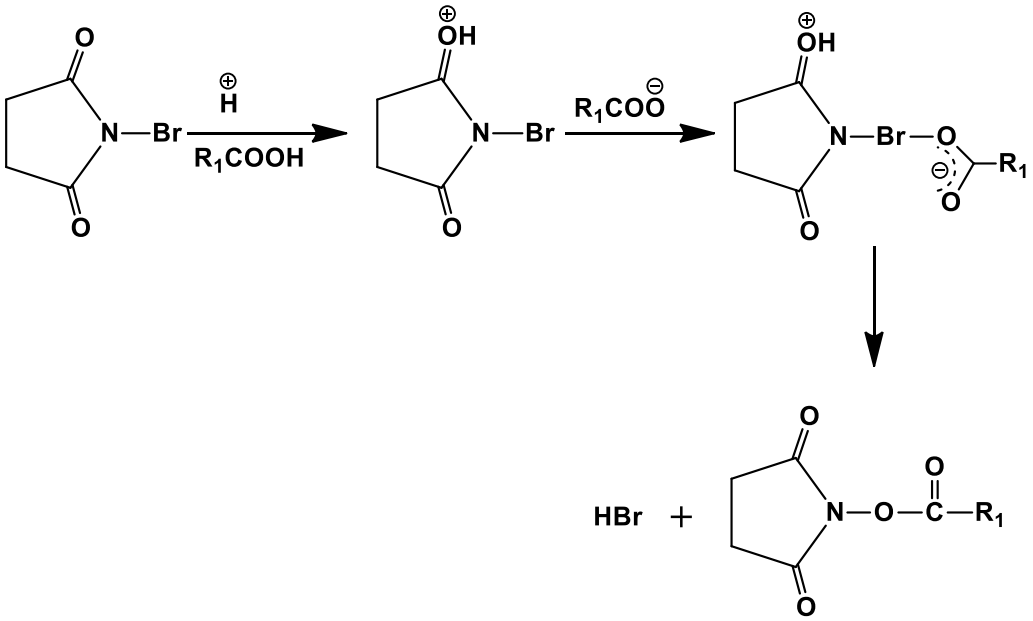

$$HBr + R_2NH_2 \longrightarrow R_2\overset{+}{N}H_3\overset{-}{Br}$$

R_1, R_2 = Alkyl group

Scheme AI.1. *Mechanism of formation of oleylammonium bromide in the reaction flask.*

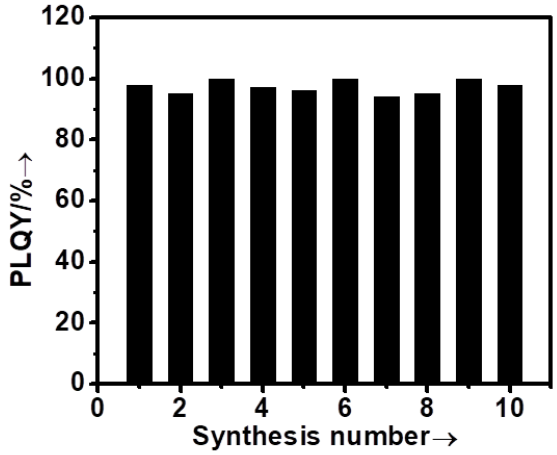

Figure AI.1. *PLQY of the $CsPbBr_3$ NCs for different batches of samples*

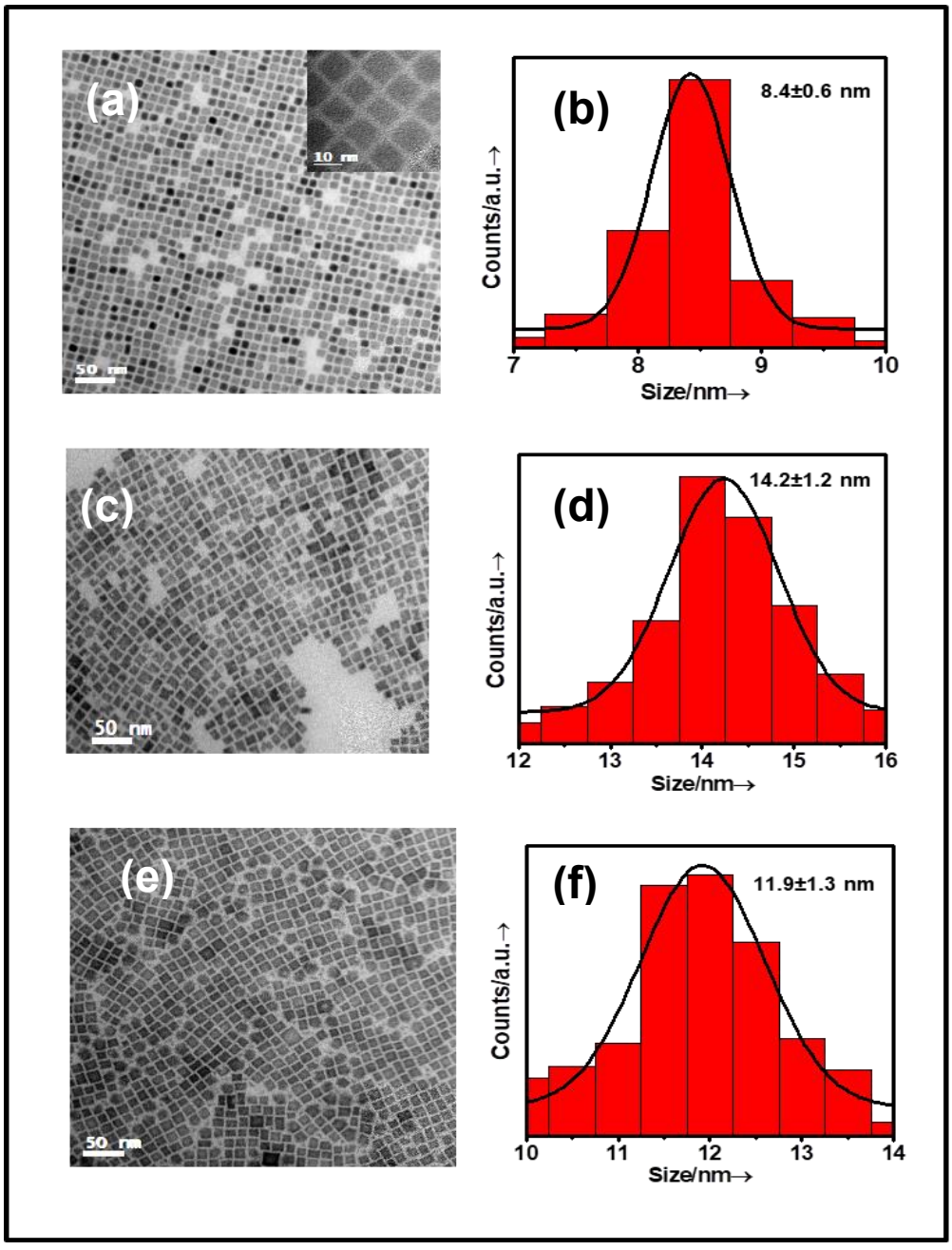

Figure AI.2. *Bright field TEM images and size distribution of (a,b) $CsPbBr_3$, (c,d)* ***MA****$PbBr_3$ and (e,f)* ***FA****$PbBr_3$ NCs. Scale bar is 50 nm in all cases.*

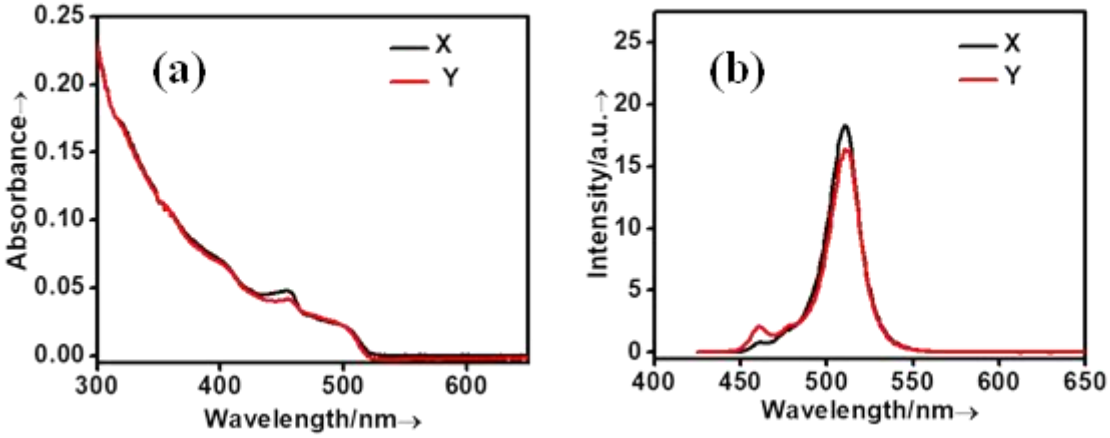

Figure AI.3. *UV-vis absorption (a) and PL emission (b) spectra of $CsPbBr_3$ NCs synthesized by injecting oleylammonium bromide (prepared separately in two differen methods) into Cs-oleate and Pb-oleate mixure.* ***X*** *corresponding to absorption and emission of NCs when oleylammonium bromide made by reaction of NBS and oleic acid and oleyl amine.* ***Y*** *corresponding to absorption and emission of NCs when oleylammonium bromide made by reaction of oleyl amine and HBr.*

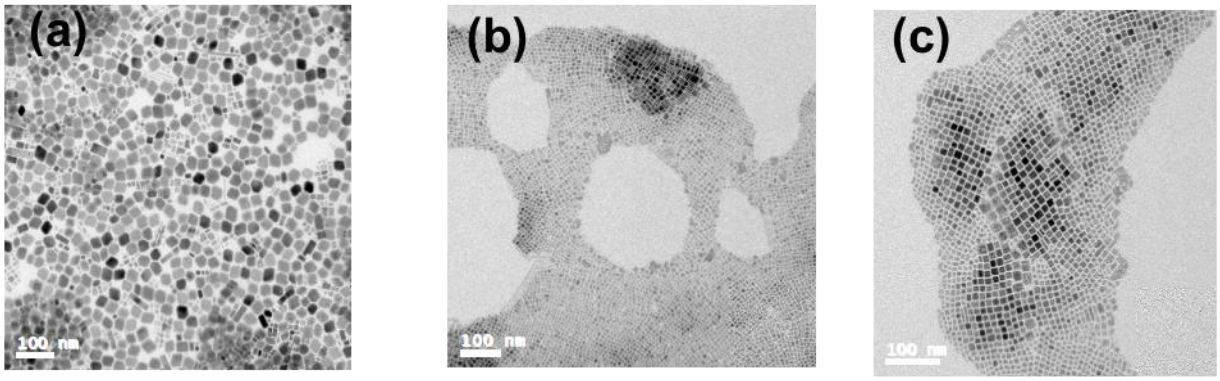

Figure AI.4. *Bright field TEM images of the $CsPbBr_3$ NCs synthesized at (a) 130°C, (b) 160°C and (c) 180°C. Scale bar is 100 nm in all cases.*

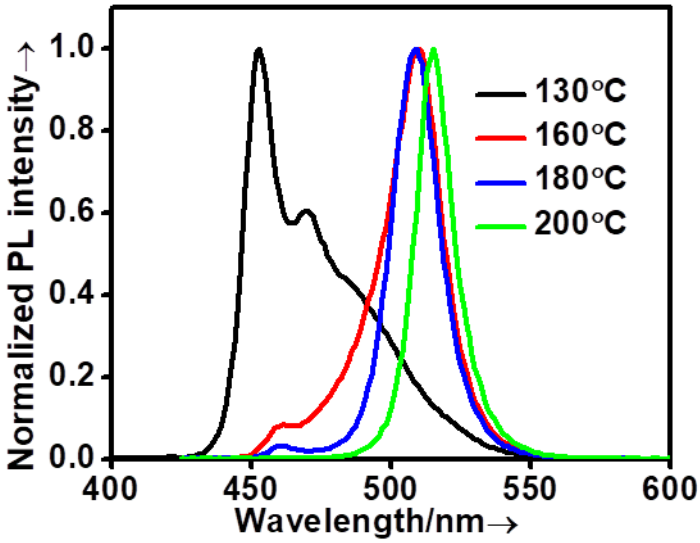

Figure AI.5. *Effect of the reaction temperature on the PL spectra of the $CsPbBr_3$ NCs.*

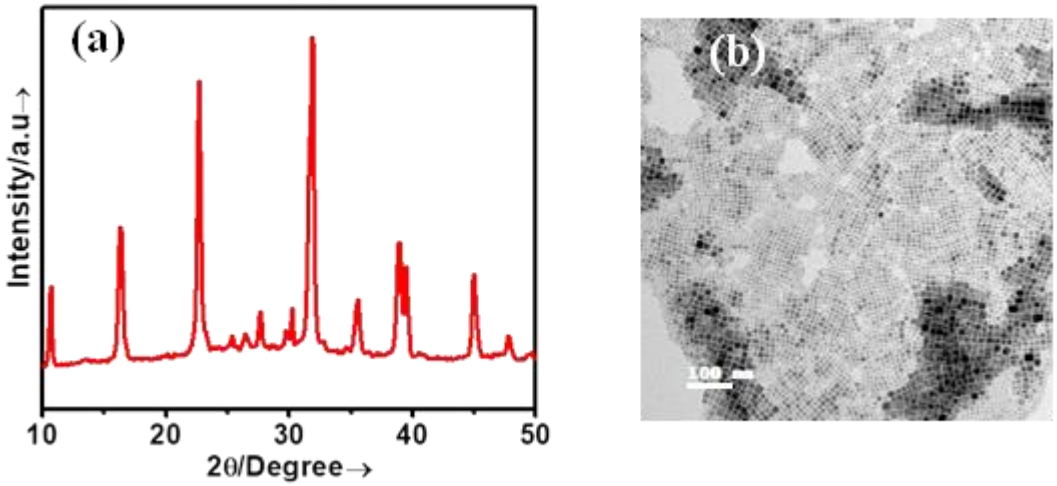

Figure AI.6. *PXRD pattern (a) and Bright field TEM image (b) of the $CsPbBr_3$ NCs obtained using a Pb:Br molar precursor ratio of 1:2.5. Scale bar is 100 nm.*

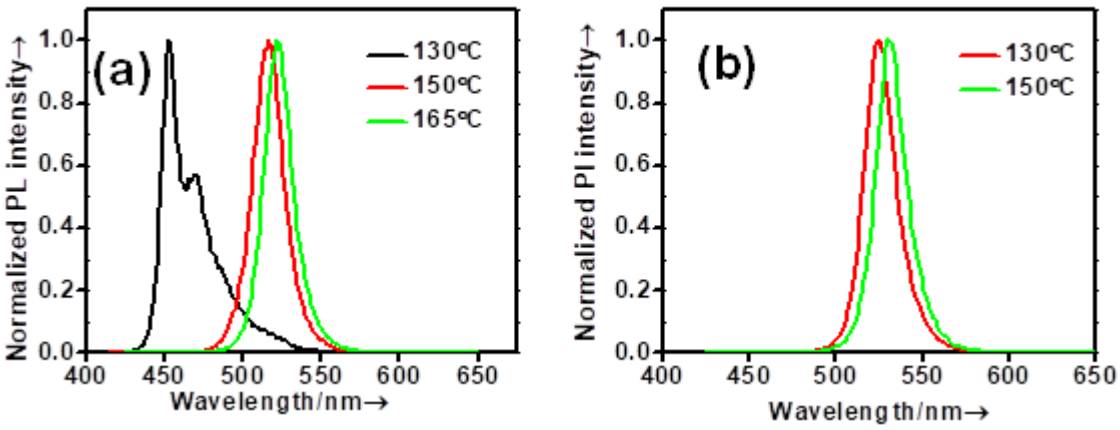

Figure AI.7. *PL spectra of (a)* ***MA****PbBr$_3$ NCs and (b)* ***FA****PbBr$_3$ NCs synthesized at different temperatures.*

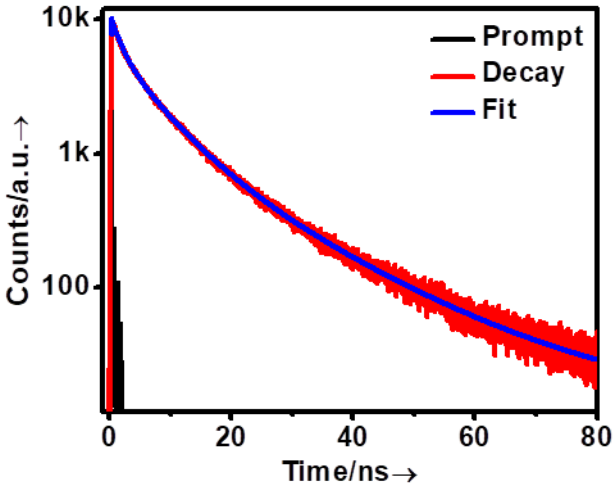

Figure AI.8. *PL decay profile of CsPbBr$_3$ NCs obtained using a Pb:Br precursor ratio of 1:2.5. Excitation wavelength is 405 nm and PL is monitored at 515 nm.*

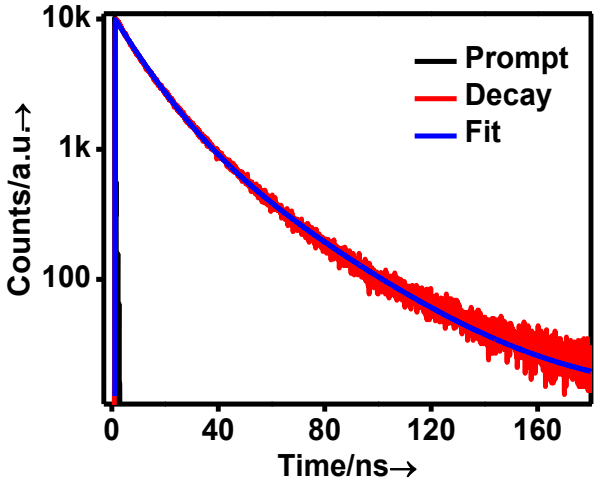

Figure AI.9. *PL decay profile of* ***FA****PbBr$_3$ NCs. Excitation wavelength is 485 nm. PL was monitored at 531 nm.*

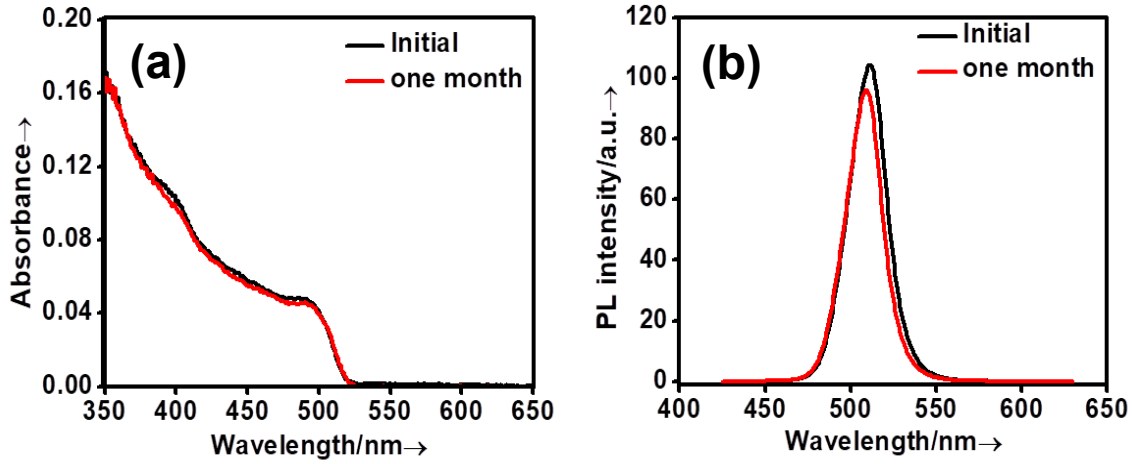

Figure AI.10. *Absorption (a) and PL emission (b) spectra of the as-synthesized CsPbBr$_3$ NCs recorded immediately after synthesis and after one month of storage in ambient condition.*

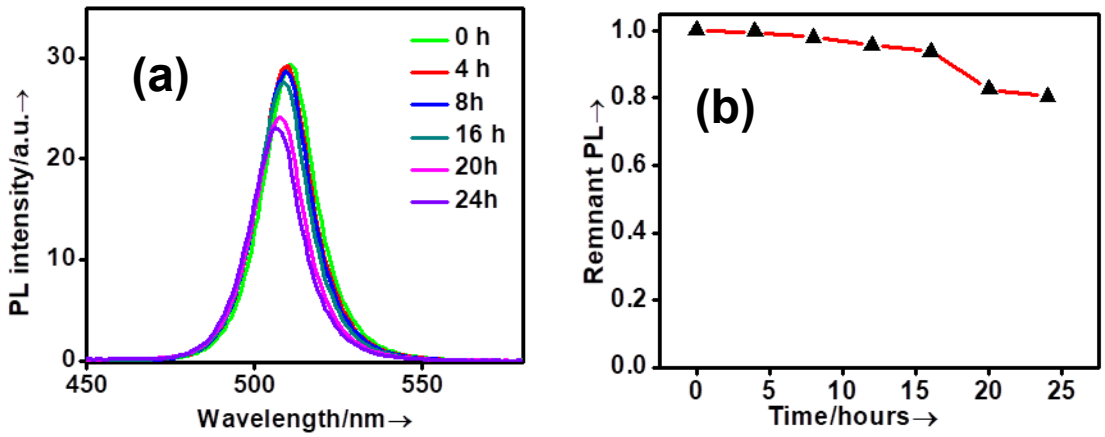

Figure AI.11. *PL spectra (a) and peak PL intensity (b) of the $CsPbBr_3$ NCs recorded after exposing the sample to 365 nm 8 W UV lamp for different periods.*

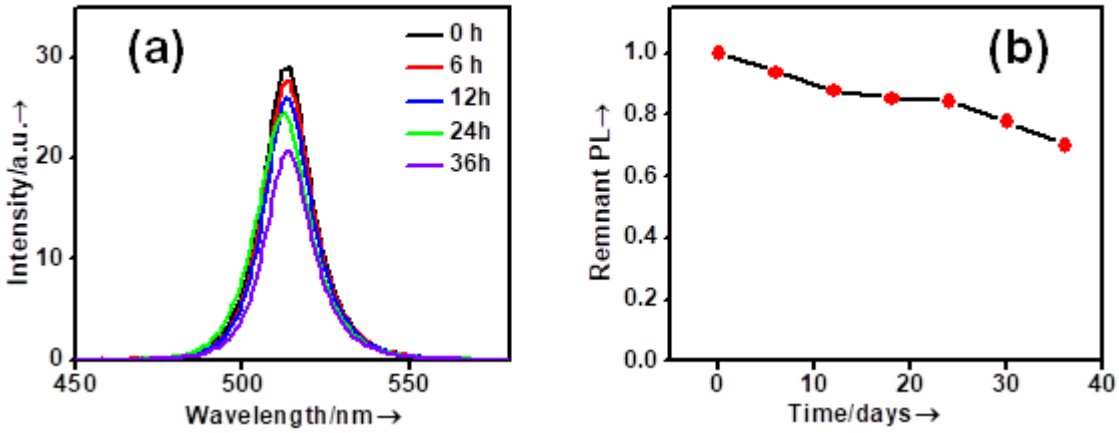

Figure AI.12. *PL spectra (a) and peak PL intensity (b) of the $CsPbBr_3$ NCs recorded at different time-interval after addition of 1.5 ml water to 2.5 ml hexane dispersion of the $CsPbBr_3$ NCs.*

.

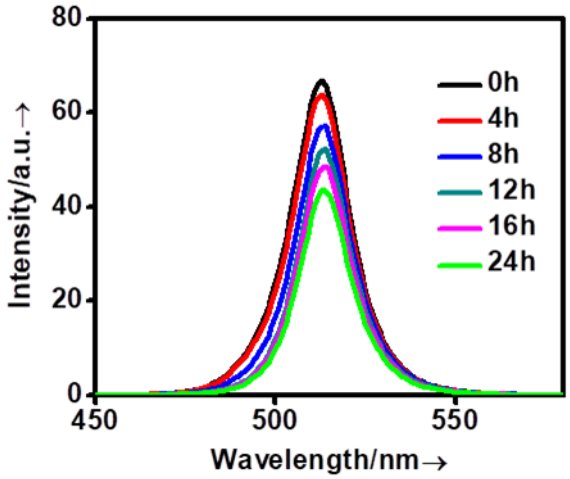

Figure AI.13. *PL emission spectra of the $CsPbBr_3$ NCs dispersed in hexane and water mixture after illumination with 365 nm, 8 W UV light for different periods.*

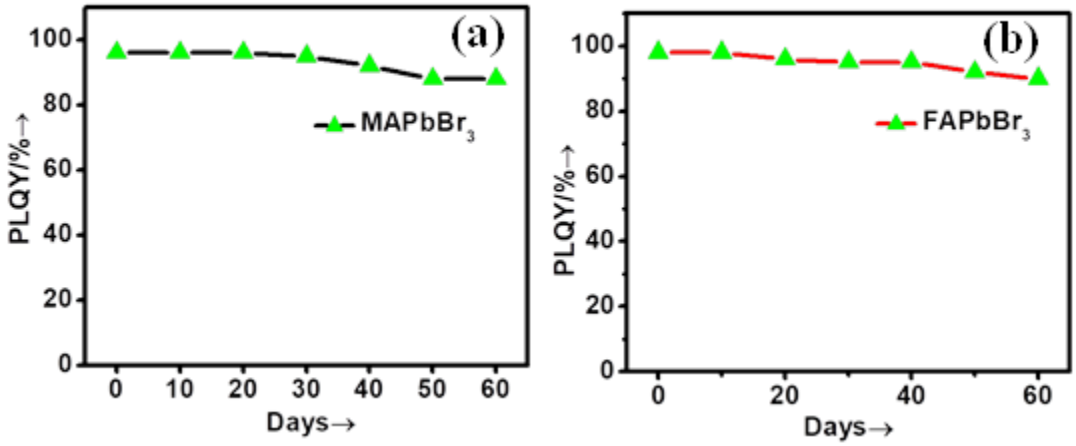

Figure AI.14. *Variation of the PLQY of* ***MA****$PbBr_3$ (a) and* ***FA****$PbBr_3$ (b) NCs after storing the samples under ambient condition for different periods.*

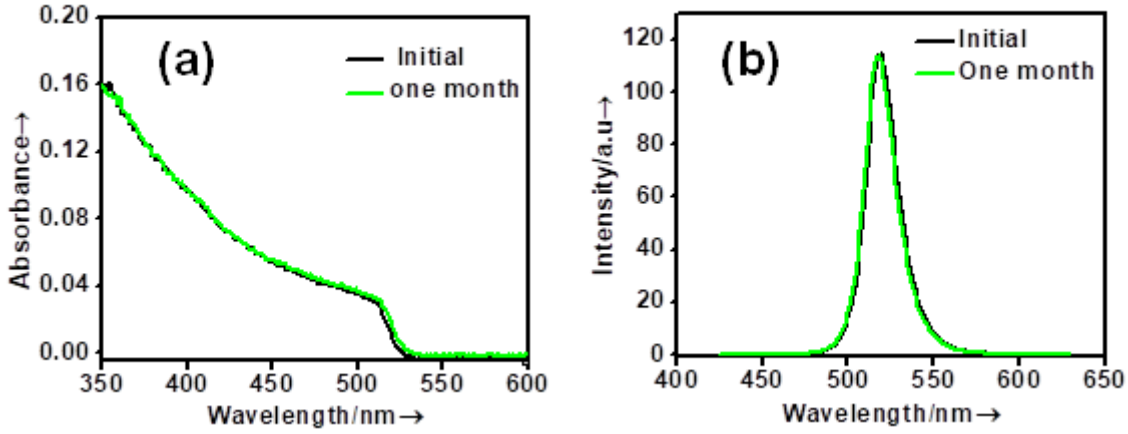

Figure AI.15. *UV-vis absorption (a) and PL emission (b) spectra of the as-synthesized and one-month old* ***MA****PbBr$_3$ NCs.*

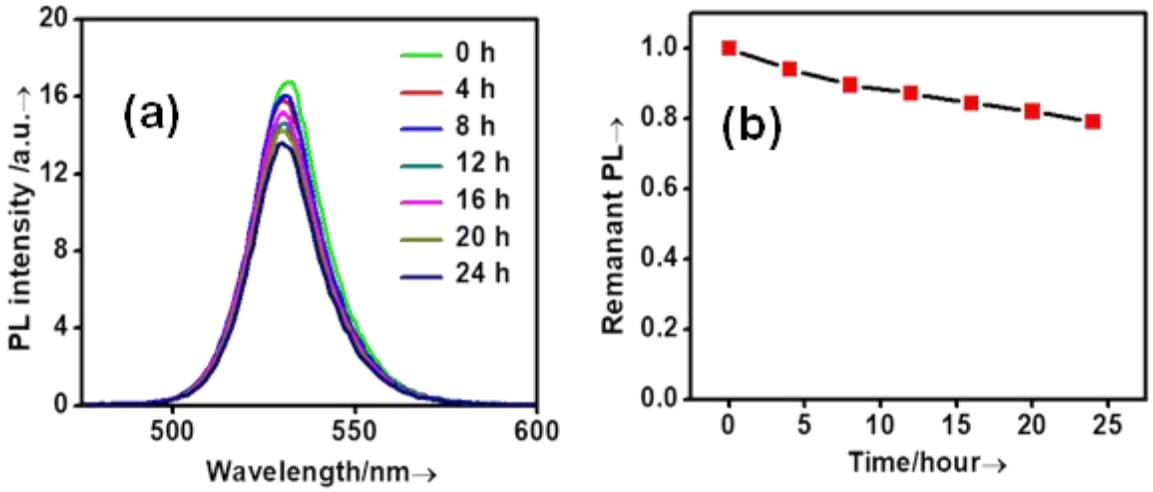

Figure AI.16. *PL spectra (a) and peak PL intensity (b) of the* ***FA****PbBr$_3$ NCs recorded after exposing the sample to 365 nm 8 W UV lamp for different periods.*

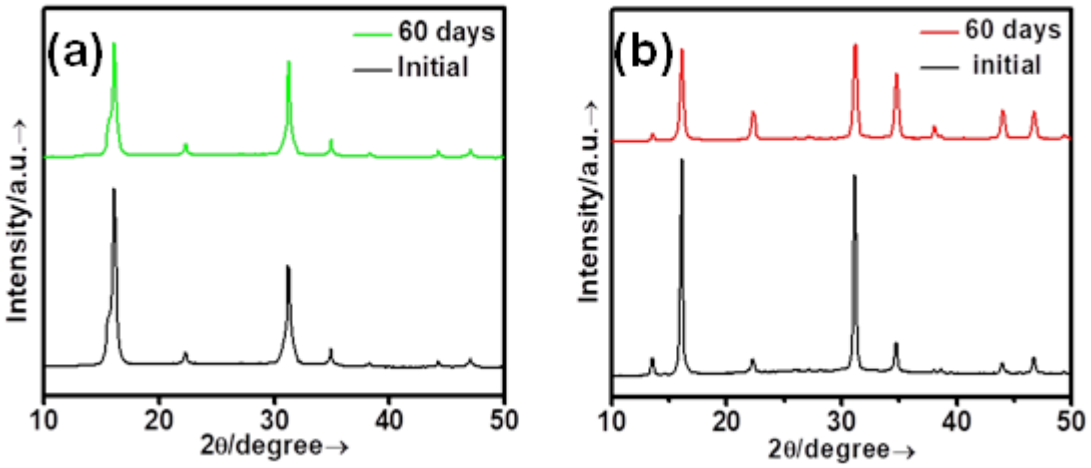

Figure AI.17. *PXRD pattern for* ***MA****PbBr$_3$ (a) and* ***FA****PbBr$_3$ (b) NCs for as-synthesized and 60 days old samples.*

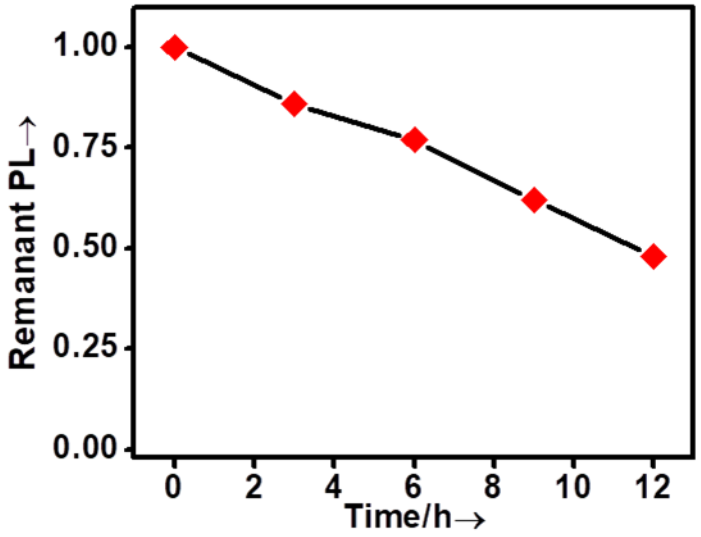

Figure AI.18. *Variation of PL intensity of the CsPbBr$_3$ NCs, which was synthesized by lower Pb:Br ratio (1:2.5), recorded after exposing the sample to 365 nm 8 W UV lamp for different periods.*

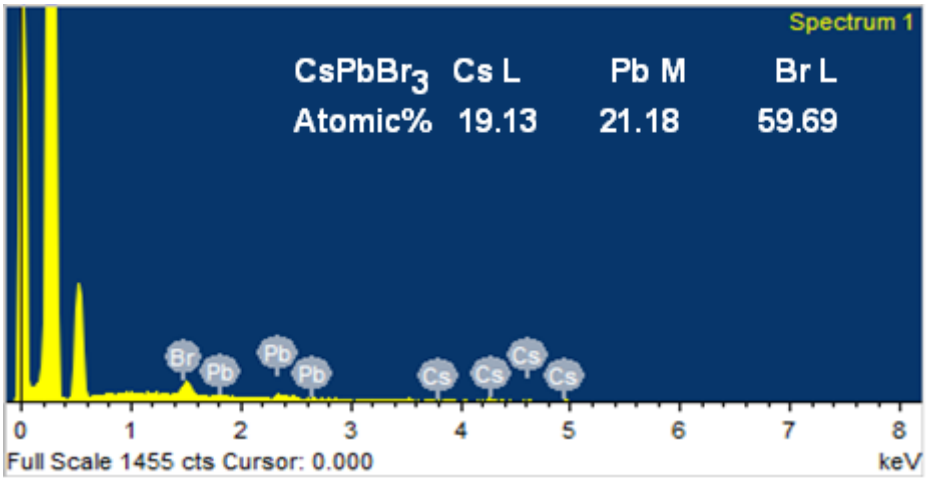

Figure AI.19. *EDX spectrum of $CsPbBr_3$ NCs obtained using a Pb:Br precursor ratio of 1:2.5 in the synthesis.*

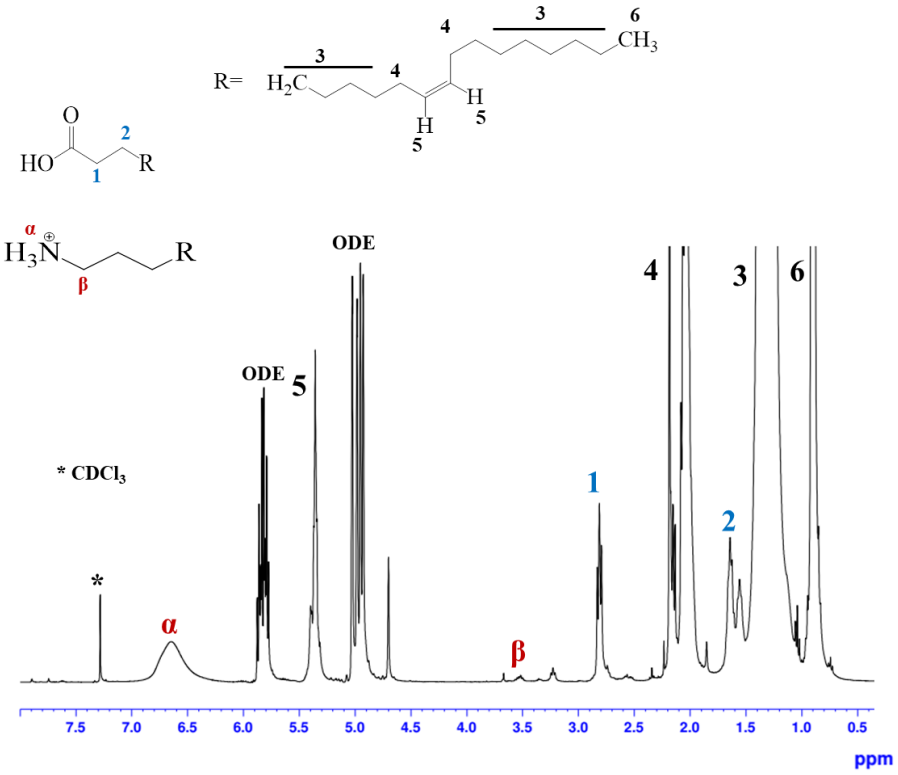

Figure AI.20: *^1H NMR spectra of $CsPbBr_3$ NCs washed with MeOAc and NBS intermediate in $CDCl_3$ solvent.*

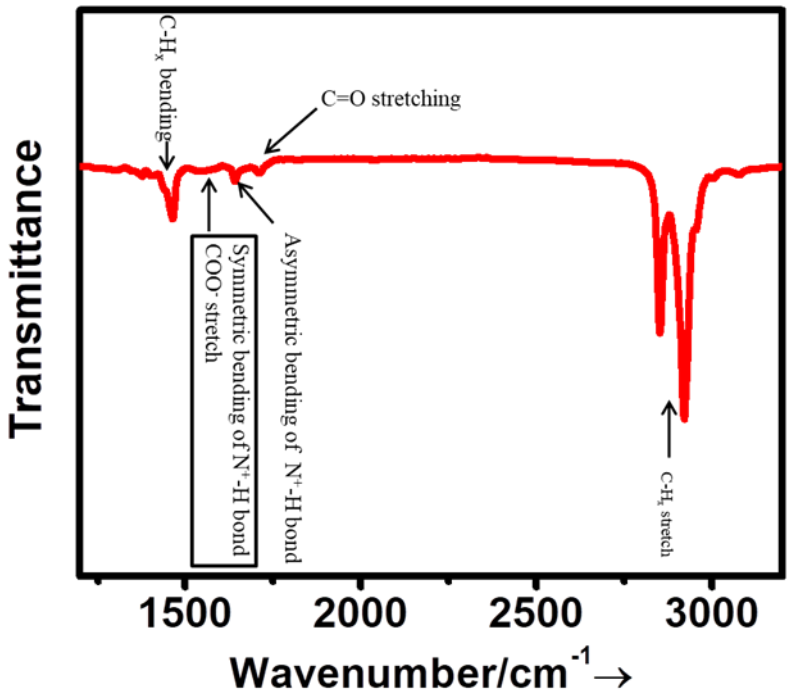

Figure AI.21: *FTIR spectrum of MeOAc washed $CsPbBr_3$ NCs.*

Table AI.1. *Photoluminescence properties of the $CsPbBr_3$ NCs synthesized by injecting oleylammonium bromide (prepared in two different way) into Cs-oleate and Pb-oleate mixure.*

Precursor	**Reaction temperature**	**PLQY**	**Emission maxima (FWHM) (nm)**
Oleylammonium bromide (prepared from NBS)	200°C	83%	459, 480 and 510
Oleylammonium bromide (prepared by reaction of oleylamine and HBr)	200°C	79%	460, 480, 509

Table AI.2. *Dependence of the photoluminescence properties of $CsPbBr_3$ NCs on the reaction temperature and Pb:Br precursor ratio.*

Reaction temperature	**Ratio of the precursors**	**PLQY**	**Emission maxima (FWHM)**
130°C	1:3	40%	453 nm (32 nm)
160°C	1:3	68%	508 nm (27 nm)
180°C	1:3	85%	508 nm (25 nm)
200°C	1:3	99%	510-515 nm (17-20 nm)
200°C	1:2.5	69%	515 nm (20 nm)

Table AI.3. *Dependence of the photoluminescence properties of* ***MA****$PbBr_3$ and* ***FA****$PbBr_3$ NCs on the reaction temperature.*

	Reaction temperature	**PLQY**	**Emission maxima (FWHM)**
MA$PbBr_3$	130°C	55%	452 nm and 471 nm (30 nm)
	150°C	84%	515 nm (22 nm)
	165°C	98%	523 nm (21 nm)
FA$PbBr_3$	130°C	75%	521 nm (24 nm)
	150°C	86%	530 nm (20 nm)
	165°C	95%	531 nm (20 nm)

Table AI.4. *Photoluminiscence decay parameters of different* ***A****PbBr$_3$ NCs.*

System	$\tau_1(A_1)$ **ns**	$\tau_2(A_2)$ **ns**	$\tau_3(A_3)$ **ns**	τ_{av} **ns**
$CsPbBr_3$(1:2.5)	6.53(0.46)	17.44(0.14)	1.65(0.40)	10.36
$CsPbBr_3$(1:3)	5.49(0.80)	15.68(0.20)		9.73
MA$PbBr_3$	11.78(0.71)	30.17(0.29)		21.18
FA$PbBr_3$	11.58(0.80)	31.18(0.20)		19.46

Table AI.5. *A comparison of the stability and PL properties of green-emitting perovskite NCs obtained by different groups under different conditions.*

System	**PLQY (%)**	**Method of synthesis**	**Stability**	**References**
$CsPbBr_3$ **MA**$PbBr_3$ **FA**$PbBr_3$	99 98 95	NBS as a bromide precursor	Air stability: Retention of 90% PLQY after 3 months of storage under ambient condition for $CsPbBr_3$ NCs. **MA**$PbBr_3$ and **FA**$PbBr_3$ NCs exhibited 85% PLQY after 60 days storage. Photo-stability: $CsPbBr_3$, **MA**$PbBr_3$ and **FA**$PbBr_3$ NCs retained 81%, 75% and 80% of the initial PL intensity, respectively after 24 h of continuous illumination with UV light. Water stability: 70% of the initial PL intensity was retained by $CsPbBr_3$ NCs when it was stored in hexane and water mixture. 65% of the initial PL intensity is retained when these NCs solution is exposed to UV light for 24 h.	This work

$CsPbBr_3$ **FA**$PbBr_3$ **MA**$PbBr_3$	92 92 92	Benzoyl bromide as bromide precursor	NA	2
FA$PbBr_3$	85	Oleylammonium bromide as bromide precursor	Retain its initial PLQY after 2-3 cycles of purification with acetonitrile. Stable under mild heating condition.	3
$CsPbBr_3$	75	Ammonium bromide as bromide precursor	Stable with respect to wash with polar solvents.	4
MA$PbBr_3$	20	Non-template synthesis using alkylammonium bromide	Stable in colloidal solution for 3 month.	5
$CsPbBr_3$	90	Zwitterionic ligands capping agent	90% quantum yield after 50 days of storage.	6
$CsPbBr_3$	48-80	Employing secondary amine of different chain length.	NA	7
FA$PbBr_3$	75	LARP strategy	PL intensity decreased to 38% after annealing with 1 h at 100°C.	8
$CsPbBr_3$	>95	Post-synthesis treatment with $PbBr_2$.	Stable for 2 months, when it is stored in dark and low temperature.	9
$CsPbBr_3$	78	*In situ* surface passivation with $ZnBr_2$.	Structural stability improves against heat.	10
$CsPbBr_3$	95-100	Post-synthesis treatment with DDAB+$PbBr_2$.	Stability improves against purification with polar solvents and retains colloidal stability up to 4 months.	11
$CsPbBr_3$	61	TOPO and oleic acid as surface capping ligand.	NA	12
MA$PbBr_3$	95-99	Benzoyl alcohol as a passivating ligand.	Retain chemical stability and optical properties up to 4 months.	13

Appendix II

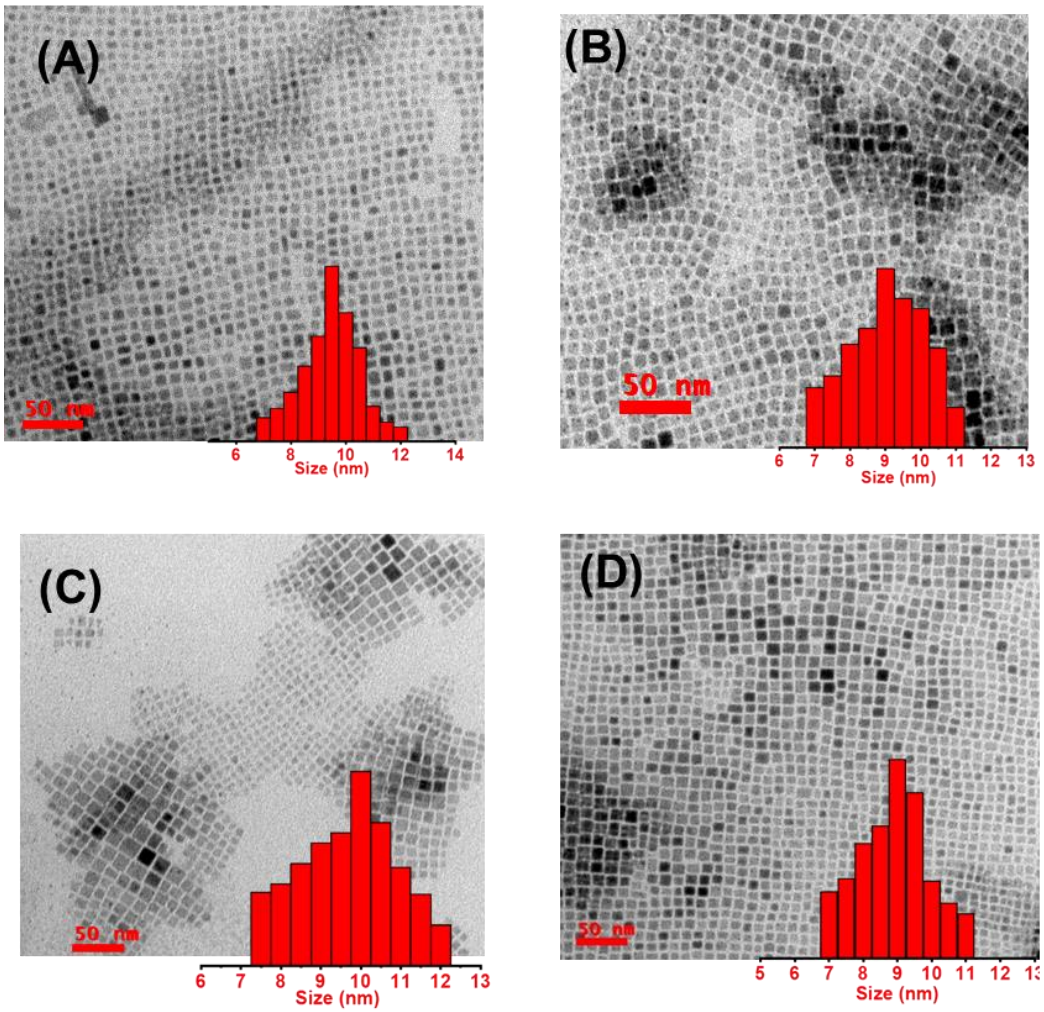

Figure AII.1. *TEM images of the* ***(A)*** *$CsPbCl_2Br(1:3)$,* ***(B)*** *$CsPbCl_{1.5}Br_{1.5}(1:3)$,* ***(C)*** *$CsPbClBr_2(1:3)$ and* ***(D)*** *$CsPbBr_3$ NCs. Scale bar is 50 nm.*

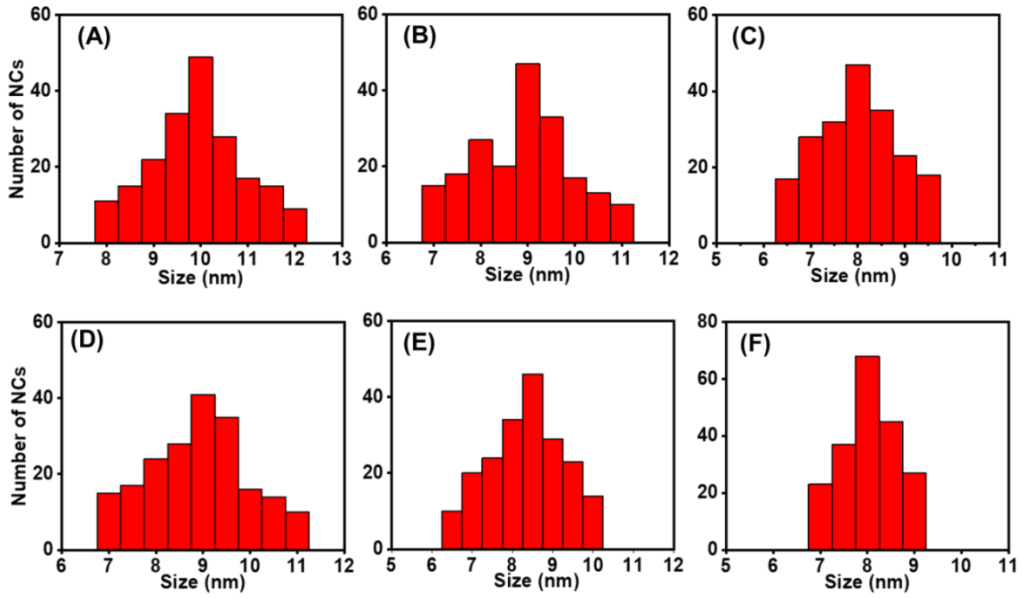

Figure AII.2. *Size distribution of the (A) $CsPbCl_3$(1:3), (B) $CsPbCl_3$(1:6), (C) $CsPbCl_3$(1:9), (D) $CsPbCl_2Br$(1:6) (E) $CsPbCl_{1.5}Br_{1.5}$(1:6) and (F) $CsPbClBr_2$(1:6) NCs.*

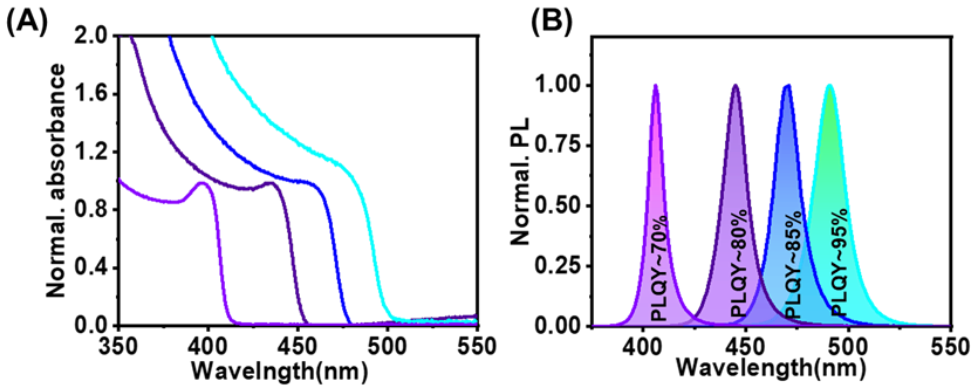

Figure AII.3. *Normalized absorption (A) and and (B) PL spectra (λ_{ex} = 350 nm) of the $CsPbCl_3$(1:9), $CsPbCl_2Br$(1:6), $CsPbCl_{1.5}Br_{1.5(}$1:6), $CsPbClBr_{2(}$1:6) and $CsPbBr_{3(}$1:3) NCs (from left to right)*

respectively synthesized by using NCS and NBS as chloride and bromide precursor respectively. PL spectra were recorded by exciting sample at 350 nm.

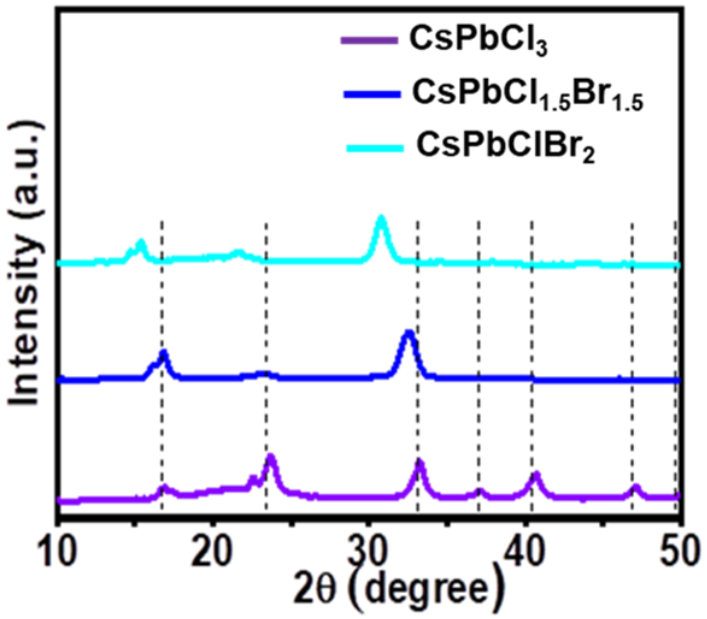

Figure AII4. *PXRD patterns of the $CsPbCl_3$ and $CsPb(Cl/Br)_3$ NCs.*

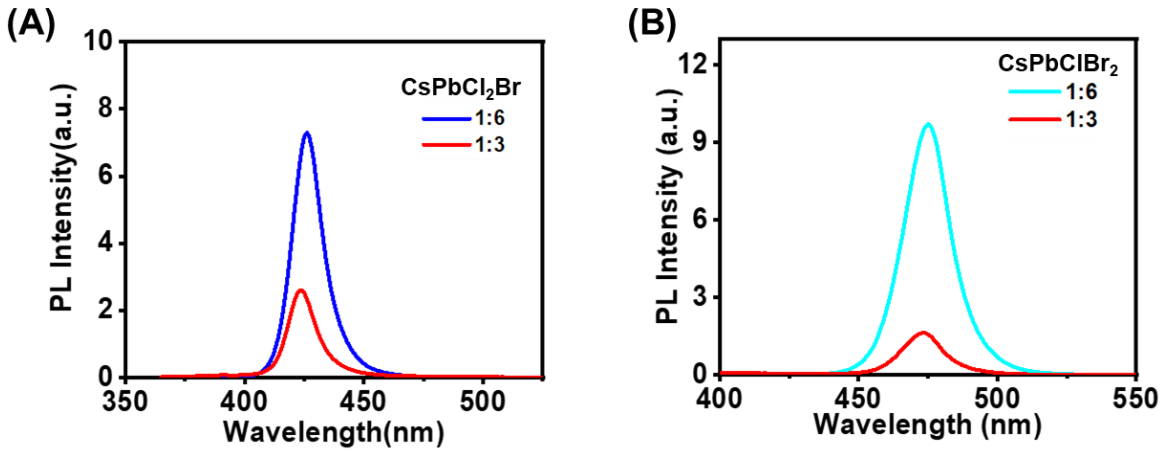

Figure AII.5. *Dependence of the PL spectra of* ***(A)*** *$CsPbCl_2Br$ and* ***(B)*** *$CsPbClBr_2$ NCs on the Pb:X precursor ratio.*

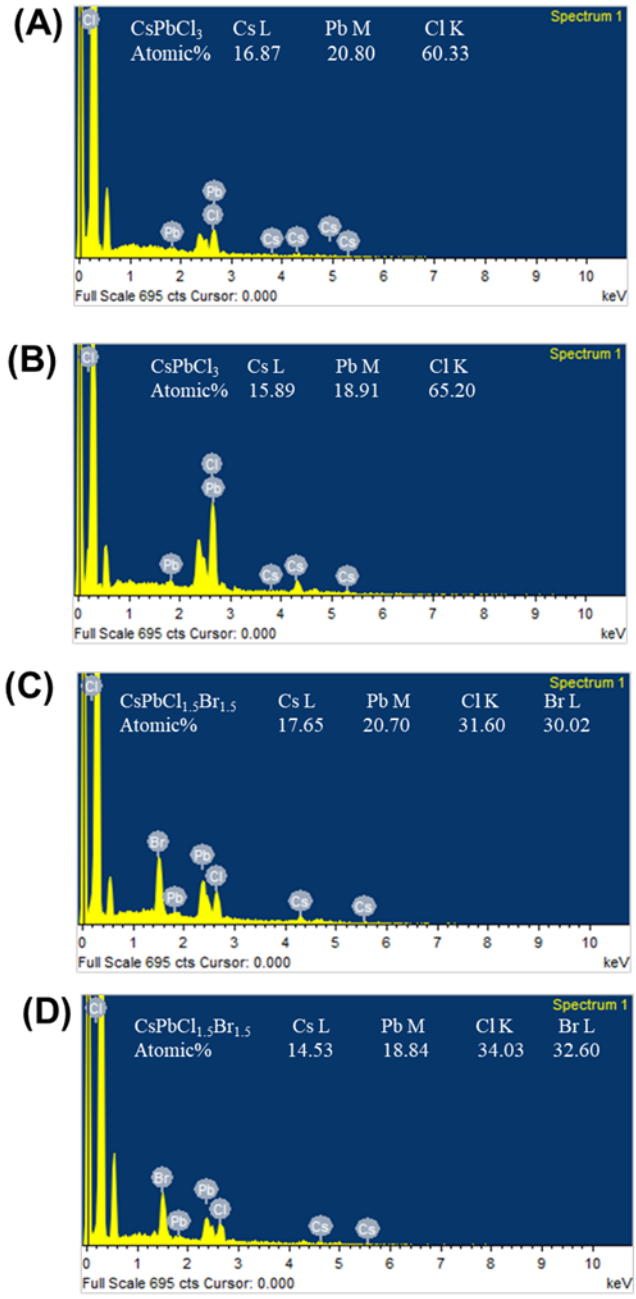

Figure AII.6. *EDX spectra of the* ***(A)*** *$CsPbCl_3$(1:3),* ***(B)*** *$CsPbCl_3$(1:9),* ***(C)*** *$CsPbCl_{1.5}Br_{1.5}$(1:3) and* ***(D)*** *$CsPbCl_{1.5}Br_{1.5}$(1:6) NCs.*

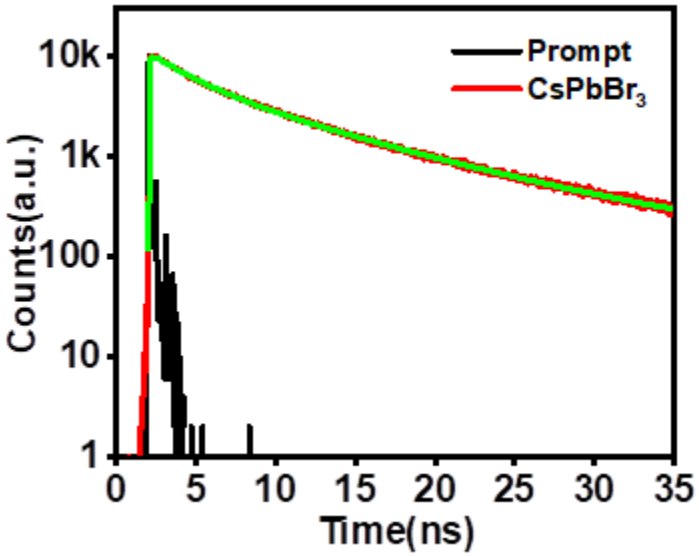

Figure AII.7. *PL decay profile of the $CsPbBr_3$ NCs. The monitoring emission and excitation wavelengths are 510 and 376 nm, respectively.*

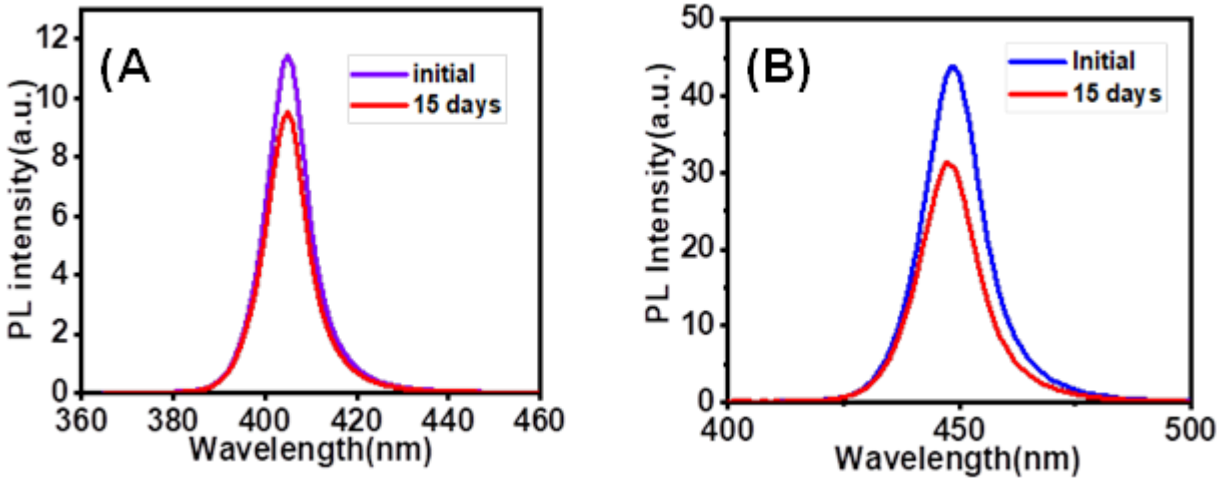

Figure AII.8. *Change in the PL spectra of optimized sample of* ***(A)*** *$CsPbCl_3$(1:9) and (B) $CsPbCl_{1.5}Br_{1.5}$(1:6) NCs after storage of 15 days in air.*

Table AI.1. *Amount of NCP and NBP taken for the synthesis of different sets of $CsPbCl_3$ and CsPb(Cl/Br)3 NCs.*

Samples	Pb:X molar ratio	NCP (g)	NBP (g)
$CsPbCl_3$	1:3	0.109	----
	1:6	0.218	----
	1:9	0.327	----
$CsPbCl_2Br$	1:3	0.073	0.045
	1:6	0.146	0.090
$CsPbCl_{1.5}Br_{1.5}$	1:3	0.054	0.068
	1:6	0.109	0.136

Table AII.2. *Atomic% of Cs, Pb and X (Cl, Br) and Pb:X ratio of different samples of $CsPbCl_3$, $CsPb(Cl/Br)_3$ and $CsPbBr_3$ NCs obtained from EDX measurements.*

System	Cs (%)	Pb (%)	Cl (%)	Br (%)	Pb:X (EDX)
$CsPbCl_3$(1:3)	16.87	20.80	60.33	----	1:2.90
$CsPbCl_3$(1:6)	16.49	19.60	63.44	----	1:3.24
$CsPbCl_3$(1:9)	15.89	18.91	65.20	----	1:3.45
$CsPbCl_2Br$(1:3)	18.97	20.30	43.57	17.16	1:2.99
$CsPbCl_2Br$(1:6)	16.30	18.85	46.03	20.82	1:3.54
$CsPbCl_{1.5}Br_{1.5}$(1:3)	17.65	20.70	31.60	30.02	1:2.98
$CsPbCl_{1.5}Br_{1.5}$(1:6)	14.53	18.86	34.03	32.60	1:3.53
$CsPbClBr_2$(1:3)	18.70	20.42	16.28	44.60	1:2.98

$CsPbClBr_2$(1:6)	18.80	17.60	18.20	45.40	1:3.61
$CsPbBr_3$	13.73	19.77	-----	66.50	1:3.36

Table AII.3. *Comparison of the PLQY and colloidal stability of different samples of $CsPbCl_3$ and $CsPb(Cl/Br)_3$ NCs obtained by direct synthesis.*

System	Method[a]/ Reaction condition[b]	PLQY (%)	Emission maxima (nm)	Remnant PL/ days	Ref
$CsPbCl_3$	LARP/ RT, PbX_2 as halide precursor	10	405	~90%, 30 days	1
	HI/ Benzoyl chloride as halide source	65	408	Not reported	2
	HI/ Oleylammonium chloride as halide source	97	405	~80%, 7 days	3
	HI/ PbX_2 as halide precursor and phthalimide as ligand	5.3	403	12%, 60 days	4
	HI/ PbX_2 and PEACl as halide precursor	62.3	405	Not reported	5
	HI/ $PhCOCl_2$ as halide precursor	71	404	Not reported	6
	HI/ N-halophthalimide as halide source	80	404	85%, 14 days	This work
$CsPb(Cl/Br)_3$	LARP/ RT, PbX_2 as halide precursor	37-70	455-478	~90%, 30 days	1
	HI/ R_4NX as ligand and PbX_2 as halide precursor	25-48	462-487	~100%, 30 days	7
	LARP/ RT, Tetrabutyl ammonium halide as halide precursor	50	440-500	Not reported	8
	HI/ PbX_2 and PEACl as halide precursor	80.2	460-470	Not reported	5

HI/ Palmitic acid and oleylamine as ligand and PbX_2 as halide source	47	430-460	Not reported	9
HI/ N-halophthalimide as halide source	85-97	425-475	75%, 14 days	This work

[a]LARP and HI represent ligand assisted re-precipitation and hot-injection. [b] RT and PEACl represent room temperature and phenylethylammonium chloride, respectively.

Appendix III

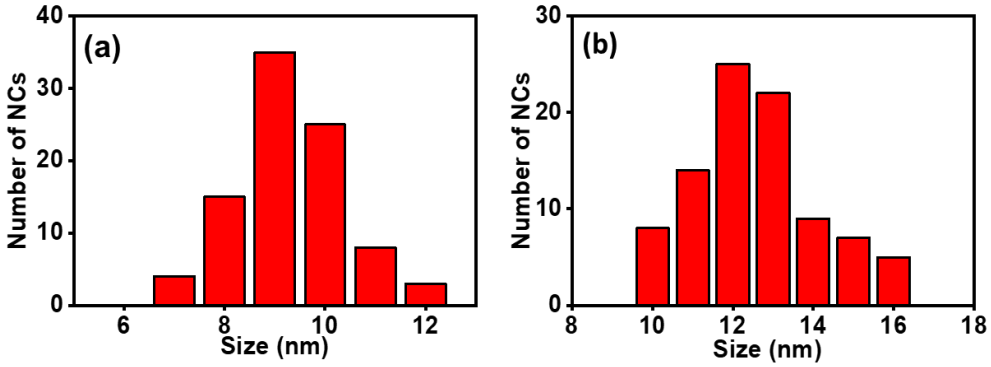

Figure AIII.1. *Size distributions of the* ***(a)*** *$CsPbI_3$(I) and* ***(b)*** *$CsPbI_3$(II) NCs.*

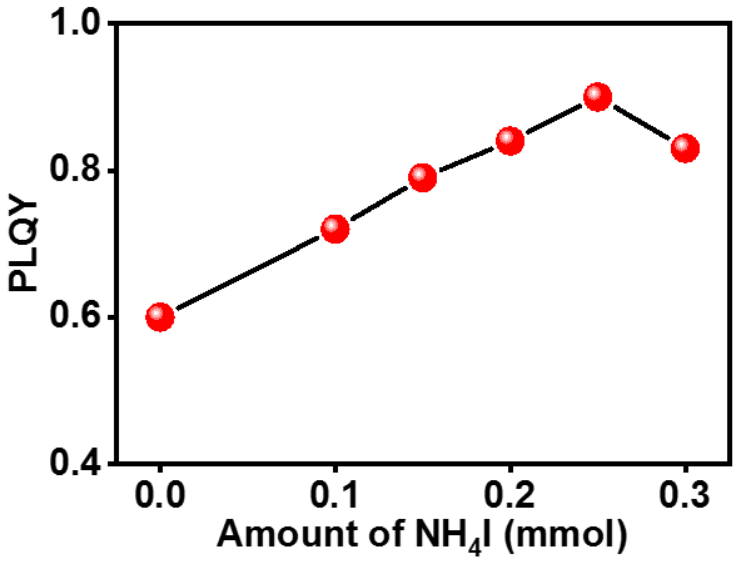

Figure AIII.2. *Variation of PLQY on varying amount of NH_4I (keeping the amount of PbI_2 fixed to 0.2 mmol) used during synthesis of the $CsPbI_3$(I) NCs.*

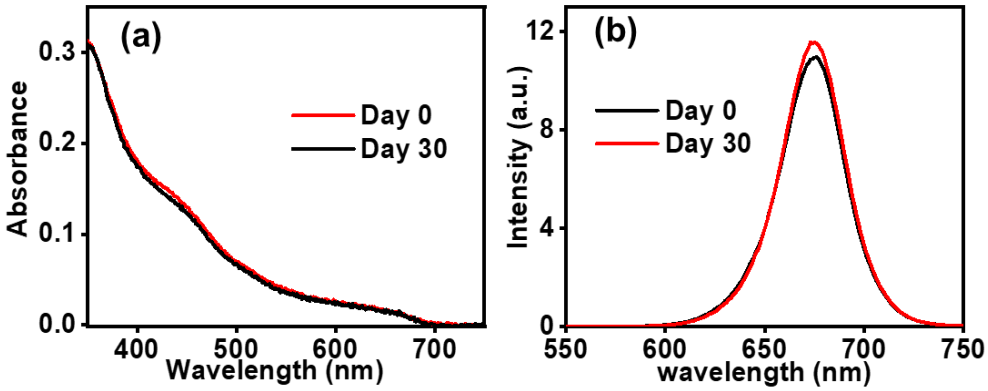

Figure AIII.3. ***(a)*** *UV–vis absorption and* ***(b)*** *PL spectra of $CsPbI_3$(I) NCs of as synthesized and 30-day old samples stored in a cuvette under ambient condition.*

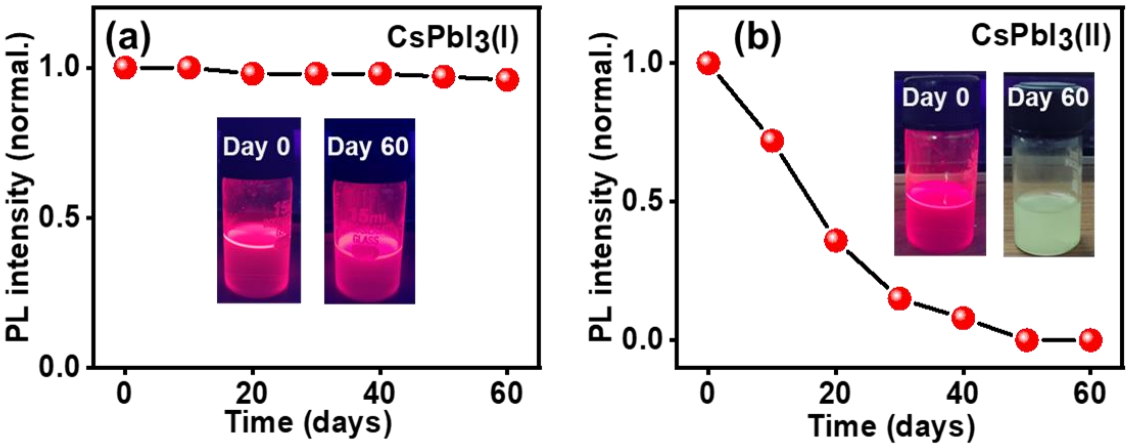

Figure AIII.4. *Air stability of the* ***(a)*** *$CsPbI_3$(I) and* ***(b)*** *$CsPbI_3$(II) NCs stored in a sealed reagent bottle.*

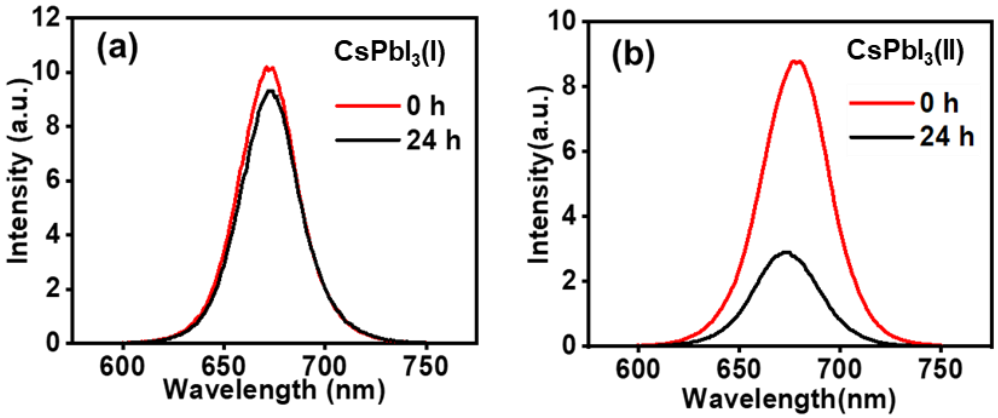

Figure AIII.5. *Time-dependence of the PL of* ***(a)*** *$CsPbI_3$(I) and* ***(b)*** *$CsPbI_3$(II) NCs under continuous illumination of UV light (365 nm, 8W) at room temperature under ambient condition.*

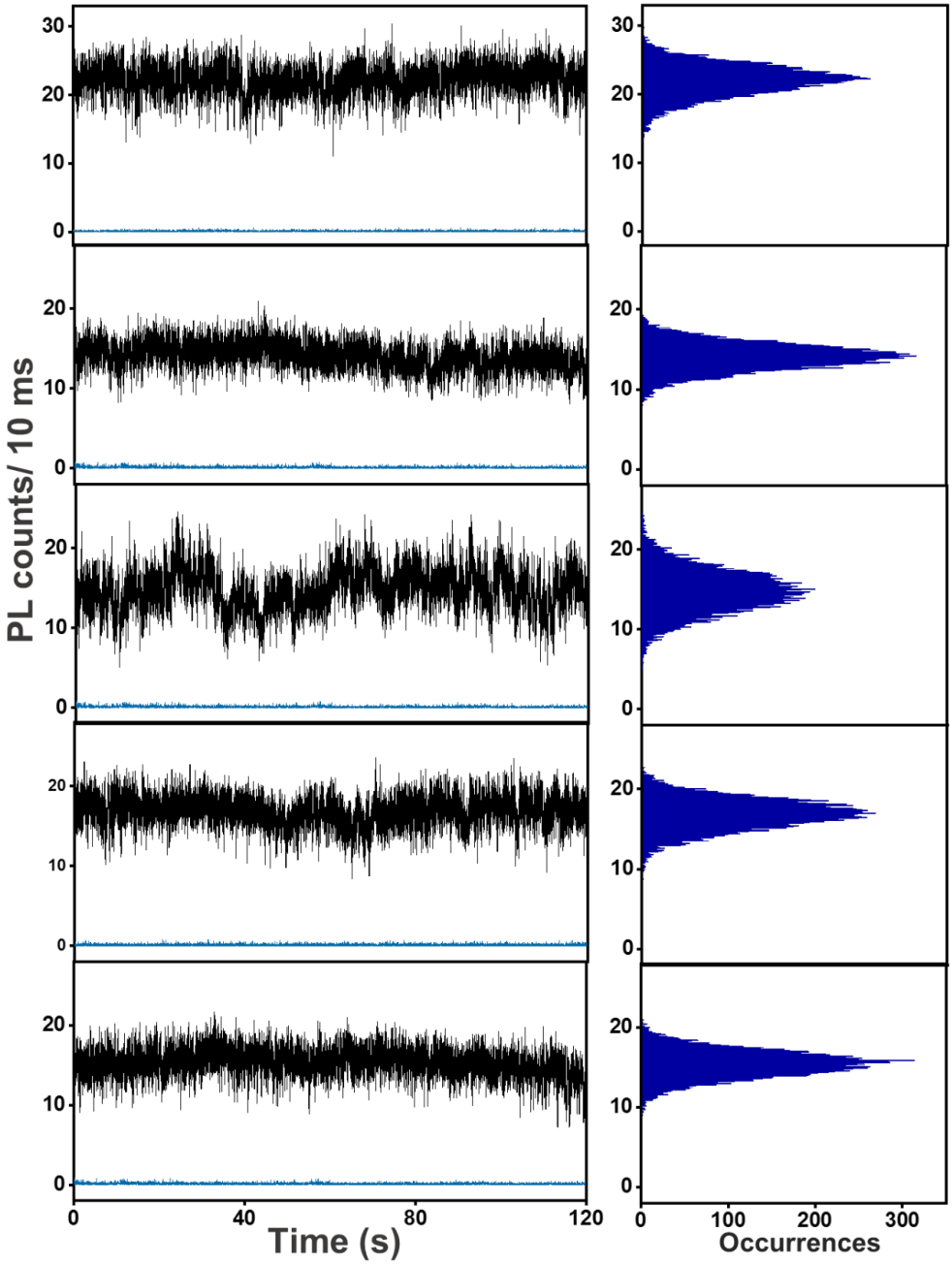
PL counts/ 10 ms
Time (s)
Occurrences
0
40
80
120
100
200
300

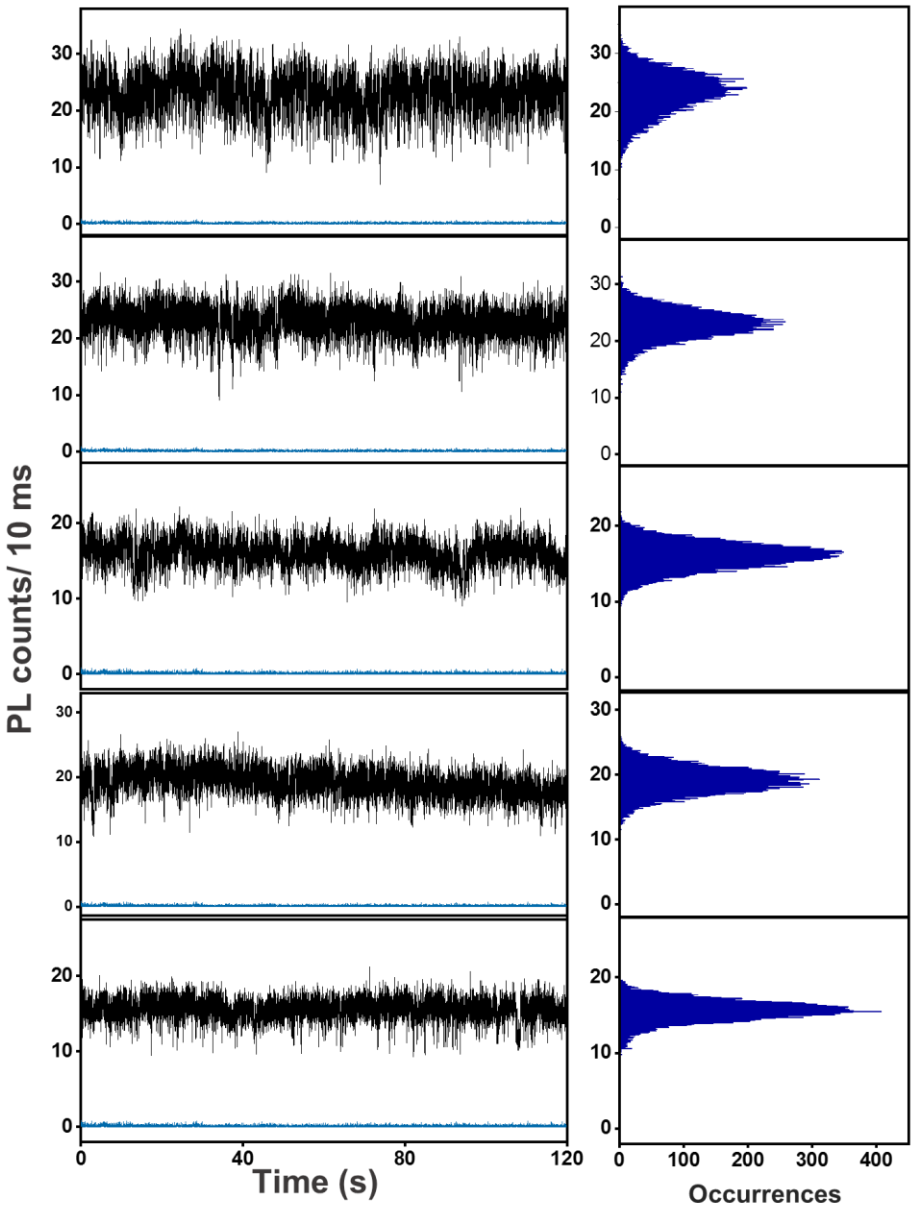

Figure AIII.6. *Representative PL intensity time-traces of 10 individual single NCs of* $CsPbI_3$*(I) (left panel) among 40 single NCs which exhibit only ON-states. Background signal is shown in cyan-blue color trace. The PL intensity distribution corresponding to each blinking trace is shown in the right panel.*

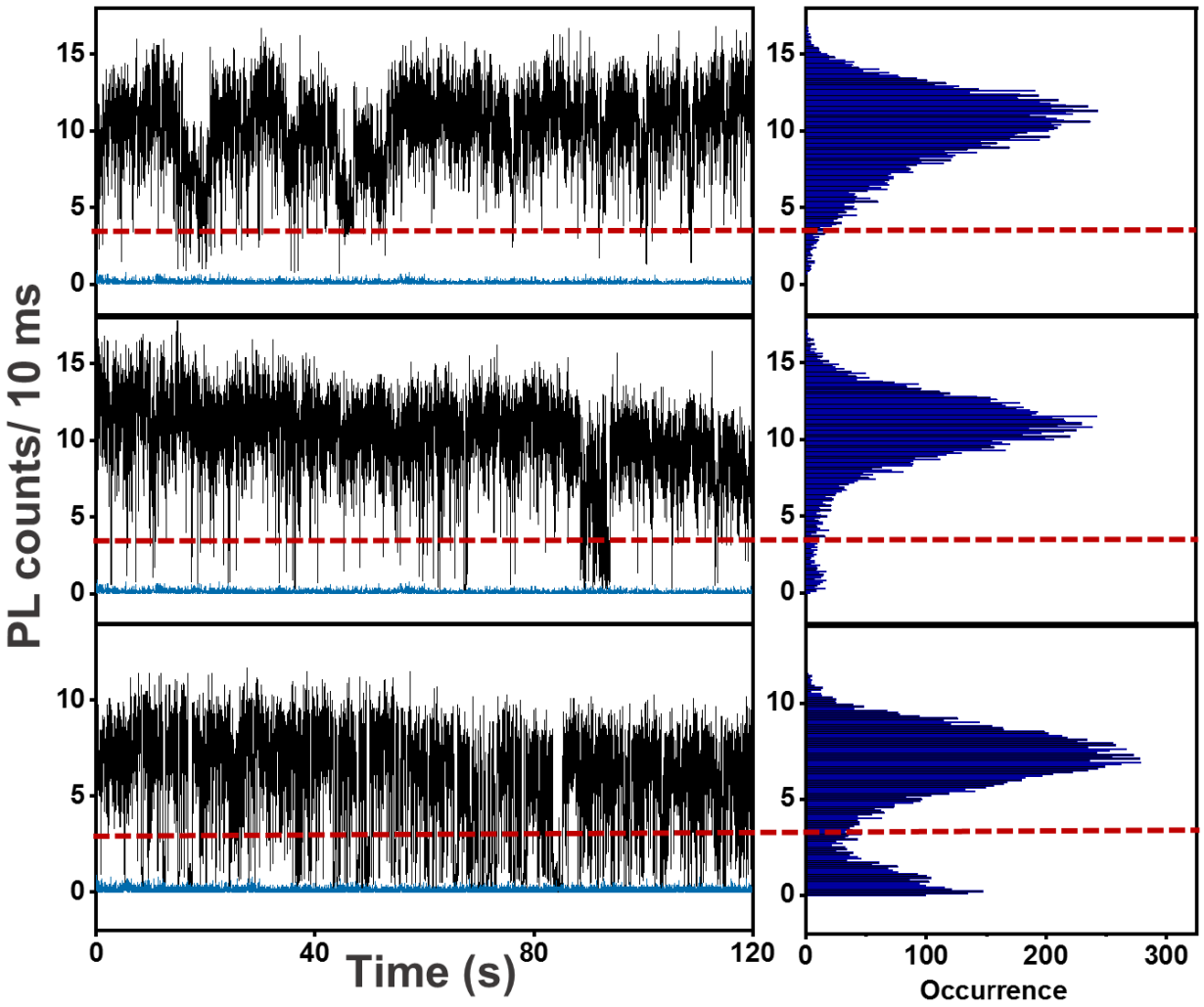

Figure AIII.7. *Representative PL intensity time-traces of 3 individual single NCs of* $CsPbI_3$*(I) among remaining 26 single NC. Background signal is shown in cyan-blue color trace. PL intensity distribution corresponding to each PL blinking trace is shown in the right panel. Threshold is shown by red dashed line.*

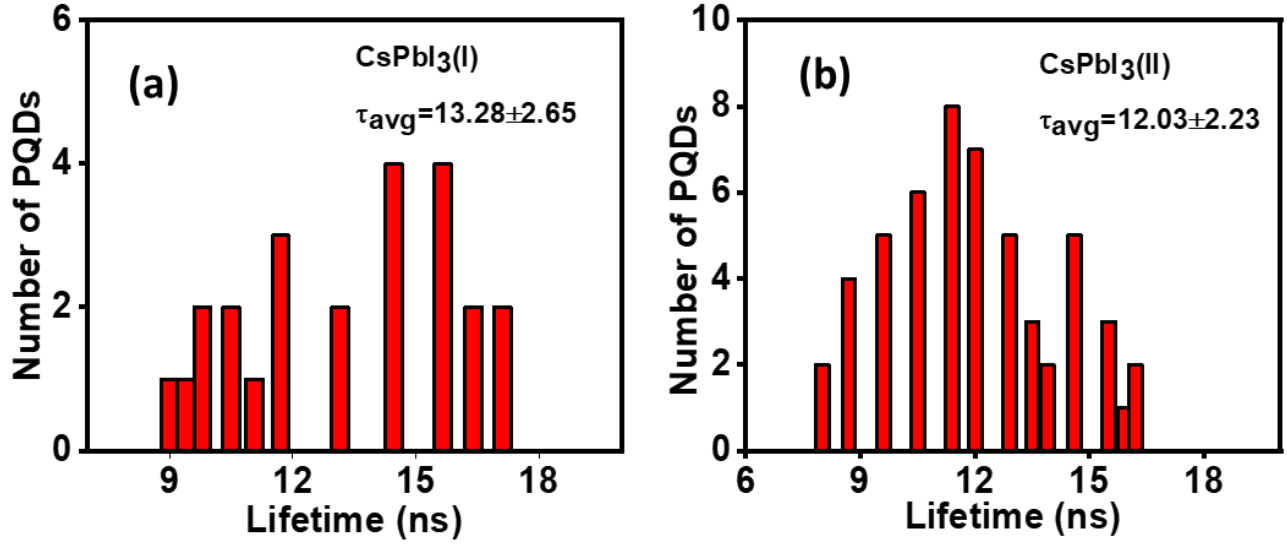

Figure AIII.8. *Lifetime histogram of the highest intensity level of (a) $CsPbI_3$(I) and (b) $CsPbI_3$(II) NCs.*

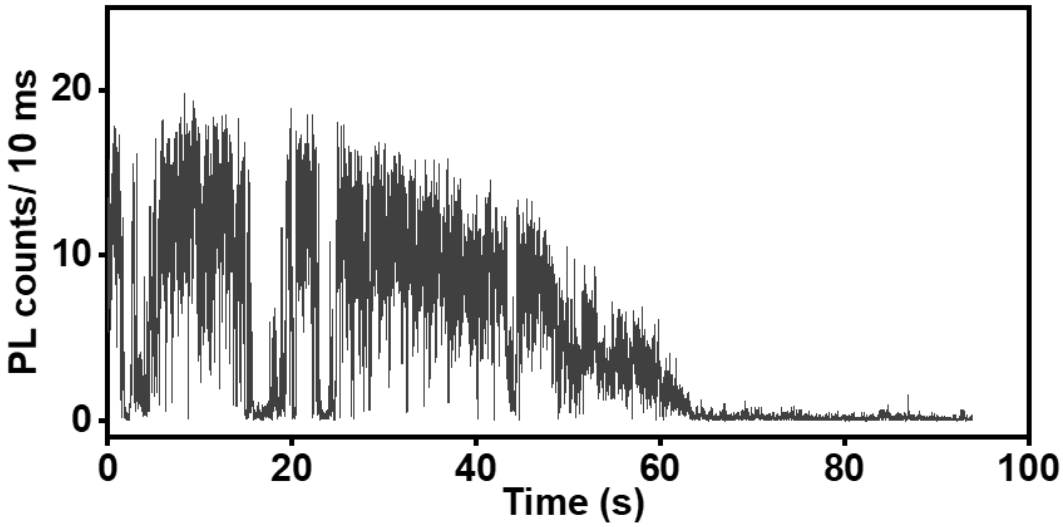

Figure AIII.9. *Representative PL intensity time-trace of a $CsPbI_3$(II) single NC, which exhibits photo-degradation within 60 s.*

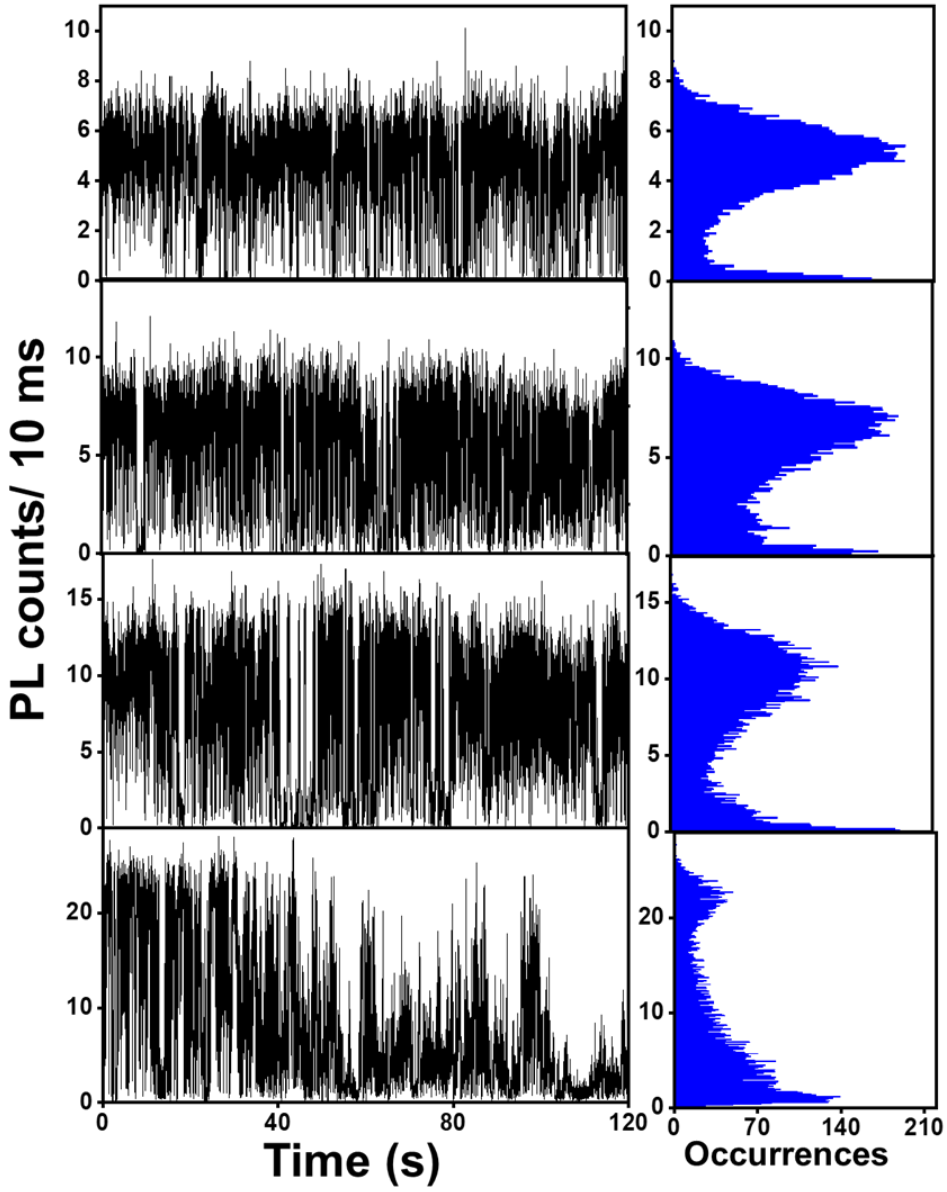

Figure AII.10. *Representative PL intensity time-traces of 4 individual single NCs of $CsPbI_3$(II) among 53 single NCs. PL intensity distribution corresponding to each PL blinking trace is shown in the right panel.*

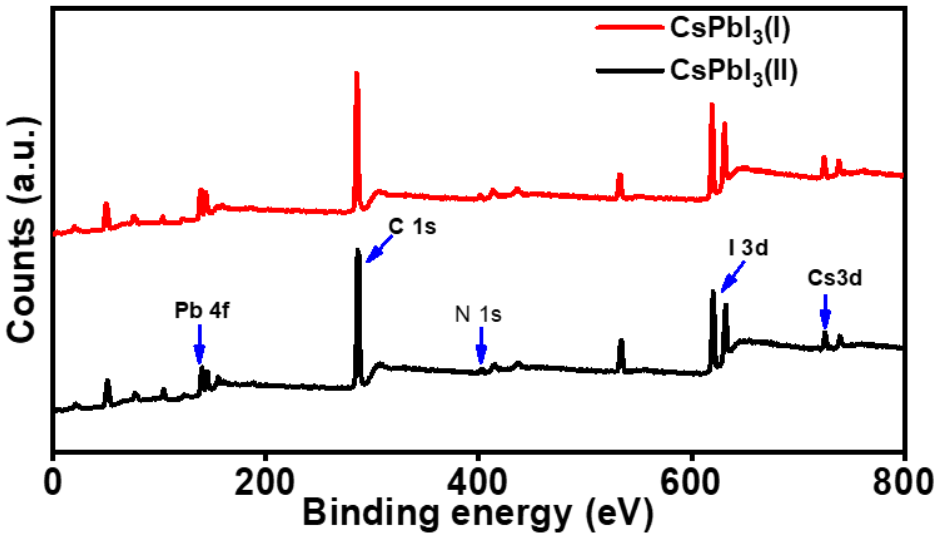

Figure AIII.11. *Survey XPS spectra of the $CsPbI_3$(I) and $CsPbI_3$(II) NCs.*

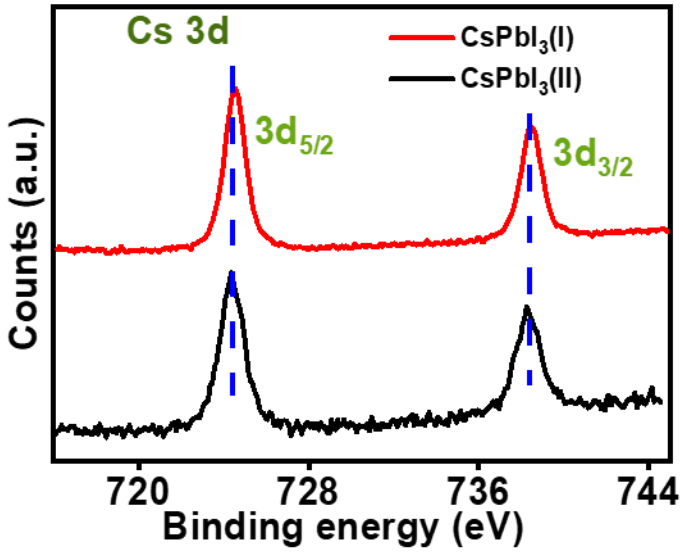

Figure AIII.12. *High resolution XPS spectra of Cs 3d ($3d_{5/2}$, $3d_{3/2}$) of $CsPbI_3$(I) and $CsPbI_3$(II) NCs.*

Table AIII.1. *Lifetime components (τ_i) and their weightages (α_i) of different PL intensity levels of the PL intensity time-trace of single $CsPbI_3$(II) NC shown in Figure* ***5a****.*

Region [Inensity (counts/10 ms)]	τ_1 (α_1) ns	τ_2(α_2) ns
P1 (14.00)	11.40	
P2 (11.00)	9.80	
P3 (7.50)	8.20	
P4 (4.00)	6.90 (0.41)	1.90 (0.59)
P5 (1.50)	4.35 (0.29)	1.33 (0.71)

Table AIII.2. *Power law exponents and truncation time of these NCs obtained from probability distribution analysis of the ON and OFF-events.*

System	α_{ON}	α_{OFF}	$\tau_{c(ON)}$
$CsPbI_3$(I)	0.59±0.16	2.11±0.28	650±120
$CsPbI_3$(II)	0.92±0.22	1.86±0.27	610±130

Table AIII.3. *Atomic percentage ratio of the constituting elements (with respect to Pb) of the $CsPbI_3$(I) and $CsPbI_3$(II) NCs calculated based on high resolution XPS data and atomic sensitivity factor of each element.*

System	**Cs (%)**	**Pb (%)**	**I (%)**	**N (%)**
$CsPbI_3$(I)	0.83	1.00	3.33	2.55
$CsPbI_3$(II)	0.90	1.00	2.89	1.53

Appendix IV

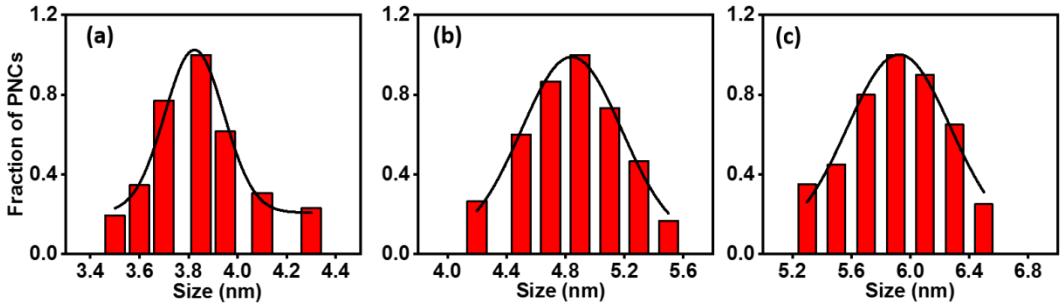

Figure AIV.1. Size histograms of $CsPbBr_3$@459 (a), $CsPbBr_3$@478 (b) and $CsPbBr_3$@488 (c) NCs.

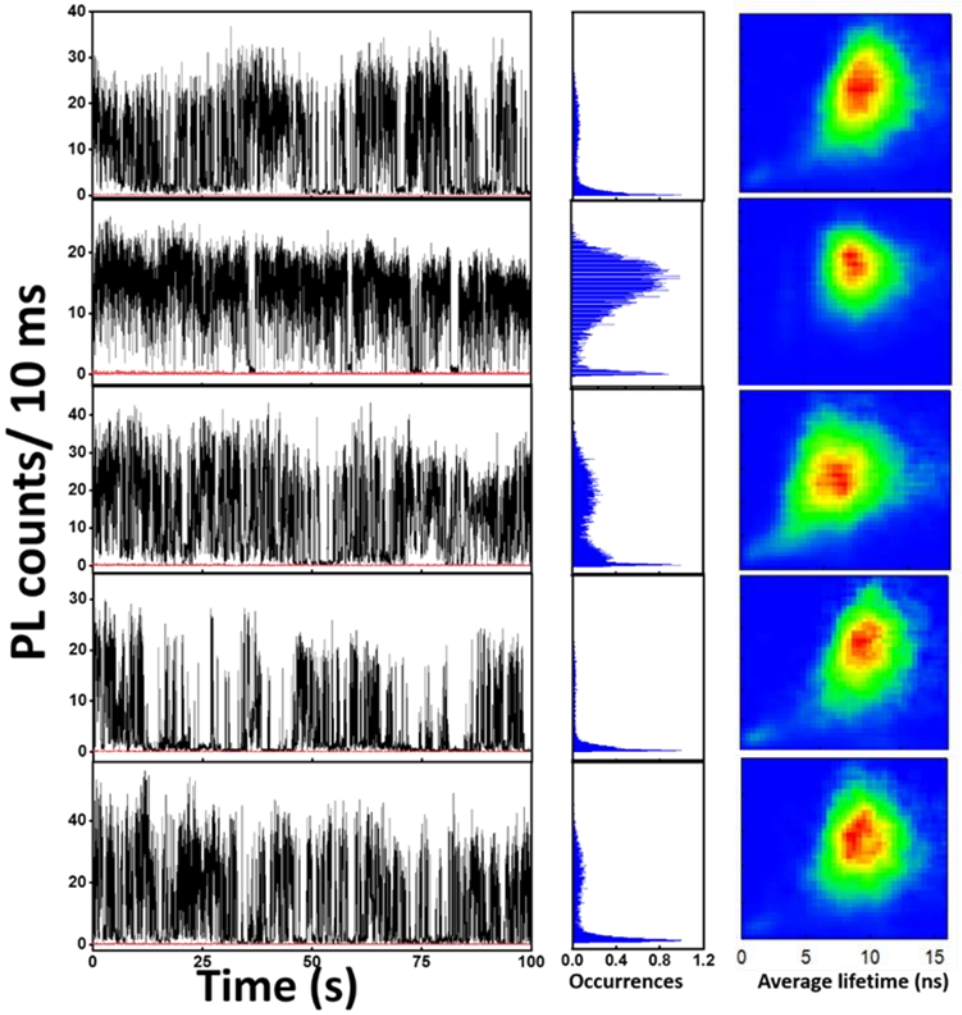

Figure AIV.2. Representative PL trajectories (left panel), occurrence histogram (middle panel) and

corresponding FLID pattern (right panel) of $CsPbBr_3$@459 NCs (3.80 nm). Background signal is shown in red trace.

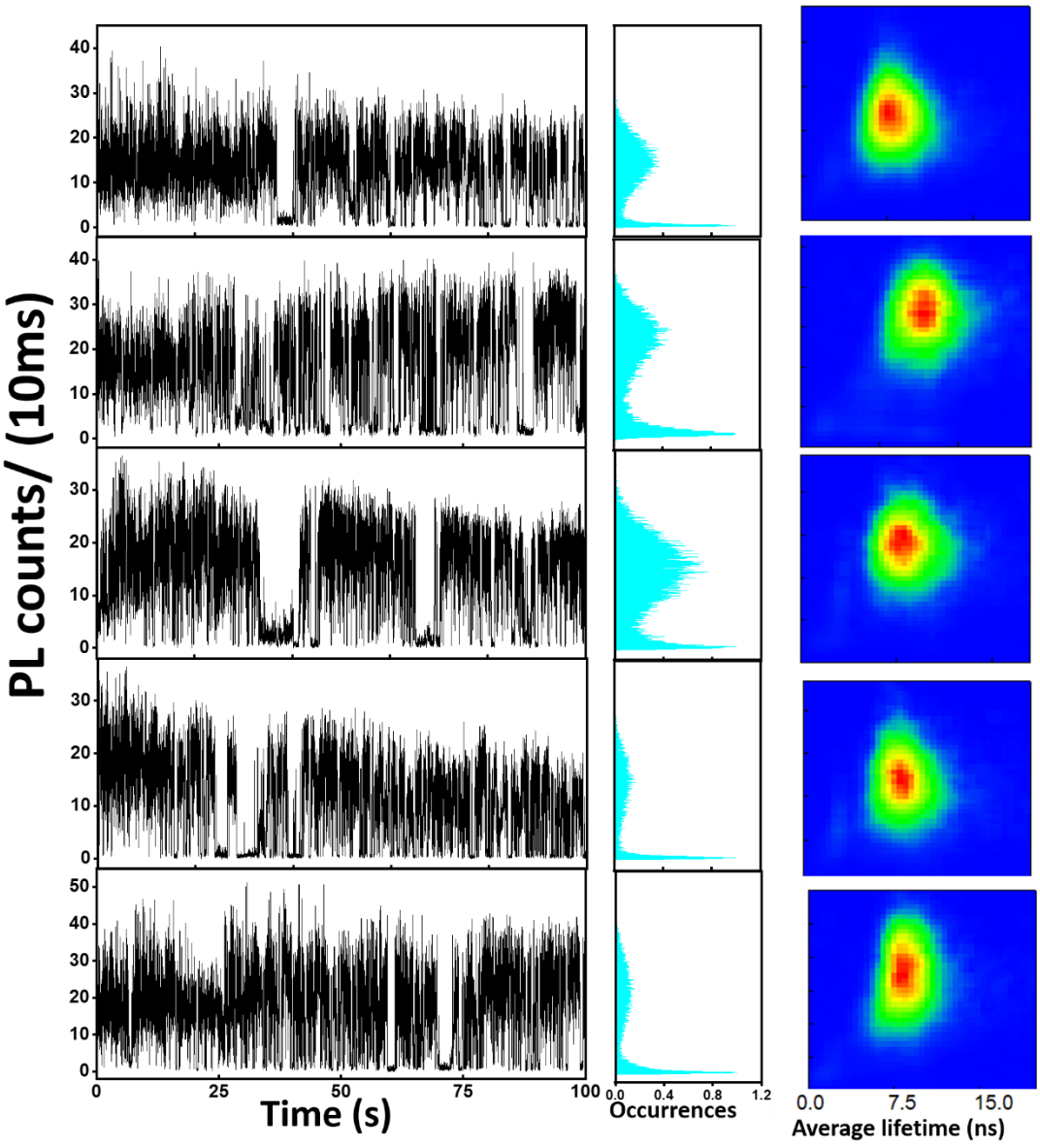

Figure AIV.3. Representative PL blinking traces (left panel), occurrence histogram (middle panel) and corresponding FLID pattern (right panel) of $CsPbBr_3$@478 NCs (4.80 nm).

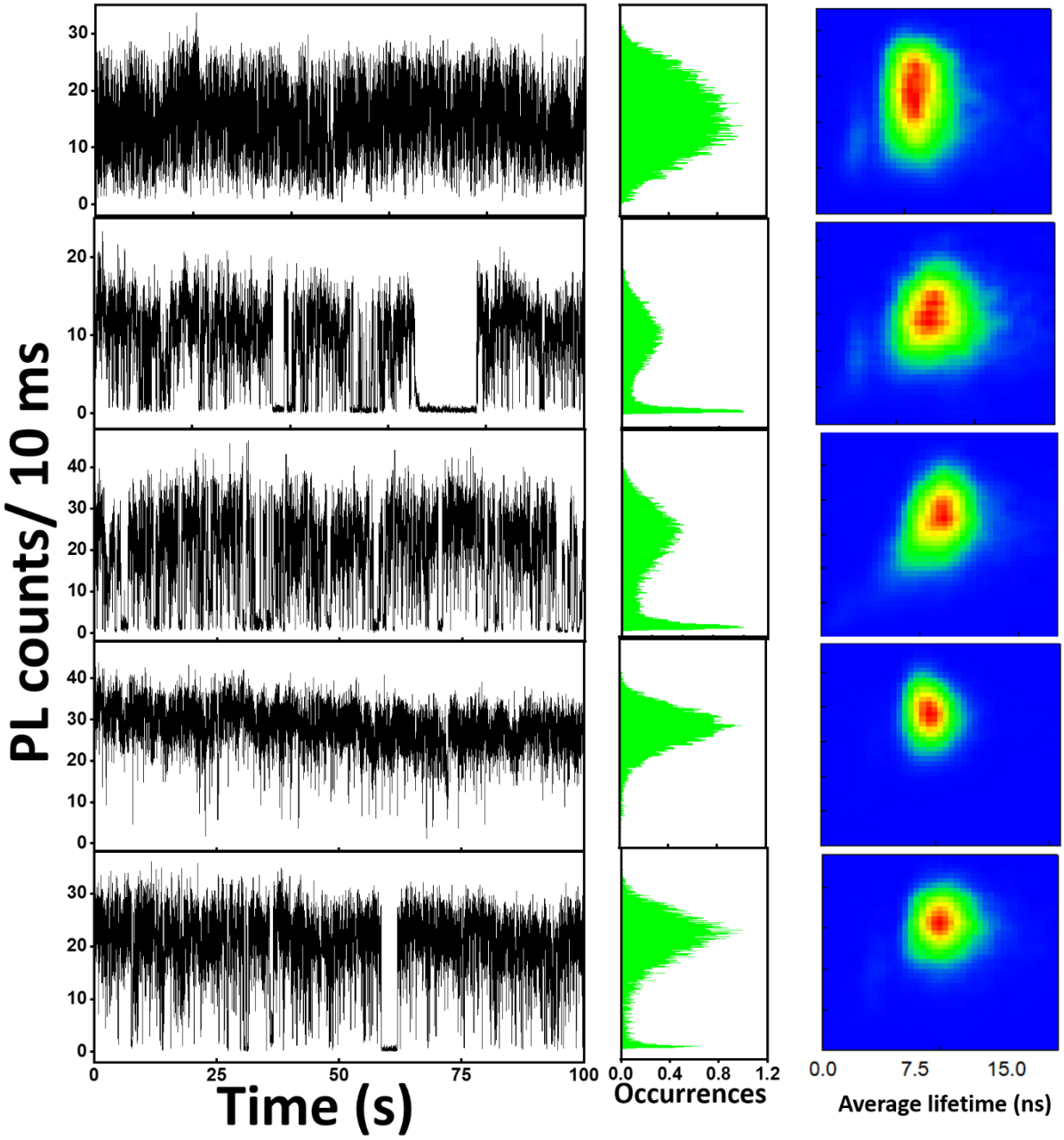

Figure AIV.4. Representative PL trajectories (left panel), occurrence histogram (middle panel) and corresponding FLID pattern (right panel) of $CsPbBr_3$@488 NCs (5.90 nm).

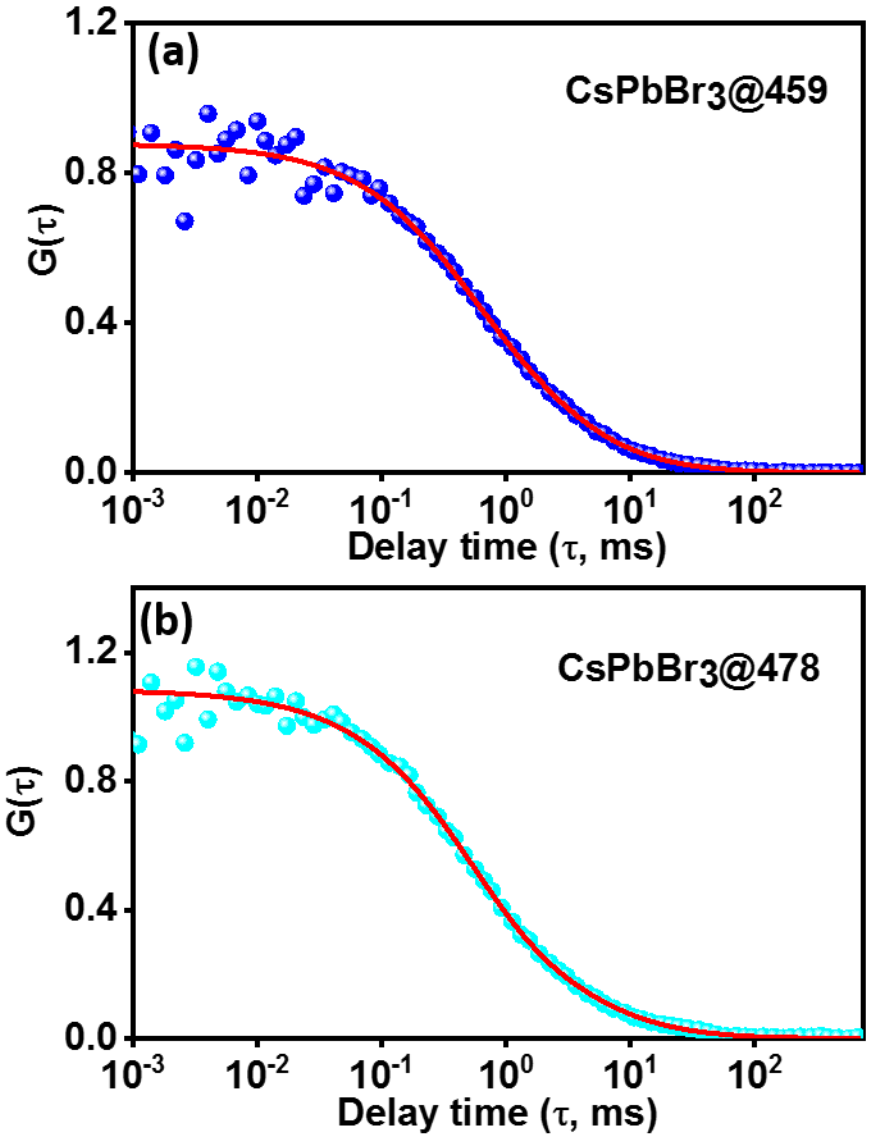

Figure AIV.5. Fluorescence correlation data of the (a) $CsPbBr_3$@459 and (b) $CsPbBr_3$@478 NCs in 1-octadecene. The red lines indicate the fit to the FCS data.

ACS Energy LETTERS

Cite This: ACS Energy Lett. 2020, 5, 64−69

http://pubs.acs.org/journal/aelccp

LETTER

N-Bromosuccinimide as Bromide Precursor for Direct Synthesis of Stable and Highly Luminescent Green-Emitting Perovskite Nanocrystals

Sumanta Paul and Anunay Samanta*

School of Chemistry, University of Hyderabad, Hyderabad 500046, India

Supporting Information

ABSTRACT: Stable green-emitting perovskite nanocrystals (NCs) with general formula $APbBr_3$, exhibiting a high photoluminescence quantum yield (PLQY), narrow bandwidth, and adjustable PL in the 510−535 nm region are coveted materials for optoelectronic applications. A generic method of obtaining both hybrid and all-inorganic perovskite NCs with the desired characteristics is, however, lacking. Herein, we report a methodology for the synthesis of $CsPbBr_3$, $FAPbBr_3$, and $MAPbBr_3$ NCs employing *N*-bromosuccinimide as the bromide precursor. The NCs show uniform size distribution, PL maxima between 512 and 531 nm, near-unity PLQY with a fwhm of 18−22 nm, and remarkable stability in ambient conditions, in the presence of water and under UV irradiation. Not only do these exceptional characteristics of the NCs indicate their high potential in real applications, but this new methodology may also open new vistas for direct synthesis of other perovskites with high PLQY and stability without resorting to any additional postsynthesis treatment.

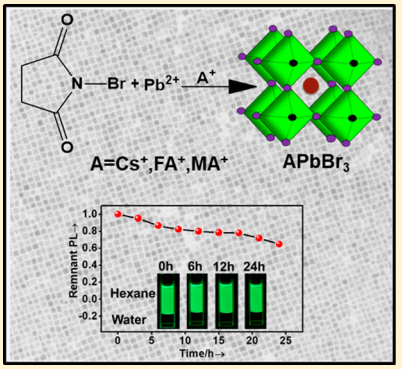

Lead halide-based perovskite nanocrystals (NCs) with general formula $APbX_3$, where **A** = Cs^+, $CH_3NH_3^+$ (**MA**), or $CH(NH_2)_2^+$ (**FA**) and X = Cl, Br, or I, have been at the forefront of research in optoelectronics and photovoltaics for nearly a decade for their impressive optical properties, such as high photoluminescence quantum yield (PLQY), narrow PL bandwidth, composition-tunable band gap, and high absorption coefficient.[1−9] Among the perovskites, the bromide-based ones ($APbBr_3$) with bright green PL and narrow full width at half-maximum (fwhm) of <25 nm are most desirable for television displays and green-emitting LEDs.[10−13] These NCs are obtained by hot-injection or ligand-assisted reprecipitation (LARP) methods.[11,14−16] The two-precursor hot-injection method, in which $PbBr_2$ is used as the precursor for both lead and bromine and which is commonly used for the synthesis of $CsPbBr_3$ NCs, is not quite effective for the organometallic (**FA**$PbBr_3$ and **MA**$PbBr_3$) perovskites.[13,16,17] For example, **FA**$PbBr_3$ NCs obtained by this method exhibit a broader size distribution and poor optical properties.[13] Even for $CsPbBr_3$ NCs, the PLQY obtained by this method is typically 60−80%[11] or even lower due to nonradiative deactivation induced by the bromide vacancies.[18−21] This is why most often an in situ or a postsynthetic treatment with bromide salt[22−25] or other reagents is necessary to improve the PLQY of these NCs.[26−28]

Kovalenko and co-workers synthesized **FA**$PbBr_3$ NCs by a three-precursor hot-injection method, wherein oleylammonium bromide was employed as the bromide source.[13] Pradhan and co-workers recently synthesized $CsPbX_3$ (X = Cl, Br, I) with 97% PLQY following this approach (i.e., using oleylammonium halides as halide precursors).[29] Although the three-precursor hot-injection method gives reasonably good quality $CsPbBr_3$ NCs and **FA**$PbBr_3$ NCs, the **MA**$PbBr_3$ NCs are still obtained by the LARP method, and they exhibit poor optical properties.[16] Except for the work of Manna and co-workers, who could succeed in obtaining all three green-emitting perovskites with 92% PLQY using benzoyl bromide as the bromide precursor, we are not aware of any other work reporting synthesis of $CsPbBr_3$, **FA**$PbBr_3$, and **MA**$PbBr_3$ following a given protocol.[30] A point to note here is that, while the $APbBr_3$ NCs obtained by this method are highly luminescent, no stability data of these NCs is available. As bright green-emitting $APbBr_3$ NCs with adjustable PL maxima in the 510−535 nm range and fwhm of <25 nm are very much essential for most optoelectronic applications (considering NTSC and the most recent rec.2020 color standard), no direct

Received: October 29, 2019
Accepted: November 25, 2019
Published: November 25, 2019

DOI: 10.1021/acsenergylett.9b02363
ACS Energy Lett. 2020, 5, 64−69

method of obtaining all three NCs that are stable with these characteristics is yet available, and we have been working toward developing a general protocol for the synthesis of all three green-emitting NCs with high stability, monodispersity, a narrow PL bandwidth, and near-unity PLQY. These efforts have led to the results that are described below.

Our three-precursor hot-injection method employs *N*-bromosuccinimide (NBS), a widely used source of bromine in organic synthesis, as the bromide precursor.[31] Reaction of NBS with organic acids generates HBr,[32] which reacts with oleylamine to form oleylammonium bromide; the latter serves as the active bromide source in the synthesis (Schemes 1 and S1). In our method, PbO and NBS were dissolved in octadecene in the presence of oleic acid and oleylamine at 120−140 °C in vacuum. The reaction temperature was then set to 200 °C for $CsPbBr_3$ and 165 °C for both **MA**$PbBr_3$ and **FA**$PbBr_3$ in a N_2 atmosphere, and the desired amount of the oleate salt of the respective **A** cation (which was prepared separately) was injected swiftly (details are in the Supporting Information). The method, which is found to be highly reproducible (Figure S1), yields brightly luminescent extremely uniform sized cubes of nanodimension (Figures 1a−c and S2).

Scheme 1. Reaction Scheme of the NBS-Mediated Synthesis of A$PbBr_3$ NCs

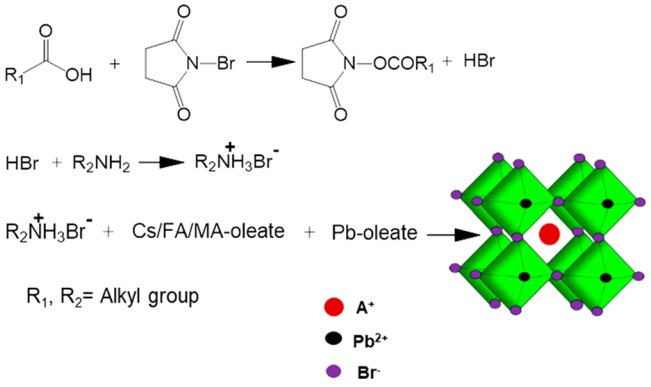

The quality of the NCs, as determined by their PLQY and size distribution, was found to be quite sensitive to the reaction conditions, particularly, the reaction temperature and Pb:Br precursor ratio. For $CsPbBr_3$ NCs, it was found that at temperatures below 200 °C a mixture of 2D nanoplates and cubes was formed (Figure S4) with a consequential increase in PL bandwidth, the appearance of multiple peaks (Figure S5), and a low PLQY (e.g., PLQY 40% at 130 °C) (Table S2). A low PLQY of the NCs was also observed for a lower Pb:Br precursor ratio (69% for a Pb:Br ratio of 1:2.5) (Figure S6, Table S2). The **MA**$PbBr_3$ NCs, when synthesized below 165 °C, exhibited broad PL spectra, and at temperatures < 150 °C, multiple emission peaks indicating a heterogeneous distribution of the size and morphology of the NCs (Figure S7a) and a significant drop in PLQY were observed (Table S3). The **FA**$PbBr_3$ NCs obtained at temperatures below 165 °C showed a lower PLQY, larger fwhm, and blue shift of the PL peak (Figure S7b, Table S3). A Pb:Br precursor molar ratio of 1:3 and a temperature of 200 °C for $CsPbBr_3$ NCs and 165 °C for both **MA**$PbBr_3$ and **FA**$PbBr_3$ NCs were found to be the optimum reaction conditions for obtaining NCs with a near-unity PLQY, uniform size distribution, and high stability.

Bright-field TEM images indicate the cubic shape and narrow size distribution of the NCs (Figures 1a−c and S2). The measured edge lengths for the $CsPbBr_3$, **MA**$PbBr_3$, and **FA**$PbBr_3$ NCs are 8.4 ± 0.62, 14.2 ± 1.2, and 11.9 ± 1 nm, respectively. The PXRD patterns nicely match with the cubic perovskite structures of $CsPbBr_3$ ICSD code 29073 and **MA**$PbBr_3$ ICSD code 252415 (Figure 1d−f). For **FA**$PbBr_3$ NCs, the PXRD pattern matches with that reported by Zhumekenov et al.[33] No secondary phases are observed in the PXRD pattern. Excellent PL properties of the NCs are exemplified by a narrow fwhm of 18 nm for $CsPbBr_3$, 21 nm for **MA**$PbBr_3$, and 20 nm for **FA**$PbBr_3$ NCs and a PLQY between 95 and 99% (Figure 1g−i). The PL decay profiles of the NCs are recorded to understand the photophysical processes involved. $CsPbBr_3$ NCs exhibit biexponential decay (Figure 2a, Table S4) with 5.49 (80%) and 15.68 (20%) ns lifetime components. The major 5.49 ns component is clearly due to excitonic recombination.[34] The absence of any subnanosecond lifetime component indicates that the $CsPbBr_3$ NCs are largely free from surface traps. This is corroborated by the fact that an additional short-lifetime component (1.65 ns) is indeed observed for the $CsPbBr_3$ NCs, which are obtained using a lower Pb:Br ratio of 1:2.5 (Figure S8 and Table S4). **MA**$PbBr_3$ and **FA**$PbBr_3$ NCs also exhibit biexponential PL decay behavior with lifetimes of 11.78 (71%) and 30.17 ns (29%) for the former and 10.00 (80%) and 31.18 ns (20%) for the latter (Figures 2b and S9 and Table S4). In both cases, the shorter-lifetime component, which has a major contribution, is assigned to excitonic recombination based on the literature.[34,35]

Perhaps the biggest problem with the perovskite NCs is their poor stability toward polar solvents (including water) and light.[1,2] The structural integrity of the $CsPbBr_3$ NCs is lost during purification with polar solvent and upon aging.[18,19] The stability of the organometallic halide perovskites, particularly for **MA**$PbBr_3$ NCs, is a major issue.[2,36] Methods such as providing an inert protection layer,[37,38] doping or alloying with heteroatoms,[20,39] changing ligands,[40−42] postsynthetic treatments, etc.[21,26,27,43] have been attempted to impart stability to the NCs. However, none of these methods yields A$PbBr_3$ NCs with the desired stability. Interestingly, all of the NCs obtained by our method show exceptional stability. For example, $CsPbBr_3$ NCs retain 90% PLQY even after 3 months of storage in ambient conditions (Figures 3a and S10). The PXRD pattern of these NCs recorded after 3 months of storage and TEM images obtained after 60 days of storage show that the cubic shape with a uniform size distribution of these NCs is retained for a long duration in ambient atmospheric conditions (Figure 3b,c). Excellent photostability of these NCs is evident from the fact that 81% of the initial PL of our $CsPbBr_3$ NCs is retained even after 24 h of continuous illumination with an 8 W, 365 nm UV light (Figure S11). Water treatment of the $CsPbBr_3$ NCs generally results in rapid degradation of the NCs with loss of PLQY. However, remarkable stability of our $CsPbBr_3$ NCs is evident from the fact that nearly 70% of the initial PL is retained even 36 h after mixing 2.5 mL of dispersed NCs in hexane with 1.5 mL of water (Figure S12). The stability of the NCs toward UV irradiation in the presence of water is evident from the fact that 65% of initial PL can be observed even after 24 h of continuous illumination (Figures 3d and S13). Table 1, which presents a comparison of the PLQY and stability of our $CsPbBr_3$ NCs with those obtained

DOI: 10.1021/acsenergylett.9b02363
ACS Energy Lett. 2020, 5, 64−69

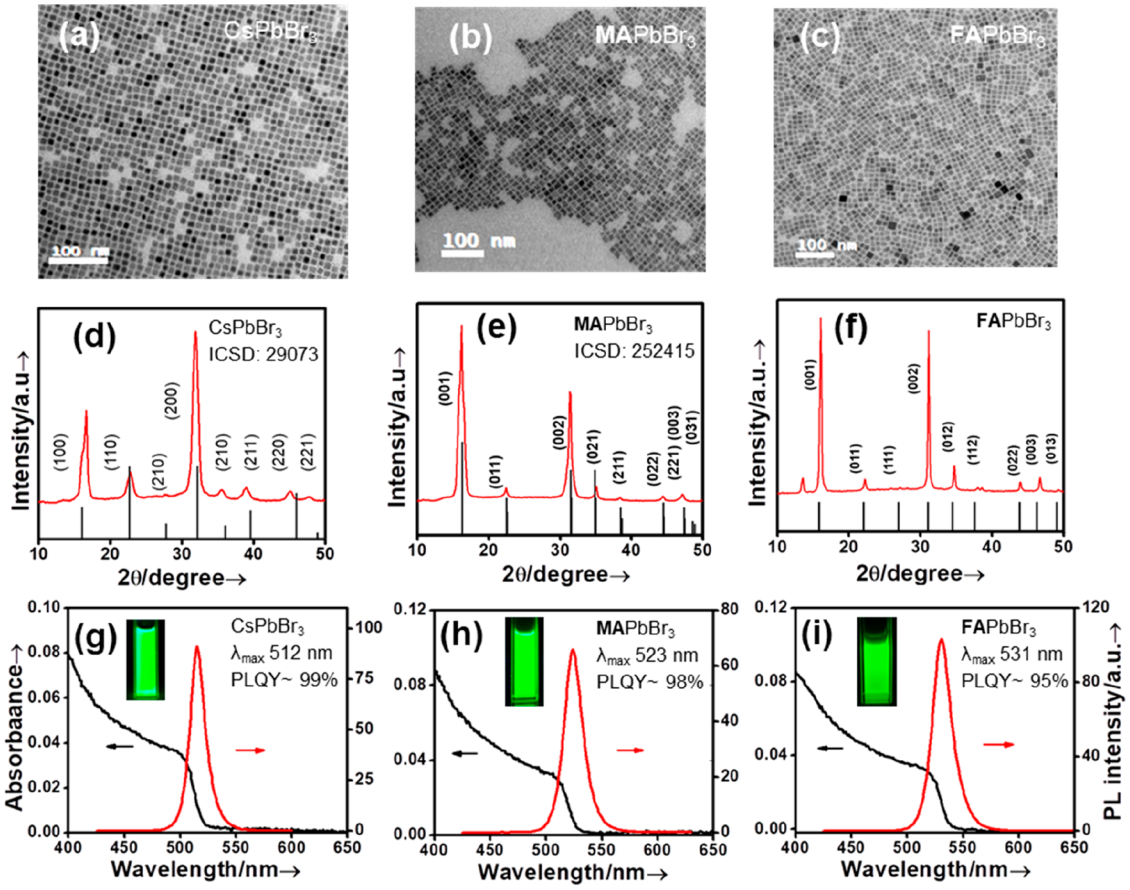

Figure 1. Bright-field TEM images of (a) $CsPbBr_3$, (b) $MAPbBr_3$, and (c) $FAPbBr_3$ NCs. The scale bar is 100 nm in all the cases. PXRD patterns of (d) $CsPbBr_3$, (e) $MAPbBr_3$, and (f) $FAPbBr_3$ NCs along with corresponding references for bulk cubic phases. In the case of $FAPbBr_3$ NCs, the PXRD pattern is compared with that of a reported crystal structure.[33] UV−vis absorption and emission spectra of (g) $CsPbBr_3$ NCs, (h) $MAPbBr_3$, and (i) $FAPbBr_3$ NCs. The excitation wavelength is 405 nm in all cases. The insets show respective NCs under UV light excitation.

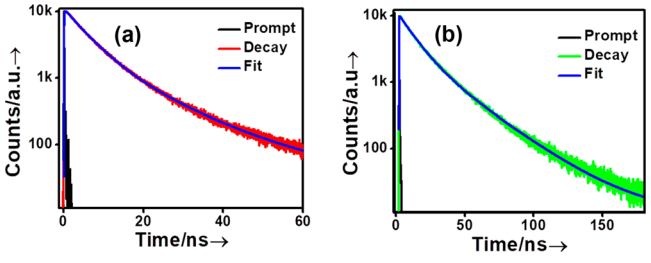

Figure 2. PL decay behavior of (a) $CsPbBr_3$ and (b) $MAPbBr_3$ NCs. Excitation wavelength is 405 nm in both cases. PL is monitored at 512 and 523 nm in (a) and (b), respectively.

by other methods so far, highlights superior characteristics of our $CsPbBr_3$ NCs.

The stability of **FA**$PbBr_3$ and **MA**$PbBr_3$ NCs is also quite impressive. Nearly 85% of the initial PL of both **FA**$PbBr_3$ and **MA**$PbBr_3$ is retained after 60 days of storage in an ambient atmosphere (Figures S14 and S15). The photostability of **MA**$PbBr_3$ NCs has been a major issue as these NCs undergo rapid photodegradation with continuous PL peak shift.[36] However, retention of 75% of the initial PL without any change of PL peak position and fwhm (Figure 4a,b) demonstrates much better photostability of our **MA**$PbBr_3$ NCs. **FA**$PbBr_3$ NCs also exhibit distinctive photostability; 80% of the initial PL is retained even after 24 h of continuous

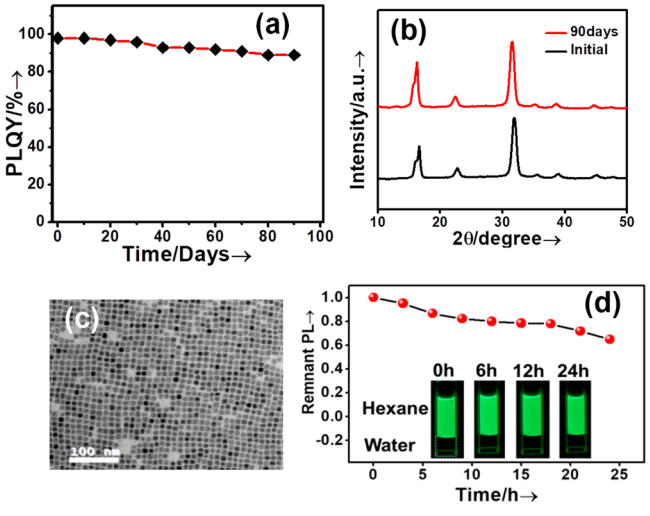

Figure 3. (a) Air stability of $CsPbBr_3$ NCs under storage in ambient atmosphere. (b) PXRD patterns after 90 days. (c) TEM image after 60 days. (d) Photostability of $CsPbBr_3$ NCs under continuous illumination of a 365 nm, 8 W UV lamp in the presence of water. Photographs at different time intervals under UV illumination are shown in the inset.

illumination (Figure S16). The PXRD patterns of **FA**$PbBr_3$ and **MA**$PbBr_3$ recorded after 60 days of storage reveal that the

DOI: 10.1021/acsenergylett.9b02363
ACS Energy Lett. 2020, 5, 64−69

Table 1. Comparison of the Stability and PLQY of $CsPbBr_3$ NCs Obtained by Different Methods

synthesis method	PLQY (%)	air stability	photostability
Zwitterionic ligands as capping agent[18]	90	50 days (90%)	NA
oleylammonium bromide as bromide precursor[29]	97	NA	NA
benzoyl bromide as bromide precursor[30]	92	NA	NA
L-type ligand-assisted synthesis[40]	100	NA	1 h (80%)
NBS as bromide precursor (this work)	99	90 days (90%)	24 h (81% in hexane, 65% in hexane/water mixture)

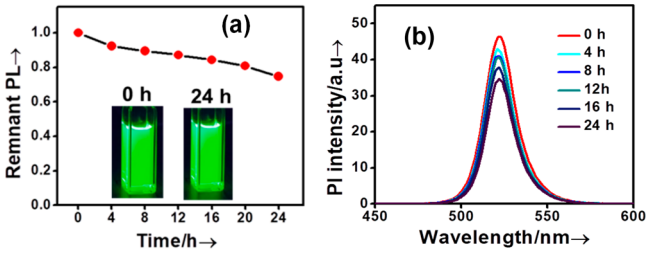

Figure 4. (a) Photostability of $MAPbBr_3$ NCs upon continuous illumination with a 365 nm, 8 W UV lamp. Photographs at different time intervals under UV illumination are shown in the inset. (b) PL emission spectra of $MAPbBr_3$ NCs at different time intervals upon continuous UV light illumination.

cubic crystal structure is retained without formation of a secondary phase (Figure S17). Table S5, which summarizes the PL properties and stability data of a variety of green-emitting perovskite NCs obtained by different approaches, clearly highlights better optical properties and stability of the NCs obtained by our method of synthesis.

The factor(s) contributing to the exceptional stability and optical properties of these $APbBr_3$ NCs can be understood considering that the $CsPbBr_3$ NCs obtained using a Pb:Br precursor ratio of 1:3 exhibit much improved stability and optical properties compared to those prepared using a lower Pb:Br ratio (Figure S18). As the EDX measurements confirm that the former samples are indeed bromide-rich (Cs:Pb:Br = 0.9:1:3.66) (Figures S19 and S20), it is evident that a bromide-rich environment helps provide better stability and PL of the NCs. This observation is consistent with current literature.[20] A second factor also needs to be considered in this context. It is well-known that alkylammonium ions enhance the stability of the $CsPbBr_3$ NCs by replacing the surface Cs^+. It is therefore very likely that oleylammonium bromide formed during our reaction replaces some surface Cs^+, forming an oleylammonium lead bromide-terminated surface, which provides necessary stability to the NCs.[44] To confirm the binding of oleylammonium cation on the surface of the NCs, we measured the NMR and FTIR spectra of the NCs (Figures S21 and S22). The NMR spectrum of MeOAc-washed $CsPbBr_3$ NCs exhibits broad peaks at 6.7 and 3.6 ppm, characteristic of the oleylammonium cation corresponding to an α-proton (NH_3^+) and β-proton (CH_2–N), respectively,[45] confirming the presence of oleylammonium cation on the surface of the NCs. The FTIR spectrum of the $CsPbBr_3$ NCs shows peaks at 1641 and 1540 cm^{-1} (Figure S22) due to the asymmetric and symmetric bending of the N^+–H bond of the oleylammonium cation[46] and reconfirms the binding of oleylammonium cation on the surface of the NCs. Hence, the superb stability and optical properties of our $APbBr_3$ NCs are the outcome of formation of an oleylammonium lead bromide-terminated surface.

In conclusion, a generic method for synthesis of three commonly used green-emitting $APbBr_3$ NCs with narrow size distribution, low PL bandwidth, near-unity PLQY, and remarkable stability under different conditions is reported for the first time employing NBS as the bromide precursor. The exceptional characteristics of these NCs, which are attributed to the formation of oleylammonium lead bromide-terminated surfaces, indicate high potential of these materials in real applications. As preliminary studies indicate applicability of this method to other halide-based perovskites using corresponding *N*-haloimide, the present protocol opens up new avenues for synthesis of a wide variety of perovskite NCs with high PL and stability.

■ ASSOCIATED CONTENT

Supporting Information

The Supporting Information is available free of charge at https://pubs.acs.org/doi/10.1021/acsenergylett.9b02363.

Experimental section, mechanism of the oleylammonium bromide formation, PLQY of different batches of synthesis, TEM images and size distribution, TEM image of $CsPbBr_3$ NCs at different temperatures, PL spectra of NCs obtained at different temperatures, PXRD and TEM images of NCs obtained by using a lower Pb:Br ratio, PL decay profile of $CsPbBr_3$ NCs, $FAPbBr_3$ NCs, air stability, photostability, water stability, EDX spectra of $CsPbBr_3$ NCs, air stability and photostability of $FAPbBr_3$ and $MAPbBr_3$ NCs, NMR spectra and FTIR spectra, decay parameters for different NCs, and comparison of stability and PLQY with other synthesis methods (PDF)

■ AUTHOR INFORMATION

Corresponding Author

*E-mail: anunay@uohyd.ac.in.

ORCID

Anunay Samanta: 0000-0003-1551-0209

Notes

The authors declare no competing financial interest.

■ ACKNOWLEDGMENTS

This work is supported by the J. C. Bose Fellowship (to A.S.) of the Science and Engineering Research Board (SERB), India and the University Grants Commission (UGC) CAS and UPE Programs. The TEM facility of the Centre for Nanotechnology, University of Hyderabad is also acknowledged. S.P thanks UGC for a Fellowship.

■ REFERENCES

(1) Akkerman, Q. A.; Rainò, G.; Kovalenko, M. V.; Manna, L. Genesis, challenges and opportunities for colloidal lead halide perovskite nanocrystals. *Nat. Mater.* **2018**, *17*, 394–405.

(2) Huang, H.; Bodnarchuk, M. I.; Kershaw, S. V.; Kovalenko, M. V.; Rogach, A. L. Lead Halide Perovskite Nanocrystals in the Research Spotlight: Stability and Defect Tolerance. *ACS Energy Lett.* **2017**, *2*, 2071–2083.

DOI: 10.1021/acsenergylett.9b02363
ACS Energy Lett. 2020, 5, 64–69

(3) Zhang, F.; Zhong, H.; Chen, C.; Wu, X.-g.; Hu, X.; Huang, H.; Han, J.; Zou, B.; Dong, Y. Brightly Luminescent and Color-Tunable Colloidal $CH_3NH_3PbX_3$ (X = Br, I, Cl) Quantum Dots: Potential Alternatives for Display Technology. *ACS Nano* **2015**, *9*, 4533−4542.
(4) He, X.; Qiu, Y.; Yang, S. Fully Inorganic Trihalide Perovskite Nanocrystals: A New Research Frontier of Optoelectronic Materials. *Adv. Mater.* **2017**, *29*, 1700775.
(5) Manser, J. S.; Christians, J. A.; Kamat, P. V. Intriguing Optoelectronic Properties of Metal Halide Perovskites. *Chem. Rev.* **2016**, *116*, 12956−13008.
(6) Ono, L. K.; Juarez-Perez, E. J.; Qi, Y. Progress on Perovskite Materials and Solar Cells with Mixed Cations and Halide Anions. *ACS Appl. Mater. Interfaces* **2017**, *9*, 30197−30246.
(7) Kovalenko, M. V.; Protesescu, L.; Bodnarchuk, M. I. Properties and potential optoelectronic applications of lead halide perovskite nanocrystals. *Science* **2017**, *358*, 745−750.
(8) Bai, S.; Yuan, Z.; Gao, F. Colloidal metal halide perovskite nanocrystals: synthesis, characterization, and applications. *J. Mater. Chem. C* **2016**, *4*, 3898−3904.
(9) Adjokatse, S.; Fang, H.-H.; Loi, M. A. Broadly tunable metal halide perovskites for solid-state light-emission applications. *Mater. Today* **2017**, *20*, 413−424.
(10) Zhang, X.; Lin, H.; Huang, H.; Reckmeier, C.; Zhang, Y.; Choy, W. C. H.; Rogach, A. L. Enhancing the Brightness of Cesium Lead Halide Perovskite Nanocrystal Based Green Light-Emitting Devices through the Interface Engineering with Perfluorinated Ionomer. *Nano Lett.* **2016**, *16*, 1415−1420.
(11) Protesescu, L.; Yakunin, S.; Bodnarchuk, M. I.; Krieg, F.; Caputo, R.; Hendon, C. H.; Yang, R. X.; Walsh, A.; Kovalenko, M. V. Nanocrystals of Cesium Lead Halide Perovskites ($CsPbX_3$, X = Cl, Br, and I): Novel Optoelectronic Materials Showing Bright Emission with Wide Color Gamut. *Nano Lett.* **2015**, *15*, 3692−3696.
(12) Shynkarenko, Y.; Bodnarchuk, M. I.; Bernasconi, C.; Berezovska, Y.; Verteletskyi, V.; Ochsenbein, S. T.; Kovalenko, M. V. Direct Synthesis of Quaternary Alkylammonium-Capped Perovskite Nanocrystals for Efficient Blue and Green Light-Emitting Diodes. *ACS Energy Lett.* **2019**, *4*, 2703−2711.
(13) Protesescu, L.; Yakunin, S.; Bodnarchuk, M. I.; Bertolotti, F.; Masciocchi, N.; Guagliardi, A.; Kovalenko, M. V. Monodisperse Formamidinium Lead Bromide Nanocrystals with Bright and Stable Green Photoluminescence. *J. Am. Chem. Soc.* **2016**, *138*, 14202−14205.
(14) Amgar, D.; Aharon, S.; Etgar, L. Inorganic and Hybrid Organo-Metal Perovskite Nanostructures: Synthesis, Properties, and Applications. *Adv. Funct. Mater.* **2016**, *26*, 8576−8593.
(15) Koolyk, M.; Amgar, D.; Aharon, S.; Etgar, L. Kinetics of cesium lead halide perovskite nanoparticle growth; focusing and de-focusing of size distribution. *Nanoscale* **2016**, *8*, 6403−6409.
(16) Vybornyi, O.; Yakunin, S.; Kovalenko, M. V. Polar-solvent-free colloidal synthesis of highly luminescent alkylammonium lead halide perovskite nanocrystals. *Nanoscale* **2016**, *8*, 6278−6283.
(17) Pradhan, N. Tips and Twists in Making High Photoluminescence Quantum Yield Perovskite Nanocrystals. *ACS Energy Lett.* **2019**, *4*, 1634−1638.
(18) Krieg, F.; Ochsenbein, S. T.; Yakunin, S.; ten Brinck, S.; Aellen, P.; Süess, A.; Clerc, B.; Guggisberg, D.; Nazarenko, O.; Shynkarenko, Y.; Kumar, S.; Shih, C.-J.; Infante, I.; Kovalenko, M. V. Colloidal $CsPbX_3$ (X = Cl, Br, I) Nanocrystals 2.0: Zwitterionic Capping Ligands for Improved Durability and Stability. *ACS Energy Lett.* **2018**, *3*, 641−646.
(19) Bodnarchuk, M. I.; Boehme, S. C.; ten Brinck, S.; Bernasconi, C.; Shynkarenko, Y.; Krieg, F.; Widmer, R.; Aeschlimann, B.; Günther, D.; Kovalenko, M. V.; Infante, I. Rationalizing and Controlling the Surface Structure and Electronic Passivation of Cesium Lead Halide Nanocrystals. *ACS Energy Lett.* **2019**, *4*, 63−74.
(20) Woo, J. Y.; Kim, Y.; Bae, J.; Kim, T. G.; Kim, J. W.; Lee, D. C.; Jeong, S. Highly Stable Cesium Lead Halide Perovskite Nanocrystals through in Situ Lead Halide Inorganic Passivation. *Chem. Mater.* **2017**, *29*, 7088−7092.
(21) Nenon, D. P.; Pressler, K.; Kang, J.; Koscher, B. A.; Olshansky, J. H.; Osowiecki, W. T.; Koc, M. A.; Wang, L.-W.; Alivisatos, A. P. Design Principles for Trap-Free $CsPbX_3$ Nanocrystals: Enumerating and Eliminating Surface Halide Vacancies with Softer Lewis Bases. *J. Am. Chem. Soc.* **2018**, *140*, 17760−17772.
(22) Liu, P.; Chen, W.; Wang, W.; Xu, B.; Wu, D.; Hao, J.; Cao, W.; Fang, F.; Li, Y.; Zeng, Y.; Pan, R.; Chen, S.; Cao, W.; Sun, X. W.; Wang, K. Halide-Rich Synthesized Cesium Lead Bromide Perovskite Nanocrystals for Light-Emitting Diodes with Improved Performance. *Chem. Mater.* **2017**, *29*, 5168−5173.
(23) Di Stasio, F.; Christodoulou, S.; Huo, N.; Konstantatos, G. Near-Unity Photoluminescence Quantum Yield in $CsPbBr_3$ Nanocrystal Solid-State Films via Postsynthesis Treatment with Lead Bromide. *Chem. Mater.* **2017**, *29*, 7663−7667.
(24) Bohn, B. J.; Tong, Y.; Gramlich, M.; Lai, M. L.; Döblinger, M.; Wang, K.; Hoye, R. L. Z.; Müller-Buschbaum, P.; Stranks, S. D.; Urban, A. S.; Polavarapu, L.; Feldmann, J. Boosting Tunable Blue Luminescence of Halide Perovskite Nanoplatelets through Postsynthetic Surface Trap Repair. *Nano Lett.* **2018**, *18*, 5231−5238.
(25) Li, F.; Liu, Y.; Wang, H.; Zhan, Q.; Liu, Q.; Xia, Z. Postsynthetic Surface Trap Removal of $CsPbX_3$ (X = Cl, Br, or I) Quantum Dots via a ZnX_2/Hexane Solution toward an Enhanced Luminescence Quantum Yield. *Chem. Mater.* **2018**, *30*, 8546−8554.
(26) Zheng, X.; Hou, Y.; Sun, H.-T.; Mohammed, O. F.; Sargent, E. H.; Bakr, O. M. Reducing Defects in Halide Perovskite Nanocrystals for Light Emitting Applications. *J. Phys. Chem. Lett.* **2019**, *10*, 2629−2640.
(27) Seth, S.; Ahmed, T.; De, A.; Samanta, A. Tackling the Defects, Stability, and Photoluminescence of $CsPbX_3$ Perovskite Nanocrystals. *ACS Energy Lett.* **2019**, *4*, 1610−1618.
(28) Ahmed, T.; Seth, S.; Samanta, A. Boosting the Photoluminescence of $CsPbX_3$ (X = Cl, Br, I) Perovskite Nanocrystals Covering a Wide Wavelength Range by Postsynthetic Treatment with Tetrafluoroborate Salts. *Chem. Mater.* **2018**, *30*, 3633−3637.
(29) Dutta, A.; Behera, R. K.; Pal, P.; Baitalik, S.; Pradhan, N. Near-Unity Photoluminescence Quantum Efficiency for All $CsPbX_3$(X = Cl, Br, and I) Perovskite Nanocrystals: A Generic Synthesis Approach. *Angew. Chem., Int. Ed.* **2019**, *58*, 5552−5556.
(30) Imran, M.; Caligiuri, V.; Wang, M.; Goldoni, L.; Prato, M.; Krahne, R.; De Trizio, L.; Manna, L. Benzoyl Halides as Alternative Precursors for the Colloidal Synthesis of Lead-Based Halide Perovskite Nanocrystals. *J. Am. Chem. Soc.* **2018**, *140*, 2656−2664.
(31) Saikia, N.; Borah, A. J.; Phukan, P. Use of Bromine and Bromo-Organic Compounds in Organic Synthesis. *Chem. Rev.* **2016**, *116*, 6837−7042.
(32) Xue, H.; Tan, H.; Wei, D.; Wei, Y.; Lin, S.; Liang, F.; Zhao, B. N-Bromosuccinimide−carboxylic acid combination: mild and efficient access to dibromination of unsaturated carbonyl compounds. *RSC Adv.* **2013**, *3*, 5382−5385.
(33) Zhumekenov, A. A.; Saidaminov, M. I.; Haque, M. A.; Alarousu, E.; Sarmah, S. P.; Murali, B.; Dursun, I.; Miao, X.-H.; Abdelhady, A. L.; Wu, T.; Mohammed, O. F.; Bakr, O. M. Formamidinium Lead Halide Perovskite Crystals with Unprecedented Long Carrier Dynamics and Diffusion Length. *ACS Energy Lett.* **2016**, *1*, 32−37.
(34) Mondal, N.; De, A.; Das, S.; Paul, S.; Samanta, A. Ultrafast carrier dynamics of metal halide perovskite nanocrystals and perovskite composites. *Nanoscale* **2019**, *11*, 9796−9818.
(35) Mondal, N.; Samanta, A. Complete ultrafast charge carrier dynamics in photo-excited all-inorganic perovskite nanocrystals ($CsPbX_3$). *Nanoscale* **2017**, *9*, 1878−1885.
(36) Liu, L.; Deng, L.; Huang, S.; Zhang, P.; Linnros, J.; Zhong, H.; Sychugov, I. Photodegradation of Organometal Hybrid Perovskite Nanocrystals: Clarifying the Role of Oxygen by Single-Dot Photoluminescence. *J. Phys. Chem. Lett.* **2019**, *10*, 864−869.
(37) Sun, C.; Zhang, Y.; Ruan, C.; Yin, C.; Wang, X.; Wang, Y.; Yu, W. W. Efficient and Stable White LEDs with Silica-Coated Inorganic Perovskite Quantum Dots. *Adv. Mater.* **2016**, *28*, 10088−10094.
(38) Wang, H.-C.; Lin, S.-Y.; Tang, A.-C.; Singh, B. P.; Tong, H.-C.; Chen, C.-Y.; Lee, Y.-C.; Tsai, T.-L.; Liu, R.-S. Mesoporous Silica

DOI: 10.1021/acsenergylett.9b02363
ACS Energy Lett. 2020, 5, 64−69

Particles Integrated with All-Inorganic $CsPbBr_3$ Perovskite Quantum-Dot Nanocomposites (MP-PQDs) with High Stability and Wide Color Gamut Used for Backlight Display. *Angew. Chem., Int. Ed.* **2016**, *55*, 7924−7929.
(39) van der Stam, W.; Geuchies, J. J.; Altantzis, T.; van den Bos, K. H. W.; Meeldijk, J. D.; Van Aert, S.; Bals, S.; Vanmaekelbergh, D.; de Mello Donega, C. Highly Emissive Divalent-Ion-Doped Colloidal $CsPb_{1-x}M_xBr_3$ Perovskite Nanocrystals through Cation Exchange. *J. Am. Chem. Soc.* **2017**, *139*, 4087−4097.
(40) Zhong, Q.; Cao, M.; Xu, Y.; Li, P.; Zhang, Y.; Hu, H.; Yang, D.; Xu, Y.; Wang, L.; Li, Y.; Zhang, X.; Zhang, Q. L-Type Ligand-Assisted Acid-Free Synthesis of $CsPbBr_3$ Nanocrystals with Near-Unity Photoluminescence Quantum Yield and High Stability. *Nano Lett.* **2019**, *19*, 4151−4157.
(41) Almeida, G.; Ashton, O. J.; Goldoni, L.; Maggioni, D.; Petralanda, U.; Mishra, N.; Akkerman, Q. A.; Infante, I.; Snaith, H. J.; Manna, L. The Phosphine Oxide Route toward Lead Halide Perovskite Nanocrystals. *J. Am. Chem. Soc.* **2018**, *140*, 14878−14886.
(42) Imran, M.; Ijaz, P.; Baranov, D.; Goldoni, L.; Petralanda, U.; Akkerman, Q.; Abdelhady, A. L.; Prato, M.; Bianchini, P.; Infante, I.; Manna, L. Shape-Pure, Nearly Monodispersed $CsPbBr_3$ Nanocubes Prepared Using Secondary Aliphatic Amines. *Nano Lett.* **2018**, *18*, 7822−7831.
(43) Mondal, N.; De, A.; Samanta, A. Achieving Near-Unity Photoluminescence Efficiency for Blue-Violet-Emitting Perovskite Nanocrystals. *ACS Energy Lett.* **2019**, *4*, 32−39.
(44) Ravi, V. K.; Santra, P. K.; Joshi, N.; Chugh, J.; Singh, S. K.; Rensmo, H.; Ghosh, P.; Nag, A. Origin of the Substitution Mechanism for the Binding of Organic Ligands on the Surface of $CsPbBr_3$ Perovskite Nanocubes. *J. Phys. Chem. Lett.* **2017**, *8*, 4988−4994.
(45) De Roo, J.; Ibanez, M.; Geiregat, P.; Nedelcu, G.; Walravens, W.; Maes, J.; Martins, J. C.; Van Driessche, I.; Kovalenko, M. V.; Hens, Z. Highly Dynamic Ligand Binding and Light Absorption Coefficient of Cesium Lead Bromide Perovskite Nanocrystals. *ACS Nano* **2016**, *10*, 2071−2081.
(46) Dutta, A.; Dutta, S. K.; Das Adhikari, S.; Pradhan, N. Phase-Stable $CsPbI_3$ Nanocrystals: The Reaction Temperature Matters. *Angew. Chem., Int. Ed.* **2018**, *57*, 9083−9087.

DOI: 10.1021/acsenergylett.9b02363
ACS Energy Lett. 2020, 5, 64−69

THE JOURNAL OF PHYSICAL CHEMISTRY C
A JOURNAL OF THE AMERICAN CHEMICAL SOCIETY

pubs.acs.org/JPCC

Article

Effect of Lead:Halide Precursor Ratio on the Photoluminescence and Carrier Dynamics of Violet- and Blue-Emitting Lead Halide Perovskite Nanocrystals

Published as part of The Journal of Physical Chemistry virtual special issue "Kankan Bhattacharyya Festschrift".

Sumanta Paul, Tasnim Ahmed, Somnath Das, and Anunay Samanta*

Cite This: *J. Phys. Chem. C* 2021, 125, 23539–23547

Read Online

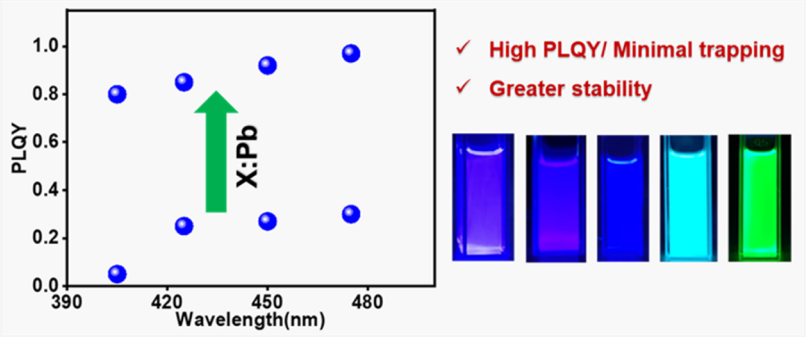

ABSTRACT: Highly luminescent cesium lead halide ($CsPbX_3$, X = Cl, Br, I) perovskite nanocrystals (NCs) are promising materials for a number of optoelectronic applications like LEDs and other display technologies. However, low photoluminescence (PL) quantum yield (QY) of the large-bandgap violet- and blue-emitting $CsPbCl_3$ and $CsPb(Cl/Br)_3$ NCs is an obstacle to the development of blue- and white-emitting LEDs. In this work, we show that these NCs with high PLQY can be obtained directly by employing an appropriate halide precursor and by optimizing the Pb:X precursor ratio. Specifically, employing *N*-chloro- and *N*-bromophthalimides as halide precursors and varying the Pb:X precursor ratio, we have obtained stable and highly luminescent (PLQY 80−99%) perovskite NCs emitting in the blue-violet region extending to green by direct synthesis. Time-resolved PL and ultrafast pump−probe studies of these systems reveal the effect of Pb:X precursor ratio on the carrier recombination processes. Rapid carrier trapping is found to be the dominant process that impairs the PLQY of the NCs obtained by using a stoichiometric (1:3) Pb:X precursor ratio. This trapping of carriers is effectively alleviated by using an excess amount of the halide precursor during the preparation of the NCs. The results brighten the potential utility of these high-quality perovskite NCs emitting in the blue-violet region in optical applications.

INTRODUCTION

Because of their great potential in diverse applications like in photovoltaics, LEDs, display technologies, lasing, and so on, the cesium lead halide ($CsPbX_3$, X = Cl, Br, I) perovskite NCs continue to receive great attention of the researchers.[1−13] High PLQY and ease of tunability of the PL band position across the entire visible region make these substances quite attractive for optoelectronic applications.[8−11,14,15] In this family of perovskites, $CsPbCl_3$ and $CsPb(Cl/Br)_3$ NCs are considered indispensable due to their violet and blue emission, which are essential color components for fabrication of white LEDs.[16−20] Unlike the conventional metal chalcogenide semiconductor NCs, the halide perovskites generally exhibit high PLQY due to their defect-tolerant nature.[5,21−23] However, compared to their green- and red-emitting counterparts, $CsPbBr_3$ and $CsPbI_3$, the large-bandgap perovskites such as violet- and blue-emitting $CsPbCl_3$ and $CsPb(Cl/Br)_3$ NCs most often exhibit much lower PLQY due to competing nonradiative recombination of the photogenerated charge carriers through the deep trap states generated by halide vacancies and distorted $[PbX_6]^{4-}$ octahedral units.[9,22,24−26] Since the first synthesis of these NCs by the hot-injection (HI) method,[9] several methodologies have been developed for the preparation of violet- and blue-emitting $CsPCl_3$ and $CsPb(Cl/Br)_3$ NCs with higher PLQY.[17,22,27−36] Doping with different

Received: September 1, 2021
Revised: October 2, 2021
Published: October 19, 2021

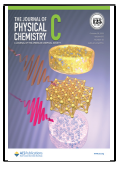

https://doi.org/10.1021/acs.jpcc.1c07740
J. Phys. Chem. C 2021, 125, 23539−23547

bivalent metal ions[16,18,19,28,29,31,33,37,38] and a variety of postsynthetic treatments of the as-synthesized NCs[17,24,32,35,36,39,40] are the most common practices for improving the PLQY of these NCs. Considering that, in the first synthesis of the $CsPbX_3$ NCs[9] PbX_2 was used as precursor for both lead and halogen, which gave a X:Pb molar precursor ratio of only 2 in the reaction system (less than the required value of 3), Manna and co-workers used a separate precursor for each constituent and succeeded in obtaining highly luminescent perovskite NCs in direct synthesis.[30] They could obtain $CsPbCl_3$ NCs with a PLQY of 65% using benzoyl chloride as the chloride precursor.[30] Pradhan and co-workers recently prepared $CsPbCl_3$ NCs with a very high PLQY (~97%) using oleylammonium chloride as the chloride source.[34] However, the blue-emitting $CsPb(Cl/Br)_3$ NCs were not reported.[34]

As halide precursor is an important element in direct synthesis of the NCs, many recent studies are directed toward finding the right candidate for this purpose. Recently, we found *N*-bromosuccinimide (NBS) as an excellent bromide precursor using which highly luminescent green-emitting $CsPbBr_3$ NCs could be obtained in direct synthesis.[41] This success prompted us to explore the efficacy of structurally related other haloimides for the preparation of quality violet- and blue-emitting NCs, which can perhaps be used in optoelectronic applications. These studies led to the identification of two phthalimide derivatives, *N*-chlorophthalimide (NCP) and *N*-bromophthalimide (NBP), as halide precursors, for obtaining high quality NCs emitting in the blue-violet region, extending even to the green region. As halide vacancies led to the formation of the mid-bandgap states, which facilitate non-radiative recombination of the photogenerated carriers and decrease the PLQY of the NCs, the PL properties of these systems are also expected to depend on the Pb:X precursor ratio during the reaction. For this reason, we have prepared different samples of each system by varying the Pb:X precursor ratios, determined the optimized conditions for obtaining these systems with high PL efficiency, and examined the influence of the Pb:X ratio on carrier recombination processes by time-resolved PL and pump−probe studies.

EXPERIMENTAL SECTION

Materials. Cesium carbonate (99%), lead oxide (99%), *N*-bromophthalimide (NBP, 95%), *N*-chlorophthalimide (NCP, 96%), oleylamine (OLA, technical grade (70%)), oleic acid (OA, technical grade (90%)), methyl acetate (MeOAc, 99.5%, anhydrous), and 1-octadecene (ODE, technical grade (90%)) were purchased from Sigma-Aldrich, USA. All solvents were purchased from Sigma-Aldrich, USA. All chemicals were used without further purification.

Preparation of $CsPbX_3$ NCs. The $CsPbX_3$ NCs were prepared in two steps. The first step involved preparation of cesium oleate, and in the second step the NCs were prepared. Cesium oleate was prepared by the high-temperature reaction between Cs_2CO_3 and oleic acid.[9] In a typical synthesis, 0.6 mmol (195.4 mg) of Cs_2CO_3 was loaded in a two-neck 50 mL round-bottom flask along with 9 mL of ODE and 1.5 mL of OA. The reaction mixture was kept in a vacuum at 140 °C for 30 min, and then it was transferred in a N_2 atmosphere for another 30 min until it became clear. The clear solution of cesium oleate was then stored in a reaction vial. As cesium oleate precipitates out at room temperature, it was preheated to 100 °C before use.

$CsPbCl_3$ NCs were obtained by a three-precursor hot injection method. 0.2 mmol of PbO and 0.6, 1.2, and 1.8 mmol of NCP as chloride precursor for the synthesis of $CsPbCl_3$(1:3), $CsPbCl_3$(1:6), and $CsPbCl_3$(1:9) NCs, respectively, were loaded into a two-neck 50 mL round-bottom flask along with 5 mL of ODE, 2 mL of OA, and 2 mL of OLAM. After complete solubilization of the reaction mixture at 140 °C, the temperature was increased to 200−220 °C in a N_2 atmosphere, and 0.6 mL of preheated cesium oleate solution was swiftly injected into the reaction mixture. After 60 s the reaction system was rapidly cooled in an ice−water bath.

Mixed halide NCs ($CsPbCl_2Br$, $CsPbCl_{1.5}Br_{1.5}$, and $CsPbClBr_2$) were prepared following a similar procedure employing NCP as the chloride source and NBP as the bromide source. Two batches of the NCs were synthesized by using Pb:X molar ratios of 1:3 and 1:6. Chloride to bromide precursor ratios used for the synthesis of $CsPbCl_2Br$, $CsPbCl_{1.5}Br_{1.5}$, and $CsPbClBr_2$ NCs were 2:1, 1:1, and 1:2, respectively. The exact amount of precursor used for the synthesis of different systems is given in Table S1. $CsPbBr_3$ NCs were obtained by following procedure used for $CsPbCl_3$ by maintaining the 1:3 Pb:Br precursor ratio.

Purification. The crude NCs were centrifuged at 7000 rpm for 6 min. After centrifugation, the supernatant liquid was discarded, and the precipitate was dispersed in hexane. After 30 min, the solution containing the NCs was again centrifuged at 12000 rpm for 10 min. The precipitate was discarded, and the supernatant solution containing the NCs was harvested. The solution of the NCs was dried in a high vacuum and dispersed again in hexane. After 10 min, the dispersed solution was again centrifuged for 3 min at 3000 rpm and the precipitate was discarded, and supernatant NCs solution was used for future studies.

Powder X-ray Diffraction Measurement (PXRD). PXRD patterns were measured in an X-ray diffractometer (Bruker AXS D8) using Cu Kα X-ray radiation (λ = 1.5406 Å). The thin film samples were prepared by drop-casting a concentrated solution of the NCs onto a thin quartz glass plate.

Transmission Electron Microscopy (TEM). The size and shape of the NCs were measured by using a transmission electron microscope (Tecnai G2 FE1 F12) operating at an accelerating voltage of 200 kV. Samples were prepared by drop-casting a dilute NCs solution on a carbon-coated copper grid, which was kept in a vacuum before use.

Energy Dispersive X-ray Spectroscopy. Energy dispersive X-ray spectra were recorded by an Oxford Instruments X-Max^N SDD (50 mm^2) system and INCA analysis software. Samples were prepared by drop-casting the NCs solution on microscope coverslips.

Steady State Optical Measurements. UV−vis absorption and photoluminescence (PL) measurements were performed by using a spectrophotometer (JASCO, V-7500) and a spectrofluorometer (Horiba Jobin Yvon, FluoroLog-3), respectively. PL measurements were performed by using very dilute colloidal solution (optical density at 350 nm <0.1 in a 1 cm path length cuvette) of the NCs.

Time-Resolved PL Measurements. Photoluminescence decay was measured by a time-correlated single photon counting instrument (Horiba Jobin Yvon IBH). A diode laser (λ_{exc} = 376 nm) and an MCP photomultiplier (Hamamatsu R3809U-50) were used as the excitation source and detector, respectively. The instrument response function, which was mainly limited by the pulse width of exciting laser

https://doi.org/10.1021/acs.jpcc.1c07740
J. Phys. Chem. C 2021, 125, 23539−23547

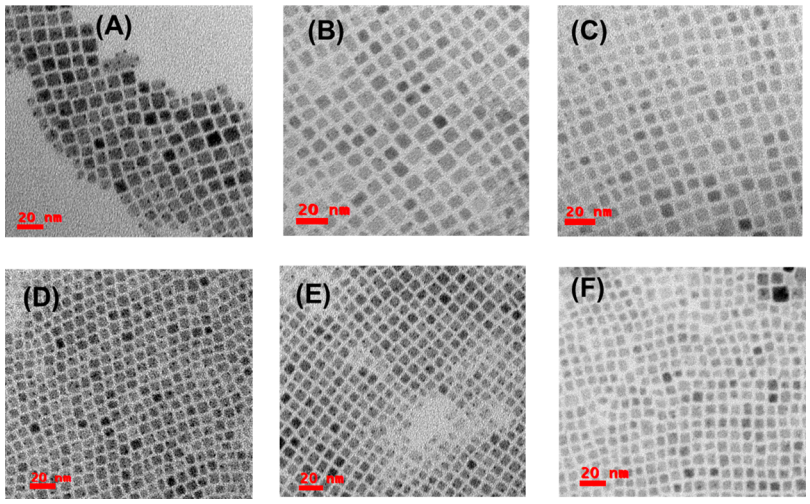

Figure 1. TEM images of the (A) $CsPbCl_3$(1:3), (B) $CsPbCl_3$(1:6), (C) $CsPbCl_3$(1:9), (D) $CsPbCl_2Br$(1:6), (E) $CsPbCl_{1.5}Br_{1.5}$(1:6), and (F) $CsPbClBr_2$(1:6) NCs. The scale bar is 20 nm in all cases.

pulse, was 54 ps, measured by recording the excitation profile by placing a scatterer solution (Ludox in water) in place of the sample. Decay profiles were analyzed by nonlinear least-squares iteration procedure using IBH DAS6 (ver. 2.2) decay analysis software. The photoluminescence decay curves were fitted to the following equation

$$I(t) = \sum_{i=1}^{n} \alpha_i \exp(-t/\tau_i)$$

where α_i and τ_i are amplitude and lifetime of the ith component, respectively. The fractional contribution of the ith component to the total steady state intensity was estimated via the equation

$$a_i = \frac{\alpha_i \tau_i}{\sum_{i=1}^{n} \alpha_i \tau_i}$$

and the average fluorescence lifetimes were enumerated by using the equation

$$\tau_{av} = \sum_{i=1}^{n} a_i \tau_i$$

Ultrafast Transient Absorption (TA) Measurement. TA measurements were performed in a setup consisting of femtosecond laser sources from a Spectra-Physics, USA, and a spectrometer from CDP Systems, Russia. The seed laser output from MaiTai (800 nm, <100 fs, 80 MHz) was directed into a Ti:sapphire regenerative amplifier, which was pumped by the second harmonic (532 nm) of an Nd:YLF laser. A portion of the amplified output (800 nm, <120 fs, 1 kHz) was passed through an optical parametric amplifier to generate the pump wavelength (350 nm) for the excitation of the NCs. The remaining portion of the output was passed through a variable optical delay line of 4 ns and then directed to a rotating CaF_2 crystal to generate the probe white light. The probe beam was divided into two parts to use as signal and reference beams. The pump and signal beams were focused onto a rotating sample cell. The transmitted signal and reference beams were received by a multichannel photodiode array through a polychromator and further processed to record difference in absorbance (ΔA) as a function of wavelength and pump−probe delay. All TA spectra were chirp-corrected, and the instrumental resolution was ∼100 fs.

Estimation of Photoluminescence Quantum Yield (PLQY). The PLQY of the NCs was measured by using the equation

$$QY_S = QY_R(I_S/I_R)(OD_R/OD_S)(n_S^2/n_R^2)$$

where I stands for the area under the emission spectrum, OD for optical density, and n for the refractive index of the medium. The subscript S and R represent the sample and reference system, respectively. 9,10-Diphenylanthracene was used as reference (ϕ_f = 0.95 in hexane) for measurement of PLQY.[42]

RESULTS AND DISCUSSION

We prepared three different samples of violet-emitting $CsPbCl_3$ NCs using molar Pb:Cl precursor ratios of 1:3, 1:6, and 1:9. For the blue (420−480 nm) region, we prepared mixed halide NCs, $CsPbCl_2Br$, $CsPbCl_{1.5}Br_{1.5}$, and $CsPbClBr_2$, and for each system two different samples were prepared by using Pb:X (Cl and Br) molar precursor ratios of 1:3 and 1:6. For each sample, the molar Pb:X precursor ratio is indicated in the parentheses after the formula of the system. We also prepared green-emitting $CsPbBr_3$ NCs using the stoichiometric Pb:Br ratio of 1:3 for comparative purposes. Bright-field TEM images (Figure 1 and Figure S1) indicate a cubic shape of the NCs obtained under optimized conditions. The average edge lengths of the $CsPbCl_3$(1:3), $CsPbCl_3$(1:6), and $CsPbCl_3$(1:9) NCs are found to be 10 ± 2.0, 9.0 ± 2.0, and 8.0 ± 1.0 nm, respectively (Figure 1A−C and Figure S2). A decrease in size and improved monodispersity of the NCs with increase in the amount of the chloride precursor (NCP) are similar to the trend observed for $CsPbBr_3$ NCs.[43] The $CsPbCl_2Br$(1:6), $CsPbCl_{1.5}Br_{1.5}$(1:6), and $CsPbClBr_2$(1:6) NCs obtained under the optimized condition show average size of 9.0 ± 1.5, 8.5 ± 1.0, and 8.0 ± 1.5 nm, respectively (Figure 1D−F and Figure S2). For these systems also a decrease in average size (by 1.5−2.5 nm) and a narrower size distribution are observed for the 1:6 Pb:X precursor ratio. Powder X-ray diffraction (PXRD) patterns suggest an orthorhombic crystal structure of the NCs (Figure S3) with no evidence of any secondary phases. For higher bromide

https://doi.org/10.1021/acs.jpcc.1c07740
J. Phys. Chem. C 2021, 125, 23539−23547

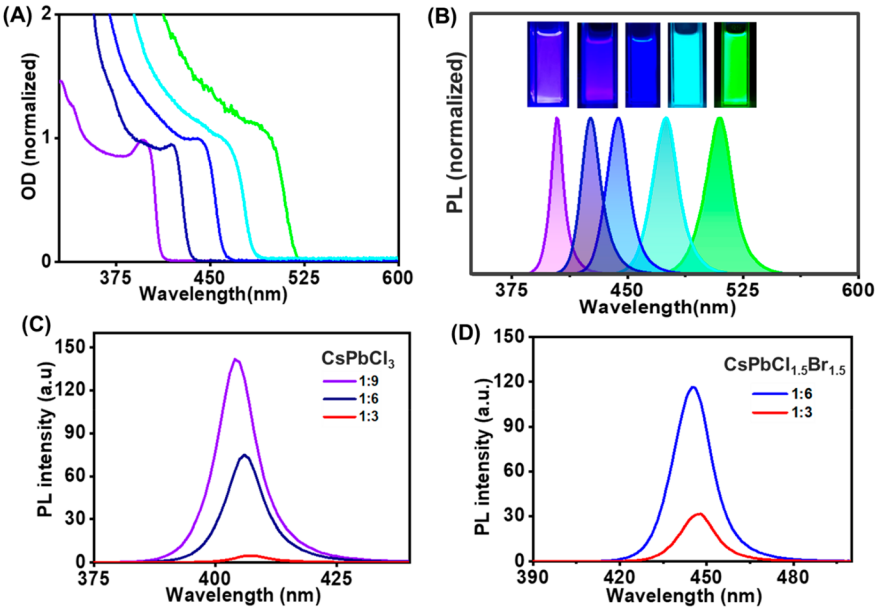

Figure 2. Normalized absorption (A) and (B) PL spectra (λ_{ex} = 350 nm) of dilute colloidal solutions of $CsPbCl_3$(1:9), $CsPbCl_2Br$(1:6), $CsPbCl_{1.5}Br_{1.5}$(1:6), $CsPbClBr_2$(1:6), and $CsPbBr_3$ NCs in hexane. Panel B also shows digital photographs of the colloidal solutions of the $CsPbCl_3$(1:9), $CsPbCl_2Br$(1:6), $CsPbCl_{1.5}Br_{1.5}$(1:6), $CsPbClBr_2$(1:6), and $CsPbBr_3$ nanocrystals under illuminations (365 nm). Panels C and D show the dependence of PL spectra of $CsPbCl_3$ and $CsPbCl_{1.5}Br_{1.5}$ NCs, respectively, on the Pb:X (Cl and Br) precursor ratio.

content, the PXRD peaks shift toward lower angle, indicating lattice expansion due to larger ionic radii of Br^- compared to Cl^-.

The UV−vis absorption and fluorescence spectra of some representative samples are shown in Figures 2A and 2B, respectively. A summary of the spectral data and PLQY values of all samples (including $CsPbBr_3$ NCs) are collected in Table 1. The PL of the $CsPbCl_3$ NCs is characterized by a peak

Table 1. PL Parameters of Different Samples of the $CsPbCl_3$, $CsPb(Cl/Br)_3$, and $CsPbBr_3$ NCs

system	Pb:X precursor ratio	PLQY (%)	λ_{max} (nm)	FWHM (nm)
$CsPbCl_3$	1:3	5	407	12
	1:6	40	406	10
	1:9	80	404	9
$CsPbCl_2Br$	1:3	25	426	15
	1:6	85	428	14
$CsPbCl_{1.5}Br_{1.5}$	1:3	27	447	17
	1:6	92	447	15
$CsPbClBr_2$	1:3	30	474	18
	1:6	97	475	17
$CsPbBr_3$	1:3	99	510	20

between 404 and 407 nm and a narrow full width at half-maximum (FWHM) of 9−12 nm. With increasing Cl:Pb molar precursor ratio a small (2−3 nm) blue-shift of the PL maximum and a slight (by 2−3 nm) decrease in FWHM are observed (Figure 2C). For the mixed halide perovskite NCs, $CsPbCl_2Br$, $CsPbCl_{1.5}Br_{1.5}$, and $CsPbClBr_2$, the PL maxima appear at 430 ± 5, 451 ± 6, and 473 ± 5 nm with a FWHM of 14−15, 15−17, and 17−18 nm, respectively (Figure 2B). For these systems, no noticeable change in PL peak position and spectral bandwidth is observed with change in the Pb:X precursor ratio. Though the spectral features of the systems show small/negligible dependence on the Pb:X precursor ratio, the PLQY values change drastically depending on this ratio. As can be seen from Table 1, the PLQY changes from 5 to 80% for $CsPbCl_3$, 25 to 85% for $CsPbCl_2Br$, 27 to 92% for $CsPbCl_{1.5}Br_{1.5}$, and 30 to 97% for $CsPbClBr_2$ NCs (Figure 2C,D and Figure S4).

An important point to note here is that $CsPbBr_3$ NCs with near-unity (~99%) PLQY is obtained by using a stoichiometric Pb:Br precursor ratio; however, for all other systems, an excess amount of halide precursor is necessary for obtaining the most luminescent sample. For the mixed halide systems, $CsPbCl_2Br$, $CsPbCl_{1.5}Br_{1.5}$, and $CsPbClBr_2$ NCs, the most luminescent system is obtained for a Pb:X precursor ratio of 1:6; however, for $CsPbCl_3$ NCs, a 1:9 Pb:Cl ratio yielded the most luminous sample (PLQY of 80%). To determine the cause of the significant dependence of PLQY on the Pb:X precursor ratio, we have determined the Pb:X ratio in the prepared samples by energy dispersive X-ray (EDX) measurements. These measurements reveal that actual Pb:Cl ratios in $CsPbCl_3$(1:3), $CsPbCl_3$(1:6), and $CsPbCl_3$(1:9) NCs are 1:2.90, 1:3.24, and 1:3.45, respectively (Figure S5 and Table S2). The actual ratios in the prepared mixed halide perovskite NCs were also determined (Figure S5 and Table S2). The Pb:X ratios in $CsPbCl_{1.5}Br_{1.5}$ NCs synthesized by using 1:3 and 1:6 Pb:X precursor ratios are found to be 1:2.98 and 1:3.53, respectively. Interestingly, the EDX data of $CsPbBr_3$ NCs prepared by stoichiometric Pb:Br precursor ratio indicated a halide-rich surface with an actual Pb:Br ratio of 1:3.36 (Table S2). A much higher X:Pb precursor ratio required for obtaining most photoluminescent sample of $CsPbCl_3$ is a reflection of greater halide vacancy in these NCs, as indicated by the EDX data (Table S2).

To understand the influence of Pb:X ratio on carrier recombination processes of the NCs, we have studied the PL decay behavior and transient absorption (TA) spectra of these systems. Except for the $CsPbBr_3$ NCs, PL decay profiles of all the samples (Figure 3) are found to be triexponential. The PL

https://doi.org/10.1021/acs.jpcc.1c07740
J. Phys. Chem. C 2021, 125, 23539−23547

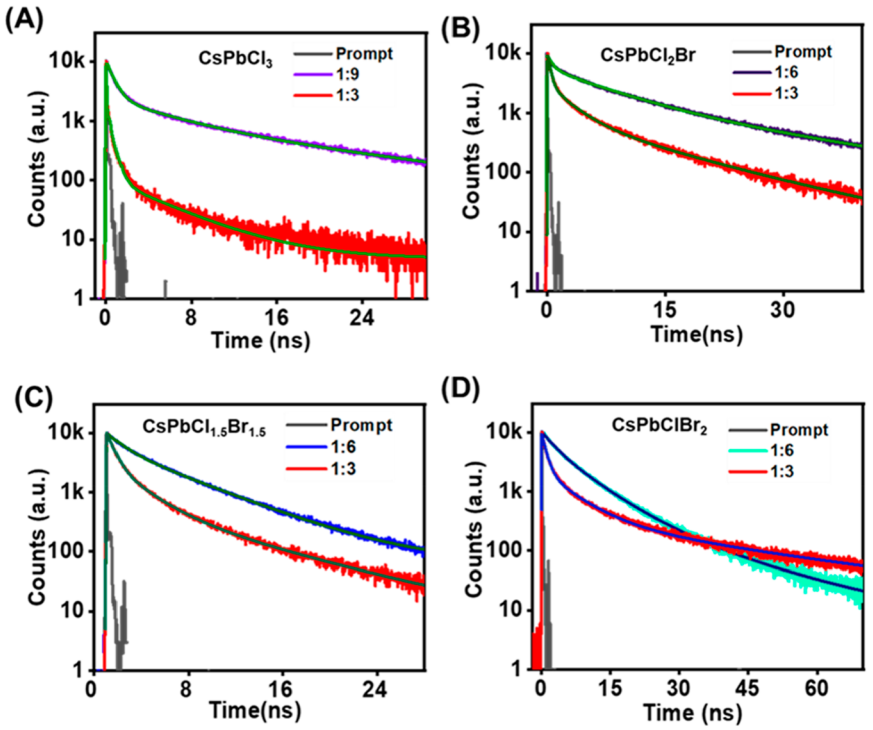

Figure 3. Dependence of the PL decay profile of the (A) $CsPbCl_3$, (B) $CsPbCl_2Br$, (C) $CsPbCl_{1.5}Br_{1.5}$, and (D) $CsPbClBr_2$ NCs on the Pb:X precursor ratio.

Table 2. PL Decay Parameters of Different Samples of $CsPbCl_3$, $CsPb(Cl/Br)_3$, and $CsPbBr_3$ NCs

system	τ_1/ns (a_1)	τ_2/ns (a_2)	τ_3/ns (a_3)	$\langle\tau_{ins}\rangle$/ns	k_{nr}[a] ($\times 10^8$ s^{-1})
$CsPbCl_3$(1:3)	0.07 (0.52)	0.49 (0.28)	5.28 (0.20)	1.23	7.77
$CsPbCl_3$(1:6)	0.60 (0.36)	2.97 (0.32)	11.90 (0.32)	4.97	1.20
$CsPbCl_3$(1:9)	0.70 (0.20)	5.50 (0.34)	21.60 (0.46)	11.95	0.16
$CsPbCl_2Br$(1:3)	0.40 (0.16)	2.86 (0.33)	11.88 (0.51)	7.06	1.06
$CsPbCl_2Br$(1:6)	0.60 (0.04)	7.60 (0.48)	22.08 (0.48)	14.27	0.105
$CsPbCl_{1.5}Br_{1.5}$(1:3)	0.62 (0.30)	2.40 (0.40)	8.17 (0.30)	3.60	2.03
$CsPbCl_{1.5}Br_{1.5}$(1:6)	1.1 (0.07)	4.64 (0.68)	12.50 (0.25)	6.36	0.12
$CsPbClBr_2$(1:3)	0.92 (0.37)	6.22 (0.26)	32.00 (0.37)	13.80	0.51
$CsPbClBr_2$(1:6)	2.48 (0.2)	6.78 (0.53)	35.40 (0.27)	13.64	0.022
$CsPbBr_3$	2.70 (0.51)	9.73 (0.49)		6.13	0.016

[a] $k_{nr} = (1 - PLQY)/\langle\tau_{ins}\rangle$.

decay parameters of the samples are collected in Table 2. As can be seen, for $CsPbCl_3$(1:3) NCs, the PL decay consists of two short components, 70 (0.52) and 490 ps (0.28), which are much faster than the radiative lifetime of $CsPbCl_3$ NCs[9,16,19] and hence can be attributed to the trap state mediated recombination processes. The long 5.28 ns component with 20% contribution clearly represents the direct excitonic recombination process. The $CsPbCl_3$(1:6) and $CsPbCl_3$(1:9) NCs are characterized by a short PL decay component (0.6−0.7 ns), a long component (11.90−21.60 ns), and a third component with lifetime of 2.97−5.50 ns. The short component is assigned to trap state mediated recombination,[9,16,19] the intermediate component (2.97−5.50 ns) to direct excitonic recombination from the band-edge, and the long component (11.90−21.60 ns) to band-edge recombination after trapping and detrapping of the carriers.[19,44] The contribution of the trapping component decreases from 36% in $CsPbCl_3$(1:6) to 20% in $CsPbCl_3$(1:9). Unlike in $CsPbCl_3$(1:3) NCs, no trapping component with time constant of <100 ps could be observed for the $CsPbCl_2Br$(1:3), $CsPbCl_{1.5}Br_{1.5}$(1:3), and $CsPbClBr_2$(1:3) NCs; however, a subnanosecond trapping component with a time constant between 0.40 and 0.92 ns can be found. For samples prepared using a higher amount of halide precursor, for example, for $CsPbCl_2Br$(1:6) and $CsPbCl_{1.5}Br_{1.5}$(1:6) NCs, the contribution of the trapping component is significantly lower (<10%), and for the $CsPbClBr_2$(1:6) NCs, no <1 ns lifetime component could be observed. The contribution of the direct excitonic recombination component (2.4−7.6 ns) increases significantly with increase in X:Pb precursor ratio from 3:1 to 6:1 for these mixed halide NCs. The nonradiative rate constant (k_{nr}), estimated from the measured PLQY and average PL lifetime (Table 2), is found to decrease from 7.77×10^8 s^{-1} in $CsPbCl_3$(1:3) NCs to 1.6×10^7 s^{-1} in $CsPbCl_3$(1:9) NCs. The k_{nr} values for the $CsPbCl_2Br$, $CsPbCl_{1.5}Br_{1.5}$, and $CsPbClBr_2$ NCs decrease by factors of 10, 17, and 23, respectively, on changing the Pb:X precursor ratio from 1:3 to 1:6. No subnanosecond trapping component could be

https://doi.org/10.1021/acs.jpcc.1c07740
J. Phys. Chem. C 2021, 125, 23539−23547

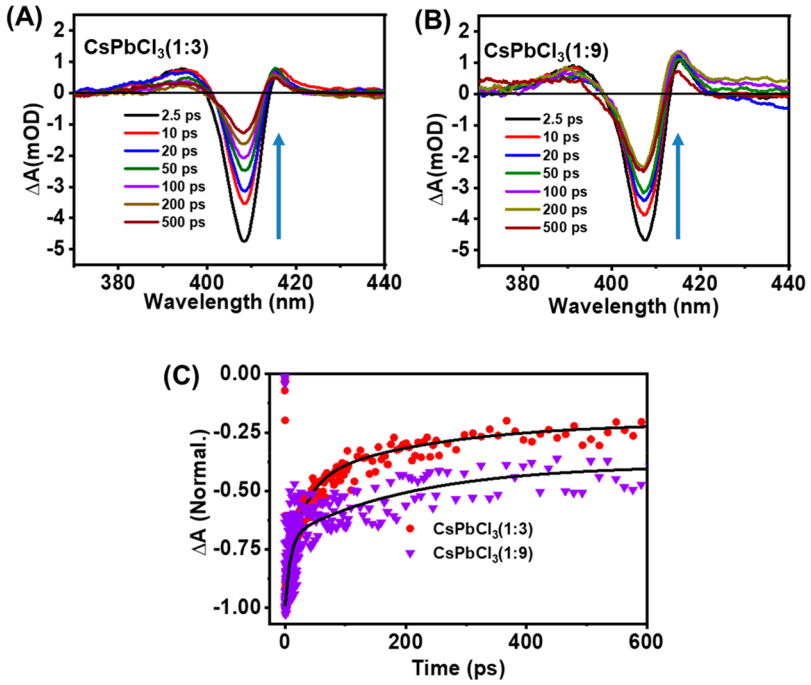

Figure 4. Panels A and B depict the TA spectra of the $CsPbCl_3$(1:3) and $CsPbCl_3$(1:9) NCs at different delay times. Panel C compares the bleach recovery kinetics of the two samples monitored at the bleach maximum position.

observed for the $CsPbBr_3$ NCs (Figure S6 and Table 2) obtained by using a stoichiometric Pb:Br precursor ratio, and this observation is consistent with its near-unity PLQY. A lower PLQY, shorter PL lifetime, and higher nonradiative recombination rate of the $CsPbCl_3$ and $CsPb(Cl/Br)_3$ NCs obtained by using a stoichiometric Pb:X precursor ratio confirm that halide deficiencies in these NCs serve as major carrier trapping centers.

Because of the limited time resolution (~54 ps) of our TCSPC setup, a faster trapping process (if any) cannot be precisely estimated by using this setup. For this reason, we have examined the transient absorption (TA) behavior of the $CsPbCl_3$ NCs using the pump−probe technique with femtosecond time resolution (λ_{exc} = 350 nm, pump power of 4−5 $\mu J/cm^2$). The TA spectra of the $CsPbCl_3$ NCs are characterized by a sharp negative signal at 403 nm and a positive signal on both sides of it (Figure 4A,B). The negative (bleach) signal is induced by state filling of the electron and hole in the band-edges.[45−47] The bleach recovery kinetics of the $CsPbCl_3$(1:3) NCs is characterized by two fast components, 4 (16%) and 41 ps (55%), and a much slower component (>750 ps (29%)) (Figure 4C and Table 3), the exact value of which cannot be estimated accurately in this setup as it falls beyond the time window of this femtosecond setup. The fast components are attributed to carrier trapping and the long component to direct band-edge carrier recombination.[19,31,46,47]

Table 3. Kinetic Parameters of the Bleach Recovery Dynamics of $CsPbCl_3$ NCs

system	τ_1/ps (a_1)	τ_2/ps (a_2)	τ_3/ps (a_3)
$CsPbCl_3$(1:3)	4.0 ± 0.15 (0.16)	41.05 ± 2.8 (0.55)	>750 (0.29)
$CsPbCl_3$(1:9)	4.73 ± 1.2 (0.41)		>750 (0.59)

The observed 41 ps time component of the bleach recovery kinetics is comparable to the 70 ps PL component of similar origin. As can be seen, the carrier trapping component is suppressed (from 71% to 41%) with change in Pb:Cl precursor ratio from 1:3 to 1:9 (Figure 4C and Table 3). This reconfirms that halide deficiency in these NCs leads to the formation of trap states and trapping of the carriers occurs on the picosecond time scale. One important point to note in this context is that the bleach recovery kinetics of the $CsPbCl_3$(1:9) NCs still comprises 41% of a fast trapping component (~4.73 ps). This suggests that, in addition to the halide vacancies, other factors like structural distortion of the octahedral $[PbX_6]^{4-}$ contribute to the defect states in these NCs, as shown recently by Sun and co-workers.[16]

In addition to high PLQY, the NCs obtained by our method exhibit very good stability. For example, when kept under ambient conditions, 85% of initial PL of a dilute (~10 nM) colloidal solution of $CsPbCl_3$(1:9) NCs in hexane is retained after 14 days with no change in PL peak position (Figure 5A and Figure S7). Under similar conditions, only 30% of initial PL intensity of $CsPbCl_3$(1:3) NCs is retained (Figure 5A). Mixed halide perovskite NCs generally exhibit low stability due to phase segregation,[48,49] but these NCs also show impressive stability. For example, $CsPbCl_{1.5}Br_{1.5}$(1:6) NCs retain 75% of its initial PL intensity without any change in PL peak position after 14 days of storage in ambient conditions, whereas, for $CsPbCl_{1.5}Br_{1.5}$(1:3) NCs, only 25% of initial PL is retained (Figure 5B and Figure S7).

The $CsPbCl_3$ and $CsPb(Cl/Br)_3$ NCs obtained by using a stoichiometric Pb:X precursor ratio are halide-deficient having a large density of the trap states, which facilitate nonradiative deactivation of the charge carriers and decrease the PLQY of the systems. However, the NCs obtained by using an excess amount of halide precursor possess a halide-rich surface with fewer trap states arising only from the inherent structural distortion in these systems. This is pictorially illustrated in

https://doi.org/10.1021/acs.jpcc.1c07740
J. Phys. Chem. C 2021, 125, 23539−23547

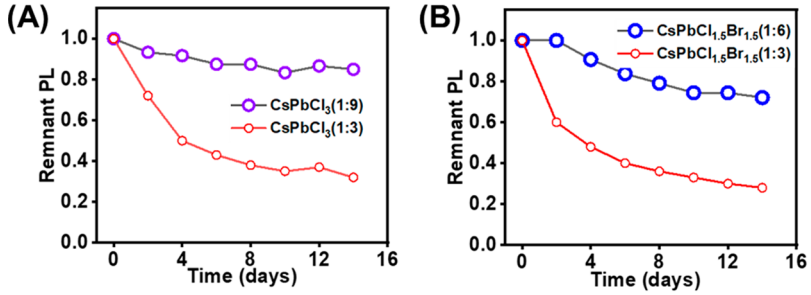

Figure 5. Air stability of different samples of (A) $CsPbCl_3$ NCs and (B) $CsPbCl_{1.5}Br_{1.5}$ NCs under ambient conditions. The stability was checked by using dilute (~10 nM) NCs solution in hexane.

Scheme 1. As the alkylammonium ions are known to enhance the stability of the $CsPbX_3$ NCs by replacing the surface Cs^+, it

Scheme 1. Schematic Illustration of the Influence of an Increasing X:Pb Precursor Ratio on the PL Properties of the $CsPbCl_3$ and $CsPb(Cl/Br)_3$ NCs[a]

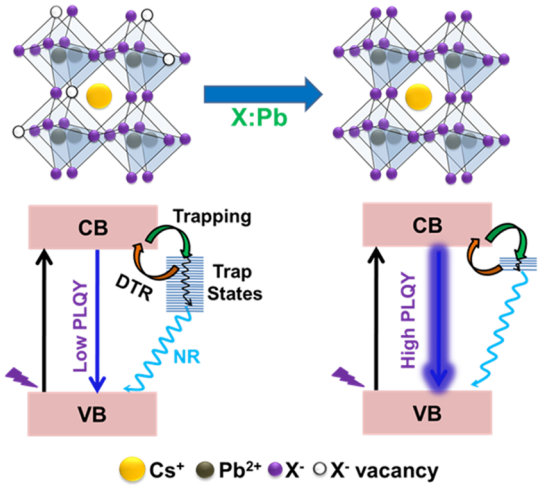

[a]NR and DTR represent nonradiative recombination and detrapping processes, respectively.

is quite likely that oleylammonium halide formed during the reaction (Scheme S1) also contributes to the stability of the systems by forming an oleylammonium halide-terminated surface. A comparison of the PLQY and stability of $CsPbCl_3$ and $CsPb(Cl/Br)_3$ NCs obtained so far by direct synthesis (Table S3) reveals the high quality of our samples. Our violet-emitting $CsPbCl_3$ NCs with 80% PLQY are the second best and blue-emitting $CsPb(Cl/Br)_3$ NCs with 85−97% PLQY are by far the best directly prepared samples as far as the PL efficiency is concerned. In terms of stability also, the present samples stand out.

CONCLUSION

Highly luminescent (PLQY ~ 80−99%) and stable $CsPbCl_3$, $CsPb(Cl/Br)_3$, and $CsPbBr_3$ NCs with narrow size distribution emitting in the violet, blue, and green region (405−510 nm) have been obtained by direct synthesis employing *N*-halophthalimides as the halide precursor and by optimizing the Pb:X precursor ratio. The results show that when the key issue, halide deficiency of the surface of the NCs, is dealt with by using an effective halide precursor and an appropriate Pb:X precursor ratio, it is indeed possible to directly obtain highly luminescent and stable NCs even for the blue-violet region. The time-resolved PL and ultrafast pump−probe measurements show the dependence of the carrier trapping processes on the Pb:X precursor ratio and that carrier trapping is greatly suppressed when these NCs are prepared by using a higher than stoichiometric X:Pb precursor ratio.

ASSOCIATED CONTENT

Supporting Information

The Supporting Information is available free of charge at https://pubs.acs.org/doi/10.1021/acs.jpcc.1c07740.

TEM images, EDX spectra, PL spectra, stability of different NCs, table for the EDX data, amount of precursor, and comparison of PL properties of our sample with other methods (PDF)

AUTHOR INFORMATION

Corresponding Author

Anunay Samanta − *School of Chemistry, University of Hyderabad, Hyderabad 500046, India;* orcid.org/0000-0003-1551-0209; Email: anunay@uohyd.ac.in

Authors

Sumanta Paul − *School of Chemistry, University of Hyderabad, Hyderabad 500046, India;* orcid.org/0000-0003-4825-0984

Tasnim Ahmed − *School of Chemistry, University of Hyderabad, Hyderabad 500046, India;* orcid.org/0000-0002-5990-3891

Somnath Das − *School of Chemistry, University of Hyderabad, Hyderabad 500046, India;* orcid.org/0000-0002-3414-9597

Complete contact information is available at: https://pubs.acs.org/10.1021/acs.jpcc.1c07740

Notes

The authors declare no competing financial interest.

ACKNOWLEDGMENTS

This work was supported by the J. C. Bose Fellowship (to A.S.) of the Science and Engineering Research Board (SERB) and the Institute of Eminence Grants to the University of Hyderabad. We thank Dr. M. Durga Prasad for the TEM measurements at the Centre for Nanotechnology, University of Hyderabad. S.P. and S.D. thank UGC and T.A. thanks CSIR for Fellowship.

REFERENCES

(1) Dey, A.; Ye, J.; De, A.; Debroye, E.; Ha, S. K.; Bladt, E.; Kshirsagar, A. S.; Wang, Z.; Yin, J.; Wang, Y.; et al. State of the Art and Prospects for Halide Perovskite Nanocrystals. *ACS Nano* **2021**, *15*, 10775−10981.

(2) Kojima, A.; Teshima, K.; Shirai, Y.; Miyasaka, T. Organometal Halide Perovskites as Visible-Light Sensitizers for Photovoltaic Cells. *J. Am. Chem. Soc.* **2009**, *131*, 6050−6051.

(3) Heo, J. H.; Im, S. H.; Noh, J. H.; Mandal, T. N.; Lim, C.-S.; Chang, J. A.; Lee, Y. H.; Kim, H.-J.; Sarkar, A.; Nazeeruddin, M. K.; et al. Efficient Inorganic−Organic Hybrid Heterojunction Solar Cells Containing Perovskite Compound and Polymeric Hole Conductors. *Nat. Photonics* **2013**, *7*, 486−491.

(4) Lee, M. M.; Teuscher, J.; Miyasaka, T.; Murakami, T. N.; Snaith, H. J. Efficient Hybrid Solar Cells Based on Meso-Superstructured Organometal Halide Perovskites. *Science* **2012**, *338*, 643−647.

(5) Kovalenko, M. V.; Protesescu, L.; Bodnarchuk, M. I. Properties and Potential Optoelectronic Applications of Lead Halide Perovskite Nanocrystals. *Science* **2017**, *358*, 745−750.

(6) Correa-Baena, J.-P.; Abate, A.; Saliba, M.; Tress, W.; Jacobsson, T. J.; Gratzel, M.; Hagfeldt, A. The Rapid Evolution of Highly Efficient Perovskite Solar Cells. *Energy Environ. Sci.* **2017**, *10*, 710−727.

(7) Sanehira, E. M.; Marshall, A. R.; Christians, J. A.; Harvey, S. P.; Ciesielski, P. N.; Wheeler, L. M.; Schulz, P.; Lin, L. Y.; Beard, M. C.; Luther, J. M. Enhanced Mobility $CsPbI_3$ Quantum Dot Arrays for Record-Efficiency, High-Voltage Photovoltaic Cells. *Sci. Adv.* **2017**, *3*, eaao4204.

(8) Sutherland, B. R.; Sargent, E. H. Perovskite Photonic Sources. *Nat. Photonics* **2016**, *10*, 295−302.

(9) Protesescu, L.; Yakunin, S.; Bodnarchuk, M. I.; Krieg, F.; Caputo, R.; Hendon, C. H.; Yang, R. X.; Walsh, A.; Kovalenko, M. V. Nanocrystals of Cesium Lead Halide Perovskites ($CsPbX_3$, X = Cl, Br, and I): Novel Optoelectronic Materials Showing Bright Emission with Wide Color Gamut. *Nano Lett.* **2015**, *15*, 3692−3696.

(10) Yakunin, S.; Protesescu, L.; Krieg, F.; Bodnarchuk, M. I.; Nedelcu, G.; Humer, M.; De Luca, G.; Fiebig, M.; Heiss, W.; Kovalenko, M. V. Low-Threshold Amplified Spontaneous Emission and Lasing from Colloidal Nanocrystals of Caesium Lead Halide Perovskites. *Nat. Commun.* **2015**, *6*, 8056.

(11) Akkerman, Q. A.; Gandini, M.; Di Stasio, F.; Rastogi, P.; Palazon, F.; Bertoni, G.; Ball, J. M.; Prato, M.; Petrozza, A.; Manna, L. Strongly Emissive Perovskite Nanocrystal Inks for High-Voltage Solar cells. *Nat. Energy* **2017**, *2*, 16194.

(12) Mondal, N.; De, A.; Seth, S.; Ahmed, T.; Das, S.; Paul, S.; Gautam, R. K.; Samanta, A. Dark Excitons of the Perovskites and Sensitization of Molecular Triplets. *ACS Energy Lett.* **2021**, *6*, 588−597.

(13) Ahmed, T.; De, A.; Paul, S.; Samanta, A. Individual Particle-Level Picture of Charge Carrier Recombination in Bi-Doped $CsPbBr_3$ Nanocrystals. *J. Phys. Chem. C* **2021**, *125*, 2156−2162.

(14) Tong, Y.; Bladt, E.; Aygüler, M. F.; Manzi, A.; Milowska, K. Z.; Hintermayr, V. A.; Docampo, P.; Bals, S.; Urban, A. S.; Polavarapu, L.; et al. Highly Luminescent Cesium Lead Halide Perovskite Nanocrystals with Tunable Composition and Thickness by Ultrasonication. *Angew. Chem., Int. Ed.* **2016**, *55*, 13887−13892.

(15) Shamsi, J.; Urban, A. S.; Imran, M.; De Trizio, L.; Manna, L. Metal Halide Perovskite Nanocrystals: Synthesis, Post-Synthesis Modifications, and Their Optical Properties. *Chem. Rev.* **2019**, *119*, 3296−3348.

(16) Yong, Z.-J.; Guo, S.-Q.; Ma, J.-P.; Zhang, J.-Y.; Li, Z.-Y.; Chen, Y.-M.; Zhang, B.-B.; Zhou, Y.; Shu, J.; Gu, J.-L.; et al. Doping-Enhanced Short-Range Order of Perovskite Nanocrystals for Near-Unity Violet Luminescence Quantum Yield. *J. Am. Chem. Soc.* **2018**, *140*, 9942−9951.

(17) Shynkarenko, Y.; Bodnarchuk, M. I.; Bernasconi, C.; Berezovska, Y.; Verteletskyi, V.; Ochsenbein, S. T.; Kovalenko, M. V. Direct Synthesis of Quaternary Alkylammonium-Capped Perovskite Nanocrystals for Efficient Blue and Green Light-Emitting Diodes. *ACS Energy Lett.* **2019**, *4*, 2703−2711.

(18) Hou, S.; Gangishetty, M. K.; Quan, Q.; Congreve, D. N. Efficient Blue and White Perovskite Light-Emitting Diodes via Manganese Doping. *Joule* **2018**, *2*, 2421−2433.

(19) Mondal, N.; De, A.; Samanta, A. Achieving Near-Unity Photoluminescence Efficiency for Blue-Violet-Emitting Perovskite Nanocrystals. *ACS Energy Lett.* **2019**, *4*, 32−39.

(20) Ahmed, G. H.; El-Demellawi, J. K.; Yin, J.; Pan, J.; Velusamy, D. B.; Hedhili, M. N.; Alarousu, E.; Bakr, O. M.; Alshareef, H. N.; Mohammed, O. F. Giant Photoluminescence Enhancement in $CsPbCl_3$ Perovskite Nanocrystals by Simultaneous Dual-Surface Passivation. *ACS Energy Lett.* **2018**, *3*, 2301−2307.

(21) Akkerman, Q. A.; Rainò, G.; Kovalenko, M. V.; Manna, L. Genesis, Challenges and Opportunities for Colloidal Lead Halide Perovskite Nanocrystals. *Nat. Mater.* **2018**, *17*, 394−405.

(22) Seth, S.; Ahmed, T.; De, A.; Samanta, A. Tackling the Defects, Stability, and Photoluminescence of $CsPbX_3$ Perovskite Nanocrystals. *ACS Energy Lett.* **2019**, *4*, 1610−1618.

(23) Ghosh, S.; Mandal, S.; Mukherjee, S.; De, C. K.; Samanta, T.; Mandal, M.; Roy, D.; Mandal, P. K. Near-Unity Photoluminescence Quantum Yield and Highly Suppressed Blinking in a Toxic-Metal-Free Quantum Dot. *J. Phys. Chem. Lett.* **2021**, *12*, 1426−1431.

(24) Behera, R. K.; Das Adhikari, S.; Dutta, S. K.; Dutta, A.; Pradhan, N. Blue-Emitting $CsPbCl_3$ Nanocrystals: Impact of Surface Passivation for Unprecedented Enhancement and Loss of Optical Emission. *J. Phys. Chem. Lett.* **2018**, *9*, 6884−6891.

(25) Zheng, X.; Hou, Y.; Sun, H.-T.; Mohammed, O. F.; Sargent, E. H.; Bakr, O. M. Reducing Defects in Halide Perovskite Nanocrystals for Light Emitting Applications. *J. Phys. Chem. Lett.* **2019**, *10*, 2629−2640.

(26) Mandal, S.; Ghosh, S.; Mukherjee, S.; De, C. K.; Roy, D.; Samanta, T.; Mandal, P. K. Unravelling Halide-Dependent Charge Carrier Dynamics in $CsPb(Br/Cl)_3$ Perovskite Nanocrystals. *Nanoscale* **2021**, *13*, 3654−3661.

(27) Kumawat, N. K.; Liu, X.-K.; Kabra, D.; Gao, F. Blue Perovskite Light-Emitting Diodes: Progress, Challenges and Future Directions. *Nanoscale* **2019**, *11*, 2109−2120.

(28) Naresh, V.; Lee, N. Zn(II)-Doped Cesium Lead Halide Perovskite Nanocrystals with High Quantum Yield and Wide Color Tunability for Color-Conversion Light-Emitting Displays. *ACS Appl. Nano Mater.* **2020**, *3*, 7621−7632.

(29) Chen, J.-K.; Ma, J.-P.; Guo, S.-Q.; Chen, Y.-M.; Zhao, Q.; Zhang, B.-B.; Li, Z.-Y.; Zhou, Y.; Hou, J.; Kuroiwa, Y.; et al. High-Efficiency Violet-Emitting All-Inorganic Perovskite Nanocrystals Enabled by Alkaline-Earth Metal Passivation. *Chem. Mater.* **2019**, *31*, 3974−3983.

(30) Imran, M.; Caligiuri, V.; Wang, M.; Goldoni, L.; Prato, M.; Krahne, R.; De Trizio, L.; Manna, L. Benzoyl Halides as Alternative Precursors for the Colloidal Synthesis of Lead-Based Halide Perovskite Nanocrystals. *J. Am. Chem. Soc.* **2018**, *140*, 2656−2664.

(31) De, A.; Das, S.; Mondal, N.; Samanta, A. Highly Luminescent Violet- and Blue-Emitting Stable Perovskite Nanocrystals. *ACS Materials Lett.* **2019**, *1*, 116−122.

(32) Li, F.; Liu, Y.; Wang, H.; Zhan, Q.; Liu, Q.; Xia, Z. Postsynthetic Surface Trap Removal of $CsPbX_3$ (X = Cl, Br, or I) Quantum Dots via a ZnX_2/Hexane Solution toward an Enhanced Luminescence Quantum Yield. *Chem. Mater.* **2018**, *30*, 8546−8554.

(33) Das, S.; De, A.; Samanta, A. Ambient Condition Mg^{2+} Doping Producing Highly Luminescent Green- and Violet-Emitting Perovskite Nanocrystals with Reduced Toxicity and Enhanced Stability. *J. Phys. Chem. Lett.* **2020**, *11*, 1178−1188.

(34) Dutta, A.; Behera, R. K.; Pal, P.; Baitalik, S.; Pradhan, N. Near-Unity Photoluminescence Quantum Efficiency for All $CsPbX_3$(X = Cl, Br, and I) Perovskite Nanocrystals: A Generic Synthesis Approach. *Angew. Chem., Int. Ed.* **2019**, *58*, 5552−5556.

(35) Ahmed, T.; Seth, S.; Samanta, A. Boosting the Photoluminescence of $CsPbX_3$ (X = Cl, Br, I) Perovskite Nanocrystals

https://doi.org/10.1021/acs.jpcc.1c07740
J. Phys. Chem. C 2021, 125, 23539−23547

Covering a Wide Wavelength Range by Postsynthetic Treatment with Tetrafluoroborate Salts. *Chem. Mater.* **2018**, *30*, 3633−3637.
(36) Wang, S.; Wang, Y.; Zhang, Y.; Zhang, X.; Shen, X.; Zhuang, X.; Lu, P.; Yu, W. W.; Kershaw, S. V.; Rogach, A. L. Cesium Lead Chloride/Bromide Perovskite Quantum Dots with Strong Blue Emission Realized via a Nitrate-Induced Selective Surface Defect Elimination Process. *J. Phys. Chem. Lett.* **2019**, *10*, 90−96.
(37) Bi, C.; Wang, S.; Li, Q.; Kershaw, S. V.; Tian, J.; Rogach, A. L. Thermally Stable Copper(II)-Doped Cesium Lead Halide Perovskite Quantum Dots with Strong Blue Emission. *J. Phys. Chem. Lett.* **2019**, *10*, 943−952.
(38) Ahmed, G. H.; Yin, J.; Bakr, O. M.; Mohammed, O. F. Near-Unity Photoluminescence Quantum Yield in Inorganic Perovskite Nanocrystals by Metal-Ion Doping. *J. Chem. Phys.* **2020**, *152*, 020902.
(39) Nenon, D. P.; Pressler, K.; Kang, J.; Koscher, B. A.; Olshansky, J. H.; Osowiecki, W. T.; Koc, M. A.; Wang, L.-W.; Alivisatos, A. P. Design Principles for Trap-Free $CsPbX_3$ Nanocrystals: Enumerating and Eliminating Surface Halide Vacancies with Softer Lewis Bases. *J. Am. Chem. Soc.* **2018**, *140*, 17760−17772.
(40) Mamgain, S.; Kunnathodi, V.; Yella, A. Humidity-Mediated Synthesis of Highly Luminescent and Stable $CsPbX_3$ (X = Cl, Br, I) Nanocrystals. *Energy Technol.* **2020**, *8*, 1900890.
(41) Paul, S.; Samanta, A. N-Bromosuccinimide as Bromide Precursor for Direct Synthesis of Stable and Highly Luminescent Green-Emitting Perovskite Nanocrystals. *ACS Energy Lett.* **2020**, *5*, 64−69.
(42) Grabolle, M.; Spieles, M.; Lesnyak, V.; Gaponik, N.; Eychmuller, A.; Resch-Genger, U. Determination of the Fluorescence Quantum Yield of Quantum Dots: Suitable Procedures and Achievable Uncertainties. *Anal. Chem.* **2009**, *81*, 6285−6294.
(43) Dong, Y.; Qiao, T.; Kim, D.; Parobek, D.; Rossi, D.; Son, D. H. Precise Control of Quantum Confinement in Cesium Lead Halide Perovskite Quantum Dots via Thermodynamic Equilibrium. *Nano Lett.* **2018**, *18*, 3716−3722.
(44) Guo, T.; Bose, R.; Zhou, X.; Gartstein, Y. N.; Yang, H.; Kwon, S.; Kim, M. J.; Lutfullin, M.; Sinatra, L.; Gereige, I.; et al. Delayed Photoluminescence and Modified Blinking Statistics in Alumina-Encapsulated Zero-Dimensional Inorganic Perovskite Nanocrystals. *J. Phys. Chem. Lett.* **2019**, *10*, 6780−6787.
(45) Mondal, N.; Samanta, A. Complete Ultrafast Charge Carrier Dynamics in Photo-excited All-Inorganic Perovskite Nanocrystals ($CsPbX_3$). *Nanoscale* **2017**, *9*, 1878−1885.
(46) Mondal, N.; De, A.; Das, S.; Paul, S.; Samanta, A. Ultrafast Carrier Dynamics of Metal Halide Perovskite Nanocrystals and Perovskite-Composites. *Nanoscale* **2019**, *11*, 9796−9818.
(47) Lai, R.; Wu, K. Picosecond Electron Trapping Limits the Emissivity of $CsPbCl_3$ Perovskite Nanocrystals. *J. Chem. Phys.* **2019**, *151*, 194701.
(48) Karlsson, M.; Yi, Z.; Reichert, S.; Luo, X.; Lin, W.; Zhang, Z.; Bao, C.; Zhang, R.; Bai, S.; Zheng, G.; et al. Mixed Halide Perovskites for Spectrally Stable and High-Efficiency blue Light-Emitting Diodes. *Nat. Commun.* **2021**, *12*, 361.
(49) Abdi-Jalebi, M.; Andaji-Garmaroudi, Z.; Cacovich, S.; Stavrakas, C.; Philippe, B.; Richter, J. M.; Alsari, M.; Booker, E. P.; Hutter, E. M.; Pearson, A. J.; et al. Maximizing and Stabilizing Luminescence from Halide Perovskites with Potassium Passivation. *Nature* **2018**, *555*, 497−501.

https://doi.org/10.1021/acs.jpcc.1c07740
J. Phys. Chem. C 2021, 125, 23539−23547

THE JOURNAL OF PHYSICAL CHEMISTRY LETTERS
A JOURNAL OF THE AMERICAN CHEMICAL SOCIETY

pubs.acs.org/JPCL

Letter

Phase-Stable and Highly Luminescent $CsPbI_3$ Perovskite Nanocrystals with Suppressed Photoluminescence Blinking

Sumanta Paul and Anunay Samanta*

Cite This: *J. Phys. Chem. Lett.* 2022, 13, 5742−5750

Read Online

ACCESS | Metrics & More | Article Recommendations | Supporting Information

ABSTRACT: Despite their low band gap, the utility of $CsPbI_3$ nanocrystals (NCs) in solar photovoltaic and optoelectronic applications is rather limited because of their phase instability and photoluminescence (PL) intermittency. Herein we show that phase-pure, monodispersed, stable and highly luminescent $CsPbI_3$ NCs can be obtained by tweaking the conventional hot-injection method employing NH_4I as an additional precursor. Single-particle studies show a significant suppression of PL blinking. Among all NCs studied, 60% exhibit only high-intensity ON states with a narrow distribution of intensity. The remaining 40% of NCs exhibit a much wider distribution of PL intensity with a significant contribution of low-intensity OFF states. Excellent characteristics of these $CsPbI_3$ NCs are shown to be the result of NH_4^+ replacing some surface Cs^+ of an iodide-rich surface of the NCs. These phase-stable and highly luminescent $CsPbI_3$ NCs with significantly suppressed PL blinking can be useful single-photon emitters and promising materials for optoelectronic and solar photovoltaic applications.

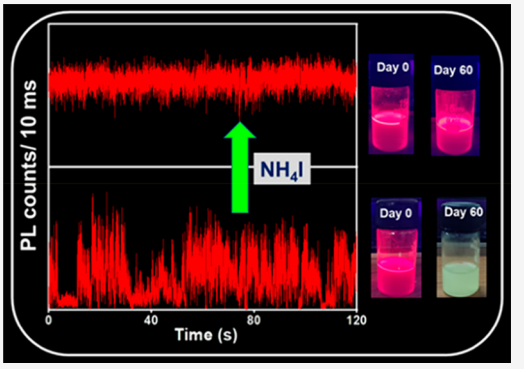

Among the cesium lead halide ($CsPbX_3$ with X = Cl, Br, and I) perovskite nanocrystals (NCs), the $CsPbI_3$ NCs, because of their low band gap, are the most promising candidates for solar photovoltaic and various optoelectronic applications.[1−13] However, poor phase stability of these NCs even under ambient condition is a major obstacle to these applications.[14−17] Apart from the stability-related issues, photoluminescence (PL) blinking of the single NCs is another factor that restricts the applications of the $CsPbI_3$ NCs as single-photon emitters and other light-emitting applications.[18−26] PL blinking is indeed an issue for all single emitters. Among different models invoked for explaining the PL blinking of semiconductor NCs, a charging model based on trapping of the carrier in long-lived trap states[19,27−39] and a multiple recombination center (MRC) model based on the trapping of the carrier in short-lived trap states[36,40−43] are the most common ones. In the charging model, the NCs are emissive (ON) when in their neutral state but are nonemissive (OFF) when in their charged state because of Auger recombination. This ON-OFF PL fluctuation is known as Auger blinking or trion blinking. Here, the OFF-state duration is determined by the lifetime of the carrier residing in the long-lived trap state. In the MRC model, the ON−OFF PL fluctuation is the result of the transformation of the trap states between the active and inactive forms. This blinking arising from time-dependent fluctuations of the carrier trapping rate is termed BC blinking. In addition, the interception of the hot carriers (HC) by trap states can also contribute to PL blinking, which is known as HC blinking.[44−47] Mulvaney and co-workers observed both Auger blinking and BC blinking in single CdSe quantum dots (QDs).[36] Ahmed et al. recently found Auger blinking, BC blinking, and HC blinking in a single $CsPbBr_3$ NC.[48] PL blinking of the $CsPbI_3$ NCs was attributed to charging and discharging of the NCs by Klimov and co-workers,[19] but later Yuan et al. showed that it arises from the activation and deactivation of the trap states.[18]

Obtaining phase-stable red-emitting $CsPbI_3$ NCs with high PL efficiency and suppressed blinking, which is necessary for many optoelectronic applications, is a challenging task.[15] Phase instability and deteriorating PL properties of these NCs arise from surface iodide vacancies, poor surface capping by the coordinating ligands, and the intrinsic disorder of the $[PbI_6]^{4-}$ units.[9,14,49] The nature of the surface of the NCs depends largely on their method of preparation.[14,50−57] The widely used two-precursor method,[3] in which PbI_2 is used as a precursor for both lead and halide, yields NCs of poor quality primarily due to halide vacancies on the surface. The use of additional iodide precursors during synthesis is known to improve the phase stability and PL of the NCs.[54,55,58,59] The doping of metal ions[60−65] and surface treatment by coordinating ligands[9,11,66−68] are also effective approaches to obtaining highly luminescent and stable $CsPbI_3$ NCs. However, despite intense investigations, phase-stable and highly luminescent $CsPbI_3$ NCs with sup-

Received: May 14, 2022
Accepted: June 14, 2022
Published: June 17, 2022

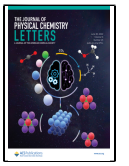

https://doi.org/10.1021/acs.jpclett.2c01463
J. Phys. Chem. Lett. 2022, 13, 5742−5750

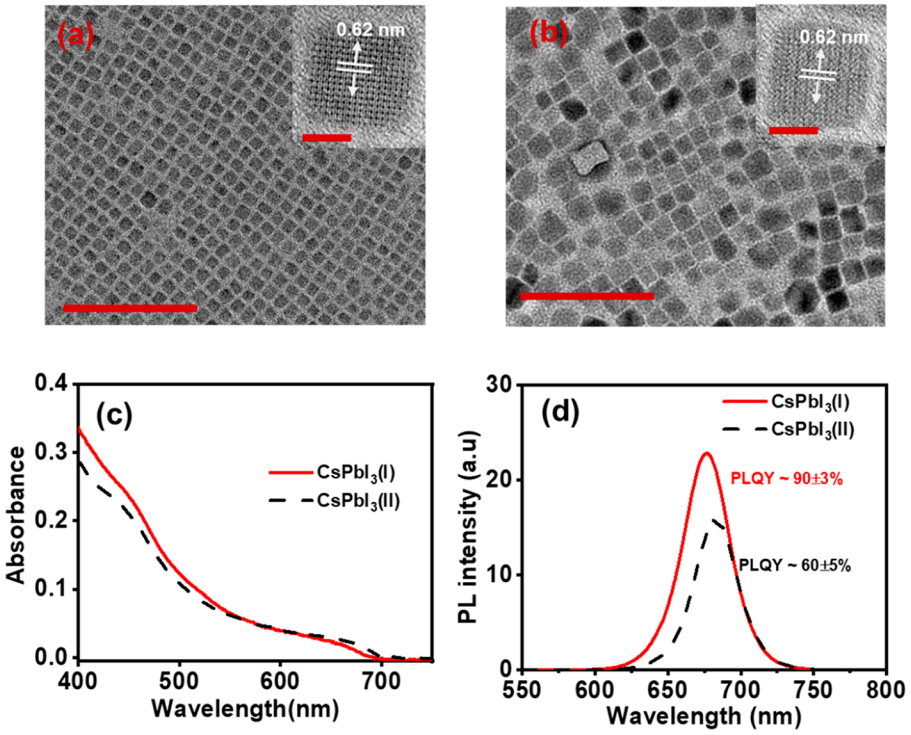

Figure 1. Bright-field TEM images of the (a) $CsPbI_3$(I) and (b) $CsPbI_3$(II) NCs with a scale bar of 100 nm. Insets show HRTEM images of the NCs (scale bar 5 nm) with interplanar spacing corresponding to the (100) planes. (c) UV−vis absorption and (d) PL spectra of the $CsPbI_3$(I) and $CsPbI_3$(II) NCs.

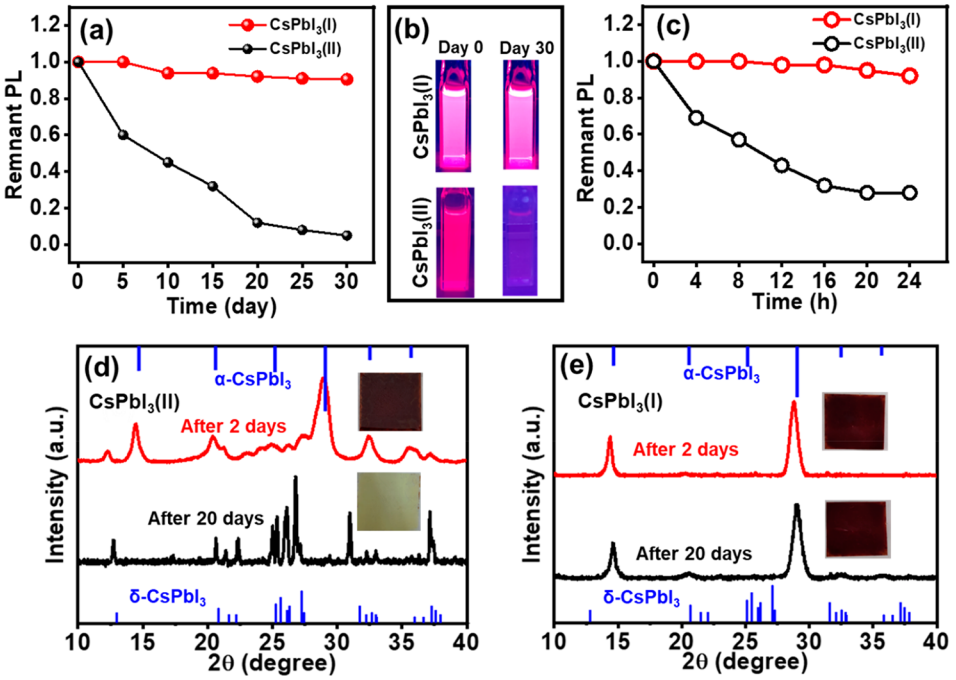

Figure 2. (a) Air stability of the colloidal dispersions of $CsPbI_3$(I) and $CsPbI_3$(II) NCs under ambient conditions. (b) Digital images (under UV illumination) of these samples at different time intervals stored under ambient conditions. (c) Photostability of $CsPbI_3$(I) and $CsPbI_3$(II) NCs under continuous UV illumination (365 nm, 8W). (d) and (e) PXRD patterns of these samples at different time periods. The insets of (d) and (e) show the digital images of the film used for the PXRD measurements.

pressed PL blinking are still not known. In this work, we show that phase-stable and highly luminescent $CsPbI_3$ NCs with significantly suppressed PL blinking can be obtained by the most widely used method of perovskite NCs[3] synthesis using the optimum amount of NH_4I as an additional reagent, which is chosen by considering that a second source of I^- provides a halide-rich synthesis condition and surface capping by NH_4^+ enhances the PLQY and colloidal stability of the NCs.[66]

The $CsPbI_3$ NCs were prepared as follows. PbI_2 (0.2 mmol), NH_4I (0.25 mmol), 1-octadecene (5 mL), oleic acid (OA, 0.8

https://doi.org/10.1021/acs.jpclett.2c01463
J. Phys. Chem. Lett. 2022, 13, 5742−5750

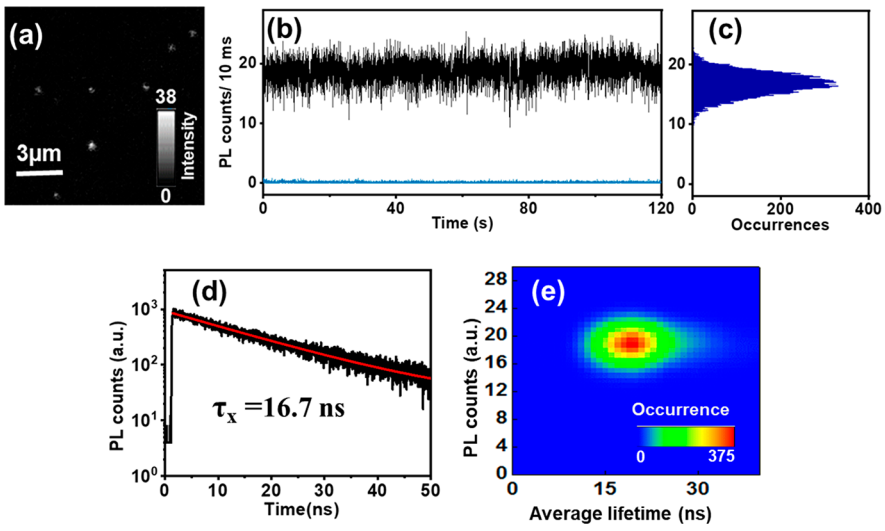

Figure 3. (a) PL intensity image of a film of $CsPbI_3$(I) NCs. (b) PL intensity time trace of a given single $CsPbI_3$(I) NC among the 40 NCs, which show the complete suppression of blinking. The background signal is shown in the cyan-blue color trace. (c) Distribution of PL intensities and occurrence. (d) PL decay profile of the trace. (e) False color representation of FLID obtained from the analyses of the intensity and lifetime of the PL intensity time trace shown in panel b.

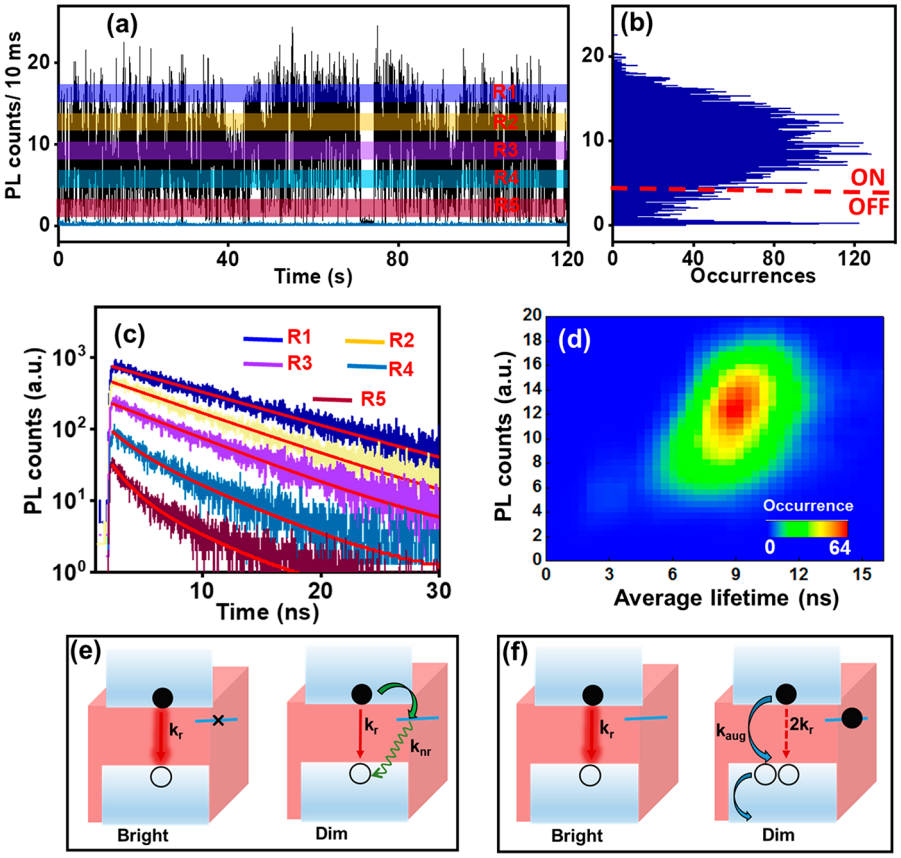

Figure 4. (a) PL intensity−time trace of a given single NC of $CsPbI_3$(I) NC (among 26 NCs exhibiting similar blinking behavior). The trace is divided into five intensity levels (R1 to R5). The background signal is shown in the cyan-blue color trace. (b) Distribution of the intensities with occurrence. Threshold is shown by the red dashed line. (c) PL decay profiles for levels R1 to R5 and (d) FLID pattern of the PL intensity−time trace shown in panel a. Schematic illustration of (e) BC blinking and (f) Auger blinking. k_r, k_{nr}, and k_{aug} represent rate constants of the radiative, nonradiative, and Auger recombination, respectively.

mL) and oleylamine (OLA, 0.8 mL) were taken in a 50 mL round-bottomed flask and stirred under vacuum for 15 min at room temperature. The reaction mixture was then held at 120 °C in a N_2 atmosphere until the formation of a clear orange-colored solution. The temperature was then raised to 160−165 °C, 0.5 mL of cesium oleate was injected into it, and the reaction mixture was quenched immediately in an ice bath. The obtained NCs were purified (details in the experimental section in

https://doi.org/10.1021/acs.jpclett.2c01463
J. Phys. Chem. Lett. 2022, 13, 5742−5750

Supporting Information (SI)) and dispersed in hexane for all measurements. We also prepared $CsPbI_3$ NCs following a conventional method[3] (i.e., without using NH_4I, details in the SI) for comparison. The $CsPbI_3$ NCs obtained by our method are labeled as $CsPbI_3$(I), and the conventional ones, as $CsPbI_3$(II) throughout the manuscript.

The bright-field transmission electron microscope (TEM) images show the uniform cubic shape of the $CsPbI_3$(I) NCs with a narrow size distribution and an average edge length of 9.0 ± 1.0 nm (Figures 1a and S1a). In contrast, the $CsPbI_3$(II) NCs exhibit a much wider size distribution and a larger average edge length (12.5 ± 2.0 nm) (Figures 1b and S1b). High-resolution TEM (HRTEM) images show an interplanar distance (d_{100}) of 0.62 nm for both samples (insets of Figure 1a,b), indicating that the crystal parameters are not affected by the use of NH_4I during synthesis. A decrease in size and improved monodispersity of the $CsPbI_3$(I) NCs are similar to those observed in the case of $CsPbBr_3$ NCs obtained under the halide-rich synthesis condition.[69] The UV−vis absorption and emission spectra of these samples are shown in Figure 1c,d, respectively. The first excitonic peak (in absorption) and the PL maximum of $CsPbI_3$(I) NCs are blue-shifted (by 6−8 nm) compared with the respective peaks of the $CsPbI_3$(II) NCs due to the smaller size of the former sample. The PL quantum yield (QY) of the $CsPbI_3$(I) NCs (90 ± 3%) is found to be much higher than that of the $CsPbI_3$(II) NCs (60 ± 5%) (Figure 1d). The high PLQY (90 ± 3%) is observed for $CsPbI_3$(I) NCs only when an optimum molar ratio of PbI_2:NH_4I (1:1.25) is used during the synthesis, and for higher or lower ratios, the PLQY values are lower (Figure S2).

The $CsPbI_3$(I) NCs are also found to display much improved stability compared to the $CsPbI_3$(II) NCs. This is evident from the fact that the PL of a freshly prepared colloidal solution of the $CsPbI_3$(I) NCs decreases only by 4% after 30 days of storage under ambient conditions with 50−60% humidity and a temperature of 25 ± 5 °C in the cuvette, whereas 95% of the PL of the $CsPbI_3$(II) NCs is lost under similar conditions (Figures 2a,b and S3). The $CsPbI_3$(I) NCs stored in a sealed reagent bottle retain almost the original PL intensity after 60 days in contrast to the $CsPbI_3$(II) NCs, which become nonluminescent during this period (Figure S4). The high photostability of our samples is evident from the fact that after the continuous UV illumination (365 nm, 8W) of a colloidal solution of the $CsPbI_3$(I) NCs (taken in a quartz cuvette) for a test period of 24 h, nearly 92% of the original PL is retained, whereas for $CsPbI_3$(II) NCs, the PL decreases to 28% under similar conditions (Figures 2c and S5). The powder X-ray diffraction (PXRD) patterns of these samples (monitored for 20 days) show that the $CsPbI_3$(II) film starts degrading to the δ-$CsPbI_3$ phase within 2 days, and a complete transition is noticed within 20 days (Figure 2d). However, no noticeable degradation of the $CsPbI_3$(I) film could be observed (Figure 2e). The sample stays in its α-phase even after 20 days under ambient conditions.

Table 1. PL Lifetime Components (τ_i) and Their Weightings (α_i) of Different PL Intensity Levels of the PL Intensity−Time Trace of $CsPbI_3$(I) NC Shown in Figure 4a

region [intensity (counts/10 ms)]	τ_1 (α_1) [ns]	τ_2(α_2) [ns]
R1 (17.00)	9.80	
R2 (13.00)	8.10	
R3 (9.00)	7.01	
R4 (5.50)	5.97 (0.63)	1.71 (0.37)
R5 (2.00)	4.99 (0.43)	1.33 (0.57)

As already mentioned, the random fluctuation of the PL intensity at the single-particle level is one of the biggest problems for the $CsPbI_3$ NCs. High PLQY and excellent stability of our samples of $CsPbI_3$(I) NCs allow us to study the PL properties of these NCs at the single-particle level. We carried out these studies by drop-casting a very dilute solution (pM, in hexane) of the NCs on a cover glass and obtaining a film by drying under vacuum. The film of the NCs was excited by a pulsed laser at 485 nm (pulsed width ∼144 ps, repetition rate 4 MHz, and power 0.1 μW) (details in the SI). The low laser power was used to avoid any nonlinear processes. Under our experimental conditions, the number of excitons generated in each NC per pulse is 0.06.

The confocal PL microscopy image of a film of $CsPbI_3$(I) NCs is shown in Figure 3a. We have examined the PL blinking behavior of 66 individual single NCs of $CsPbI_3$(I) (Figures 3b and S6 and S7), among which 40 single NCs show the complete suppression of PL blinking, indicating the presence of only the ON states (bright states) with a narrow distribution of intensity. A representative PL intensity time trace and PL intensity distribution corresponding to the blinking trace of a single NC of this type are depicted in Figure 3b,c, respectively (and in Figure S6). The single-exponential decay of the PL intensity indicates that the photogenerated charge carriers recombine only through the radiative excitonic recombination process (Figures 3d). A fluorescence lifetime intensity distribution (FLID) plot also shows the presence of only the high-intensity ON states (Figure 3e). The complete elimination of the low-intensity OFF states for a majority of the single NCs of $CsPbI_3$(I) is consistent with the sample's bulk PL properties.

The PL intensity time trace of a representative single NC belonging to the remaining 26 NCs is shown in Figure 4a. The PL intensity fluctuation in this case is much wider with no clear separation of the ON and OFF states (Figure 4b). To understand the mechanism of PL blinking of these NCs, we have examined the PL decay behavior of five different intensity levels (R1 to R5) for each NC. Although the PL decay is single-exponential for the high intensity levels (R1 to R3), the decay profile is biexponential for the bottom two intensity levels (R4 and R5) (Figure 4c). The highest intensity level (R1), which is characterized by a lifetime of 9.80 ns for the representative NCs, is due to radiative excitonic recombination. The PL lifetime of the highest intensity state, when averaged for all ∼26 NCs studied, is ∼13.28 ± 2.65 ns (Figure S8). The lifetime decreases gradually with the lowering of the PL intensity (Table 1). The intensity−lifetime scaling parameter (η) (details in the SI) for first three intensity levels is

$$\eta = k_{R1}:k_{R2}:k_{R3} = I_1/\tau_1:I_2/\tau_2:I_3/\tau_3 = 1.00:0.93:0.74$$

A near-unity ratio of the radiative recombination rates of two high intensity levels indicates the competition between a fixed radiative rate and variable nonradiative rates in the NC. This is typical of BC blinking arising from trapping and detrapping of the charge carrier in/from short-lived trap states.[36] The deviation of the η value from near unity from the R3 level onward indicates the involvement of additional competing recombination process(es). These levels are associated with a second lifetime component (between 1.30 and 1.70 ns), and the contribution of this component increases from the R4 to the R5 level. This short-lived component must arise from trion

https://doi.org/10.1021/acs.jpclett.2c01463
J. Phys. Chem. Lett. 2022, 13, 5742−5750

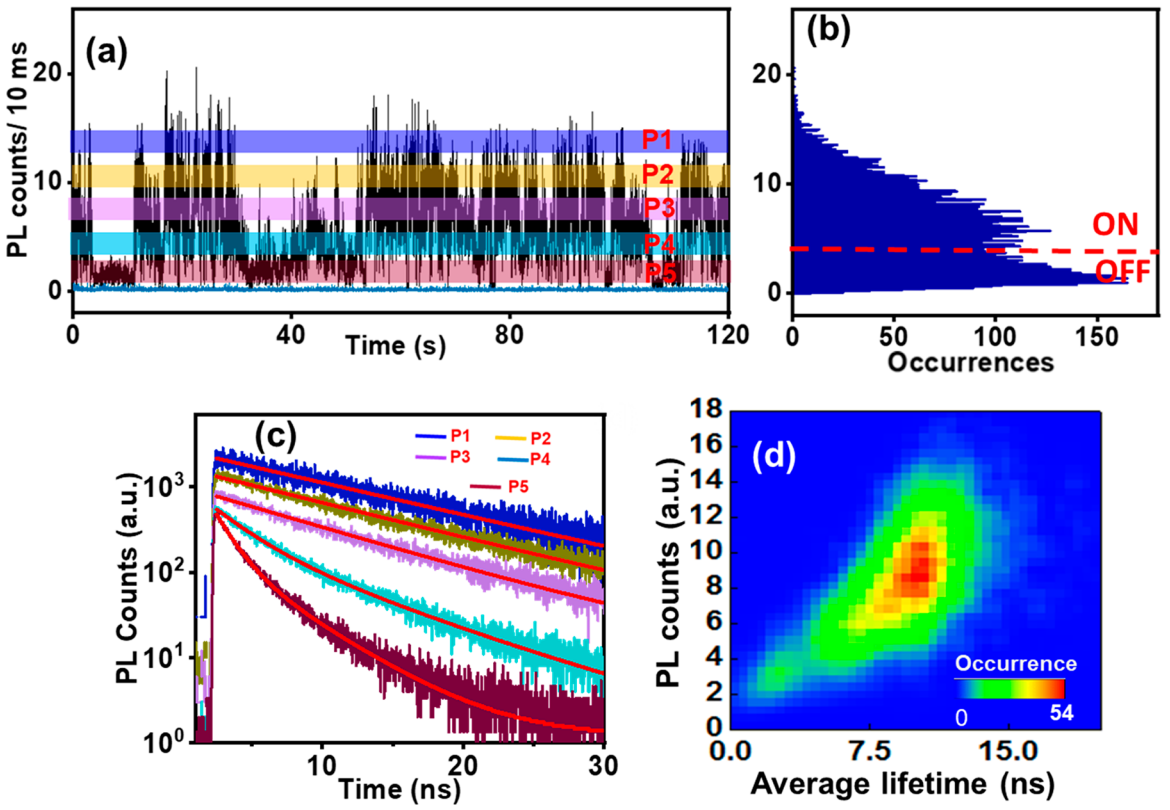

Figure 5. (a) PL blinking trace of a single $CsPbI_3$(II) NC. The trace is divided into five intensity levels (P1 to P5). The background signal is shown in the cyan-blue color trace. (b) Distribution of the intensities observed in the blinking trace. The threshold is shown by the red dashed line. (c) PL decay profiles for levels P1 to P5. (d) FLID patterns of the PL blinking trace shown in panel a with false color representation.

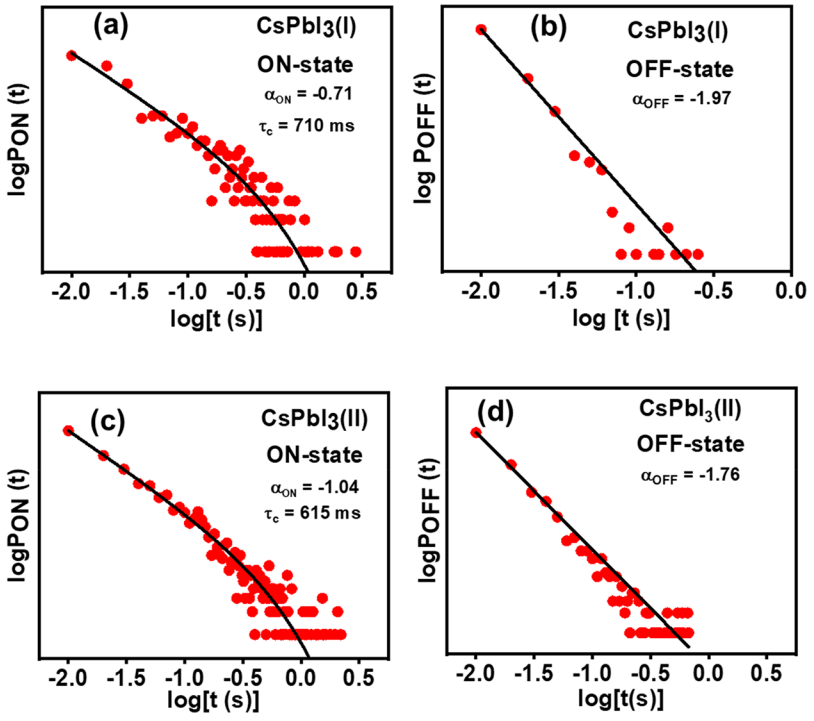

Figure 6. Log–log distributions of (a, c) the ON-time and (b, d) the OFF-time probability of representative NCs of $CsPbI_3$(I) and $CsPbI_3$(II).

recombination because multiexcitonic recombination is ruled out under our experimental conditions.[19,30] The involvement of two simultaneously occurring processes is not very clear in the FLID pattern (Figure 4d) because of the low occurrences of the OFF states. BC blinking and Auger blinking occurring in these samples are represented schematically in (4e,f) respectively.

It was difficult to investigate the single-particle PL properties of the $CsPbI_3$(II) NCs because of their poor stability.[12,18,19] We

https://doi.org/10.1021/acs.jpclett.2c01463
J. Phys. Chem. Lett. 2022, 13, 5742−5750

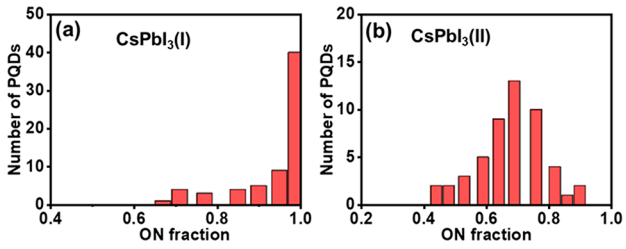

Figure 7. Distribution of the ON-state fractions of (a) $CsPbI_3$(I) and (b) $CsPbI_3$(II) NCs.

observed that several single NCs often degrade within a minute during the recording of the PL intensity−time traces (Figure S9). However, we could manage to record the PL blinking traces of 53 NCs for up to 60 s (Figures 5a and S10), during which no significant photodegradation could be observed. A representative PL blinking trace of these NCs, depicted in Figure 5a, shows a broad distribution of intensity levels with no clear separation between the ON and OFF states (Figure 5b). To determine the origin of PL blinking of this system, the PL intensity trace is marked for five different intensity regions, P1 to P5 (Figure 5a), and their PL decay behavior is studied (Figure 5c and Table S1). The intensity−lifetime scaling parameter (η) for the first three intensity levels is

$$\eta = k_{P1}{:}k_{P2}{:}k_{P3} = I_1/\tau_1{:}I_2/\tau_2{:}I_3/\tau_3 = 1.00{:}0.92{:}0.75$$

A near-unity ratio of the radiative recombination rates of the two high-intensity levels indicates BC blinking arising from the fluctuating trapping rate of the carriers.[36] The deviation of the η value from near-unity from the P3 level onward and the appearance of a short-lifetime component for levels P4 and P5 indicate Auger blinking or trion blinking in these NCs. The FLID plot shows a combination of linear and curvature behavior confirming both Auger and BC blinking in the same NC (Figure 5d). The competition between the fixed radiative and fluctuating

Scheme 1. Schematic Illustration of the Surface Passivation of the $CsPbI_3$ NCs by NH_4I

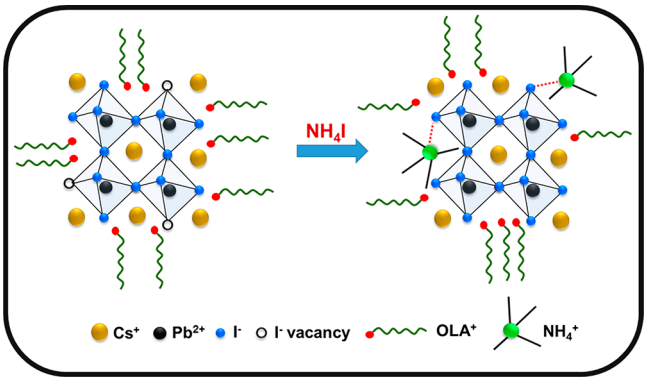

nonradiative relaxations leads to the linear behavior in the FLID pattern, whereas trion recombination leads to nonlinearity in the FLID pattern.

To shed additional light on the nature of the trap states and their effect on carrier recombination, we have analyzed blinking statistics by constructing the probability distributions of the ON and OFF events (Figure 6). Although the ON and OFF events are not so well separated, we have used a threshold of 5 times the maximum background noise level (red dashed line in Figure 4b) for the calculation of the probability distributions of ON and OFF events. The probability distributions of the OFF events are best represented by a power-law function of the form $P_{OFF}(t) \propto t^{\alpha OFF}$; however, for the ON state, it follows a truncated power-law behavior, $P_{ON}(t) \propto t^{\alpha ON} \exp(-t/\tau_c)$ (details in the SI). Here, α and τ_c indicate the power-law exponent and truncation time, respectively. The power-law behavior indicates the dispersive kinetics of carrier trapping and detrapping arising from the (i) the difference in the static distribution of trap states, (ii) the energetic diffusion of the barrier between the core and surface

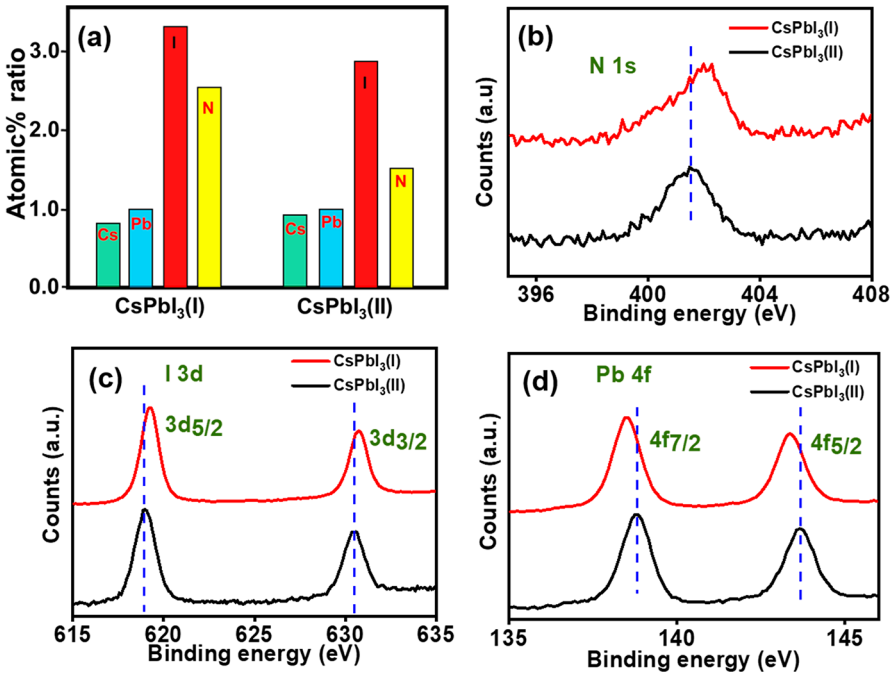

Figure 8. (a) Atomic % ratio (with respect to Pb) of the constituting elements of the $CsPbI_3$(I) and $CsPbI_3$(II) NCs calculated using high-resolution XPS data. High-resolution XPS spectra of (b) N 1s, (c) I 3d ($3d_{5/2}$, $3d_{3/2}$), and (d) Pb 4f ($4f_{5/2}$, $4f_{7/2}$) of these samples.

https://doi.org/10.1021/acs.jpclett.2c01463
J. Phys. Chem. Lett. 2022, 13, 5742−5750

trap states for charge tunneling, and (iii) the difference in the number of time-fluctuating active trap sites.[34,40,70] A larger value of the power-law exponent for the OFF state and a smaller value for the ON state of the $CsPbI_3$(I) NCs compared to the $CsPbI_3$(II) NCs indicate a much longer ON duration of the former sample (Figure 6a−d and Table S2).

The average time fractions spent by the NCs in their ON state, calculated for both $CsPbI_3$(I) and $CsPbI_3$(II) NCs from an individual PL blinking trace (up to 60 s) and corresponding distributions, are shown in Figure 7a,b, respectively. The $CsPbI_3$(I) NCs show an average ON-state fraction of 0.945 ± 0.09, which is quite remarkable. It is also important to note here that 60% of these NCs exhibit an average ON-state fraction of ∼1.0. However, in the case of the $CsPbI_3$(II) NCs, the average ON-state fraction is much lower (0.676 ± 0.11).

The factors contributing to the exceptional phase stability and PL properties of the $CsPbI_3$(I) NCs compared to the $CsPbI_3$(II) NCs can be understood by comparing the XPS spectra of the two samples (Figures 8 and S11). First, the areas under the spectral bands (considering the atomic sensitivity factor[71]) of the constituting elements show Cs:Pb:I atomic percentage ratios of 0.83:1.00:3.33 and 0.90:1.00:2.89 in $CsPbI_3$(I) and $CsPbI_3$(II) NCs, respectively (Figure 8a and Table S3), indicating a halide-rich surface of the former sample. Second, an inspection of the atomic percentage of Cs and N indicates a decrease in Cs content and an increase in N content for the $CsPbI_3$(I) NCs (Figure 8a). This indicates the replacement of some surface Cs^+ by NH_4^+.[72] Third, the N 1s core-level XPS spectrum for $CsPbI_3$(I) NCs is seen to be broader and blue-shifted compared to $CsPbI_3$(II) NCs (Figure 8b). This reflects the presence of two different types of ammonium cations, namely, NH_4^+ and OLA^+ and a higher binding energy of NH_4^+ compared to that of OLA^+. Fourth, a higher binding energy of I^- $3d_{3/2}$ and $3d_{5/2}$ electrons in the $CsPbI_3$(I) NCs compared with the corresponding signals in $CsPbI_3$(II) (Figure 8c) implies a stronger binding of the surface I^- with NH_4^+ in the former sample. Fifth, a decrease in the binding energy of the Pb $4f_{7/2}$ and Pb $4f_{5/2}$ levels (Figure 8d) indicates weakening of the Pb−I bond because of the stronger interaction between NH_4^+ and I^-. It is thus evident that an improved phase stability and significant suppression of PL blinking of the $CsPbI_3$(I) NCs arises from the replacement of some surface Cs^+ by NH_4^+ of an iodide-rich surface of the NCs (Scheme 1).

In short, by focusing on the core issues of phase instability and PL blinking of the $CsPbI_3$ nanocrystals that restrict the utility of these low-band-gap substances in photovoltaic, light-emitting and single-photonic applications, it is shown that exceptionally phase-stable and highly luminescent $CsPbI_3$ NCs with significantly suppressed PL blinking can be obtained by tweaking the conventional hot-injection method of synthesis employing NH_4I as an additional reagent. The PL blinking characteristics of a large number of single $CsPbI_3$ NCs reveal an average ON-state fraction of 0.945 with 60% of them exhibiting the complete suppression of PL blinking. The remaining 40% of the NCs exhibit OFF states due to both Auger recombination of the trion- and trap-induced recombination of the band-edge carrier. The extraordinary features of these NCs are attributed to NH_4I serving as both a halide precursor and a surface capping agent. This work, which provides a simple approach to obtaining high-quality $CsPbI_3$ NCs hitherto unknown, is expected to be of great significance in photovoltaic, light-emitting and single-photonic applications.

■ ASSOCIATED CONTENT

Supporting Information

The Supporting Information is available free of charge at https://pubs.acs.org/doi/10.1021/acs.jpclett.2c01463.

Experimental section, details of single-particle data analysis, variation of PLQY with NH_4I concentration, stability data, additional PL blinking traces, XPS spectra and table of lifetime components, parameters obtained from the statistical analysis of ON and OFF events, and atomic percentages of different elements (PDF)

■ AUTHOR INFORMATION

Corresponding Author

Anunay Samanta − *School of Chemistry, University of Hyderabad, Hyderabad 500046, India;* orcid.org/0000-0003-1551-0209; Email: anunay@uohyd.ac.in

Author

Sumanta Paul − *School of Chemistry, University of Hyderabad, Hyderabad 500046, India;* orcid.org/0000-0003-4825-0984

Complete contact information is available at: https://pubs.acs.org/10.1021/acs.jpclett.2c01463

Notes

The authors declare no competing financial interest.

■ ACKNOWLEDGMENTS

This work is supported by the J. C. Bose Fellowship (to A.S.) of the Science and Engineering Research Board (SERB) and the Institute of Eminence Grants (to the University of Hyderabad) of the Ministry of Human Resource and Development (MHRD), Government of India. We thank Dr. M. Durga Prasad for TEM measurements. S.P. thanks UGC India for a fellowship.

■ REFERENCES

(1) Sanehira, E. M.; Marshall, A. R.; Christians, J. A.; Harvey, S. P.; Ciesielski, P. N.; Wheeler, L. M.; Schulz, P.; Lin, L. Y.; Beard, M. C.; Luther, J. M. Enhanced Mobility $CsPbI_3$ Quantum Dot Arrays for Record-Efficiency, High-Voltage Photovoltaic Cells. *Sci. Adv.* **2017**, *3*, No. eaao4204.

(2) Swarnkar, A.; Marshall, A. R.; Sanehira, E. M.; Chernomordik, B. D.; Moore, D. T.; Christians, J. A.; Chakrabarti, T.; Luther, J. M. Quantum Dot−Induced Phase Stabilization of α-$CsPbI_3$ Perovskite for High-Efficiency Photovoltaics. *Science* **2016**, *354*, 92−95.

(3) Protesescu, L.; Yakunin, S.; Bodnarchuk, M. I.; Krieg, F.; Caputo, R.; Hendon, C. H.; Yang, R. X.; Walsh, A.; Kovalenko, M. V. Nanocrystals of Cesium Lead Halide Perovskites ($CsPbX_3$, X = Cl, Br, and I): Novel Optoelectronic Materials Showing Bright Emission with Wide Color Gamut. *Nano Lett.* **2015**, *15*, 3692−3696.

(4) Bai, S.; Yuan, Z.; Gao, F. Colloidal Metal Halide Perovskite Nanocrystals: Synthesis, Characterization, and Applications. *J. Mater. Chem. C* **2016**, *4*, 3898−3904.

(5) Huang, H.; Polavarapu, L.; Sichert, J. A.; Susha, A. S.; Urban, A. S.; Rogach, A. L. Colloidal Lead Halide Perovskite Nanocrystals: Synthesis, Optical Properties and Applications. *NPG Asia Mater.* **2016**, *8*, No. e328.

(6) Zhang, J.; Yang, X.; Deng, H.; Qiao, K.; Farooq, U.; Ishaq, M.; Yi, F.; Liu, H.; Tang, J.; Song, H. Low-Dimensional Halide Perovskites and Their Advanced Optoelectronic Applications. *Nano-Micro Lett.* **2017**, *9*, 36.

(7) Huang, H.; Bodnarchuk, M. I.; Kershaw, S. V.; Kovalenko, M. V.; Rogach, A. L. Lead Halide Perovskite Nanocrystals in the Research

Spotlight: Stability and Defect Tolerance. *ACS Energy Lett.* **2017**, *2*, 2071−2083.
(8) Mondal, N.; De, A.; Seth, S.; Ahmed, T.; Das, S.; Paul, S.; Gautam, R. K.; Samanta, A. Dark Excitons of the Perovskites and Sensitization of Molecular Triplets. *ACS Energy Lett.* **2021**, *6*, 588−597.
(9) Pan, J.; Shang, Y.; Yin, J.; Bastiani, M. D.; Peng, W.; Dursun, I.; Sinatra, L.; El-Zohry, A. M.; Hedhili, M. N.; Emwas, A.-H.; et al. Bidentate Ligand-Passivated $CsPbI_3$ Perovskite Nanocrystals for Stable Near-Unity Photoluminescence Quantum Yield and Efficient Red Light-Emitting Diodes. *J. Am. Chem. Soc.* **2018**, *140*, 562−565.
(10) Chen, K.; Jin, W.; Zhang, Y.; Yang, T.; Reiss, P.; Zhong, Q.; Bach, U.; Li, Q.; Wang, Y.; Zhang, H.; et al. High Efficiency Mesoscopic Solar Cells Using $CsPbI_3$ Perovskite Quantum Dots Enabled by Chemical Interface Engineering. *J. Am. Chem. Soc.* **2020**, *142*, 3775−3783.
(11) Lan, Y.-F.; Yao, J.-S.; Yang, J.-N.; Song, Y.-H.; Ru, X.-C.; Zhang, Q.; Feng, L.-Z.; Chen, T.; Song, K.-H.; Yao, H.-B. Spectrally Stable and Efficient Pure Red $CsPbI_3$ Quantum Dot Light-Emitting Diodes Enabled by Sequential Ligand Post-Treatment Strategy. *Nano Lett.* **2021**, *21*, 8756−8763.
(12) Dey, A.; Ye, J.; De, A.; Debroye, E.; Ha, S. K.; Bladt, E.; Kshirsagar, A. S.; Wang, Z.; Yin, J.; Wang, Y.; et al. State of the Art and Prospects for Halide Perovskite Nanocrystals. *ACS Nano* **2021**, *15*, 10775−10981.
(13) Tang, X.; Yang, J.; Li, S.; Liu, Z.; Hu, Z.; Hao, J.; Du, J.; Leng, Y.; Qin, H.; Lin, X.; et al. Single Halide Perovskite/Semiconductor Core/Shell Quantum Dots with Ultrastability and Nonblinking Properties. *Adv. Sci.* **2019**, *6*, 1900412.
(14) Dutta, A.; Pradhan, N. Phase-Stable Red-Emitting $CsPbI_3$ Nanocrystals: Successes and Challenges. *ACS Energy Lett.* **2019**, *4*, 709−719.
(15) Protesescu, L.; Yakunin, S.; Kumar, S.; Bar, J.; Bertolotti, F.; Masciocchi, N.; Guagliardi, A.; Grotevent, M.; Shorubalko, I.; Bodnarchuk, M. I.; et al. Dismantling the "Red Wall" of Colloidal Perovskites: Highly Luminescent Formamidinium and Formamidinium−Cesium Lead Iodide Nanocrystals. *ACS Nano* **2017**, *11*, 3119−3134.
(16) Matuhina, A.; Grandhi, G. K.; Liu, M.; Smatt, J.-H.; Viswanath, N. S. M.; Ali-Löytty, H.; Lahtonen, K.; Vivo, P. Octahedral Distortion Driven by $CsPbI_3$ Nanocrystal Reaction Temperature − the Effects on Phase Stability and Beyond. *Nanoscale* **2021**, *13*, 14186−14196.
(17) Straus, D. B.; Guo, S.; Abeykoon, A. M.; Cava, R. J. Understanding the Instability of the Halide Perovskite $CsPbI_3$ through Temperature-Dependent Structural Analysis. *Adv. Mater.* **2020**, *32*, 2001069.
(18) Yuan, G.; Ritchie, C.; Ritter, M.; Murphy, S.; Gomez, D. E.; Mulvaney, P. The Degradation and Blinking of Single $CsPbI_3$ Perovskite Quantum Dots. *J. Phys. Chem. C* **2018**, *122*, 13407−13415.
(19) Park, Y.-S.; Guo, S.; Makarov, N. S.; Klimov, V. I. Room Temperature Single-Photon Emission from Individual Perovskite Quantum Dots. *ACS Nano* **2015**, *9*, 10386−10393.
(20) Hu, F.; Yin, C.; Zhang, H.; Sun, C.; Yu, W. W.; Zhang, C.; Wang, X.; Zhang, Y.; Xiao, M. Slow Auger Recombination of Charged Excitons in Nonblinking Perovskite Nanocrystals without Spectral Diffusion. *Nano Lett.* **2016**, *16*, 6425−6430.
(21) Hsu, B.-W.; Chuang, Y.-T.; Cheng, C.-Y.; Chen, C.-Y.; Chen, Y.-J.; Brumberg, A.; Yang, L.; Huang, Y.-S.; Schaller, R. D.; Chen, L.-J.; et al. Very Robust Spray-Synthesized $CsPbI_3$ Quantum Emitters with Ultrahigh Room-Temperature Cavity-Free Brightness and Self-Healing Ability. *ACS Nano* **2021**, *15*, 11358−11368.
(22) Bose, R.; Zhou, X.; Guo, T.; Yang, H.; Yin, J.; Mishra, A.; Slinker, J. D.; Bakr, O. M.; Mohammed, O. F.; Malko, A. V. Single-Particle Spectroscopy as a Versatile Tool to Explore Lower-Dimensional Structures of Inorganic Perovskites. *ACS Energy Lett.* **2021**, *6*, 3695−3708.
(23) Mandal, S.; Roy, D.; De, C. K.; Ghosh, S.; Mandal, M.; Das, A.; Mandal, P. K. Instantaneous, Room-Temperature, Open-Air Atmosphere, solution-Phase Synthesis of Perovskite Quantum Dots Through Halide Exchange Employing Non-Metal Based Inexpensive HCl/HI: Ensemble and Single Particle Spectroscopy. *Nanoscale Adv.* **2019**, *1*, 3506−3513.
(24) Halder, A.; Pathoor, N.; Chowdhury, A.; Sarkar, S. K. Photoluminescence Flickering of Micron-Sized Crystals of Methylammonium Lead Bromide: Effect of Ambience and Light Exposure. *J. Phys. Chem. C* **2018**, *122*, 15133−15139.
(25) Rainò, G.; Nedelcu, G.; Protesescu, L.; Bodnarchuk, M. I.; Kovalenko, M. V.; Mahrt, R. F.; Stöferle, T. Single Cesium Lead Halide Perovskite Nanocrystals at Low Temperature: Fast Single-Photon Emission, Reduced Blinking, and Exciton Fine Structure. *ACS Nano* **2016**, *10*, 2485−2490.
(26) Zhang, A.; Dong, C.; Ren, J. Tuning Blinking Behavior of Highly Luminescent Cesium Lead Halide Nanocrystals through Varying Halide Composition. *J. Phys. Chem. C* **2017**, *121*, 13314−13323.
(27) Efros, A. L.; Rosen, M. Random Telegraph Signal in the Photoluminescence Intensity of a Single Quantum Dot. *Phys. Rev. Lett.* **1997**, *78*, 1110.
(28) Krauss, T. D.; Brus, L. E. Charge, Polarizability, and Photoionization of Single Semiconductor Nanocrystals. *Phys. Rev. Lett.* **1999**, *83*, 4840−4843.
(29) Yarita, N.; Tahara, H.; Saruyama, M.; Kawawaki, T.; Sato, R.; Teranishi, T.; Kanemitsu, Y. Impact of Postsynthetic Surface Modification on Photoluminescence Intermittency in Formamidinium Lead Bromide Perovskite Nanocrystals. *J. Phys. Chem. Lett.* **2017**, *8*, 6041−6047.
(30) Kanemitsu, Y. Trion Dynamics in Lead Halide Perovskite Nanocrystals. *J. Chem. Phys.* **2019**, *151*, 170902.
(31) Yumoto, G.; Tahara, H.; Kawawaki, T.; Saruyama, M.; Sato, R.; Teranishi, T.; Kanemitsu, Y. Hot Biexciton Effect on Optical Gain in $CsPbI_3$ Perovskite Nanocrystals. *J. Phys. Chem. Lett.* **2018**, *9*, 2222−2228.
(32) Vishnu, E. K.; Nair, A. A. K.; Thomas, K. G. Core-Size-Dependent Trapping and Detrapping Dynamics in CdSe/CdS/ZnS Quantum Dots. *J. Phys. Chem. C* **2021**, *125*, 25706−25716.
(33) Chouhan, L.; Ito, S.; Thomas, E. M.; Takano, Y.; Ghimire, S.; Miyasaka, H.; Biju, V. Real-Time Blinking Suppression of Perovskite Quantum Dots by Halide Vacancy Filling. *ACS Nano* **2021**, *15*, 2831−2838.
(34) Cordones, A. A.; Leone, S. R. Mechanisms for Charge Trapping in Single Semiconductor Nanocrystals Probed by Fluorescence Blinking. *Chem. Soc. Rev.* **2013**, *42*, 3209−3221.
(35) Li, B.; Huang, H.; Zhang, G.; Yang, C.; Guo, W.; Chen, R.; Qin, C.; Gao, Y.; Biju, V. P.; Rogach, A. L.; et al. Excitons and Biexciton Dynamics in Single $CsPbBr_3$ Perovskite Quantum Dots. *J. Phys. Chem. Lett.* **2018**, *9*, 6934−6940.
(36) Yuan, G.; Gomez, D. E.; Kirkwood, N.; Bold, K.; Mulvaney, P. Two Mechanisms Determine Quantum Dot Blinking. *ACS Nano* **2018**, *12*, 3397−3405.
(37) Gibson, N. A.; Koscher, B. A.; Alivisatos, A. P.; Leone, S. R. Excitation Intensity Dependence of Photoluminescence Blinking in $CsPbBr_3$ Perovskite Nanocrystals. *J. Phys. Chem. C* **2018**, *122*, 12106−12113.
(38) Trinh, C. T.; Minh, D. N.; Ahn, K. J.; Kang, Y.; Lee, K.-G. Organic−Inorganic $FAPbBr_3$ Perovskite Quantum Dots as a Quantum Light Source: Single-Photon Emission and Blinking Behaviors. *ACS Photonics* **2018**, *5*, 4937−4943.
(39) Park, Y.-S.; Bae, W. K.; Pietryga, J. M.; Klimov, V. I. Auger Recombination of Biexcitons and Negative and Positive Trions in Individual Quantum Dots. *ACS Nano* **2014**, *8*, 7288−7296.
(40) Frantsuzov, P. A.; Volkan-Kacso, S.; Janko, B. Model of Fluorescence Intermittency of Single Colloidal Semiconductor Quantum Dots Using Multiple Recombination Centers. *Phys. Rev. Lett.* **2009**, *103*, 207402.
(41) Frantsuzov, P. A.; Marcus, R. A. Explanation of Quantum Dot Blinking without the Long-Lived Trap Hypothesis. *Phys. Rev. B* **2005**, *72*, 155321.
(42) Gerhard, M.; Louis, B.; Frantsuzov, P. A.; Li, J.; Kiligaridis, A.; Hofkens, J.; Scheblykin, I. G. Heterogeneities and Emissive Defects in

https://doi.org/10.1021/acs.jpclett.2c01463
J. Phys. Chem. Lett. 2022, 13, 5742−5750

$MAPbI_3$ Perovskite Revealed by Spectrally Resolved Luminescence Blinking. *Adv.Optical Mater.* **2021**, *9*, 2001380.
(43) Seth, S.; Ahmed, T.; Samanta, A. Photoluminescence Flickering and Blinking of Single $CsPbBr_3$ Perovskite Nanocrystals: Revealing Explicit Carrier Recombination Dynamics. *J. Phys. Chem. Lett.* **2018**, *9*, 7007−7014.
(44) Galland, C.; Ghosh, Y.; Steinbruck, A.; Sykora, M.; Hollingsworth, J. A.; Klimov, V. I.; Htoon, H. Two Types of Luminescence Blinking Revealed by Spectroelectrochemistry of Single Quantum Dots. *Nature* **2011**, *479*, 203−207.
(45) Kim, T.; Jung, S. I.; Ham, S.; Chung, H.; Kim, D. Elucidation of Photoluminescence Blinking Mechanism and Multiexciton Dynamics in Hybrid Organic−Inorganic Perovskite Quantum Dots. *Small* **2019**, *15*, 1900355.
(46) Trinh, C. T.; Minh, D. N.; Ahn, K. J.; Kang, Y.; Lee, K.-G. Verification of Type-A and Type B-HC Blinking Mechanisms of Organic−Inorganic Formamidinium Lead Halide Perovskite Quantum Dots by FLID Measurements. *Sci. Rep.* **2020**, *10*, 2172.
(47) Reid, K. R.; McBride, J. R.; Croix, A. D. L.; Freymeyer, N. J.; Click, S. M.; Macdonald, J. E.; Rosenthal, S. J. Role of Surface Morphology on Exciton Recombination in Single Quantum Dot-in-Rods Revealed by Optical and Atomic Structure Correlation. *ACS Nano* **2018**, *12*, 11434−11445.
(48) Ahmed, T.; Seth, S.; Samanta, A. Mechanistic Investigation of the Defect Activity Contributing to the Photoluminescence Blinking of $CsPbBr_3$ Perovskite Nanocrystals. *ACS Nano* **2019**, *13*, 13537−13544.
(49) Seth, S.; Ahmed, T.; De, A.; Samanta, A. Tackling the Defects, Stability, and Photoluminescence of $CsPbX_3$ Perovskite Nanocrystals. *ACS Energy Lett.* **2019**, *4*, 1610−1618.
(50) Dutta, A.; Dutta, S. K.; Adhikari, S. D.; Pradhan, N. Phase-Stable $CsPbI_3$ Nanocrystals:The Reaction Temperature Matters. *Angew.-Chem., Int.Ed.* **2018**, *57*, 9083−9087.
(51) Paul, S.; Samanta, A. N-Bromosuccinimide as Bromide Precursor for Direct Synthesis of Stable and Highly Luminescent Green-Emitting Perovskite Nanocrystals. *ACS Energy Lett.* **2020**, *5*, 64−69.
(52) Paul, S.; Ahmed, T.; Das, S.; Samanta, A. Effect of Lead:Halide Precursor Ratio on the Photoluminescence and Carrier Dynamics of Violet- and Blue-Emitting Lead Halide Perovskite Nanocrystals. *J. Phys. Chem. C* **2021**, *125*, 23539−23547.
(53) Pradhan, N. Tips and Twists in Making High Photoluminescence Quantum Yield Perovskite Nanocrystals. *ACS Energy Lett.* **2019**, *4*, 1634−1638.
(54) Imran, M.; Caligiuri, V.; Wang, M.; Goldoni, L.; Prato, M.; Krahne, R.; Trizio, L. D.; Manna, L. Benzoyl Halides as Alternative Precursors for the Colloidal Synthesis of Lead-Based Halide Perovskite Nanocrystals. *J. Am. Chem. Soc.* **2018**, *140*, 2656−2664.
(55) Dutta, A.; Behera, R. K.; Pal, P.; Baitalik, S.; Pradhan, N. Near-Unity Photoluminescence Quantum Efficiency for All $CsPbX_3$(X = Cl, Br, and I) Perovskite Nanocrystals: A Generic Synthesis Approach. *Angew. Chem., Int. Ed.* **2019**, *58*, 5552−5556.
(56) Liu, P.; Chen, W.; Wang, W.; Xu, B.; Wu, D.; Hao, J.; Cao, W.; Fang, F.; Li, Y.; Zeng, Y.; et al. Halide-Rich Synthesized Cesium Lead Bromide Perovskite Nanocrystals for Light-Emitting Diodes with Improved Performance. *Chem. Mater.* **2017**, *29*, 5168−5173.
(57) Park, J.; Kim, Y.; Ham, S.; Woo, J. Y.; Kim, T.; Jeong, S.; Kim, D. A Relationship Between the Surface Composition and Spectroscopic Properties of Cesium Lead Bromide ($CsPbBr_3$) Perovskite Nanocrystals: Focusing on Photoluminescence Efficiency. *Nanoscale* **2020**, *12*, 1563−1570.
(58) Cai, Y.; Wang, H.; Li, Y.; Wang, L.; Lv, Y.; Yang, X.; Xie, R.-J. Trimethylsilyl Iodine-Mediated Synthesis of Highly Bright Red-Emitting $CsPbI_3$ Perovskite Quantum Dots with Significantly Improved Stability. *Chem. Mater.* **2019**, *31*, 881−889.
(59) Das, S.; Samanta, A. Highly Luminescent and Phase-Stable Red/NIR-Emitting All-Inorganic and Hybrid Perovskite Nanocrystals. *ACS Energy Lett.* **2021**, *6*, 3780−3787.
(60) Yao, J.-S.; Ge, J.; Wang, K.-H.; Zhang, G.; Zhu, B.-S.; Chen, C.; Zhang, Q.; Luo, Y.; Yu, S.-H.; Yao, H.-B. Few-Nanometer-Sized α-$CsPbI_3$ Quantum Dots Enabled by Strontium Substitution and Iodide Passivation for Efficient Red-Light Emitting Diodes. *J. Am. Chem. Soc.* **2019**, *141*, 2069−2079.
(61) Shen, X.; Zhang, Y.; Kershaw, S. V.; Li, T.; Wang, C.; Zhang, X.; Wang, W.; Li, D.; Wang, Y.; Lu, M.; et al. Zn-Alloyed $CsPbI_3$ Nanocrystals for Highly Efficient Perovskite Light-Emitting Devices. *Nano Lett.* **2019**, *19*, 1552−1559.
(62) Akkerman, Q. A.; Meggiolaro, D.; Dang, Z.; Angelis, F. D.; Manna, L. Fluorescent Alloy $CsPbxMn_{1-x}I_3$ Perovskite Nanocrystals with High Structural and Optical Stability. *ACS Energy Lett.* **2017**, *2*, 2183−2186.
(63) Behera, R. K.; Dutta, A.; Ghosh, D.; Bera, S.; Bhattacharyya, S.; Pradhan, N. Doping the Smallest Shannon Radii Transition Metal Ion Ni(II) for Stabilizing α-$CsPbI_3$ Perovskite Nanocrystals. *J. Phys. Chem. Lett.* **2019**, *10*, 7916−7921.
(64) Chen, Z.; Zhou, B.; Yuan, J.; Tang, N.; Lian, L.; Qin, L.; Zhu, L.; Zhang, J.; Chen, R.; Zang, J. Cu^{2+}-Doped $CsPbI_3$ Nanocrystals with Enhanced Stability for Light Emitting Diodes. *J. Phys. Chem. Lett.* **2021**, *12*, 3038−3045.
(65) Shu, B.; Chang, Y.; Zhang, J.; Cheng, X.; Yu, D. Synthesis and Photoluminescence Kinetics of Ce^{3+}-Doped $CsPbI_3$ QDs with Near-Unity PLQY. *Nano Res.* **2021**, *14*, 3352−3357.
(66) Zhu, Y.; Zhao, J.; Yang, G.; Xu, X.; Pan, G. Ammonium Acetate Passivated $CsPbI_3$ Perovskite Nanocrystals for Efficient Red Light-Emitting Diodes. *Nanoscale* **2020**, *12*, 7712−7719.
(67) Lu, M.; Guo, J.; Lu, P.; Zhang, L.; Zhang, Y.; Dai, Q.; Hu, Y.; Colvin, V. L.; Yu, W. W. Ammonium Thiocyanate-Passivated $CsPbI_3$ Perovskite Nanocrystals for Efficient Red Light-Emitting Diodes. *J. Phys. Chem. C* **2019**, *123*, 22787−22972.
(68) Chen, Q.; Cao, S.; Xing, K.; Ning, M.; Zeng, R.; Wang, Y.; Zhao, J. Mg^{2+}-Assisted Passivation of Defects in $CsPbI_3$ Perovskite Nanocrystals for High-Efficiency Photoluminescence. *J. Phys. Chem. Lett.* **2021**, *12*, 11090−11097.
(69) Dong, Y.; Qiao, T.; Kim, D.; Parobek, D.; Rossi, D.; Son, D. H. Precise Control of Quantum Confinement in Cesium Lead Halide Perovskite Quantum Dots via Thermodynamic Equilibrium. *Nano Lett.* **2018**, *18*, 3716−3722.
(70) Tang, J.; Marcus, R. A. Mechanisms of Fluorescence Blinking in Semiconductor Nanocrystal Quantum Dots. *J. Chem. Phys.* **2005**, *123*, 054704.
(71) Balakrishnan, S. K.; Kamat, P. V. Ligand Assisted Transformation of Cubic $CsPbBr_3$ Nanocrystals into Two-Dimensional $CsPb_2Br_5$ Nanosheets. *Chem. Mater.* **2018**, *30*, 74−78.
(72) Ravi, V. K.; Santra, P. K.; Joshi, N.; Chugh, J.; Singh, S. K.; Rensmo, H.; Ghosh, P.; Nag, A. Origin of the Substitution Mechanism for the Binding of Organic Ligands on the Surface of $CsPbBr_3$ Perovskite Nanocubes. *J. Phys. Chem. Lett.* **2017**, *8*, 4988−4994.

https://doi.org/10.1021/acs.jpclett.2c01463
J. Phys. Chem. Lett. 2022, 13, 5742−5750

THE JOURNAL OF PHYSICAL CHEMISTRY C
A JOURNAL OF THE AMERICAN CHEMICAL SOCIETY

pubs.acs.org/JPCC

Article

Photoluminescence Blinking of Quantum Confined $CsPbBr_3$ Perovskite Nanocrystals: Influence of Size

Published as part of The Journal of Physical Chemistry C virtual special issue "The Physical Chemistry of Perovskites".

Sumanta Paul, Gautam Kishore, and Anunay Samanta*

Cite This: *J. Phys. Chem. C* 2023, 127, 10207−10214

Read Online

ACCESS | Metrics & More | Article Recommendations | Supporting Information

ABSTRACT: Quantum confined $CsPbBr_3$ nanocrystals (NCs) with adjustable photoluminescence (PL) in the range of 470−500 nm are particularly desirable for applications in light-emitting diodes and many quantum technologies. Exploration of the full potential of these perovskite NCs requires an understanding of the random fluctuation of their PL at the single-particle level, commonly termed as blinking. In this work, we study the PL blinking of quantum confined single NCs of $CsPbBr_3$ of three different sizes between 3.80 and 5.90 nm in immobilized and fluid conditions to understand the recombination pathways and dynamics of the photogenerated charge carriers. In the immobilized state, the PL intensity trajectories and PL lifetime-intensity distributions of these single NCs reveal the contributions of both Auger recombination and trapping of hot carriers to the PL fluctuation. The results suggest a higher carrier trapping rate constant for smaller NCs. The fluorescence correlation spectroscopy and fluorescence lifetime correlation spectroscopy measurements on freely diffusing NCs show a higher off-state fraction and lower per-particle brightness of the smaller NCs. It is concluded that a larger trap depth and higher probability density of the carriers at the surface in smaller NCs make the trapping process more feasible and detrapping more difficult. The results provide first information on the effect of size on PL blinking of the quantum confined $CsPbBr_3$ NCs, and this knowledge is expected to be useful in better designing photoluminescent samples of this class for optoelectronic applications.

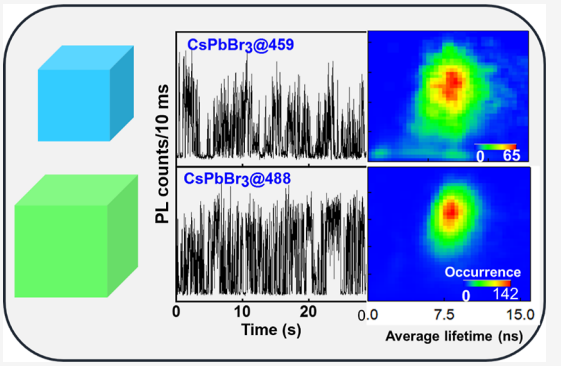

INTRODUCTION

The cesium lead halide ($CsPbX_3$, X= Cl, Br and I) perovskite nanocrystals (NCs) continue to receive great attention owing to their potential applications in optoelectronic devices such as in light-emitting diodes[1−8] and single-photon sources.[9−13] However, the fluctuation of photoluminescence (PL) of the single NCs of these substances between bright (on) and dark (off) states,[9,12,14−20] and sometimes between the "on" and a low-intensity gray state,[16,18,21] is impediment to these applications. The PL fluctuation occurs over a rather broad timescale ranging from tens of microseconds to hundreds of seconds.[22,23] While the PL of these perovskite NCs originates from the radiative recombination of the electron and hole produced on photoexcitation, the fluctuation of PL is caused by the involvement of various trap states in these systems. Several processes can contribute to the PL blinking of the semiconductor NCs.[9,14,17,21,22,24] When one of the charge carriers is trapped for a longer duration, the NCs become charged. When the absorption of another photon by a charged NC produces an exciton, the system becomes a trion.[9,21,24−26] The trion can recombine nonradiatively by Auger recombination or/and radiatively at a much faster rate (twice the neutral exciton recombination rate).[9,21,24,26] PL blinking arising from trion-mediated recombination is known as Auger or A-type blinking.[24] Trapping of the charge carrier in a short-lived trap state can facilitate its instant relaxation by a nonradiative pathway.[16,18,19,21,27] Random activation and deactivation of these trap states result in a constantly changing nonradiative rate constant.[21,22,27] This time-dependent fluctuation of the nonradiative rate constant leads to PL blinking, which is termed as band-edge carrier (BC) blinking when the trapping of the charge carriers takes place from the band-edge states.[21] Blinking can also be caused by the trapping of the hot carriers (HC blinking).[14,22,24,28] Trapping of the hot carriers allows their rapid relaxation through a nonradiative recombination

Received: February 27, 2023
Revised: April 22, 2023
Published: May 18, 2023

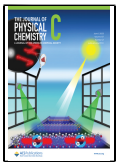

https://doi.org/10.1021/acs.jpcc.3c01336
J. Phys. Chem. C 2023, 127, 10207−10214

route, and one observes a large drop of PL intensity without any noticeable change in lifetime. As both BC and HC blinking arise from the activation and deactivation of the trap states, these two types of blinking are often referred to as B-type blinking.[24,28] In many cases, more than one mechanism of blinking is observed.[16,18,19,21,24] The coexistence of Auger, BC, and HC blinking in single perovskite NCs has also been reported.[16,29]

PL blinking studies on perovskite single NCs, except a few on $MAPbBr_3$ NCs,[14,15] have been carried out on large systems (size range 6−20 nm) with no/weak quantum confinement.[9,11,14,16−18,30−38] One main reason for the dearth of PL blinking studies on smaller particles was the lack of any method of their preparation with uniform size distribution and control on size. A very recent report on the synthesis of quantum confined $CsPbX_3$ NCs with uniform size distribution[39] has enabled photophysical studies on these smaller NCs.[40−42] These studies have revealed blue-shifted emission with a larger Stokes shift,[39,42] faster biexciton auger recombination rate,[40,43,44] intense dark exciton emission,[41] and higher single-photon purity[11] of the quantum confined perovskite NCs compared to the non-quantum confined system. The smaller NCs are found to have higher trion and biexciton binding energy due to stronger Coulomb interaction between the electrons and holes.[45,46] As the size of the NCs plays an important role in the charge carrier trapping and detrapping processes,[14,47,48] an investigation of the PL blinking of quantum confined perovskite NCs of different sizes is expected to provide an understanding of the charge carrier trapping and detrapping processes in these substances, which may help unleash these materials' full application potentials.

In order to study the PL blinking behavior of quantum confined perovskite NCs of different sizes, we have prepared $CsPbBr_3$ NCs with 3.80, 4.80, and 5.90 nm edge length and investigated their PL blinking by analyzing PL blinking traces, fluorescence lifetime-intensity distribution (FLID) patterns, and statistical distribution of the on- and off-events. PL blinking of freely diffusing NCs is also studied by employing fluorescence correlation spectroscopy (FCS) and fluorescence lifetime correlation spectroscopy (FLCS) techniques.

EXPERIMENTAL SECTION

Preparation of Quantum Confined $CsPBr_3$ NCs. These NCs of different sizes were synthesized by the hot injection method following a reported procedure with minor changes in the reaction conditions.[39] In the first step, Cs-oleate was prepared from its precursors. For this purpose, 0.25 g Cs_2CO_3, 0.9 mL oleic acid (OA), and 9 mL 1-octadecene (ODE) were loaded onto a 50 mL 2-neck round-bottom flask and dried under vacuum for 1 h at 120 °C. The mixture was then heated under a N_2 atmosphere to 150 °C until Cs_2CO_3 dissolved completely. The Cs-oleate solution was then kept at 100 °C to prevent the precipitation of Cs-oleate. For the preparation of the $CsPbBr_3$ NCs, in another 50 mL 2-neck round-bottom flask, 75 mg $PbBr_2$ and $ZnBr_2$ (250 mg) were dissolved in a mixture of ODE (5 mL), OA (3 mL), and oleylamine (3 mL) at 120 °C in vacuum. Then, 0.4 mL Cs-oleate was injected swiftly into the reaction mixture at a preset reaction temperature (in a N_2 atmosphere). The reaction temperatures used for the synthesis of the NCs of three different sizes were 80, 140, and 180 °C, respectively. The reaction was quenched after 120 s by cooling the system in an ice bath. The crude product was then purified (details in the Supporting Information).

Single-Particle PL Measurements. *Sample Preparation.* A pM solution (in hexane) of the NCs was drop-cast on a cover glass and dried under vacuum to obtain a film of the sample. The film was kept on the microscope stage for measurements. The experiments were carried out at a relative humidity of 55 ± 5% and a temperature of 25 °C. For the FCS and FLCS measurements, a drop of nM solution of the NCs (in ODE) was placed on a cover glass and studied under the microscope.

Photon Antibunching and PL Blinking Measurement. These measurements were performed using a PicoQuant MicroTime 200 time-resolved confocal fluorescence microscope system consisting of an inverted microscope (Olympus IX71) equipped with a Piezo scanning stage. Samples were excited at 405 nm by a pulsed (8 MHz repletion rate) picosecond diode laser (PDL 828 S Sepia II, PicoQuant). A water immersion objective (UplanSApo 60× NA 1.2) was used for the collection of photons. The sample-emitted photons were spectrally filtered by a 430 nm long-pass filter. A 50 μm diameter pinhole was used in the optical path for the spatial filtration of photons. For antibunching measurement, the filtered photons were passed through a 50:50 beam splitter and focused onto two identical SPADs arranged in the Hanbury Brown−Twiss configuration. For the blinking measurement, emitted photons were focused on a single detector. The detector signal was processed using a PicoHarp300 time correlated single-photon counting (TCSPC) unit. For photon antibunching and PL blinking measurements, the TCSPC unit was operated in time-tagged (T_2) and time-tagged time resolved (T_3) modes, respectively. The recording and analysis of the data was done using the SymPhoTime software.

FCS and FLCS Measurement. FCS and FLCS measurements were also carried out using the same MicroTime 200 setup. The emitted photons from NCs, after the spectral and spatial filtration, were passed through a 50:50 beam splitter and focused onto two identical SPAD detectors. Then, the cross-correlation of the PL intensity observed in the two detectors was performed. The recording and analysis of the data were made using the SymPhoTime software.

Calculation of the Number of Excitons (N) Generated per Pulse. The number of excitons (N) generated per pulse was calculated using the formula: $N = J_p \times \sigma$, where J_p is the per-pulse photon fluence and σ is the absorption cross section.[49] J_p was calculated by using[50]

$$J_p = P/f \times E(\lambda) \quad (1)$$

where P, f, and $E(\lambda)$ are power density at the center of the focused excitation spot, the repetition rate of the laser, and the energy of the photon, respectively. The laser power density was maintained low such that on an average each NC absorbed ~0.08 photon per pulse. The possibility of any nonlinear process under this condition can be ruled out.

Calculation of Probability Densities of the On- and Off-Events. The on- and off-events were distinguished in the PL intensity time trace by applying a threshold, which was typically 10 times the maximum intensity of the background noise. Probability densities of the on- and off-events, $P_{on}(t)$ and $P_{off}(t)$, were then calculated using the following equation[18,48]

https://doi.org/10.1021/acs.jpcc.3c01336
J. Phys. Chem. C 2023, 127, 10207−10214

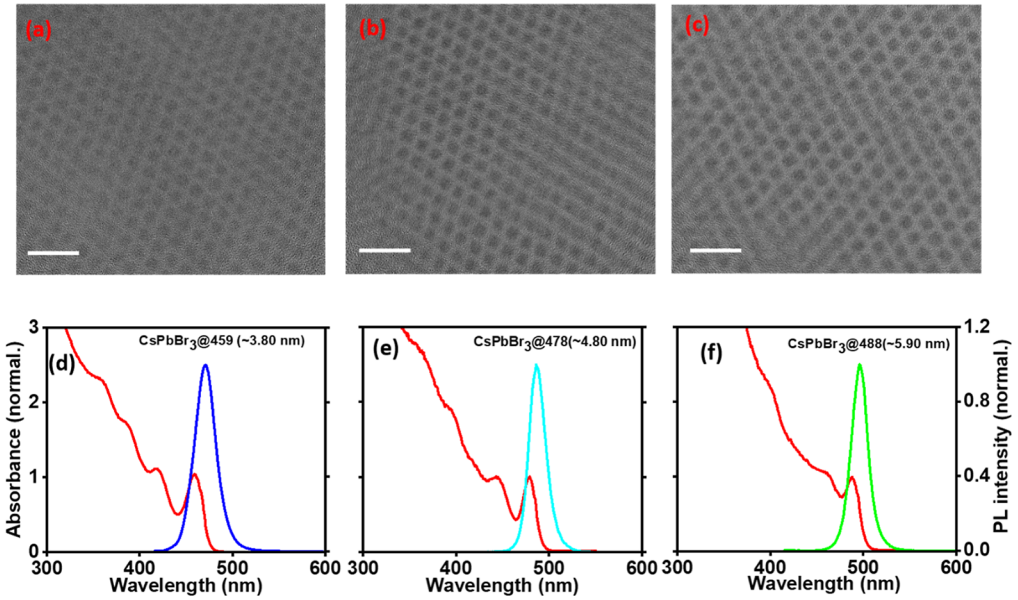

Figure 1. TEM images (top panel; a–c) and absorption and PL spectra (bottom panel; d–f) of the $CsPbBr_3$ NCs of different sizes. Scale bar is 20 nm for the TEM images. PL spectra were recorded by exciting the colloidal dispersion of these NCs at 405 nm.

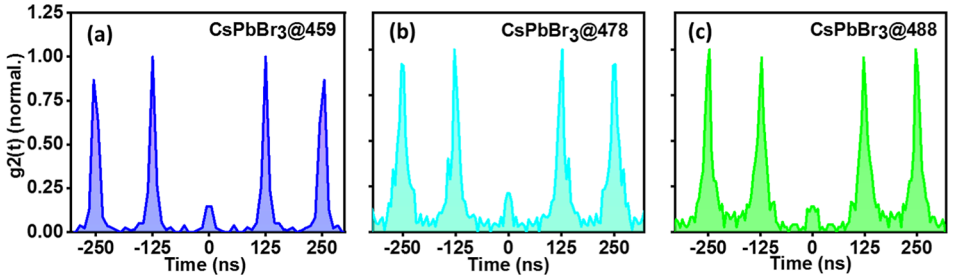

Figure 2. Second-order photo-correlation plots of $CsPbBr_3$@459 (a), $CsPbBr_3$@478 (b), and $CsPbBr_3$@488 (c) NCs. Samples were excited at 405 nm using a pulsed laser with 8 MHz repetition rate.

$$P_i(t) = \frac{N_i}{N_{i,\text{total}}} 1/\Delta t_{\text{avg}} \tag{2}$$

where i represents the on- or off-event, N_i the number of on- or off-events with the duration time of t, N_{total} is the total number of on- or off-events, and Δt_{avg} is the average time interval between the nearest neighboring events. The probability density distributions (PDD) were generated by writing a code in the Python Jupyter notebook.

RESULTS AND DISCUSSION

The transmission electron microscopy (TEM) images indicate an edge length of 3.80 ± 0.24, 4.80 ± 0.60, and 5.90 ± 0.70 nm for the $CsPbBr_3$ NCs obtained at 80, 140, and 180 °C, respectively (Figures 1a–c and S1). The absorption and PL spectra of these NCs are shown in Figure 1d–f. We have labeled these NCs with the numerical extension of their respective first excitonic peak position. The PL peaks of the $CsPbBr_3$@459, $CsPbBr_3$@478, and $CsPbBr_3$@488 NCs are observed at 470, 486, and 496 nm, respectively. Photoluminescence quantum yield (PLQY) of the $CsPbBr_3$@459, $CsPbBr_3$@478, and $CsPbBr_3$@488 NCs are estimated to be 0.45 ± 0.03, 0.75 ± 0.03, and 0.90 ± 0.05, respectively.

Before carrying out the PL blinking measurements on the immobilized NCs, we performed the photon antibunching experiment to ensure that each fluorescent particle represents a single NC. The single-photon purity is characterized by the second-order intensity correlation function

$$g^{(2)}(t) = \frac{\langle I_1(t) I_2(t+\tau)\rangle}{\langle I_1(t)\rangle \langle I_2(t+\tau)\rangle} \tag{3}$$

as a function of the delay time τ between the two photon detection events, measured in a Hanbury Brown and Twiss (HBT)-type setup (details in the Experimental Section). Here, $I_1(t)$ is the emission intensity at time t in detector 1, and $I_2(t+\tau)$ is the intensity after a time delay of τ in detector 2. For a single particle, $g^{(2)}(0)$ is expected to be 0 as it cannot emit more than one photon at any given time. This implies that a dip at "zero" time in the correlation curves indicates photon antibunching. For our samples, as can be seen from Figure 2, $g^{(2)}(0)$ is not zero but is very small compared to the side peaks at other time delays. The non-zero value of $g^{(2)}(0)$ is attributed to biexciton, whose formation cannot be completely prevented even at low laser power.[9,48,51]

PL blinking trajectories of the representative NCs of $CsPbBr_3$@459, $CsPbBr_3$@478, and $CsPbBr_3$@488 NCs, depicted in Figure 3a–c (and also in S2–S4), show that the PL of these NCs fluctuates over a range of intensity levels. The occurrence histograms (Figure 3d–f) indicate no clear separation between the on- and off-PL intensity states. In order to understand the blinking mechanism, we have measured PL decay profiles of three different intensity regions

https://doi.org/10.1021/acs.jpcc.3c01336
J. Phys. Chem. C 2023, 127, 10207–10214

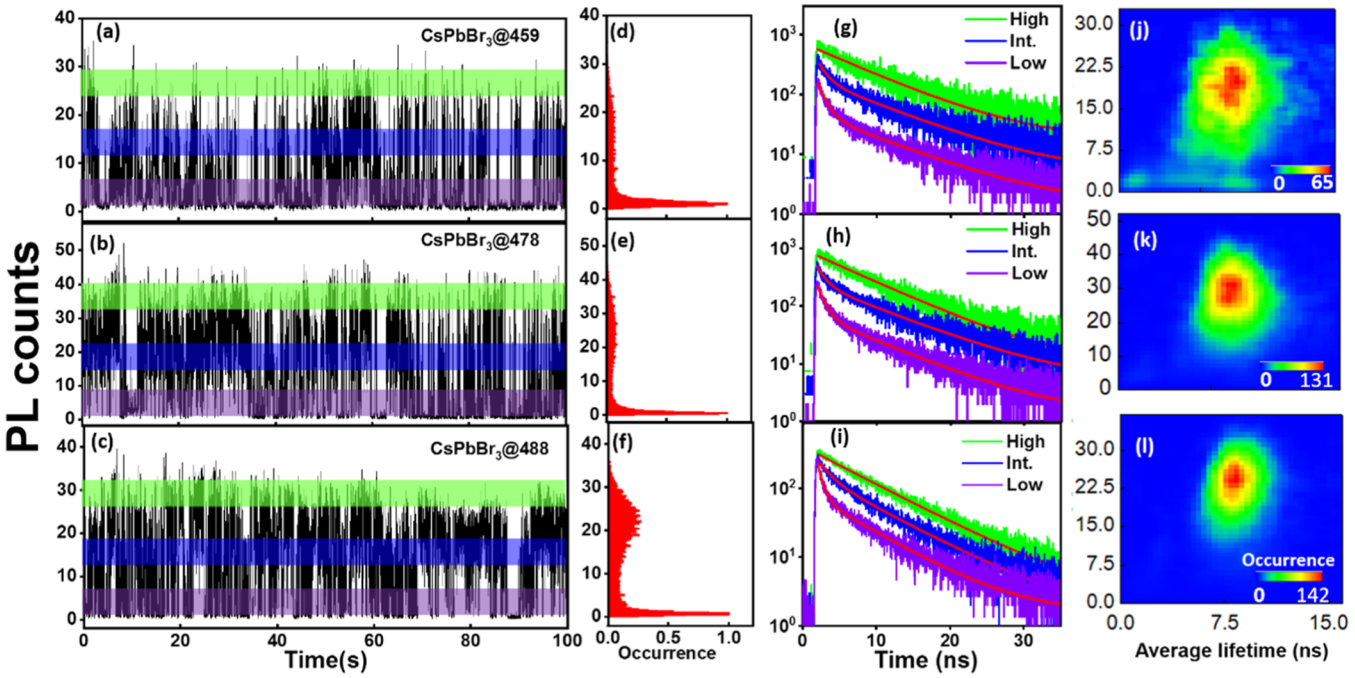

Figure 3. Representative PL intensity trajectories (a–c) (binning time 10 ms) and occurrence histograms (d–f) of the NCs of different sizes. Green, blue, and violet shades indicate high-, intermediate-, and low-intensity regions, respectively, for which PL decay profiles were measured (g–i). FLID plots of these NCs are shown in panels (j–l).

(indicated by green, blue, and violet shades) of the blinking traces (Figure 3g–i). The high-intensity level of these NCs is characterized by the single exponential decay with lifetime around 8–9 ns (Table 1). The PL decays of the intermediate- and low-intensity levels are bi-exponential, with one long (~8 ns) and one short (~1 ns) component (Table 1). The long 8–9 ns component of the highest intensity levels arises clearly from band-edge excitonic recombination. For the intermediate- and low-intensity regions, a lifetime close to that of the high-intensity region is possible only if the electron or hole is trapped prior to its relaxation to the band edge. Hence, this implies that trapping of the hot carriers contributes to the PL fluctuation of these NCs. The short component is attributed to the Auger recombination of trion.[9,16,26,40]

Table 1. PL Lifetime Components (τ_i) and Their Contributions (a_i) for Different PL Intensity Levels of Different Samples of $CsPbBr_3$ NCs

system	region	τ_1/ns (a_1)	τ_2/ns (a_2)
$CsPbBr_3$@459	high	8.56	
	intermediate	8.69 (0.44)	1.07 (0.56)
	low	7.70 (0.17)	0.82 (0.83)
$CsPbBr_3$@478	high	8.20	
	intermediate	8.40 (0.52)	0.83 (0.70)
	low	7.20 (0.30)	1.37 (0.48)
$CsPbBr_3$@488	high	7.90	
	intermediate	7.60 (0.57)	1.60 (0.43)
	low	6.90 (0.42)	0.73 (0.58)

The FLID of these NCs also provides an understanding of the PL blinking mechanism. For the $CsPbBr_3$@459 NCs, the FLID plot (Figure 3j) consists of (i) a high intensity–high lifetime, (ii) a low intensity–low lifetime, and (iii) a low intensity–high lifetime component. The nonlinear nature of the FLID plot and low intensity–low lifetime component are a reflection of Auger blinking,[9,21,24] and the low intensity–high lifetime component is indicative of HC blinking.[16,24,28] For $CsPbBr_3$@478 and $CsPbBr_3$@488 NCs (Figure 3k,l), both types of blinking are not clearly observable in the FLID plots due to the low occurrence of the off-intensity levels. Coexistence of HC blinking and Auger blinking for each single NC indicates that these NCs have both short-lived and long-lived trap states.

We have analyzed the PDD of the on- and off-events, P_{on} and P_{off}, to further understand the trapping and detrapping processes in these samples. For this purpose, we have sorted the data into on and off categories by assigning a threshold, above which the NCs are considered on and below which they are considered off. The PDD plots of the off-events (Figure 4)

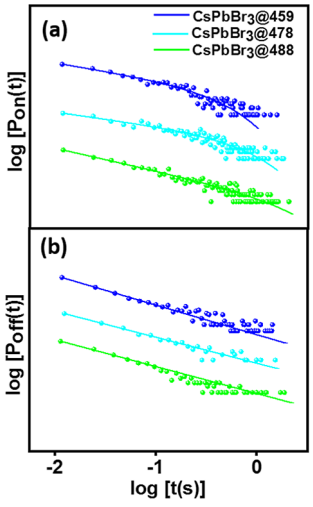

Figure 4. PDD of the on- and off-events (top and bottom panels) of the $CsPbBr_3$@459, $CsPbBr_3$@478, and $CsPbBr_3$@488 NCs.

https://doi.org/10.1021/acs.jpcc.3c01336
J. Phys. Chem. C 2023, 127, 10207–10214

are best represented by a power law function (eq 4), indicating widely distributed off → on switching rates. However, the PDD plots of the on events (Figure 4) are best represented by a truncated power law (eq 5), indicating that the events which are power-law distributed at shorter times become exponential at longer times.

$$P_{off}(t) = t_{off}^{-m_{off}} \tag{4}$$

$$P_{on}(t) = t_{ON}^{-m_{on}} \exp -\left(t_{on}/\tau_c^{on}\right) \tag{5}$$

where $m_{off/on}$ is the power-law exponent and τ_c^{on} represents the time corresponding to the exponential truncation of the power law. The exponential truncation of the on-events at long times implies that the on → off switching at the long on-duration occurs at a single rate or the distributed rate process saturates at the long on-duration.[22,52,53]

A much higher m_{off} value of these NCs compared to their m_{on} value indicates that PL blinking is dominated by longer on-events and shorter off-events. A distinct variation of the truncation time with the size of the NCs is observable (Figure 5a and Table 2). With the increase in size of the NCs, an

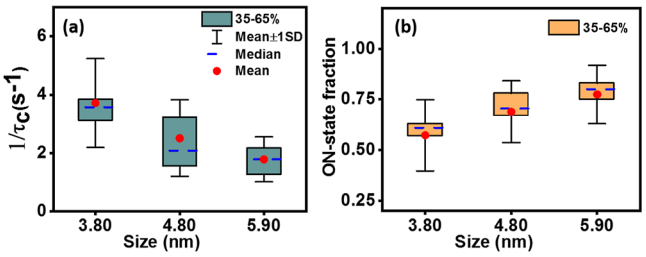

Figure 5. (a) Box plot of the inverse of the truncation time ($1/\tau_c^{on}$) and (b) on-state fraction of the $CsPbBr_3$ NCs of different sizes. Interquartile range is equal to 35−65th percentile. Spheres indicate the mean. Whiskers indicate standard deviation from the mean. Dashed lines in the box indicate the median.

increase in the truncation time [0.31 ± 0.15 s ($CsPbBr_3$@459), 0.51 ± 0.28 s ($CsPbBr_3$@478), and 0.69 ± 35 s ($CsPbBr_3$@488)] indicates a decrease in the trapping rate constant (k_t).[48,54−56] The average time fraction in the on-state (Figure 5b) is estimated from the measured blinking trajectory of nearly 100 NCs of a particular size. With the increase in size of the NCs, this number increases as follows: 0.58 ± 0.17 ($CsPbBr_3$@459), 0.69 ± 0.15 ($CsPbBr_3$@478), and 0.77 ± 0.16 ($CsPbBr_3$@488). A lower on-state fraction for the smaller $CsPbBr_3$ NCs is attributed to a higher carrier trapping rate and lower detrapping rate in these systems. In larger NCs, charge carrier wave functions are localized in the core of the NCs, and with the decrease in size of the NCs, the carrier probability density at the surface increases,[57] thus making the trapping process more feasible. As $CsPbBr_3$ NCs possess shallow trap states,[1,8,58] and the depth of these trap states decreases with the increase in size of the NCs, the trapping process is more feasible and detrapping is more difficult for smaller NCs.

Additional insights into the PL blinking of these NCs are obtained from the FCS and FLCS studies of freely diffusing NCs. While the time resolution of PL blinking data discussed so far for the immobilized samples is limited by the binning time (10 ms here) of the measurement, the FCS and FLCS measurements can be used for extracting information on the PL fluctuation occurring in the μs timescale.[32,59] In these techniques, one measures the fluctuations of the PL intensity of a highly dilute solution (nM) of the NCs in a small volume of the sample (typically ∼1 fL) using a confocal fluorescence microscope (details in the Experimental Section). While the FCS experiment records only the macroscopic arrival time of each detected photon (τ, with resolution μs) with respect to the beginning of the experiment, the FLCS additionally measures the microscopic delay time (t, with ps resolution) of the detected photons relative to the excitation pulse,[60] which allowed us to study the autocorrelation function of the PL fluctuation of the neutral exciton (∼8.5 ns) and trion (∼1.6 ns) separately. The FCS and FLCS data of these NCs (Figures 6a,b, S5 and S6) are best described by eq 6, which considers the PL fluctuation due to (i) the diffusion of the NCs in and out of the observation volume and (ii) the trapping of the charge carriers, represented by a stretched exponential decay component. The amplitude of the correlation at time τ, $G(\tau)$, is expressed as

$$G(\tau) = \left[1 + \frac{T}{1-T}\exp\left(-\frac{\tau}{\tau_T}\right)^{\beta}\right]\frac{1}{N}\left(1 + \frac{\tau}{\tau_D}\right)^{-1}\left(1 + \frac{\tau}{k^2\tau_D}\right)^{-1/2} \tag{6}$$

where N is the average number of particles undergoing reversible PL intensity fluctuation in the observation volume, τ_D is the diffusion time of the NCs, T is the fraction of the particles in their "off" state, and τ_T is the dark-state relaxation time or blinking time. β is the stretching exponent with a value between 0 and 1 and is related to the distribution of τ_T. $\kappa(=\omega_z/\omega_{xy})$ is the structure parameter of the observation volume; ω_z and ω_{xy} are the longitudinal and transverse radii of the observation volume, respectively. The per-particle brightness (PPB) of the NCs is estimated by $I/\langle N\rangle$, where I is the average count rate of the PL intensity trace.

A close look at various parameters associated with the PL fluctuation (Table 3), as obtained from an analysis of the FCS and FLCS curves, reveals a large deviation of the β values from unity. This indicates a broadly distributed kinetics of PL blinking, indicating the involvement of multiple trap states with varying carrier trapping and detrapping rates. The data also show a decrease in the off-state fraction with an increase in the size of the NCs (Table 3). While this trend is similar to that observed in the case of immobilized samples, the absolute values differ significantly in the two cases. The FCS and FLCS measurements provide a higher off-state fraction compared to the blinking measurements on immobilized NCs simply

Table 2. Power Law Exponents and Truncation Time for the $CsPbBr_3$ NCs of Different Sizes

system	NCs size (nm)	m_{off}	m_{on}	τ_c^{on} (s)
$CsPbBr_3$@459	3.80 ± 0.24	1.58 ± 0.26	0.75 ± 0.12	0.31 ± 0.15
$CsPbBr_3$@478	4.80 ± 0.60	1.78 ± 0.32	0.71 ± 0.13	0.51 ± 0.28
$CsPbBr_3$@488	5.90 ± 0.70	1.77 ± 0.40	0.72 ± 0.14	0.69 ± 0.35

https://doi.org/10.1021/acs.jpcc.3c01336
J. Phys. Chem. C 2023, 127, 10207−10214

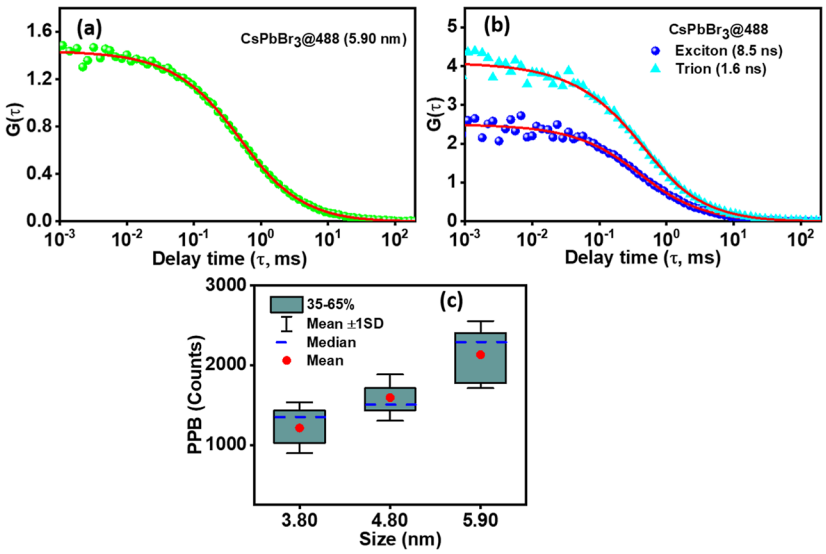

Figure 6. (a) Fluorescence correlation data (green dots) and the fit (red line) to the data of the $CsPbBr_3$@488 NCs in ODE. (b) Autocorrelation amplitudes of 8.5 ns (exciton) and 1.6 ns (trion) component as a function of delay time of this NCs. (c) PPBs of three different size NCs.

Table 3. Estimated Values of the Stretching Exponent (β), Off-State Fraction (T), and Off-State Relaxation Time (τ_T)

system	experiment	β	T	τ_T (ms)
	FCS	0.67 ± 0.10	0.58 ± 0.08	0.49 ± 0.09
$CsPbBr_3$@459	FLCS (exciton)	0.65 ± 0.12	0.63 ± 0.09	0.43 ± 0.05
	FLCS (trion)	0.53 ± 0.08	0.68 ± 0.12	0.44 ± 0.05
	FCS	0.69 ± 0.03	0.51 ± 0.07	0.45 ± 0.05
$CsPbBr_3$@478	FLCS (exciton)	0.71 ± 0.10	0.55 ± 0.07	0.37 ± 0.06
	FLCS (trion)	0.63 ± 0.09	0.57 ± 0.11	0.40 ± 0.08
	FCS	0.76 ± 0.05	0.42 ± 0.07	0.43 ± 0.05
$CsPbBr_3$@488	FLCS (exciton)	0.79 ± 0.11	0.46 ± 0.06	0.42 ± 0.06
	FLCS (trion)	0.65 ± 0.08	0.47 ± 0.07	0.35 ± 0.05

because the former captures PL fluctuations at a faster timescale. As can be seen (Figure 6c), the PPB of these NCs increases with the increase in size of the NCs: 1213.60 ± 317.70 cps ($CsPbBr_3$@459), 1593.40 ± 289.90 cps ($CsPbBr_3$@478), and 2131.50 ± 421.70 cps (CsPbBr3@488). This trend is consistent with the size-dependent variation of the PLQY of the systems. A higher value of the off-state fraction and a lower PPB value of the smaller NCs reconfirm that with decrease in NCs, size trapping becomes more feasible and detrapping becomes difficult.

CONCLUSIONS

The PL blinking of three different size quantum confined single NCs of $CsPbBr_3$ has been studied. Both hot carrier trapping and Auger recombination are found to contribute to the PL fluctuations of the immobilized NCs, indicating the presence of both short-lived and long-lived trap states. The results also suggest an increase in the trapping rate constant with a decrease in size of the NCs. The FCS and FLCS measurements indicate a lower off-state fraction and higher per-particle brightness for the bigger NCs. The observation is rationalized considering a smaller trap depth and the localization of the charge-carrier wavefunction in the core region for large size NCs. The findings provide first insights into the charge carrier recombination pathway and the dynamics of the quantum confined $CsPbBr_3$ NCs from PL blinking studies, and the findings will be useful in the design and development of small size highly luminescent perovskite NCs for optoelectronic applications.

ASSOCIATED CONTENT

Supporting Information

The Supporting Information is available free of charge at https://pubs.acs.org/doi/10.1021/acs.jpcc.3c01336.

Details of the purification method and TEM, steady state absorption and PL measurements, size histograms of these NCs, additional blinking traces of representative NCs of the different size NCs, and FCS and FLCS curves of $CsPbBr_3$@478 and $CsPbBr_3$@459 NCs (PDF)

AUTHOR INFORMATION

Corresponding Author

Anunay Samanta − *School of Chemistry, University of Hyderabad, Hyderabad 500046, India;* orcid.org/0000-0003-1551-0209; Email: anunay@uohyd.ac.in

Authors

Sumanta Paul − *School of Chemistry, University of Hyderabad, Hyderabad 500046, India;* orcid.org/0000-0003-4825-0984

Gautam Kishore − *School of Chemistry, University of Hyderabad, Hyderabad 500046, India;* Present Address: School of Computer & Information Science, University of Hyderabad, Hyderabad 500046, India

Complete contact information is available at: https://pubs.acs.org/10.1021/acs.jpcc.3c01336

Notes

The authors declare no competing financial interest.

■ ACKNOWLEDGMENTS

This work was supported by the J. C. Bose Fellowship (to A.S.) of the Science and Engineering Research Board (SERB) and the Institute of Eminence Grants (to the University of Hyderabad) of the Ministry of Human Resource and Development (MHRD), Government of India. S.P. and G.K. thank the University Grants Commission and University of Hyderabad for fellowships, respectively. We thank E. Krishnan Vishnu and Prof. K. George Thomas of IISER, Thiruvananthapuram, for their help with the antibunching measurements at IISER TVM.

■ REFERENCES

(1) Protesescu, L.; Yakunin, S.; Bodnarchuk, M. I.; Krieg, F.; Caputo, R.; Hendon, C. H.; Yang, R. X.; Walsh, A.; Kovalenko, M. V. Nanocrystals of Cesium Lead Halide Perovskites ($CsPbX_3$, X = Cl, Br, and I): Novel Optoelectronic Materials Showing Bright Emission with Wide Color Gamut. *Nano Lett.* **2015**, *15*, 3692−3696.

(2) Paul, S.; Ahmed, T.; Das, S.; Samanta, A. Effect of Lead:Halide Precursor Ratio on the Photoluminescence and Carrier Dynamics of Violet- and Blue-Emitting Lead Halide Perovskite Nanocrystals. *J. Phys. Chem. C* **2021**, *125*, 23539−23547.

(3) Liu, X.-K.; Xu, W.; Bai, S.; Jin, Y.; Wang, J.; Friend, R. H.; Gao, F. Metal Halide Perovskites for Light-Emitting Diodes. *Nat. Mater.* **2021**, *20*, 10−21.

(4) Fakharuddin, A.; Gangishetty, M. K.; Abdi-Jalebi, M.; Chin, S.-H.; bin Mohd Yusoff, A. R.; Congreve, D. N.; Tress, W.; Deschler, F.; Vasilopoulou, M.; Bolink, H. J. Perovskite Light-Emitting Diodes. *Nat. Electron.* **2022**, *5*, 203−216.

(5) Wei, Z.; Xing, J. The Rise of Perovskite Light-Emitting Diodes. *J. Phys. Chem. Lett.* **2019**, *10*, 3035−3042.

(6) Ji, K.; Anaya, M.; Abfalterer, A.; Stranks, S. D. Halide Perovskite Light-Emitting Diode Technologies. *Adv. Opt. Mater.* **2021**, *9*, 2002128.

(7) Paul, S.; Samanta, A. N-Bromosuccinimide as Bromide Precursor for Direct Synthesis of Stable and Highly Luminescent Green-Emitting Perovskite Nanocrystals. *ACS Energy Lett.* **2020**, *5*, 64−69.

(8) Dey, A.; Ye, J.; De, A.; Debroye, E.; Ha, S. K.; Bladt, E.; Kshirsagar, A. S.; Wang, Z.; Yin, J.; Wang, Y.; et al. State of the Art and Prospects for Halide Perovskite Nanocrystals. *ACS Nano* **2021**, *15*, 10775−10981.

(9) Park, Y.-S.; Guo, S.; Makarov, N. S.; Klimov, V. I. Room Temperature Single-Photon Emission from Individual Perovskite Quantum Dots. *ACS Nano* **2015**, *9*, 10386−10393.

(10) Rainò, G.; Yazdani, N.; Boehme, S. C.; Kober-Czerny, M.; Zhu, C.; Krieg, F.; Rossell, M. D.; Erni, R.; Wood, V.; Infante, I.; et al. Ultra-Narrow Room-Temperature Emission from Single $CsPbBr_3$ Perovskite Quantum Dots. *Nat. Commun.* **2022**, *13*, 2587.

(11) Zhu, C.; Marczak, M.; Feld, L.; Boehme, S. C.; Bernasconi, C.; Moskalenko, A.; Cherniukh, I.; Dirin, D.; Bodnarchuk, M. I.; Kovalenko, M. V.; et al. Room-Temperature, Highly Pure Single-Photon Sources from All-Inorganic Lead Halide Perovskite Quantum Dots. *Nano Lett.* **2022**, *22*, 3751−3760.

(12) Feld, L. G.; Shynkarenko, Y.; Krieg, F.; Rainò, G.; Kovalenko, M. V. Perovskite Quantum Dots for Super-Resolution Optical Microscopy: Where Strong Photoluminescence Blinking Matters. *Adv. Opt. Mater.* **2021**, *9*, 2100620.

(13) Mir, W. J.; Alamoudi, A.; Yin, J.; Yorov, K. E.; Maity, P.; Naphade, R.; Shao, B.; Wang, J.; Lintangpradipto, M. N.; Nematulloev, S.; et al. Lecithin Capping Ligands Enable Ultrastable Perovskite-Phase $CsPbI_3$ Quantum Dots for Rec. 2020 Bright-Red Light-Emitting Diodes. *J. Am. Chem. Soc.* **2022**, *144*, 13302−13310.

(14) Kim, T.; Jung, S. I.; Ham, S.; Chung, H.; Kim, D. Elucidation of Photoluminescence Blinking Mechanism and Multiexciton Dynamics in Hybrid Organic−Inorganic Perovskite Quantum Dots. *Small* **2019**, *15*, 1900355.

(15) Han, X.; Zhang, G.; Li, B.; Yang, C.; Guo, W.; Bai, X.; Huang, P.; Chen, R.; Qin, C.; Hu, J.; et al. Blinking Mechanisms and Intrinsic Quantum-Confined Stark Effect in Single Methylammonium Lead Bromide Perovskite Quantum Dots. *Small* **2020**, *16*, 2005435.

(16) Ahmed, T.; Seth, S.; Samanta, A. Mechanistic Investigation of the Defect Activity Contributing to the Photoluminescence Blinking of $CsPbBr_3$ Perovskite Nanocrystals. *ACS Nano* **2019**, *13*, 13537−13544.

(17) Yarita, N.; Tahara, H.; Saruyama, M.; Kawawaki, T.; Sato, R.; Teranishi, T.; Kanemitsu, Y. Impact of Postsynthetic Surface Modification on Photoluminescence Intermittency in Formamidinium Lead Bromide Perovskite Nanocrystals. *J. Phys. Chem. Lett.* **2017**, *8*, 6041−6047.

(18) Seth, S.; Ahmed, T.; Samanta, A. Photoluminescence Flickering and Blinking of Single $CsPbBr_3$ Perovskite Nanocrystals: Revealing Explicit Carrier Recombination Dynamics. *J. Phys. Chem. Lett.* **2018**, *9*, 7007−7014.

(19) Paul, S.; Samanta, A. Phase-Stable and Highly Luminescent $CsPbI_3$ Perovskite Nanocrystals with Suppressed Photoluminescence Blinking. *J. Phys. Chem. Lett.* **2022**, *13*, 5742−5750.

(20) Bose, R.; Zhou, X.; Guo, T.; Yang, H.; Yin, J.; Mishra, A.; Slinker, J. D.; Bakr, O. M.; Mohammed, O. F.; Malko, A. V. Single-Particle Spectroscopy as a Versatile Tool to Explore Lower-Dimensional Structures of Inorganic Perovskites. *ACS Energy Lett.* **2021**, *6*, 3695−3708.

(21) Yuan, G.; Gomez, D. E.; Kirkwood, N.; Boldt, K.; Mulvaney, P. Two Mechanisms Determine Quantum Dot Blinking. *ACS Nano* **2018**, *12*, 3397−3405.

(22) Cordones, A. A.; Leone, S. R. Mechanisms for Charge Trapping in Single semiconductor Nanocrystals Probed by Fluorescence Blinking. *Chem. Soc. Rev.* **2013**, *42*, 3209−3221.

(23) Efros, A. L.; Nesbitt, D. J. Origin and Control of Blinking in Quantum Dots. *Nat. Nanotechnol.* **2016**, *11*, 661−671.

(24) Galland, C.; Ghosh, Y.; Steinbruck, A.; Sykora, M.; Hollingsworth, J. A.; Klimov, V. I.; Htoon, H. Two Types of Luminescence Blinking Revealed by Spectroelectrochemistry of Single Quantum Dots. *Nature* **2011**, *479*, 203−207.

(25) Nirmal, M.; Dabbousi, B. O.; Bawendi, M. G.; Macklin, J. J.; Trautman, J. K.; Harris, T. D.; Brus, L. E. Fluorescence Intermittency in Single Cadmium Selenide Nanocrystals. *Nature* **1996**, *383*, 802−804.

(26) Kanemitsu, Y. Trion Dynamics in Lead Halide Perovskite Nanocrystals. *J. Chem. Phys.* **2019**, *151*, 170902.

(27) Frantsuzov, P. A.; Volkan-Kacso, S.; Janko, B. Model of Fluorescence Intermittency of Single Colloidal Semiconductor Quantum Dots Using Multiple Recombination Centers. *Phys. Rev. Lett.* **2009**, *103*, 207402.

(28) Trinh, C. T.; Minh, D. N.; Ahn, K. J.; Kang, Y.; Lee, K.-G. Verification of Type-A and Type B-HC Blinking Mechanisms of Organic−Inorganic Formamidinium Lead Halide Perovskite Quantum Dots by FLID Measurements. *Sci. Rep.* **2020**, *10*, 2172.

(29) Park, J.; Kim, Y.; Ham, S.; Woo, J. Y.; Kim, T.; Jeong, S.; Kim, D. A Relationship Between the Surface Composition and Spectroscopic Properties of Cesium Lead Bromide ($CsPbBr_3$) Perovskite Nanocrystals: Focusing on Photoluminescence Efficiency. *Nanoscale* **2020**, *12*, 1563−1570.

(30) Yuan, G.; Ritchie, C.; Ritter, M.; Murphy, S.; Gomez, D. E.; Mulvaney, P. The Degradation and Blinking of Single $CsPbI_3$ Perovskite Quantum Dots. *J. Phys. Chem. C* **2018**, *122*, 13407−13415.

(31) Ahmed, T.; Paul, S.; Samanta, A. Photoluminescence Blinking Revealing Static and Dynamic Heterogeneity of the Hole Transfer Process in Phenothiazine-Adsorbed $FAPbBr_3$ Single Nanocrystals. *J. Phys. Chem. C* **2022**, *126*, 9109−9116.

(32) Ahmed, T.; De, A.; Paul, S.; Samanta, A. Individual Particle-Level Picture of Charge Carrier Recombination in Bi-Doped $CsPbBr_3$ Nanocrystals. *J. Phys. Chem. C* **2021**, *125*, 2156−2162.

(33) Mandal, S.; Ghosh, S.; Mukherjee, S.; Roy, D.; De, C. K.; Mukhuti, K.; Mandal, P. K. Near-Ergodic $CsPbBr_3$ Perovskite

Nanocrystal with Minimal Statistical Aging. *J. Phys. Chem. Lett.* **2021**, *12*, 10169−10174.
(34) Mandal, S.; Mukherjee, S.; De, C. K.; Roy, D.; Ghosh, S.; Mandal, P. K. Extent of Shallow/Deep Trap States beyond the Conduction Band Minimum in Defect-Tolerant $CsPbBr_3$ Perovskite Quantum Dot: Control over the Degree of Charge Carrier Recombination. *J. Phys. Chem. Lett.* **2020**, *11*, 1702−1707.
(35) Li, B.; Huang, H.; Zhang, G.; Yang, C.; Guo, W.; Chen, R.; Qin, C.; Gao, Y.; Biju, V. P.; Rogach, A. L.; et al. Excitons and Biexciton Dynamics in Single $CsPbBr_3$ Perovskite Quantum Dots. *J. Phys. Chem. Lett.* **2018**, *9*, 6934−6940.
(36) Gibson, N. A.; Koscher, B. A.; Alivisatos, A. P.; Leone, S. R. Excitation Intensity Dependence of Photoluminescence Blinking in $CsPbBr_3$ Perovskite Nanocrystals. *J. Phys. Chem. C* **2018**, *122*, 12106−12113.
(37) Trinh, C. T.; Minh, D. N.; Ahn, K. J.; Kang, Y.; Lee, K.-G. Organic−Inorganic $FAPbBr_3$ Perovskite Quantum Dots as a Quantum Light Source: Single-Photon Emission and Blinking Behaviors. *ACS Photonics* **2018**, *5*, 4937−4943.
(38) Hou, L.; Zhao, C.; Yuan, X.; Zhao, J.; Krieg, F.; Tamarat, P.; Kovalenko, M. V.; Guo, C.; Lounis, B. Memories in the Photoluminescence Intermittency of Single Cesium Lead Bromide Nanocrystals. *Nanoscale* **2020**, *12*, 6795−6802.
(39) Dong, Y.; Qiao, T.; Kim, D.; Parobek, D.; Rossi, D.; Son, D. H. Precise Control of Quantum Confinement in Cesium Lead Halide Perovskite Quantum Dots via Thermodynamic Equilibrium. *Nano Lett.* **2018**, *18*, 3716−3722.
(40) Li, Y.; Luo, X.; Ding, T.; Lu, X.; Wu, K. Size- and Halide-Dependent Auger Recombination in Lead Halide Perovskite Nanocrystals. *Angew. Chem., Int. Ed.* **2020**, *59*, 14292−14295.
(41) Rossi, D.; Liu, X.; Lee, Y.; Khurana, M.; Puthenpurayil, J.; Kim, K.; Akimov, A. V.; Cheon, J.; Son, D. H. Intense Dark Exciton Emission from Strongly Quantum-Confined $CsPbBr_3$ Nanocrystals. *Nano Lett.* **2020**, *20*, 7321−7326.
(42) Cheng, O. H.-C.; Qiao, T.; Sheldon, M.; Son, D. H. Size- and Temperature-Dependent Photoluminescence Spectra of Strongly Confined $CsPbBr_3$ Quantum Dots. *Nanoscale* **2020**, *12*, 13113−13118.
(43) Dana, J.; Binyamin, T.; Etgar, L.; Ruhman, S. Unusually Strong Biexciton Repulsion Detected in Quantum Confined $CsPbBr_3$ Nanocrystals with Two and Three Pulse Femtosecond Spectroscopy. *ACS Nano* **2021**, *15*, 9039−9047.
(44) Lubin, G.; Yaniv, G.; Kazes, M.; Ulku, A. C.; Antolovic, I. M.; Burri, S.; Bruschini, C.; Charbon, E.; Yallapragada, V. J.; Oron, D. Resolving the Controversy in Biexciton Binding Energy of Cesium Lead Halide Perovskite Nanocrystals through Heralded Single-Particle Spectroscopy. *ACS Nano* **2021**, *15*, 19581−19587.
(45) Cho, K.; Yamada, T.; Tahara, H.; Tadano, T.; Suzuura, H.; Saruyama, M.; Sato, R.; Teranishi, T.; Kanemitsu, Y. Luminescence Fine Structures in Single Lead Halide Perovskite Nanocrystals: Size Dependence of the Exciton−Phonon Coupling. *Nano Lett.* **2021**, *21*, 7206−7212.
(46) Cho, K.; Tahara, H.; Yamada, T.; Suzuura, H.; Tadano, T.; Sato, R.; Saruyama, M.; Hirori, H.; Teranishi, T.; Kanemitsu, Y. Exciton−Phonon and Trion−Phonon Couplings Revealed by Photoluminescence Spectroscopy of Single $CsPbBr_3$ Perovskite Nanocrystals. *Nano Lett.* **2022**, *22*, 7674−7681.
(47) Naghadeh, S. B.; Luo, B.; Pu, Y.-C.; Schwartz, Z.; Hollingsworth, W. R.; Lindley, S. A.; Brewer, A. S.; Ayzner, A. L.; Zhang, J. Z. Size Dependence of Charge Carrier Dynamics in Organometal Halide Perovskite Nanocrystals: Deciphering Radiative Versus Nonradiative Components. *J. Phys. Chem. C* **2019**, *123*, 4610−4619.
(48) Vishnu, E. K.; Kumar Nair, A. A.; Thomas, K. G. Core-Size-Dependent Trapping and Detrapping Dynamics in CdSe/CdS/ZnS Quantum Dots. *J. Phys. Chem. C* **2021**, *125*, 25706−25716.
(49) Puthenpurayil, J.; Cheng, O. H.-C.; Qiao, T.; Rossi, D.; Son, D. H. On the Determination of Absorption Cross Section of Colloidal Lead Halide Perovskite Quantum Dots. *J. Chem. Phys.* **2019**, *151*, 154706.
(50) Qin, H.; Niu, Y.; Meng, R.; Lin, X.; Lai, R.; Fang, W.; Peng, X. Single-Dot Spectroscopy of Zinc-Blende CdSe/CdS Core/Shell Nanocrystals: Nonblinking and Correlation with Ensemble Measurements. *J. Am. Chem. Soc.* **2014**, *136*, 179−187.
(51) Peterson, J. J.; Nesbitt, D. J. Modified Power Law Behavior in Quantum Dot Blinking: A Novel Role for Biexcitons and Auger Ionization. *Nano Lett.* **2009**, *9*, 338−345.
(52) Tang, J.; Marcus, R. A. Diffusion-Controlled Electron Transfer Processes and Power-Law Statistics of Fluorescence Intermittency of Nanoparticles. *Phys. Rev. Lett.* **2005**, *95*, 107401.
(53) Tang, J.; Marcus, R. A. Mechanisms of Fluorescence Blinking in Semiconductor Nanocrystal Quantum Dots. *J. Chem. Phys.* **2005**, *123*, 054704.
(54) Roy, D.; Mandal, S.; De, C. K.; Kumar, K.; Mandal, P. K. Nearly Suppressed Photoluminescence Blinking of Small-Sized, Blue−Green−Orange−Red Emitting Single CdSe-Based Core/Gradient Alloy Shell/Shell Quantum Dots: Correlation between Truncation Time and Photoluminescence Quantum Yield. *Phys. Chem. Chem. Phys.* **2018**, *20*, 10332−10344.
(55) Bixby, T. J.; Cordones, A. A.; Leone, S. R. CdSe/ZnS quantum dot intermittency in N,N′-diphenyl-N,N′-bis(3-methylphenyl)-(1,1′-biphenyl)-4,4′-diamine (TPD). *Chem. Phys. Lett.* **2012**, *521*, 7−11.
(56) Xu, Z.; Cotlet, M. Photoluminenscence Blinking Dynamics of Colloidal Quantum Dots in the Presence of Controlled External Electron Traps. *Small* **2012**, *8*, 253−258.
(57) Luo, X.; Lai, R.; Li, Y.; Han, Y.; Liang, G.; Liu, X.; Ding, T.; Wang, J.; Wu, K. Triplet Energy Transfer from $CsPbBr_3$ Nanocrystals Enabled by Quantum Confinement. *J. Am. Chem. Soc.* **2019**, *141*, 4186−4190.
(58) Nenon, D. P.; Pressler, K.; Kang, J.; Koscher, B. A.; Olshansky, J. H.; Osowiecki, W. T.; Koc, M. A.; Wang, L.-W.; Alivisatos, A. P. Design Principles for Trap-Free $CsPbX_3$ Nanocrystals: Enumerating and Eliminating Surface Halide Vacancies with Softer Lewis Bases. *J. Am. Chem. Soc.* **2018**, *140*, 17760−17772.
(59) Das, A.; Mishra, K.; Ghosh, S. Revealing Explicit Microsecond Carrier Diffusion from One Emission Center to Another in an All-Inorganic Perovskite Nanocrystal. *J. Phys. Chem. Lett.* **2021**, *12*, 5413−5422.
(60) Kapusta, P.; Wahl, M.; Benda, A.; Hof, M.; Enderlein, J. Fluorescence Lifetime Correlation Spectroscopy. *J. Fluoresc.* **2006**, *17*, 43−48.

https://doi.org/10.1021/acs.jpcc.3c01336
J. Phys. Chem. C 2023, 127, 10207−10214

Deciphering Photoluminescence and Charge Carrier Recombination Dynamics of the Lead Halide Perovskite Nanocrystals at the Single-Particle and Ensemble Level

by Sumanta Paul

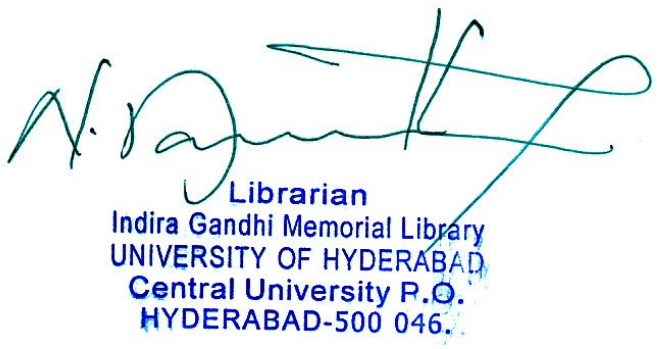

Deciphering Photoluminescence and Charge Carrier Recombination Dynamics of the Lead Halide Perovskite Nanocrystals at the Single-Particle and Ensemble Level

ORIGINALITY REPORT

58%	21%	56%	8%
SIMILARITY INDEX	INTERNET SOURCES	PUBLICATIONS	STUDENT PAPERS

PRIMARY SOURCES

1	Sumanta Paul, Gautam Kishore, Anunay Samanta. " Photoluminescence Blinking of Quantum Confined CsPbBr Perovskite Nanocrystals: Influence of Size ", The Journal of Physical Chemistry C, 2023 Publication	16%
2	Sumanta Paul, Tasnim Ahmed, Somnath Das, Anunay Samanta. "Effect of Lead:Halide Precursor Ratio on the Photoluminescence and Carrier Dynamics of Violet- and Blue-Emitting Lead Halide Perovskite Nanocrystals", The Journal of Physical Chemistry C, 2021 Publication	13%
3	Sumanta Paul, Anunay Samanta. " Phase-Stable and Highly Luminescent CsPbI Perovskite Nanocrystals with Suppressed Photoluminescence Blinking ", The Journal of Physical Chemistry Letters, 2022 Publication	12%

Own publication

PROF. ANUNAY SAMANTA
SCHOOL OF CHEMISTRY
UNIVERSITY OF HYDERABAD
HYDERABAD - 500 046

Own publication

PROF. ANUNAY SAMANTA
SCHOOL OF CHEMISTRY
UNIVERSITY OF HYDERABAD
HYDERABAD - 500 046

Own publication

PROF. ANUNAY SAMANTA
SCHOOL OF CHEMISTRY
UNIVERSITY OF HYDERABAD
HYDERABAD - 500 046

4	pubs.acs.org ACS Energy Lett. 2020, 5, 64-69 Internet Source ACS EL 2020, 5, 64-69	9%
5	Submitted to University of Hyderabad, Hyderabad Student Paper	3%
6	Sumanta Paul, Anunay Samanta. " - Bromosuccinimide as Bromide Precursor for Direct Synthesis of Stable and Highly Luminescent Green-Emitting Perovskite Nanocrystals ", ACS Energy Letters, 2019 Publication	1%
7	www.researchgate.net Internet Source	1%
8	escholarship.org Internet Source	<1%
9	"Principles of Fluorescence Spectroscopy", Springer Science and Business Media LLC, 2006 Publication	<1%
10	pubs.rsc.org Internet Source	<1%
11	www.ncbi.nlm.nih.gov Internet Source	<1%
12	Sudipta Seth, Tasnim Ahmed, Apurba De, Anunay Samanta. " Tackling the Defects, Stability, and Photoluminescence of CsPbX	<1%

PROF. ANUNAY SAMANTA
SCHOOL OF CHEMISTRY
UNIVERSITY OF HYDERABAD
HYDERABAD - 500 046
Own work

PROF. ANUNAY SAMANTA
SCHOOL OF CHEMISTRY
UNIVERSITY OF HYDERABAD
HYDERABAD - 500 046

29	Javad Shamsi, Alexander S. Urban, Muhammad Imran, Luca De Trizio, Liberato Manna. "Metal Halide Perovskite Nanocrystals: Synthesis, Post-Synthesis Modifications, and Their Optical Properties", Chemical Reviews, 2019 Publication	<1 %
30	Nathan S. Claxton, Thomas J. Fellers, Michael W. Davidson. "Microscopy, Confocal", Wiley, 2006 Publication	<1 %
31	Tasnim Ahmed, Sumanta Paul, Anunay Samanta. " Photoluminescence Blinking Revealing Static and Dynamic Heterogeneity of the Hole Transfer Process in Phenothiazine-Adsorbed FAPbBr Single Nanocrystals ", The Journal of Physical Chemistry C, 2022 Publication	<1 %
32	opus4.kobv.de Internet Source	<1 %
33	9pdf.org Internet Source	<1 %
34	Ayendrila Das, Krishna Mishra, Subhadip Ghosh. "Revealing Explicit Microsecond Carrier Diffusion from One Emission Center to Another in an All-Inorganic Perovskite	<1 %

Nanocrystal", The Journal of Physical Chemistry Letters, 2021
Publication

35 Submitted to University of Nottingham
Student Paper <1%

Exclude quotes	On	Exclude matches	< 14 words
Exclude bibliography	On		